Deutsche Gesellschaft für Kristallographie

21. Jahrestagung

19. bis 21. März 2013

Freiberg, Sachsen

Referate

Oldenbourg Verlag – München

Deutsche Gesellschaft für Kristallographie

21. Jahrestagung

19. bis 21. März 2013

Freiberg, Sachsen

Referate

Oldenbourg Verlag – München

Table of Contents

Talks

Poster

Plenary Talks

P01

Heusler compounds: From spintronics to topological insulators

C. Felser[1]
[1]*Max Planck Institute for Chemical Physics of Solids, Dresden, Germany*

Heusler compounds are a remarkable class of intermetallic materials with 1:1:1 (often called Half-Heusler) or 2:1:1 composition comprising more than 1500 members [1]. New properties and potential fields of applications emerge constantly; the prediction of topological insulators is the most recent example [2]. Surprisingly, the properties of many Heusler compounds can easily be predicted by the valence electron count or within a rigid band approach. The subgroup of more than 250 semiconductors is of high relevance for the development of novel materials for energy technologies. Their band gaps can readily be tuned from zero to 4 eV by changing the chemical composition. Thus, great interest has been attracted in the fields of thermoelectrics and topological insulator research. Ternary materials based on multifunctional properties, i.e. the combination of two or more functions such as superconductivity and topological edge states will revolutionize technological applications. The wide range of the multifunctional properties of Heusler compounds is reflected in extraordinary magneto-optical, magneto-electronic, and magneto-caloric properties. Tetragonal Heusler compounds Mn_2YZ as potential materials for STT applications can be easily designed by positioning the Fermi energy at the van Hove singularity in one of the spin channels [3]. The high magneto crystalline anisotropy identifies this group of Heusler compounds as potential candidates for spin transfer torque applications (data storage, wireless communications) and rare earth free hard magnets [3].

[1] Simple Rules for the Understanding of Heusler Compounds, Tanja Graf, Stuart S. P. Parkin, and Claudia Felser, Progress in Solid State Chemistry 39 (2011) 1.

[2] Tunable Multifunctional Topological Insulators in Ternary Heusler Compounds, S. Chadov, X.-L. Qi, J Kübler, G. H. Fecher, C. Felser, S.-C. Zhang, Nature Mat. 9 (2010) 541, arXiv:1003.0193.

[3] J. Winterlik et al. Advanced Materials 24 (2012) 6283

P02

QUASI-PERIODIC MATERIALS - CRYSTAL REDEFINED

D. Shechtman[1,2]
[1]*Technion, Haifa, Israel*
[2]*ISU, Ames, Iowa, USA, Israel*

Crystallography has been one of the mature sciences. Over the years, the modern science of crystallography that started by experimenting with x-ray diffraction from crystals in 1912, has developed a major paradigm - that all crystals are ordered and periodic. Indeed, this was the basis for the definition of "crystal" in textbooks of crystallography and x-ray diffraction. Based upon a vast number of experimental data, constantly improving research tools, and deepening theoretical understanding of the structure of crystalline materials no revolution was anticipated in our understanding the atomic order of solids.

However, such revolution did happen with the discovery of the Icosahedral phase, the first quasi-periodic crystal (QC) in 1982, and its announcement in 1984 [1, 2]. QCs are ordered materials, but their atomic order is quasiperiodic rather than periodic, enabling formation of crystal symmetries, such as icosahedral symmetry, which cannot exist in periodic materials. The discovery created deep cracks in this paradigm, but the acceptance by the crystallographers' community of the new class of ordered crystals did not happen in one day. In fact it took almost a decade for QC order to be accepted by most crystallographers. The official stamp of approval came in a form of a new definition of "Crystal" by the International Union of Crystallographers. The paradigm that all crystals are periodic has thus been changed. It is clear now that although most crystals are ordered and periodic, a good number of them are ordered and quasi-periodic.

While believers and nonbelievers were debating, a large volume of experimental and theoretical studies was published, a result of a relentless effort of many groups around the world. Quasi-periodic materials have developed into an exciting interdisciplinary science.

This talk will outline the discovery of QCs and describe the important role of electron microscopy as an enabling discovery tool.

[1] D. Shechtman, I. Blech, Met. Trans. 16A (June 1985) 1005-1012.

[2] D. Shechtman, I. Blech, D. Gratias, J.W. Cahn, Phys. Rev. Letters, Vol 53, No. 20 (1984) 1951-1953.

P03

Electronic materials seen by x-rays

V. Holy[1]
[1]*Charles University in Prague, Department of Condensed Matter Physics, Praha, Czech Republic*

Materials used in electronic technology represent a very broad spectrum of various structures ranging from amorphous layers, standard polycrystalline and epitaxial layers, and the most perfect man-made crystal structures (Si wafers), as well as quantum dot and quantum wire systems. The performance of these materials is substantially influenced by their chemical composition, crystal structure and crystal quality, and x-ray based methods represent a relatively simple, effective and reliable tool for their investigation.

Standard x-ray methods such as x-ray diffraction and reflectivity are routinely used for the determination of basic parameters such as lattice parameters and thicknesses of layers in multilayer systems. They make it possible to determine also simple parameters of real structure like interface roughness, and sizes of coherently scattering domains in polycrystalline and mosaic materials.

Application of powerful synchrotron sources of x-rays allowed us to combine x-ray absorption spectroscopy with high-resolution diffraction, and to use diffraction at various photon energies close to an absorption edge (anomalous diffraction). These methods extend the possibilities of the scattering methods to the determination of local chemical composition in the length scales of about 1 micron. A substantial progress in the x-ray scattering theory made it possible to determine physically relevant parameters of the crystal structure (types and densities of individual defects like stacking faults, dislocations, precipitates etc.) from x-ray diffraction data.

Another rapidly developing field of application of x-rays for the investigation of electronic materials is initiated by the improved coherence of an x-ray beam. Using extremely narrow beams with the cross-sections far below 1 micrometer it is possible to produce almost fully spatially coherent x-ray radiation that can be used in various coherent-scattering methods making possible to recover fully the phase of the scattered radiation. At the moment, these methods are still under development but their more frequent application for various electronic materials is expected in near future. Furthermore, very narrow x-ray beams make it possible to investigate in detail single nano-objects so that the experimental data do not suffer from a statistical averaging over an ensemble of many slightly different objects that inevitably smears out interesting details in the investigated structure. New emerging x-ray sources based on free-electron lasers open new possibilities of material research that are not yet fully understood and appreciated.

In parallel to the tendency to more and more intense x-ray sources, the progress in x-ray optics and x-ray detectors made it possible to combine x-ray scattering set-ups with semiconductor technology yielding in-situ information during a technological process.

P04

Quantitative local strain mapping of semiconductor heterostructures

P. A. van Aken[1], V. B. Özdöl[2], C. T. Koch[3]
[1]*Max Planck Institute for Intelligent Systems, Center for Electron Microscopy, Stuttgart, Germany*
[2]*Lawrence Berkeley National Laboratory, National Center for Electron Microscopy, Berkeley, United States*
[3]*Universität Ulm, Institut für Experimentelle Physik, Ulm, Germany*

Today's state-of-the-art semiconductor electronic devices utilize the charge transport within very small volumes of the active device regions. The structural, chemical and optical material properties in these small dimensions can critically affect the performance of these devices. The present contribution will cover the advances in nanometer scale characterization of the strain state in semiconductor heterostructures discussing various transmission electron microscopy techniques.

Be it process-induced strain in the latest generation MOSFETs or biaxial strain in high efficiency optoelectronic structures, optimization of device performance requires quantitative methods for strain analysis. Although high-resolution transmission electron microscopy (HRTEM) has shown to provide the required accuracy at the nanometer scale, optimization of imaging conditions is necessary for accurate strain measurements. In the last years, dark-field holography techniques have been introduced to overcome the limitations for HRTEM based methods [1,2], such as limited field of view or requirements for high quality specimens. Unlike dark-field off-axis electron holography [3], dark-field inline holography (DIH) [4] relies on the reconstruction of the geometric phase from a focal series of dark-field images. It requires therefore even less electron dose [5] and does not rely on the presence of a large area of undistorted reference lattice and can thus be applied to nanomaterials or semiconductor heterostructures where no such area exists (e.g. Fig 2).

Owing to the much lower electron doses used in holography experiments when compared to conventional quantitative HRTEM methods [5,6], the DIH approach allows to map compositional distribution in electron beam sensitive materials without alteration of the original morphology and chemical composition. Apart from its simpler experimental setup and better signal to noise properties, DIH experiments can be performed on thicker specimens than the ones required for HRTEM, which in turn reduces the thin foil relaxation. As an example, Figures 1 and 2 display the strain state analysis of 45nm technology p-MOSFET structure of a commercial processor [4] and of InGaN multi QWs from the active region of a light emitting diode (LED) [6], respectively.

References

[1] K. Du, F. Phillipp, *J. Microsc.* **221** (2006) 63.

[2] M. J. Hÿtch, E. Snoeck, and R. Kilaas, *Ultramicrosc.* **74** (1998) 131.

[3] M. Hÿtch, F. Houdellier, F. Hüe, and E. Snoeck, *Nature* **453** (2008) 1086 109.

[4] C. T. Koch, V. B. Özdöl, and P. A. van Aken, *Appl. Phys. Lett.* **96** (2010) 091901.

[5] C.T. Koch, and A. Lubk, *Ultramicrosc.* **110** (2010) 460.

[6] V. B. Özdöl, C.T. Koch, and P.A. van Aken, *J. Appl. Phys.* **108** (2010) 056103.

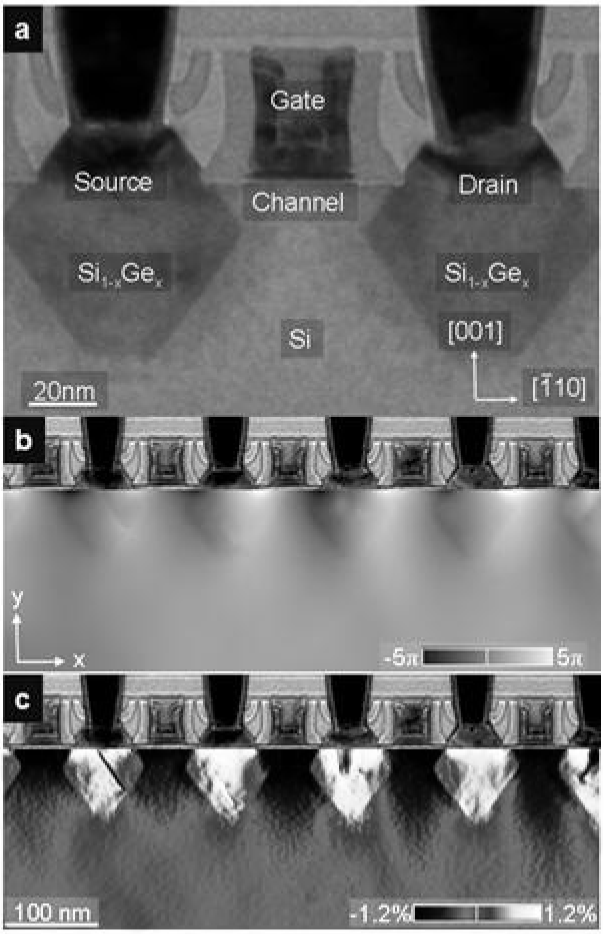

FIG. 1: a) Bright-field image of the 45nm technology p-MOSFET structure of a commercial processor. The individual transistor components are labeled. b) Geometric phase reconstructed from a focal series of 15 dark-field inline electron holograms for the (220) reflection. c) Map of the ε_{xx} strain component extracted from the geometric phase map shown in b). The gate channels are compressively strained.

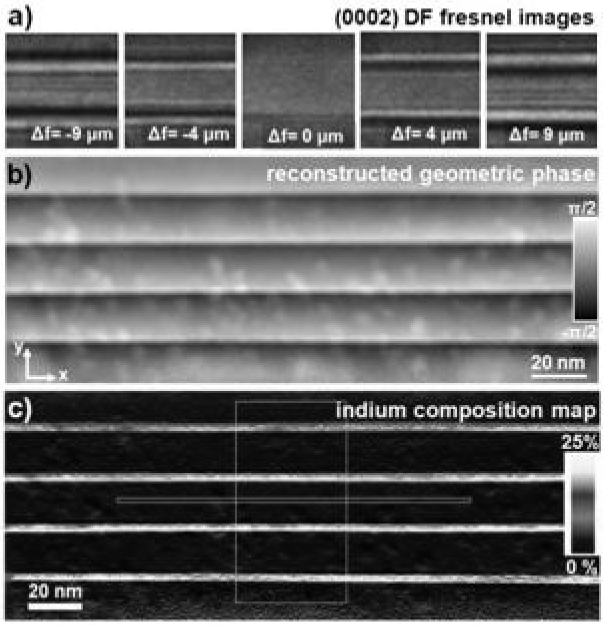

FIG. 2: a) Sub-areas of the dark-field Fresnel images of two InGaN QWs acquired at different defocus values. b) Geometric phase reconstructed from a focal series of 11 dark-field images covering the whole active region of the LED. c) Indium composition map derived from the geometric phase image reveals homogenous distribution without any evidence of nanometer scale gross indium clustering.

P05

HOW DO BIOLOGICAL MACROMOLECULES RESPOND TO LIGHT? TIME-RESOLVED CRYSTALLOGRAPHY AND PROTEIN DESIGN

K. Moffat[1]

[1] *The University of Chicago, Department of Biochemistry & Molecular Biology, Chicago, United States*

All chemical and biochemical reactions involve dynamic, not merely static structures, in which atoms move from their positions in reactants via intermediate structures towards those in products. Atomic motion in biomolecules spans an extremely wide time range, from femtoseconds to seconds or even to the generation time of the organism. How shall this atomic motion be probed and the reaction mechanisms identified? Are these chemical kinetic mechanisms based on a relatively small number of discrete intermediate states and well-defined pathways for interconversion among these states? Or, is there essentially a continuous distribution of intermediate states? More generally, can X-ray crystallography, usually thought of as a static technique, be applied to study dynamic structural changes?

We explore these questions by studying light-sensitive biomolecules and in particular, signaling photoreceptors. Such molecules absorb a photon in the visible region of the spectrum, undergo structural changes over a wide time range that constitute a thermodynamic signal, then ultimately respond to this signal by a change in the “behavior” of the organism e.g. a change in the swimming behavior of bacteria or the light-dependent developmental processes of plants (1). That is, signaling photoreceptors harness the energy in a photon to generate information, in contrast with processes such as photosynthesis in which the energy in the photon ultimately generates chemical energy and drives metabolic processes.

We apply a combination of ultrafast time-resolved X-ray crystallography (2,3,9) and UV/visible spectroscopies (see e.g. 4) to explore the static and dynamic structures of signaling photoreceptors, in crystals and in solution. Some photoreceptors absorb blue light e.g. flavin-based LOV receptors; others absorb red/far red light e.g. bilin-based bacteriophytochromes. The primary photochemistry differs from system to system: isomerization about a double bond, rupture of a covalent bond, formation of a covalent bond, or electron transfer (1).

Obviously, not all biological systems are light-sensitive and techniques devised for natural photoreceptors are not directly applicable to them. To explore generality, we are implementing biologically-inspired approaches to conferring light sensitivity on light-inert biological systems. That is, we design and engineer artificial biological photoreceptors, in which a desired biological activity such as catalysis by a histidine kinase or binding to a specific DNA sequence by a transcription factor is placed under the control of light. This approach is becoming known as "optogenetics" (5-8).

References

1) Moeglich, A., Yang, X-J., Ayers, R.A. & Moffat, K. (2010) Ann. Rev. Plant. Biol. 61, 21-47.
2) Moffat, K. (2001) Chem. Revs. 101, 1569-81.
3) Ihee, H., Wulff, M., Kim, J. and Adachi, S-I. (2010) Int. Rev. Phys. Chem. 29, 453-520.
4) Toh, K.C., Stojkovic, E.A., van Stokkum, I.H.M., Moffat, K. and Kennis, J.T.M. (2010) Proc. Nat. Acad. Sci. USA 107, 9170-5.
5) Deisseroth, K., Feng, G., Majewska, A.K., Miesenbock, G., Ting, A. and Schnitzer, M.J. (2006) J. Neurosci. 26, 10380-6.
6) Miesenbock, G. (2009) Science 326, 395-398.
7) Moeglich, A., Ayers, R.A. and Moffat, K. (2009) J. Mol. Biol. 385, 1433-44.
8) Moeglich, A. and Moffat, K. (2010) Photochem. Photobiol. Sci. 9, 1286-300.
9) Jung, Y.O., Lee, J.H., Kim, J., Schmidt, M., Moffat, K., Srajer, V., and Ihee, H. (2013) Nature Chem., in press.

P06

Biomimetic Mineralization: Nanocomposite Superstructures as Fundctional Materials of the Human Body

R. Kniep[1]
[1]*Max-Planck-Institute for Chemical Physics of Solids, Dresden, Germany*

The human body contains two different kinds of biominerals acting as functional materials: Bone and teeth (apatite-protein-nanocomposites; hardness and mechanical stability) and otoconia (calcite-(glyco?)protein-nanocomposites; gravity sensors responding to linear accelerations). The general principles of biomineralization (nucleation, transfer of information, formation of hierarchical structures, shape development) are still only poorly understood. Suitable model systems based on processes of self-organization of chemical components which are optimized during millions of years of evolution hold the chance to get deeper insight into these scenarios of high complexity. By this it becomes possible to follow and investigate the morphogenetic principles from the atomic level via embryonic composite states to hierarchical macroscopic structures [1,2].

[1] Apatite-Protein

- P. Simon, E. Rosseeva, J. Buder, W. Carrillo-Cabrera, R. Kniep: Embryonic States of Fluorapatite-Gelatine Nanocomposites and Their Intrinsic Electric-Field-Driven Morphogensis:The Missing Link on the Way from Atomistic Simulations to Pattern Formation on the Mesoscale. Adv. Funct. Mater. 19, 3596-3603 (2009).

- J. Brickmann, R. Paparcone, S. Kokolakis, D. Zahn, P. Duchstein, W. Carrillo-Cabrera, P. Simon, R. Kniep: Fluorapatite-Gelatine-Nanocomposite Superstructures: New Insights into a Biomimetic System of High Complexity. ChemPhysChem 11, 1851-1853 (2010).

[2] Calcite-(Glyco?)Protein

- Y.-X. Huang, J. Buder, R. Cardoso-Gil, Yu. Prots, W. Carrillo-Cabrera, P. Simon, R. Kniep: Shape Development and Structure of a Complex (Otoconia-Like?) Calcite-Gelatine Composite. Angew. Chem. Int. Ed. 120, 8404-8408 (2008).

- P. Simon, W. Carrillo-Cabrera, Y.-X. Huang, J. Buder, H. Borrmann, R. Cardoso-Gil, E. Rosseeva, Yu. Yarin, Th. Zahnert, R. Kniep: Structural relations between biomimetic and human calcite statoliths (otoconia) Eur. J. Inorg. Chem. 5370-5377 (2011).

P07

Tetrahedrally coordinated compound semiconductors for photovoltaic applications

S. Schorr[1]
[1]*Helmholtz-Zentrum Berlin für Materialien und Energie, Kristallographie, Berlin, Germany*

The current market dominating photovoltaic devices and modules made from crystalline silicon are 1st generation solar cells. Employing the thin film technology resulted in a significant cost reduction, thus thin film solar cells are considered as 2nd generation solar cells. Thin film photovoltaic modules can processed on large areas and alternative substrates like glass, polyimide foils or stainless steel.

Ternary and quaternäry compound semiconductors like $CuInSe_2$ (CISe) $Cu(In,Ga)Se_2$ (CIGSe) and $Cu_2ZnSn(S,Se)_4$ (CZTSSe) are candidates for an absorber material in 2nd generation solar cells due to their direct band gap in the range 1- 1.5 eV and high absorption coefficient ($> 10^4 cm^{-1}$) for solar radiation in the corresponding spectral range. World record device efficiencies reached in the laboratory are 20.3% for CIGSe based [1] and 11% for CZTSSe based solar cells [2].

These compounds belong to the group of materials with tetrahedral coordination, i. e. each atom has four nearest neighbours. Such a group of materials is the adamantine compound family, which is based on diamond and lonsdaleite, respectively. Comparing with other semiconductors, for instance Pyrite (FeS_2) or transition metal chalcogenides (photovoltaic devices with these compounds as absorber layer have shown only low efficiency values), the tetrahedral bonding structure in the adamantine compounds is advantageous in controlling the semiconducing properties of the material.

The chalcopyrite type compound CIGSe is extremely tolerant to defects that naturally arise for large deviations from stoichiometry as present in the highest-efficiency devices. These deviations, especially Cu/(In+Ga)Cu+In_{Cu}. For the kesterite type compound CZTSSe the homogeneity region is much smaller, i. e. the deviations from stoichiometry are small and secondary phases occur.

In order to understand the correlation between growth conditions, material properties and final device quality much has to be understood regarding the basic material properties of the absorber material, for instance the occupation density of the different sites within the crystal structure, i.e. defect formation at certain material compositions. Among various experimental possibilities structural analysis of compound semiconductors by diffraction techniques using X-rays or neutrons has come a key technique of choice. Especially neutron diffraction can provide valuable results, because it allows the differentiation electronical similar elements.

The presentation will give an overview of our structural studies [3-7] of off stoichiometric chalcopyrite type and kesterite type compound semiconductors and will demonstrate the advantages of neutron diffraction.

[1] P. Jackson, et al., Progr. Photovolt.: Res. Appl. **19** (7), 894-897 (2011).
[2] D. Aaron et al., Progr. Photovolt.: Res. Appl. **20** (2012) 6-11.
[3] S. Schorr, Thin Solid Films **515** (15) (2007) 5985-5991.
[4] S. Schorr et al., Europ. Jour. Mineral. **19** (2007)65 - 73.
[5] S. Schorr, Sol. En. Mat. Sol. Cells, **95** (2011) 1482-1488.
[6] C. Stephan et al., Appl Phys Lett **98** (2011) 091906 (091901) - 091906 (091903).
[7] C. Stephan, et al., Appl Phys Lett **101** (2012) 101907(101901)-101907(101904).

MS01 - Non-ambient Conditions: Pressure, Temperature and Fields at Work I

MS01-T01

Neutrondiffraction at the Swiss Neutron Spallation Source SINQ

M. Frontzek[1], D. Cheptiakov [1], O. Zaharko[1], S. Van Petegem[1], J. Gavilano[1]
[1]Paul Scherrer Institut, Laboratory for Neutron Scattering, Villigen-PSI, Switzerland

In our contribution we want to present an overview how neutronscattering at the Paul Scherrer Institute (PSI) is used to answer crystallographic questions beyond the scope of x-rays. The PSI is home of the Swiss Spallation Neutron Source (SINQ) and several instruments dedicated to diffraction have beamports. The ***Q***-range suitable for investigations of hard condensed matter is covered by two powder- (DMC, cold neutrons and HRPT, thermal neutrons) and the thermal 4-circle diffractometer TriCS. Additionally, the time-of-flight diffractometer POLDI is dedicated to strain-stress ananlysis. In the lower ***Q***-range required for protein diffractometry two Small Angle Instruments (SANS-I,II) are available.

Additionally, we will adress the complementarity of x-ray and neutron scattering which is reflected by the special possibility to submit a joint proposal for neutron at SINQ and synchrotron experiments at the Swiss Light Source, PSI.

The strenght of neutron scattering lies in the availability of extreme sample environments from mk to 2000 K range in temperature, high pressure to 100 kBar and applied electric and magnetic fields. Furthermore neutrons often offer high diffraction contrast between neighboured elements in the periodic table and high cross-section for light elements. We will emphasize the strengths of neutron diffraction with recent experimental results from different instruments as for instance the in-situ annealing of Ho_2PdSi_3 on the cold neutron powder diffractometer DMC shown in Fig. 1. Here, additional reflections due to Pd/Si order on the B-sites of the AlB_2-structure emerge over time. In this case the in-situ neutron scattering experiment allowed identifying suitable temperature ranges for compound synthesis with Pd/Si order.

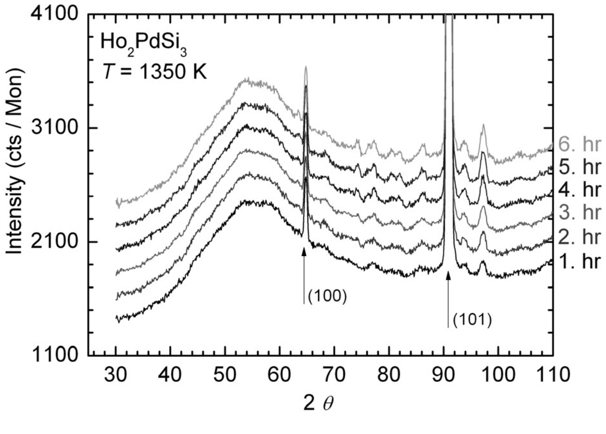

Caption Fig. 1: In-situ annealing of Ho_2PdSi_3 powder sealed in a quartz-tube, measured on DMC, SINQ. In the timespan of 6 hrs additional superstructure reflections emerge in the angular range around 80°. The broad peak around 55° originates from the quartz tube. The reflections from the primitive hexagonal structure are marked.

MS01-T02

X-ray diffraction investigations under non ambient conditions at the Rossendorf Beamline ROBL

C. Baehtz[1], J. Grenzer[1], O. Roshchupkina[1], P. Kidambi[2], B. Bayer[2], S. Hofmann[2], R. Weatherup[2]
[1]Helmholtz-Zentrum Dresden-Rossendorf, Institute of Ion Beam Physics and Materials Research, Dresden, Germany
[2]University of Cambridge, Dept. of Engineering, Cambridge, United Kingdom

The Rossendorf Beamline ROBL at the ESRF is operated since 1998 by the Institute of Resource Ecology and Ion Beam Physics and Materials Research of the HZDR. In 2011-2012 the optics of the beamline such as mirrors, double crystal monochromator and diagnostic was modernized to meet future experimental demands. The Materials Research Station is focusing on in-situ investigations. These are in thin film synthesis by magnetron sputtering, in-operando measurements on lithium ion batteries, materials modification by ion implantation and high temperature investigations using reactive atmosphere like in chemical vapor deposition (CVD) processes.

Iron nano-crystals are a common catalyst in the CVD growth reaction of carbon nano tubes [1,2]. These crystals were formed by dewetting of the corresponding iron thin film at raised temperatures. Under reaction condition different iron phases such as Fe3C, alpha-Fe and gamma-Fe were detected. Their concentrations are strongly varying before, after and during the CVD process. This leads to the conclusion that besides Fe3C also metallic iron is catalytically active [1].

In graphene CVD nickel and copper are commonly used as catalyst. High resolution diffraction data were collected at reaction temperature. The lattice parameter was calculated using Lebail fit, corrected due to small shifts in sample surface temperature by the thermal expansion determined before. The results show a lattice expansion of nickel under different CVD atmospheres, indicating an uptake of hydrogen and carbon on interstitials in the metallic Ni. The carbon uptake is only partially reversible, but additional hydrogen can be assimilated [3,4].

[1] B.C. Bayer, Chem. Mater., doi: 10.1021/cm301402g

[2] B. C. Bayer, J. Phys. Chem. C, 2011, 115, 4359

[3] R. S. WeatherupNano Lett., 2011, 11 4154

[4] R. S. Weatherup et al,ChemPhysChem, 2012 , 13, 2544

MS01-T03

Diamond anvils with a spherical support designed for X-ray and neutron diffraction experiments in DAC

N. Dubrovinskaia[1], L. Dubrovinsky[1], M. Hanfland[2], M. Hofmann[3]
[1]*Universität Bayreuth, Bayreuth, Germany*
[2]*ESRF, Grenoble, France*
[3]*FM II, Garching, Germany*

Here we present new diamond anvils with a spherical support designed for applications in diamond anvil cell technique. The main feature of the anvils is the diamond crown of a spherical shape. The assembly of the spherical diamond fixed within a spherical support of a seat made of WC or hard metals provides enhanced stability, simple alignment, and large optical and X-ray aperture that makes it very useful for broad applications in diamond anvil cell technique, particularly for single crystal X-ray and powder neutron diffraction. The anvils were tested in various experiments conducted in a wide pressure-temperature range and showed a very good performance.

MS01-T04

Oxygen diffusivity in silicon derived from dynamical X-ray diffraction

J. Will[1], A. Gröschel[1], C. Bergmann[1], A. Magerl[1]
[1]*FAU Erlangen-Nürnberg, Lehrstuhl für Kristallographie und Strukturphysik, Erlangen, Germany*

Thickness dependent Pendellösung oscillations [1] are highly sensitive to strain fields from defects in a host crystal [2-4]. Based on this, we present a novel technique to determine the precipitation kinetics of oxygen in silicon at early stages of clustering at high temperatures.

The measurements were performed using the characteristic $K_{\alpha 1}$-line of a high voltage tungsten X-ray tube at 59.31 keV, which allows recording the SiO_x precipitation process in silicon in-situ through complex sample environments at high temperatures.

The measured static Debye-Waller factors [5-8] are evaluated as a function of time within a diffusion limited model of a growing spherical precipitates [9-10].

We investigated two moderately boron doped Czochralski silicon crystalls. One in the range of normal diffusivity [11] at 900°C to compare our technique with established methods. The second measurement was performed in the low temperature range at 650°C, where a wide spread of experimental data exists [12]. The final size, density and morphology of the precipitates were determined by STEM and EDX.

At 900°C, precipitates with a radius smaller than 4 nm and with a density of 10^{13} 1/cm³ were observed. The determined diffusion constant of (**see Fig. 1**) is close to the literature value of [11].

The determined diffusion constant at 650°C of is slightly enhanced compared to the extrapolated value for normal diffusion of [11]. However, it is close to the value from dislocation unlocking experiments () [12], and one order of magnitude lower compared to SIMS measurements [13].

[1] A. Authier, Dynamical Theory of X-Ray Diffraction, Oxford University Press, Oxford, 2001.
[2] J. Will, A. Gröschl, M. Weißer, A. Magerl, Appl. Phys. Lett., Vol. 98 (2011), 041910.
[3] J. Will, A. Gröschel, C. Bergmann, A. Magerl Phys. Status Solidi C, Vols. 10-11 (2012), 1920.
[4] J. R. Schneider, R. Bouchard, H. A. Graf, H. Nagasawa, Acta Cryst. A48 (1992), 471.
[5] N. Kato, Acta Cryst., A36 (1980) 763-769.
[6] N. Kato, Acta Cryst.,. A36 (1980) 770-778.
[7] M. Al Haddad, P. J. Becker, Acta Cryst., A48 (1992) 121-134.
[8] P. H. Dederichs, J. Phys. F, 3 (1973) 471-496.
[9] S. Iida, H. Sugiyama, Y. Sugita, H. Kawata, Japanese J. Appl. Physics, 27 (1988) 1081-1087.
[10] F. S. Ham J. Phys. Chem. Solids, Vol. 6 (1958), 335.
[11] J. C. Mikkelsen Jr.: Mater. Res. Soc. Symp. Proc. Vol. 59 (1986), 19.
[12] S. Senkader, P. R. Wilshaw, R. J. Falster: J. Appl. Phys. Vol. 89 (2001), 4803.
[13] S.-T. Lee, P. Fellinger, S. Chen J. Appl. Phys. Vol. 63 (1988), 1924.

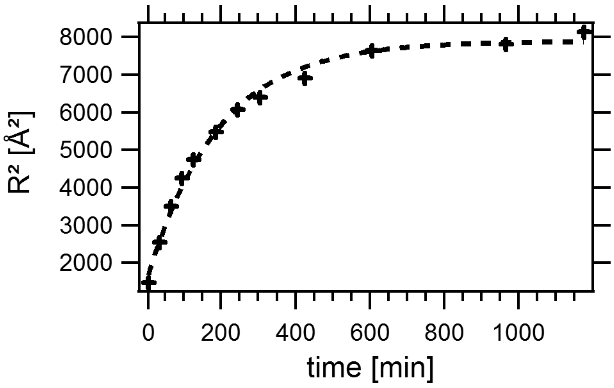

Fig. 1. Fit of the square of the precipitate radius against annealing time at 900°C within Ham's theory of precipitation.

MS01-T05

XRD In-Situ Studies of Crystallization of Different TiO_2 Thin Films

R. Kuzel[1], L. Nichtova[1], A. Kadlecova[1], Z. Matej[1], Z. Hubicka[2], S. Kment[2], J. Bursik[3]
[1]*Charles University in Prague, Faculty of Mathematics and Physics, Department of Condensed Matter Physics, Prague, Czech Republic*
[2]*Institute of Physics, Academy of Sciences of the Czech Republic, Prague, Czech Republic*
[3]*Institute of Inorganic Chemistry, Academy of Sciences of the Czech Republic, Prague, Czech Republic*

Crystallization of different amorphous TiO_2 thin films deposited on Si substrates was investigated by in-situ high-temperature X-ray diffraction (XRD). The films prepared by different methods were compared - deposited by dual magnetron, by the pulsed double hollow Ti cathodes plasma jet sputtering and by the sol-gel method. The time evolution of crystallization expressed in terms of integrated intensity of diffraction peaks (anatase phase was observed only) could be always well described by the modified Avrami equation. Stress analysis at room temperature revealed the presence of tensile stresses after the crystallization confirmed by the observation of diffraction peak shifts with annealing time. The stresses increased rapidly with decreasing film thickness and inhibit further crystallization that was consequently also dependent on film thickness [1]. However, the plasma jet sputtered films, less dense as indicated by the reflectivity, showed low tensile stresses and the dependence of crystallization on film thickness was not so pronounced, either. Differences were found in texture evolution. In more dense films, at the beginning of crystallization the orientations of {101} were supressed but at the end of process XRD indicated nearly random grain orientations. In the films of low density, {101} preferred orientation was found and did not change much during crystallization. All these films crystallized at relatively low temperatures by a fast forming of relatively large crystallites (very small XRD profile broadening already from the beginning of crystallization). More compact films crystallize at lower temperature starting below 200 °C while sparse films only at about 250 °C. Annealing of sol-gel films showed very different results. Crystallization started by forming small crystallites and at higher temperatures. Unlike the other films, some adjustment of crystallite size is possible by setting up the temperature and time of annealing.

1. Z. Matěj, R. Kužel and L. Nichtová, *Metallurgical and Materials Transactions* **A42** (2011) 3323-3332.

MS01-T06

Diffusion constants from time-resolved powder diffraction data analysed with a shrinking-core model.

A. Falenty[1], M. Jansen[1], A. N. Salamatin[1], W. F. Kuhs[1]
[1]*Universität Göttingen, GZG Abt. Kristallographie, Göttingen, Germany*

Multiphase reactions of solid materials often proceed from the surface into the interior and can be described in a shrinking-core modeling *ansatz*. If phase transitions are involved such reactions can conveniently be followed by in-situ diffraction methods, given that the reaction can be followed within the time-resolution of the data collection. The analysis then proceeds *via* Rietveld refinement in a batch processing of the time-dependent data-sets. The shrinking-core model of the formation of gas hydrates from ice spheres with well-defined geometry gives experimental access to the gas permeation in bulk hydrates (1,2,3). Here we report on results obtained for CO_2 clathration experiments in the temperature range from 185 to 272 K extending earlier work to much lower temperature conditions (4). Neutron diffraction was used as it allows easily for the operation gas pressure cells in the beam. The reactions were followed for up to 3 days. For longer reaction times laboratory-based pressure-volume-temperature set-ups were used to follow the reactions (by recording the gas consumption) and were combined with a diffractometric determination of the phase fraction at the end of the reaction. The activation energy deduced from the permeation coefficients changes its value from ~ 46 kJ/mol at higher temperatures to ~ 19 kJ/mol below 225 K. We compare our results with published molecular dynamics simulation as well as nuclear magnetic resonance studies and provide arguments that the rate limiting process at lower temperatures is the cage-to-cage jumping of CO_2 molecules *via* a “hole-in-the-cage” mechanism involving extrinsic water vacancies in cage walls. The rate-limiting process at higher temperatures can be explained by the temperature-dependent creation of intrinsic water-vacancy-interstitial pairs. The results obtained for CO_2-hydrate are compared to earlier results for CH_4-hydrate formation, including a detailed discussion of the slight structural differences of both phases. The permeation of CO_2 molecules through bulk hydrate is found to be an order-of-magnitude faster when compared to the CH_4 case. This explains the faster clathration reaction of CO_2-hydrate in comparison to CH_4-hydrate.

1. DK Staykova, WF Kuhs, AN Salamatin and T Hansen (2003) *J Phys. Chem. B*, *107*:10299-10311.

2. WF Kuhs, DK Staykova, and AN Salamatin (2006), *J Phys. Chem. B*, *110* :13283-13295.

3. A Falenty, DY Genov, TC Hansen, WF Kuhs, and AN Salamatin (2011) *J Phys. Chem. C*, *115*: 4022-4032.

4. A Falenty, AN Salamatin, and WF Kuhs, submitted to *J.Phys.Chem. B*

MS02 - General Crystallography: Modelling and Analysis Bridging the Scales I

MS02-T01

Struktur und Dynamik von Einzelmolekülen eingebettet in Nanoporen

T. Woike[1]
[1]*TU-Dresden, Inst. für Strukturphysik, Dresden, Germany*

Die Bestimmung der Atomabstände in Einzelmolekülen kann prinzipiell mittels der Debye-Analyse oder der Paarverteilungsfunktion erfolgen. Jedoch müssen zur Messung der gebeugten Röntgen-Photonen oder Neutronen hinreichend viele Moleküle vorhanden sein. Dies wird erreicht, indem man diese Moleküle in Nanoporen einbettet. Dabei muss jedoch sichergestellt sein, dass wirklich je Pore nur ein Molekül vorhanden ist und dass diese keine Kopplung mit den Wänden eingehen, da sonst ihre Struktur geändert werden kann.

Wir zeigen, dass Komplexe aus $Na_2[Fe(CN)_5NO]$ als Einzelmoleküle in Nanoporen aus SiO_2-Xerogelen eingebaut werden können und dass diese Komplexe in den Poren frei rotieren. Als Nachweismethode verwenden wir die Röntgen- und Neutronenstreuung sowie die ^{29}Si, ^{13}C und ^{23}Na NMR . Die Auswertung der Streuspektren erfolgt mittels Debye-Analyse und Paar-Verteilungsfunktion. Damit kann eindeutig zwischen Monomeren, Dimeren oder Trimeren in den Poren unterschieden werden und es können alle Atomabstände bestimmt werden. Mittels ^{13}C und ^{23}Na NMR wird die isotrope Rotation der Monomere auf der µs-Zeitskala nachgewiesen.

Dieses Verfahren kann auf eine Vielzahl weiterer Komplexe zur Bestimmung ihrer Struktur angewandt werden.

A. Cervellino et al., J. Appl. Cryst. **43**, 1040-1045 (2010)

MS02-T02

Nucleation of ZnO Nanoparticles: Structural Changes of Precursor and Nuclei

M. Zobel[1], R. B. Neder[1]
[1]*University Erlangen, Institute of Crystallography and Structural Physics, Erlangen, Germany*

Monodisperse zinc oxide nanoparticles are produced in a sol-gel process based on the dissolution of zinc acetate dihydrate in ethanol, which results in the formation of a precursor [1-3]. Upon addition of the alkaline tetramethylammonium hydroxide (TMAH), ZnO nanoparticles start to nucleate. However, the nucleation kinetics as well as the stability and structure of the precursor solution have not been resolved yet. It had been shown with EXAFS that the initial precursor solution of the metal salt consists of a tetrahedral precursor of the form Zn4O coordinated with six acetate molecules [4]. Though it is commonly accepted that the addition of TMAH initiates the transformation into ZnO nuclei, the structural changes within the solution induced by TMAH are unknown.
Using high-energy synchrotron radiation, it is possible to study this nucleation process in-situ via x-ray wide angle diffraction, even in salt solutions with very low concentration (30 mM). Fig. 1 shows background corrected scattering curves collected during the nucleation of ZnO from a zinc acetate solution. The reaction was observed for a total of 9 hours, and the time difference between two successive curves is 5 min. The turquoise filling represents the structure of the precursor solution prior to adding TMAH, yellow filling the structure afterwards. Obviously, the TMAH addition results in a spontaneous change of the precursor structure prior to the nucleation of nanoparticles. In order to tune the nanoparticle size, organic ligands are added to the precursor solution. Therefore, the experiment was repeated in the presence of the ligand dimethyl-L-tartrate (DMLT). Fig. 2 shows the nucleation process for a total time of 11 hours, again with 5 min intervals between two curves. Under these conditions, TMAH changes the precursor structure much more dramatically than without an additional ligand. Moreover, by comparing Fig. 1 and Fig. 2, distinct differences between the precursor structure in presence and absence of an additional ligand are obvious. These differences have not been observed before.

Consequently, we can state for the first time that in-situ high-energy x-ray wide angle diffraction experiments with synchrotron radiation are possible and that furthermore, detailed insight into structural changes during chemical reactions can be gained. By deducing the pair distribution function, the detailed structure of the different phases can be assessed.

[1] L. Spanhel and M. A. Anderson, J. Am. Chem. Soc. 113 (1991), 2826
[2] N. S. Pesika, Z. Hu, K.J. Stebe, P. C. Searson, J. Phys. Chem. B 106 (2002), 6985
[3] Ch. Chory, R. B. Neder, V. I. Korsunskiy, et al., phys. stat. sol. c 4 (2007), 3260
[4] M. S. Tokumoto, S. H. Pulcinelli, C. V. Santilli, V. Briois, J. Phys. Chem. B 107 (2003), 568

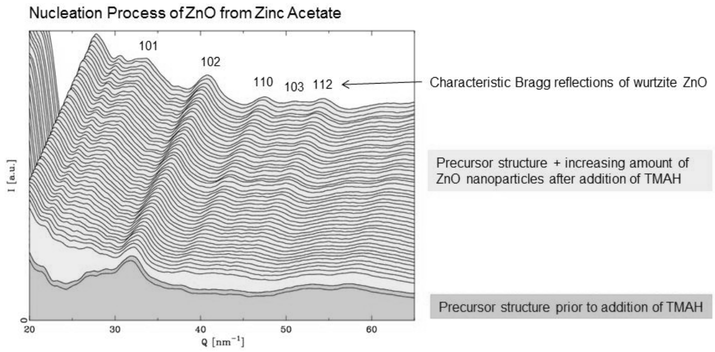

Fig. 1: Nucleation Process of ZnO from Zinc Acetate

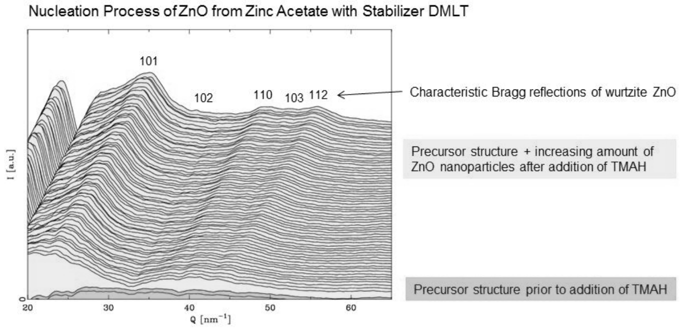

Fig. 2: Nucleation Process of ZnO from Zinc Acetate with Stabilizer DMLT

MS02-T03

Experimental evidence of orbital order for icosahedral B_{12} cluster in boron-rich solids

S. Mondal[1], S. van Smaalen[1], N. Dubrovinskaia[1], L. Dubrovinsky[2]
[1]*University of Bayreuth, Laboratory of Crystallography, Bayreuth, Germany*
[2]*University of Bayreuth, Bayerisches Geoinstitut, Bayreuth, Germany*

Many boron-rich solids including boron polymorphs show unusual properties like, super hardness and low compressibility [1]. All boron-rich solids that posses such properties contain icosahedral B_{12} clusters as structural building blocks. Explanations of unusual properties of such solids thus require the understanding of bonding mechanism of these clusters. Knowledge of electron density distribution in boron-rich solids will provide insight into the nature of chemical bonding between B_{12} clusters and between the B_{12} cluster and other atoms. On the basis of experimental electron-density studies of rhombohedral α boron [2] and orthorhombic γ boron [3], we have found evidence for orbital order in the icosahedral B_{12} cluster. Electron-density studies were performed using the computer program XD2006 [4] against low-temperature single-crystal X-ray diffraction data. Final multipole models yield excellent fits to the data for both polymorphs (For α boron: R_F(obs) = 0.0117; For γ boron: R_F(obs) = 0.0120). Electron densities were analyzed using the Quantum Theory of Atoms in Molecules [5]. These studies reveal strongly directional spatial distribution of electron density at the corners of the B_{12} cluster pointing outward perpendicularly to the surface of the cluster. This exo-cluster orbital order is persistent in both α and γ boron, irrespective of the fact that they participate in completely different kinds of inter-cluster bonds. Geometric calculation on other boron-rich compounds also indicate the same orbital order, suggesting an unifying bonding mechanism in these solids due to the persistent orbital order in the icosahedral B_{12} cluster.

References

[1] B. Albert, H. Hillebrecht, Angew. Chem. Int. Ed. **48**, 8640-8668, (2009).

[2] S. Mondal, S. Van Smaalen, G. Parakhonskiy1, S. J. Prathapa, E. Bykova, N. Dubrovinskaia, D. Chernyshov, L. Dubrovinsky, unpublished, (2012).

[3] S. Mondal, S. Van Smaalen, A. Schönleber, Y. Filinchuk, D. Chernyshov, S. I. Simak, A. S. Mikhaylushkin, I. A. Abrikosov, E. Zarechnaya, L. Dubrovinsky, N. Dubrovinskaia, Phys. Rev Lett. **106**, 215502, (2011).

[4] A. Volkov, P. Macchi, L. J. Farrugia, C. Gatti, P. R. Mallinson, T. Richter, T. Koritsanszky, XD2006, *A Computer Program Package for Multipole Refinement, Topological Analysis of Charge Densities and Evaluation of Intermolecular Energies from Experimental or Theoretical Structure Factors*, (2000).

[5] R. F. W. Bader, Atoms in Molecules, Oxford University Press, (1990).

MS03 - Aperiodic and Modulated Structures: Potential in Higher Dimensions

MS03-T01

The modulated structure of 1-Adamantanammonium 4-fluorobenzoate

A. Schönleber[1], S. van Smaalen[1], H.- C. Weiss[2], A. J. Kesel[3]
[1] *University of Bayreuth, Laboratory of Crystallography, Bayreuth, Germany*
[2] *Currenta GmbH & Co. OHG, Leverkusen, Germany*
[3] *Chammünsterstr. 47, 81827 München, Germany*

1-Adamantanammonium 4-fluorobenzoate, $N_{10}H_{18}N^+ \cdot C_7H_4FO_2^-$ exhibits at low temperature an incommensurately modulated structure. 1-Adamantanammonium (tricyclo[3.3.1.1^{3,7}]decan-1-amine, is a tricyclic amine with diamondoid structure. In this organic salt the cations and the anions are linked by N-H···O hydrogen bonds [1].

We have performed in-house single crystal X-ray diffraction with an Agilent Xcalibur diffractometer, equipped with a CCD detector, at T = 97 K. A first inspection of the data has shown, that the main reflections are regularly surrounded by satellite reflections up to second order. All observed peaks can be indexed within monoclinic symmetry with a = 10.8499(1) Å, b = 6.5245(1) Å, c = 21.3829(1) Å, β = 98.27(1)° and the **q**-vector components σ_1 = 0.4237(5) and σ_3 = 0.4284(7). The (3+1)-dimensional superspace group is $P\ 2_1/n\ (\sigma_1 0 \sigma_3)\ 00$.

To describe the modulated structure, for the atomic modulation functions (AMFs) harmonic waves up to second order are applied for the displacive modulation and also for the modulation of the anisotropic atomic displacement parameters (ADPs). The H-bond motif forms endless ribbons along crystallographic **b**-axis, with the anions oriented parallel to the plane (-2,0,3) and the cations to the plane (1,0,3).

[1] A. J. Kesel, H.-C. Weiss, A. Schönleber, C. W. Day, D. L. Barnard, M. A. Detorio, R.F. Schinazi: Antiviral agents derived from novel 1-adamantyl singlet nitrenes, *Antiviral Chemistry & Chemotherapy* (2013) accepted for publication.

MS03-T02

The theory of proper ferroelectrics with an incommensurate phase in complex compounds with structural defects

B. Gadjiev[1]
[1] *International University for Nature, Science and Man, SAM, Dubna, Russian Federation*

Generalization of the theory of phase transitions shows that the phase diagrams of complex crystals with structural defects exhibit a number of peculiarities [1, 2].

In the present paper we analyze the influence of defects on physical properties of the layered semiconductor compounds in the region of a sequence of phase transitions paraelectric - incommensurate - commensurate phase. Using the obtained theoretical results, we describe a number of physical properties that discovered in layered ferroelectric semiconductors with structural defects [3].

We proceed from the fact that deviations from the ideal crystal structure induced by structural defects, creates a new critical regime with new universal critical exponents.

We derive a fractional generalization of the equation of motion for the major order parameter for the proper ferroelectrics in an incommensurate phase in the absence of the *Lifshitz* invariant and obtain a nonlinear dispersion law.

We solve the fractional equation of motion for the order parameter and determine the spatial distribution of the order parameter in the incommensurate phase. Special attention is given to the analysis smearing of the soliton lattice and loss the inversion element of superspace group symmetry of incommensurate phase.

From the solution of the fractional kinetic equation, we define the frequency dependence of the imaginary part of the dielectric susceptibility in the paraelectric phase has a number of local maxima the position of which depends on temperature. It means that a phase transition from a paraelectric phase to an incommensurate phase is accompanied not only by a soft mode but also by the modes with the square of frequencies having a nonlinear dependence on temperature.

By using a renormalization group method we describe a phase transition from paraelectrical to an incommensurate phase and obtain a dependence of critical indexes on the measure complexity of the system.

References

1. Leo P. Kadanoff, Theories of Matter: Infinities and Renormalization, arXiv:1002.2985v1 [physics.hist-ph] (2010).

2. B.R. Gadjiev, On the theory of phase transition in muliferroics, J. Phys. 200 (1) 012044 (2010).

3. A. M. Panich, S. Kashida, Single-crystal NMR for the layered semiconductor TlGaSe2, J. Phys.: Condens. Matter 20 395211 (2008).

MS03-T03

The crystal structure of modulated 2:1 mullite ($Al_{4.8}Si_{1.2}O_{9.6}$) revisited

J. Birkenstock[1], V. Petříček[2], B. Pedersen[3], H. Schneider[1,4], R. X. Fischer[1]
[1]*Universität Bremen, Fachbereich Geowissenschaften/ Kristallographie, Bremen, Germany*
[2]*Academy of Science, Inst. of Physics, Dept. of Structure Analysis, Praha, Czech Republic*
[3]*TU München, Forschungsneutronenquelle Heinz Maier-Leibniz (FRM II), Garching, Germany*
[4]*Universität Köln, Institut für Kristallographie, Köln, Germany*

The structural short range order of mullite, especially the distribution of oxygen vacancies, has been discussed controversially for many years. In a first step to a more detailed understanding Czochralski-grown single crystals of mullite (by S. Uecker, IKZ, Berlin-Adlershof, Germany, after Guse & Mateika, 1974) were examined to revisit its modulated crystal structure. X-ray diffraction data were collected for a 0.15x0.26x0.31 mm^3 crystal on a Bruker diffractometer (APEX II area detector, Mo-Kα) and neutron diffraction data for a ~4x4x4 mm^3 crystal at FRM II (RESI with MAR345 detector).

For the X-ray data the refined lattice parameters were a=7.5911(2) Å, b=7.6923(2) Å, c=2.8899(1) Å (space group *P b a m*) and the q-vector was $\mathbf{q}$ = (0.3137(3) 0 ½), respectively, considering 13584 reflections with JANA 2006 (Petříček et al., 2006). The lattice parameters compare well to those of Fischer et al. (1994) for a 2:1 mullite, while the q-vector is somewhat larger (q_1 = 0.3137 compared to 0.30 there) than that of Angel & Prewitt (1987). Two further q-vectors, $\mathbf{q_2}$ = (0 0.4021(5) 0.1834(2)) and $\mathbf{q_3}$ = (0 0.5991(5) 0.1840(2)) were found - not reported hitherto.

The average and the 1d-modulated structures were refined with JANA 2006. Due to the similar scattering power of Si^{4+}, Al^{3+} and O^{2-} in the X-ray case (10 electrons each) the occupancies of T = (Al2,Si2), T* = (Al3,Si3), O3 and O4 atoms were constrained to preserve electrostatic neutrality, yielding a final R_{obs}(main) = 2.14 %. The refinement of the occupancy SOF of O4, accounting for a possible chemical variation in the mullite series (see, e.g., Fischer & Schneider, 2005), resulted in a composition of $Al_{4.803(8)}Si_{1.197(8)}O_{9.598(14)}$, i.e., exactly 2:1 mullite within one sigma. The refinement of SOF(Si3), accounting for the distribution of Si and Al over T and T*, resulted in an Al/Si ratio of ~2/1 on site T*, yet with no improvement of R_{obs}.

The tedious refinement of the 1d-modulated structure - with frequent false minima and R_{obs}(satellites) of 20 to 40 % - was restricted to harmonic waves of first order as only first order satellites were observed. The predominant factor in the final solution (R_{obs}(sat) = 10.9%) was the modulation of the occupancies of O3 and O4 which turned out to be coupled in an anti-phase manner, i.e., that of O3 is low where that of O4 is high and vice versa. Further results are expected from the ongoing investigation of neutron data and the 3d-modulated structure.

We gratefully acknowledge the DFG for grant FI 442/17-1 and Holger Ott, Bruker Co., for the high quality X-ray diffraction data.

Angel, R. J. & Prewitt, C. T. (1987). Acta Cryst. B43, 116-126.

Fischer, R.X. & Schneider, H. in: Mullite (Schneider, H. & Komarneni, S., eds.) Wiley-VCH Verlag (2005) 1-46, 128-141.

Guse, W. & Mateika, D. (1974). J. Crystal Growth 22, 237-240.

Petříček, V., Dušek, M. & Palatinus, L. (2006). Jana2006. The crystallographic computing system. Inst. of Physics, Praha, Czech Republic.

MS04 - Crystallography in Materials Science: Real Structures I

MS04-T01

Stacking fault energy obtained from in-situ X-ray diffraction experiments under bending

D. Rafaja[1], S. Martin[1], P. Gallardo Martinez[1]
[1]*TU Bergakademie Freiberg, Materials Science, Freiberg, Germany*

The stacking fault energy is a very important quantity, as it significantly controls the behaviour of dislocations during plastic deformation of metallic materials. Although the first experimental methods for determining the stacking fault energy were developed in early 1950's, there is still a need to establish a technique, which would be concurrently reliable and easy to use, because the majority of the experimental methods that are currently applied to determine the stacking fault energy are either laborious or indirect [1]. Consequently, the differences in the stacking fault energy revealed by different techniques may be large. For face-centred cubic (fcc) materials in particular, the experimentally determined stacking fault energies differ frequently by factor 2 or more [2]. As based on the classical Peach-Koehler theory [3], Byun [4] quantified the effect of the applied stress on the separation distance between two partial dislocations terminating a stacking fault. He showed that when the energy induced by the applied stress exceeds the stacking fault energy, a rapid growth of the stacking faults is observed, which impedes a further accumulation of the internal stress.

In a recent paper [5], we have shown on the example of austenitic steels that X-ray diffraction (XRD) is capable of judging the width of the stacking faults in fcc materials. The width of the stacking faults (i.e. the separation of the partial dislocations) was classified by means of the crystallographic anisotropy of the lattice deformation. For wide and rapidly growing stacking faults which compensate a further rise of the internal stress during a continuous deformation of the material, the anisotropy of the lattice deformation was found to comply with the orientation factors obtained from the classical Warren theory [6]. On the contrary, both short stacking faults and stacking faults interfering with other microstructure defects produce local strain fields with a different symmetry. This can be recognised as a change in the dependence of the interplanar spacing on the crystallographic direction. In this contribution, the in-situ XRD during a quasi-continuous deformation experiment will be shown to be able to reveal the magnitude of the internal stress, which is needed to balance the stacking fault energy and which can be used to calculate the stacking fault energy quite reliably. Exemplarily, the stacking fault energies in austenitic steels showing the transformation induced plasticity (TRIP) effect will be presented.

References:
[1] M.F. de Campos, Mat. Sci. Forum 591-593 (2008) 708.
[2] R.P. Reed, R.E. Schramm, J. Appl. Phys. 45 (11) (1974) 4705.
[3] M.O. Peach, J.S. Koehler, Phys. Rev. 80 (1950) 436.
[4] T.S. Byun, Acta Mater. 51 (2003) 3063.
[5] D. Rafaja, C. Krbetschek, D. Borisova, G. Schreiber, V. Klemm, Thin Solid Films (2012), in press, DOI: 10.1016/j.tsf.2012.07.067.
[6] B.E. Warren, X-Ray Diffraction, Dover Inc., New York, 1969.

MS04-T02
Electric field stabilized polar phase in strontium titanate single crystals at room temperature

J. Hanzig[1], M. Zschornak[1,2], B. Abendroth[1], F. Hanzig[1,3], E. Mehner[1], H. Stöcker[1], C. Röder[4], A. Talkenberger[4], G. Schreiber[3], D. Rafaja[3], S. Gemming[2], D. C. Meyer[1]
[1]TU Bergakademie Freiberg, Institut für Experimentelle Physik, Freiberg, Germany
[2]HZ Dresden-Rossendorf, Institut für Ionenstrahlphysik und Materialforschung, Dresden, Germany
[3]TU Bergakademie Freiberg, Institut für Werkstoffwissenschaft, Freiberg, Germany
[4]TU Bergakademie Freiberg, Institut für Theoretische Physik, Freiberg, Germany

Stoichiometric perovskite-type strontium titanate acts as an insulator because of its wide electronic band gap and has therefore great potential as high-k dielectric and storage material in memory applications. Degradation phenomena of insulating properties of transition metal oxides occur during long time voltage application. From the defect chemistry point of view the question arises how mobile species react on an external electric field and which impact redistribution of mobile species has on the stability of the crystal structure. In $SrTiO_3$ oxygen vacancies are well-known charged defects to migrate during electroformation and to establish a concentration gradient through the bulk. Here, we discuss the local and reversible structural changes in $SrTiO_3$ single crystals caused by oxygen vacancy redistribution in an external electric field. We present *in-situ* X-ray diffraction measurements during and after electroformation. Several reflections are monitored and show a tetragonal elongation of the cubic unit cell of strontium titanate. *In-situ* Raman investigations were carried out to verify that the expansion of the unit cell involves a transition from the centro-symmetric to a less symmetric structure. Regarding a whole formation cycle, two different time scales occur: a slow one during the increase of the lattice constant and a fast one at the end. Based on the experimental data we suggest a model containing the formation of a polar strontium titanate unit cell stabilized by the electric field, which is referred to as migration induced field stabilized polar (MFP) phase at room temperature.

MS04-T03
Multi-temperature high-resolution study of diffuse X-ray scattering in $Na_{0.5}Bi_{0.5}TiO_3$

S. Gorfman[1], D. Keeble[2], P. Thomas[2]
[1]University of Siegen, Department of Physics, Siegen, Germany
[2]University of Warwick, Department of Physics, Coventry, United Kingdom

$Na_{0.5}Bi_{0.5}TiO_3$ (NBT) is the perovskite-based ferroelectric that attracts a strong interest as a potential lead-free piezoelectric material. The large variety of structural transformations and intriguing physical properties [1-5] make NBT an interesting system for fundamental crystallography and material science. The number of NBT properties remain unexplained so far. For example piezoelectricity of NBT is irreversibly lost above 420 K, while no aparent changes of an average structure is observed at these temperatures. It is known that real structure of NBT must be characterized by structural disorder, which produces strong and anisotropic L-shaped diffuse X-ray scattering. Neither the exact nature of the disorder nor its role in NBT properties is established.

This work aimed to reinforce the investigation of diffuse X-ray scattering and structural disorder in NBT and clarify if it is realted to the physical properties of NBT (primarily loss of the piezoelectric properties at higher temperature).

Multi-temperature diffuse scattering was collected at the I16 beamline at the Diamond Light Source. We benefited from highest intensity of the beam, high dynamical range of PILATUS detector and targeting of a small region of interest in reciprocal space. The diffuse scattering of an extraordinary high resolution (~ 0.001 in reciprocal space units) was collected around pseudocubic {320} reflection. We took the data in a temperature range between 20 and 620 K, passing the temperature of thermal depoling phase transition from the monoclinic to tetragonal phase [5].

We have found that, similarly to the average structure, the structural disorder can not be accounted for the thermal depoling in NBT. We have however, discovered a few previously unknown features of the topology of the diffuse scattering.

The details of the high-resolution diffuse scattering, possible models of disorder and its temperatire dependence will be discussed in the presentation.

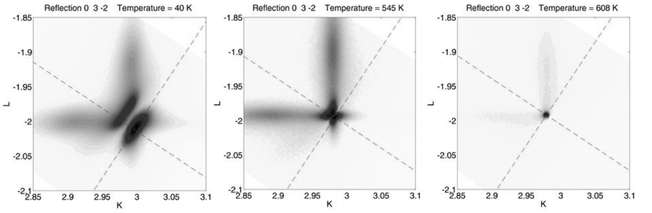

Figure 1. Diffuse scattering around (0 3 -2) pseudocubic Bragg peak collected at 40, 545 and 610 K. Dashed lines indicate two perpendicular directions, one of them pointing to the origin of reciprocal space.

[1] Kreisel, J., Bouvier, P., Dkhil, B., Thomas, P.A, Glazer, M., Wellbery, T.R., Chaabane, B., Mezouar. Phys Rev B68, 014113, (2003)
[2] Jones, G.O., Thomas, P.A. Acta Cryst B68, 168-178, (2002)
[3] Gorfman, S., Thomas, P.A. J. Appl. Cryst. 43, 1409-1414, (2010)
[4] Thomas, P. A., Trujillo, S., Boudard, M., Gorfman, S. and Kreisel, J. Solid State Sciences, 12 (3): 311-317 (2010)
[5] Gorfman, S., Glazer, A.M., Noguchi, Y., Miyayama, M., Luo, H., Thomas, P., J Appl Cryst 45, 444-452, (2012)

MS04-T04

Quantitative phase analysis in partially stabilised zirconia by combined XRD and EBSD characterisation

S. Martin[1], D. Rafaja[1]
[1]*TU Bergakademie Freiberg, Institut für Werkstoffwissenschaft, Freiberg, Germany*

The addition of selected elements into the host structure of ZrO_2 stabilises the tetragonal and cubic phases of zirconia, which are, in their undoped binary form, only stable at high temperatures. From the crystallographic point of view, the increasing amount of the stabiliser causes a continuous transition of the tetragonal zirconia to its cubic modification. In partially stabilised zirconia, local concentration gradients of the stabiliser are present frequently as a consequence of the production process that results in a coexistence of zirconia domains having different degrees of tetragonality. The presence of the local concentration gradients in the analysed samples and the continuous nature of the phase transformation complicate the quantitative phase analysis in partially stabilised zirconia. On the example of zirconia partially stabilised by magnesium, this contribution illustrates the capabilities and limitations of X-ray and electron back-scatter diffraction. In particular, the ability of these experimental methods to reveal the gradual lattice distortion, which is associated with the cubic to tetragonal phase transformation in zirconia and the reliability of the quantitative phase analysis are discussed. In this context, it is shown in which amount the choice of the microstructure model influences the result of the phase analysis.

MS04-T05

Anisotropic 1D domain pattern in $NaNbO_3$ epitaxial thin films grown on (110) $TbScO_3$

M. Schmidbauer[1], A. Duk[1], J. Schwarzkopf[1]
[1]*Leibniz-Institut for Crystal Growth, Berlin, Germany*

$NaNbO_3$ based materials have attracted considerable scientific interest due to their complex phase diagram and promising optical and piezoelectric properties. The formation of domain structures in $NaNbO_3$ single bulk crystal is known for a long time. However, less is known for epitaxial thin films, in particular, the evolution of domain structure with increasing film thickness and the impact of plastic strain relaxation on the domain formation have not been studied yet in detail. In the present work $NaNbO_3$ thin films were grown under anisotropic tensile strain on orthorhombic (110) $TbScO_3$ (TSO) single crystalline substrates with liquid-delivery spin metal organic chemical vapor deposition. Films with thicknesses ranging from 7 nm to 66 nm were deposited at a temperature of 700 °C.

In order to study the domain structure and the local piezoelectric responses of the films piezoresponse force microscopy was performed. Our measurements show that the tensily strained $NaNbO_3$ films appear in the antiferroelectric *aa*-phase. Here the vector of electric antipolarization is parallel to the film plane with no out-of-plane component. 90° stripe domain patterns with domain walls parallel to the $[001]_{TSO}$ direction are observed for all film thicknesses. This domain configuration has been asigned as .. $a_1/a_2/a_1$ .. type for tetragonal films on cubic substrates.

High-resolution x-ray diffraction proves that films with thicknesses below 21 nm are coherently grown on the underlying substrate. They show a highly regular one-dimensional periodic array of 90° domains with coherent domain walls which are aligned along the $[001]_{TSO}$ direction. A 1D to 2D transformation of the 90° domain pattern is observed at a critical thickness of about 21 nm. This transformation is accompanied by a characteristic change in the dependence of lateral domain size from film thickness. At about the same thickness the onset of plastic strain relaxation is observed. Grazing incidence in-plane x-ray diffraction using highly brilliant synchrotron radiation reveals that the pseudocubic $NaNbO_3$ unit cells exhibit an in-plane monoclinic distortion. For the coherently grown thin films the distortion is very small. With larger thicknesses it increases and reaches the bulk value of 0.67° at about 21 nm film thickness.

The observed anisotropic 1D domain formation at small film thickness cannot be reduced to the small elastic strain anisotropy caused by the TSO substrate lattice. Further microscopic mechanisms will be discussed.

MS04-T06

Characterization of dislocations and cracks in freestanding GaN single crystals

I. Ratschinski[1], H. S. Leipner[1], F. Heyroth[1], W. Fränzel[2], G. Leibiger[3], F. Habel[3]
[1]*Martin-Luther-Universität Halle-Wittenberg, Interdisziplinäres Zentrum für Materialwissenschaften, Halle, Germany*
[2]*Martin-Luther-Universität Halle-Wittenberg, Institut für Physik, Halle, Germany*
[3]*Freiberger Compound Materials GmbH, Freiberg, Germany*

The (0001) surface of freestanding GaN single crystals having a thickness of more than 3 mm and a density of in-grown dislocations about 10^6 cm^{-2} has been deformed at room temperature using a Vickers indenter. Dislocations and cracks at the indentations were investigated by optical microscopy, transmission electron microscopy and scanning electron microscopy in secondary electron contrast and by cathodoluminescence (CL). The dislocation arrangement conforms to the symmetry of the indented surface, whereas the crack formation depends on the orientation of the indenter. In addition, the propagation of dislocations in the strain field of indentations was analyzed by heating and subsequent CL imaging at temperature levels from 200 °C up to 1000 °C. The results of the investigations of GaN crystals are compared to measurements at indentation-induced dislocations and cracks in GaAs wafers.

MS05 - Non-ambient Conditions: Pressure, Temperature and Fields at Work II

MS05-T01

Synthesis and thermal behavior of pauflerite, β-$VOSO_4$, and its polymorph modification, α-$VOSO_4$

S. Filatov[1], R. Bubnova[1,2], M. Krzhizhanovskaya[1]
[1]*Saint Petersburg State University, Department of Crystallography, St. Petersburg, Russian Federation*
[2]*Institute of Silicate Chemistry RAS, St. Petersburg, Russian Federation*

Pauflerite, β-modification of vanadylsulfate, was discovered among exhalative products of Tolbachik volcano (Kamchatka peninsula, Russia), erupted in 1975-1976 and was named after well-known German crystal physicists Professor Peter Paufler [1]. Powder of the mineral was synthesized by boiling of V_2O_5 in H_2SO_4.

In-situ high-temperature powder X-ray diffractometry (Stoe Stadi P, CuKα, HTK 1600 Buehler GmbH) was performed in air, 25 - 500 °C, step 25 °C. Cell parameters, their thermal dependencies and main coefficients of thermal expansion were calculated using Theta To Tensor program complex (V.A. Firsova, R.S. Bubnova, S.K. Filatov. St. Petersburg State University).

Under ambient conditions $VOSO_4$ exists in α- (structural type of $MoOPO_4$) and β- modifications, those crystal structures represent three dimensional frameworks from chains of cornersharing VO_6 octahedra condensed through SO_4-tetrahedra. Although oxygen atoms build almost an ideal octahedron, vanadium is displaced from the center forming vanadyl-ion with characteristic V-O bond lengths: one very short (1.63 Å) and one very long (2.47 Å).

Long bond V-O = 2.47 Å breaks the chains transforming $VOSO_4$ frameworks into layered structures. Due to this specific feature, the tetragonal α-$VOSO_4$ demonstrates extremely intensive thermal expansion parallel to vanadyl-ion elongation (along *c* axis): $\alpha_a = 3$, $\alpha_c = 40 \cdot 10^{-6}$ °C^{-1} [2] and $\alpha_a = 8$, $\alpha_c = 50 \cdot 10^{-6}$ °C^{-1}, according present work).

From this point of view, it was unexpected to reveal nearly middle thermal expansion along vanadyl-ion (along *a* axis) of the orthorhombic pauflerite (β-$VOSO_4$) crystal structure: $\alpha_a = 20$, $\alpha_b = 3$, $\alpha_c = 18 \cdot 10^{-6}$ °C^{-1} (present work). This phenomenon can be explained using the following specific feature of pauflerite crystal structure.

The chains of VO_6 cornersharing octahedra are branched (through oxygen atoms) by SO_4 tetrahedra. It is notable that SO_4 tetrahedra connect each pair of neighboring octahedra from one side of the chain and from the opposite one in turn. Well known that SO_4 tetrahedra practically do not change their size on heating.

For this reason the chains of VO_6 octahedra and branching SO_4 tetrahedra in crystal structure of pauflerite (β-$VOSO_4$) do not demonstrate most intensive thermal expansion along vanadyl-ion (*a* axis). The structure of α-$VOSO_4$ shows maximum expansion parallel to vanadyl- ion because of each SO_4 tetrahedron shares oxygen atom with one VO_6 octahedron only.

References. 1. Krivovichev S.V., Vergasova L.P., Britvin S.N., Filatov S.K., Kahlenberg V., Ananiev V.V. Canad. Mineral. 2007. Vol. 45. P. 921-927. 2. Long J.M., Arnott R.J. J. Solid State Chem. 1970. Vol. 1. P. 394-398.

MS05-T02

High-pressure crystal structure of $Bi_{12}GeO_{20}$ sillenite from single-crystal X-ray diffraction and theory

L. Wiehl[1], A. Friedrich[1], E. Haussühl[1], W. Morgenroth[1], B. Winkler[1]
[1]*Goethe-Universität Frankfurt/Main, Geowissenschaften/Abt. Kristallographie, Frankfurt/Main, Germany*

$Bi_{12}GeO_{20}$ crystallizes in the sillenites structure type with the non-centrosymmetric cubic space group *I23*. Sillenites $Bi_{12}MO_{20}$ (M = Si, Ge, Ti) are used in technical applications, such as optical data storage, holography, interferometry [1] or as photorefractive waveguides [2] because of their outstanding electrical and nonlinear optical properties. These properties are assumed to be correlated with the stereochemical activity of the $6s^2$ lone electron pair of Bi^{3+}. Lone electron pairs are associated with (apparently) empty space in crystal structures. Therefore a significant response to high pressure is expected.

The evolution of the $Bi_{12}GeO_{20}$ crystal structure under high pressure was investigated by experiment and theory using single-crystal X-ray diffraction and density functional theory (DFT) calculations. The crystal structure was determined from X-ray intensity data collected at ambient conditions in house and at high pressure with synchrotron radiation at HASYLAB (D3). Pressures up to 21 GPa were generated in diamond anvil cells. DFT calculations were performed using the CASTEP code [3] up to 50 GPa. The pressure dependence of interatomic distances indicates a reduced eccentricity of the Bi^{3+} coordination at high pressure, but not a collapse of the Bi^{3+} lone electron pair. The results are discussed in comparison with the isotypic Si sillenite [4].

Financial support from the DFG (HA 5137/3-1) and from HASYLAB is gratefully acknowledged. We thank HASYLAB for synchrotron beamtime and Martin Tolkiehn for assistance at D3.

[1] Buse K, Appl. Phys. B 64, 1997, 273-291 & 391-407
[2] Kip D, Appl. Phys. B 67, 1998, 131-150
[3] Clark S J, Segall M D, Pickard C J, Hasnip P J, Probert M I J, Refson K, Payne M C (2005) Z. Kristallogr. 220, 567-570
[4] Wiehl L, Friedrich A, Haussühl E, Morgenroth W, Grzechnik A, Friese K, Winkler B, Refson K, Milman V (2010) J. Phys.: Condens. Matter 22, 505401(16pp)

MS05-T03

Structures and stabilities of $NaLnF_4$ and $KLnF_4$ compounds at ambient and high pressures

K. Friese[1], A. Grzechnik[2]
[1]*Research Centre Jülich GmbH, Jülich Centre for neutron Science, Jülich, Germany*
[2]*RWTH Aachen, Institute fro Crystallography, Aachen, Germany*

Efficient upconversion properties are observed for many MXF_4 host lattices and are in general related to the multisite characters of the underlying crystal structure [1]. We studied the structures and stabilities of the $NaLnF_4$ (Ln = La, Ce, Pr, Nd, Sm or Gd) and $KLnF_4$ (Ln=Y, Ho, Er, Tm, Yb) compounds [2,3] with laboratory and synchrotron single-crystal and powder diffraction.

$NaLnF_4$ materials with Ln = La, Ce, Nd, Sm and Gd [2] have the average β structure (P- 6 , Z = 1) and a disordered distribution of the mono- and trivalent cations. For $NaPrF_4$ we found a new type of superstructure (P3, Z = 6) due to partial ordering of cations and vacancies in the lattice. The structure can be derived from the P- 6 structure through group-subgroup relationships. Our observations suggest that the β structure is unstable and that the ordering is a slow process at ambient conditions. Upon compression, β-$NaNdF_4$, β-$NaGdF_4$ and the superstructure $NaPrF_4$ are stable to at least 8 GPa with no evidence for any pressure-induced disorder-order phenomena.

At atmospheric conditions, $KHoF_4$ and $KErF_4$ crystallize in space group $P3_1$, while $KTmF_4$, Er:$KYbF_4$, and KYF_4 crystallize in space group $P3_2$ [3]. In both enantiomorphic structures, the K^+ and Ln^{3+} cations are completely ordered. The pseudo-symmetry of the structures with respect to the two minimal supergroups k = 3 ($P3_1$ and $P3_2$) and t = 2 ($P3_112$ and $P3_212$) increases with decreasing radius of the Ln^{3+} cation, respectively. No phase transition is detected in KYF_4 at low temperatures down to 100 K at atmospheric pressure. Er:$KYbF_4$ and KYF_4 undergo irreversible pressure-induced phase transitions at about 4 GPa. In each case, the single crystals become fragmented into several crystallites as observed during single-crystal measurements in diamond anvil cells. Up to the phase transitions, both Er:$KYbF_4$ and KYF_4 are more compressible along the c axis and their bulk compressibility predominantly results from the contraction of the KF_8 polyhedra. The application of pressure does not affect the distribution of the cations in the crystal structures of Er:$KYbF_4$ and KYF_4 up to the phase transitions at about 4 GPa.

References

1. M. Haase & H. Schäfer, Angew. Chem., Int. Ed., 2011, 50, 5808; A. Aebischer et.al., Angew. Chem., Int. Ed., 2006, 45, 2802;. C. Renero-Lecuna et.al., Chem. Mater., 2011, 23, 3442.

2. A. Grzechnik & K. Friese, Dalton Trans. 2012, 41, 10258.

3. A. Grzechnik, N. Khaidukov & K. Friese, Dalton Trans. 2013, 42, 441.

MS05-T04

Compressibility of orthorhombic FeB_4 studied on a single crystal sample

E. Bykova[1], H. Gou[1], N. Dubrovinskaia[1], M. Merlini[2], M. Hanfland[2], L. Dubrovinsky[3]
[1]*Materialphysik und Technologie, Lehrstuhl für Kristallographie , Physikalisches Institut, Universität Bayreuth, Bayreuth, Germany*
[2]*ESRF, ID09A beamline, Grenoble, France*
[3]*Universität Bayreuth, Bayerisches Geoinstitut, Bayreuth, Germany*

Metal borides are an important class of compounds having a number of remarkable properties like high superconductivity (MgB_2 [1]), low compressibility (OsB_2 [2]), and high hardness (tungsten borides [3], for example). Therefore synthesis of novel metal borides and investigation of their properties have a great interest for material science and technology. Theoretical calculations can help in a search for the compounds with a combination of beneficial properties. Recently [4] two novel phases in the Fe-B system, FeB_2 and FeB_4, were predicted, and the phonon-mediated superconductivity with the T_c = 15-20 K for the latter phase was theoretically suggested. Later [5] the formation conditions of these borides were calculated and it was proposed that the phases are stabilized by high pressure.

These predictions formed a basis of our search for the novel iron borides, and a series of high pressure and high temperature experiments in multi-anvil apparatus have been undertaken. As the result a novel predicted phase of FeB_4 was revealed. The single crystals were characterized by X-ray diffraction. Compressibility of FeB_4 was studied up to 38 GPa in a diamond anvil cell (ID09a beamline, ESRF).

FeB_4 crystallizes in an orthorhombic structure (space group *Pnnm*) with the unit cell parameters a = 4.5782(3), b = 5.2972(4), c = 2.9990(3) Å. The crystal structure consists of distorted FeB12 polyhedra packed through sharing tetragonal faces in columns parallel to the c axis. Figure below shows that each column is connected with 4 neighbors by common edges of polyhedra and all neighbors are shifted in 1/2 c, forming a chess-like packing. Similar packing exists in CrB_4 but the CrB12 polyhedra are not distorted.

Compressibility of FeB_4 was studied both under compression and decompression. No significant differences between the two datasets were observed; therefore the combined data were fit with the 3rd order Birch-Murnaghan equation of state. The resulting bulk modulus K = 252(5) GPa appeared to be rather high among those known for borides. This points at potential high hardness of FeB_4. The compressibility of the iron tetraboride is not uniform in different directions. Along the b axis (b is the largest unit cell parameter) the structure is least compressible and as stiff as diamond.

1. Nagamatsu J., Nakagawa N., Muranaka T., *et al.* // *Nature* (2001), **410**, 63-64.
2. Cumberland R.W., Weinberger M.B., Gilman J.J., *et al.* // *J. Am. Chem. Soc.* (2005), **127**, 7264-7265.
3. Mohammadia R., Lecha A.T., Xiea M., *et al.* // *PNAS* (2011), **108**, 10958-10962.

4. Kolmogorov A.N., Shah S., Margine E.R., *et al.* // *Phys. Rev. Lett.* (2010), **105**, 217003.
5. Bialon A.F., Hammerschmidt T., Drautz R., *et al.* // *Appl. Phys. Lett.* (2011), **98**, 081901.

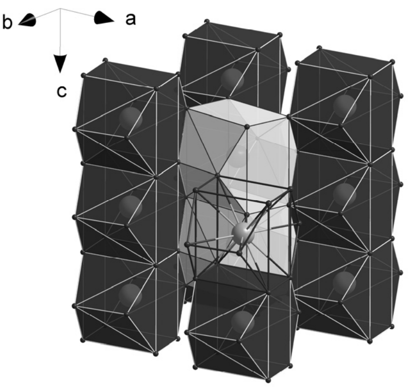

MS05-T05
Single crystal elasticity of $Na_{1.07}Mg_{1.58}Al_{4.91}Si_{1.26}O_{12}$ NAL phase at high-pressure and temperature.

M. G. Pamato[1], A. Kurnosov[1], T. Boffa Ballaran[1], D. M. Trots[1], D. J. Frost[1]
[1]*Universitaet Bayreuth, Bayerisches Geoinstitut, Bayreuth, Germany*

The subduction of oceanic lithosphere plays an important role in the dynamics of mantle convection and is believed to be responsible for the creation of lateral chemical heterogeneity in the mantle. At lower mantle conditions, subducting mid-ocean ridge basalt (MORB) can contain more than 20% of an aluminium rich phase, which is referred to as NAL (short for new Al-rich) phase. NAL exhibits complex solid solutions and has the general chemical formula $XY_2Z_6O_{12}$ being X a large monovalent or divalent cation (Ca^{2+}, K^+, Na^+); Y a middle-sized cations (Mg^{2+}, Fe^{2+} or Fe^{3+}); and Z a small sized cation (Al^{3+} and Si^{4+}).

To date several studies have been conducted on the stability and compression of NAL phases both in complex and simplified systems. However, most data refer to powdered samples. This is the first study reporting of large single-crystals (up to 120 mm) of $Na(Mg,Al)_2(Al,Si)_6O_{12}$ which were synthesized at 2260 °C and at 20.5 GPa. NAL crystallises in the space group $P6_3/m$ and its crystal structure consists of a double chain of $M1O_6$ octahedra connected by shared edges with disordered occupancy of Al^{3+} and Si^{4+}. Mg^{2+} occupies the M2 site (six fold coordinated triangular tunnel-like spaces along the **c**-axis and surrounded by three double chains of $M1O_6$ octahedra) whereas Na^+ occupies the M3 site (tunnel-like cavity surrounded by six double chains of $M1O_6$ octahedra and coordinated by nine O atoms).

We will present the compressibility and structural behavior both at high pressures and temperatures as well as the variation with pressures of the elastic constants of this NAL sample. To this end a crystal of 70 x 70 µm has been doubled side polished to a thickness of approximately 15 µm and loaded in a piston cylinder diamond anvil cell, together with a Sm-doped Yag as pressure standard and neon as pressure transmitting medium. A specially designed internal resistive heater was prepared and placed for high temperature measurements. *P-V* data are collected using a Huber 4-circles diffractometer and a point detector, whereas structural data at high pressure will be collected using an X-calibur diffractometer equipped with a CCD detector. Brillouin spectra will be collected at several pressures for calculating the elastic behavior of such sample.

MS05-T06
Stability of K_2ThF_6 and $K_7Th_6F_{31}$ on compression

A. Grzechnik[1], K. Friese[2]
[1]*RWTH Aachen University, Institute of Crystallography, Aachen, Germany*
[2]*Juelich Centre for Neutron Science, Juelich, Germany*

The first crystallographic studies of actinide fluorides were carried out during the Manhattan Project [1]. Recently, the interest in these materials, especially in the thorium fluorides, has been revived due to stricter safety requirements regarding modern nuclear power generation and waste storage [2]. Our work on these materials is focused on their structural properties and their stability at various P-T conditions [3-5].

Experiments on K_2ThF_6 and $K_7Th_6F_{31}$ to 9 GPa at room temperature were carried out in the Ahsbahs diamond anvil cells on a Stadivari diffractometer equipped with a high-flux delivery system Genix-3D (Mo radiation) and a detector Pilatus 300 k. All data sets were processed with the software X-Area. Further data treatment followed the procedures described by Friese et al. [6]. Structure refinements were performed with the program Jana2006 [7].

The crystal structure of K_2ThF_6 (P-62m, Z = 1) is stable to 9 GPa. It is built of chains of ThF_9 face-sharing tricapped trigonal prisms along the *c* axis. The KF_9 tricapped trigonal prisms share faces with each other. The K-F distances are the most sensitive to increasing pressure resulting in a larger axial compressibility in the *a* direction.

In the crystal structure of $K_7Th_6F_{31}$ (R-3, Z = 3), the Th and K atoms form layers perpendicular to the *c* axis. The ThF_8 coordination polyhedra are square antiprisms and form Th_2F_{14} doublets. They enclose a cubooctahedral cavity in which a disordered F atom is located. The coordination numbers for the K atoms are 6 and 7.

$K_7Th_6F_{31}$ is stable up to the highest pressures reached in this study. The Th-F distances essentially do not change upon compression. Increasing pressure has no significant effect on the cuboctahedral building unit. $K_7Th_6F_{31}$ is most compressible in the *c* direction, because the distances K-F**,** which are approximately directed along the *c* axis, are shortened considerably more at high pressures than those within the layers perpendicular to *c*.

Our observations on the behaviour of K_2ThF_6 and $K_7Th_6F_{31}$ on compression suggest that moderate high pressure has no effect on the coordination polyhedra around the Th atoms and the topology of the structure of complex thorium fluorides. The bulk compressibility of the thorium fluorides entirely depends on the alkali metal present in the structure.

References
1. W.H. Zachariasen, *Acta Cryst*., 1948, **1**, 265.
2. N. Cooper et al., *Environ. Sci. Technol*., 2011, **45**, 6237.
3. A. Grzechnik et al., *J. Phys.: Condens. Matter*, 2007, **19**, 266219.
4. A. Grzechnik et al., *J. Solid State Chem*., 2008, **181**, 971.
5. K. Friese et al., *Dalton Trans*., 2011, **40**, 1902.6
6. K. Friese et al., *High Press. Res.*, 2012, accepted.
7. V. Petricek, M. Dusek and L. Palatinus, JANA2006 - Crystallographic Computing System, Institute of Physics, Academy of Sciences of the Czech Republic, Praha, 2006.

MS06 - General Crystallography: Modelling and Analysis Bridging the Scales II

MS06-T01
Dynamic effects in a neutron diffraction experiment

M. Gutmann[1], S. Mukhopadhyay[1], K. Refson[1], M. von Zimmermann[2]
[1]*Rutherford Appleton Laboratory, Chilton Didcot, United Kingdom*
[2]*DESY, HASYLAB, Hamburg, Germany*

Thermal diffuse scattering is often observed in diffraction experiments at room temperature using X-rays, neutrons or electron diffraction. This is caused by phonons and is well described using the Born-von Karman formalism. Uniquely, direct phonon excitation can occur in a neutron diffraction experiment if the energy and q-vector of neutrons matches that of a phonon and dynamic effects are observed. An example of NaCl will be shown, where strong inelastic effects are observed for two different crystals with the time-of-flight Laue neutron diffractometer SXD installed at the ISIS neutron spallation source and comparisons are made with ab-initio DFT calculations.

MS06-T02
Evaluation of site occupancy factors in crystal structure refinements using Boolean satisfiability techniques

M. Soeken[1], R. Drechsler[1], R. X. Fischer[2]
[1]*Universität Bremen, Fachbereich Mathematik/Informatik, Bremen, Germany*
[2]*Universität Bremen, Fachbereich Geowissenschaften, Bremen, Germany*

Site occupancies of mixed atom positions or not fully occupied positions are usually determined in least squares refinements of crystal structures based on X-ray or neutron diffraction data. Especially in those cases where two atom positions are too close to each other to be simultaneously occupied by atoms the plausibility of the refinement results have to be evaluated. That means, it has to be verified that there does exist a distribution of atoms avoiding such close contacts to next neighbors. This is trivial when there are just two positions being too close to each other. In that case it has to be obeyed that the total occupancy of the two positions must not exceed 100%. If a position has more than one distance to next neighbors too short for simultaneous occupancies the situation becomes more complex. If more than one set of atom postions is present in the unit cell with conflicting distances to nearest neighbors it is impossible to verify possible atom distributions by simple methods.

Here we introduce a method for the evaluation of site occupancy factors using Boolean satisfiability (SAT) techniques which are, e.g., successfully employed in the field of circuit and system design [1]. A Boolean variable is assigned to each atom position in the unit cell being true if it is occupied and false if it is vacant. Restrictions due to site occupancies are encoded as Boolean expressions which are combined and passed to the SAT algorithm. The optimization yields the highest possible occupancy of one site and/or the validation of the occupancy factors from crystal structure refinements. That way it could be shown that the occupancy factors of many published structures with a statistical distribution of atoms are not correct. That means, it is impossible in these cases to find a possible distribution of atoms avoiding any distace too close for simultaneous occupancy. Thus, this approach could be used to routinely evaluate the results of occupancy refinements for plausible distributions of atoms.

References:
[1] R. Drechsler, S. Eggersglüß, G. Fey, A. Glowatz, F. Hapke, J. Schlöffel, D. Tille. On Acceleration of SAT-Based ATPG for Industrial Designs. IEEE Trans. on CAD (TCAD) 27 (2008) 1329-1333.

MS06-T03
Random numbers and their application to the real and dual space description of crystal structures

W. Hornfeck[1]
[1]*German Aerospace Center (DLR), Institute of Materials Physics in Space, Cologne, Germany*

Crystal structures are commonly conceived as prime examples for ordered states of condensed matter and crystallographic group theory appears as the method of choice for their description in real and dual space.

However, symmetry alone merely accounts for a *qualitative* picture of a crystal structure, thereby largely ignoring the incidental occurrence of non-trivial *quantitative* relations regarding either metrical relations between the lattice vectors [1,2] or arithmetical patterns with respect to the set of atomic coordinates.

Moreover, ordered patterns may emerge in a fully deterministic way from very simple rules primarily invented for the effective generation of pseudo- or quasirandom number sequences [3,4].

Illustrative examples are given for (i) pseudorandom point sets generated by multiplicative congruential generators, exhibiting a sublattice structure [3], and for (ii) quasirandom point sets and their associated planar tilings generated by a bit-reversal procedure, exhibiting features of quasicrystals, namely pseudo-decagonal short-range order. Both methods start from a finite set of integers ultimately yielding characteristic permutations, with the symmetry resulting from and encoded by their corresponding cycle representations [3,4].

Both methods may be applied as effective solutions for certain sampling tasks, e.g. in the context of numerical integration and, notably, with respect to the solution of crystal structures employing direct methods (magic integer method, [5]). Ideas of uniform distribution theory such as discrepancy measures and distance optimization algorithms may be used to extend the crystallographer's toolkit for the analysis and description of crystal structures, e.g. via a utilization of pattern recognition methods or via the establishment of distinct definitions of long- and short-range order beyond classical concepts.

A survey is given on possible applications to other fields of crystallographic interest, e.g. regarding the algorithmic generation of crystal structures as well as combinatorial ways of their enumeration and classification.

[1] R. de Gelder & A. Janner. *Acta Cryst. B* (2005) **61**, 287-295.

[2] R. de Gelder & A. Janner. *Acta Cryst. B* (2005) **61**, 296-303.

[3] W. Hornfeck & B. Harbrecht. *Acta Cryst. A* (2009) **65**, 532-542.

[4] W. Hornfeck. *Acta Cryst. A* (2012) **68**, 167-180.

[5] P. S. White & M. M. Woolfson. *Acta Cryst. A* (1975) **31**, 53-56.

MS06-T04
Structural systematization of the polymorph transitions in crystals: a recent experience

S. Filatov[1]
[1]*Saint Petersburg State University, Crystallography, Saint Petersburg, Russian Federation*

The types of polymorphism were discussed and systematized in the middle of 20th century by M. Buerger [1]. The principles of the systematization were repeatedly adopted by the successors during more than half a century . In the present work, we attempt to expand the systematization of M. Buerger.

The advantageous feature of the Buerger's theory of polymorphism is that it discriminates between the transitions involving the first and the second coordination sphere (1st parameter of the systematization) and between the transitions with reconstruction (involves bond breaking) and deformation (all the chemical bonds retained) (2nd parameter). Nevertheless, a system based on these two parameters can not account for the transformations of single atoms or ions: displacements or rotations of atoms or ions, electronic transitions within an atom, spin transitions, magnetic ordering etc.

This vagueness can be remedied by (1) introducing an additional sphere - the trivial zeroth coordination sphere, represented by the atom (ion) itself, and (2) introducing an intermediate level of the second parameter, characterized by a local breaking of chemical bonds due to the change in the type of thermal motion (rotations, hoppings)

Then, *the first parameter* of the systematization denotes the coordination sphere affected by the transformation: the zeroth coordination sphere (atom or ion), the first coordination sphere ("the coordination polyhedron", e.g., SiO_4, SeO_3, MgO_6 etc.), and the second coordination sphere (the environment of the coordination polyhedron).

And *the second parameter* denotes the level of the transformation: deformational level (all the chemical bonds retained), reconstructive level (involves bond breaking) and intermediate level caused by rotations, hoppings (by the change in the type of thermal motion).

Thus, we can systematize the polymorph transitions by considering the three types of coordination spheres and three levels of their transformations. That systematization covers the whole variety of the types of polymorphism.

1. Buerger M.J. Crystallographic aspects of phase transphormations. In: Phase transphormations in solids, Smoluchowski R., Mayer J.E., Weyl W.A., eds., N.-Y.: John Wiley and Sons, 183-211, 1951.

MS06-T05
Modeling frameworks: from polyhedral conformations and distortions to macroscopic strains

R. Angel[1], N. Ross[2], J. Zhao[2], L. Sochalski-Kolbus[2], H. Krueger[3]
[1]*University of Padova, Geosciences, Padova, Italy*
[2]*Virginia Tech, Dept Geosciences, Blacksburg, United States*
[3]*University of Innsbruck, Institute for Mineralogy and Petrography, Innsbruck, Austria*

Unraveling the total response of crystal structures to changes in temperature, pressure or composition in order to understand the relationship between structure and properties is often very challenging. This is especially true for framework materials such as zeolites, perovskites and MOFs in which several levels of structural response interact.

For strongly-bonded frameworks (e.g. zeolites or other silicate minerals), with relatively weak interactions between the framework and the extra-framework cations or molecular species, the polyhedral distortions are small and often remain unchanged. The structural response is then dominated by the tilting of the framework units. Forward geometric modeling allows the elastic response (and hence thermodynamic properties) of the material to be directly related to these tilts. The key question is then: do the distortions of the polyhedra contribute significantly to the anisotropy of the strains induced in a structure by changes in P, T or composition? For octahedral frameworks such as perovskites it is trivial to show that if the octahedral distortions remain constant, the anisotropy is unchanged. For tetrahedral frameworks the application of a new modeling approach [Angel et al., 2012] confirms that networks of deformed tetrahedra exhibit the same anisotropy as those of regular tetrahedra. This leads to three significant conclusions. The elastic anisotropy of frameworks can be determined from models that employ the tilting of rigid regular polyhedra. If the strains displayed by real structures differ significantly from those of model structures, then the framework polyhedra are undergoing significant distortions. And, the total structural response can be considered as the sum of the separate contributions of tilts of rigid structural units together with the deformation of those units.

Angel RJ, Sochalski-Kolbus LM, Tribaudino M (2012) Tilts and tetrahedra: the origin of anisotropy of feldspars. American Mineralogist 97:765-778.

MS06-T06

Single crystal diffraction from powders - Collecting complete 3D electron diffraction data using the automatic rotation method RED

S. Hovmöller[1], W. Wan[1], X. Zou[1], J. Sun[1]
[1]*Stockholm University, Structural chemistry, Stockholm, Sweden*

Atomic structures of crystals < 1µm^{3}can only be solved by electron crystallography. The most complicated zeolites and quasicrystal approximants that have been solved were by electron diffraction (ED) and electron microscopy (EM). Yet, there are still problems. One is the uncertain quality of ED and EM, due to multiple scattering of electrons; even in very thin (< 20 nm) samples. This problem is less severe when the crystal is not viewed along a main crystal axis or a main diagonal. Electron precession reduces multiple diffraction and makes the diffracted intensities more reliable i.e. closer to kinematical. Another problem of electron crystallography has been that it can only be done by highly skilled and well trained persons. Also, it is virtually impossible to collect complete 3D ED or HRTEM data considering all the diagonal views that are needed for complex structures. This is in great contrast to for example X-ray powder diffraction, where you just put a powder sample into an instrument and it collects the data. There is a strong demand for automatic and simple methods for collecting high-quality complete 3D ED data.

We have developed the rotation electron diffraction (RED) method, where complete 3D diffraction data to 1 Å resolution or even higher is collected. This has become possible because the modern electron microscopes and CCD cameras are computer controlled.

The rotation steps must be < 0.1º if reflections with resolution higher than 1.0 Å are to be collected. Only then are they sampled finely enough. Such an accuracy of rotation cannot be reached by the goniometer, but it is possible using the beam tilt. We collect series of 80 frames at 0.05º intervals, covering a total of 4º rotation by automatic beam tilt control. Then we tilt the goniometer by 3.5º (allowing some overlap between series) and start a new series etc. The whole data set, with some 2000 frames may be collected within one hour.

References: Zhang,D.L., Hovmöller,S., Oleynikov,P. and Zou,X.D. Collecting 3D electron diffraction data by the rotation method. Z. Kristallogr. 225 (2010) 94-102.

Zou, Hovmöller and Oleynikov: Electron Crystallography; Electron microscopy and Electron Diffraction. IUCr series of Crystallography Textbooks, Oxford University Press (2011).

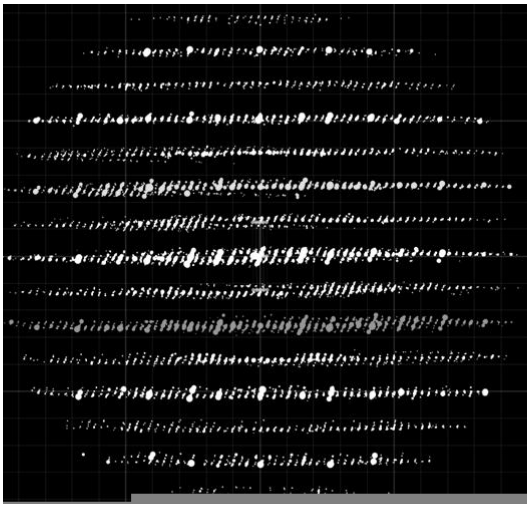

Figure 1. Complete 3D electron diffraction pattern of the Al-Co-Ni approximant PD2. The diffraction goes to 0.5 Å resolution but is here trimmed to only show data upp to 1.0 Å resolution. Unit cell dimensions *a* = 46.4 Å, *b* = 64.0 Å, *c* = 8.1 Å.

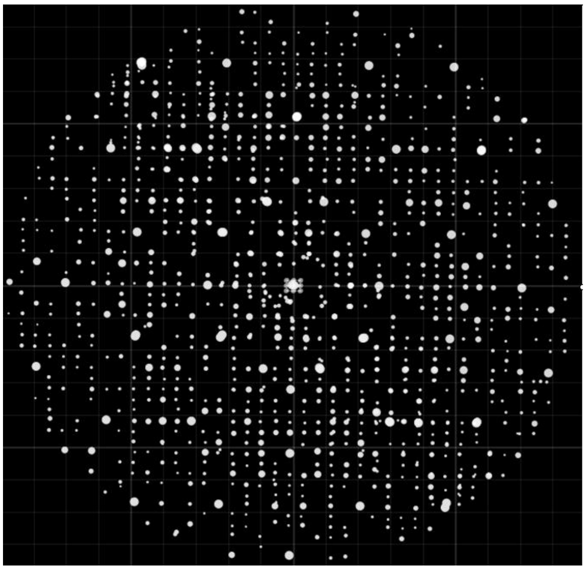

Figure 2. The layers *hk4* and *hk-4* in the Al-Co-Ni quasicrystal approximant PD2 obtained by RED (Rotation Electron Diffraction) from a sub-micron sized crystal. Notice the 10-fold symmetry!

MS07 - Spectroscopy and other Tools for Analysis I

MS07-T01

Spectroscopic methods acting as a supplementary benefit to solve crystallographic research questions - An overview

M. Fechtelkord[1]
[1]*Ruhr-Universität Bochum, Institut für Geologie, Mineralogie und Geophysik, Bochum, Germany*

A wide variety of analytical methods such as diffraction methods, electron microscopy, thermal analysis and spectroscopy is used in the different research fields of crystallography, each method contributing small pieces to the large puzzle of unsolved scientific questions. Often several methods fail in the investigation of structural aspects as in the case of amorphous materials (e.g., glasses and ceramics) or microcrystalline materials and for specific structural questions, e.g., the location and dynamics of hydrogen atoms in minerals. Spectroscopic methods can be of an ideal supplementary benefit here.

For example, in Nuclear Magnetic Resonance all nuclei, that possess a magnetic moment ($I > 0$), are able to provide detailed information about their local environments as local probe e.g., about bond angles, neighbouring atoms (1st and 2nd coordination sphere), the local symmetry, the coordination number, as well as being sensitive to dynamic processes. This is due to the fact that, beside the outside static magnetic field, there are small internal local fields that contain the appropriate structural information, which influence the effective magnetic field at the nucleus.

Similarly, Mössbauer spectroscopy has an extremely fine energy resolution and can detect even small deviations in the nuclear environment of the relevant atoms. Typically, there are three types of nuclear interactions that are detected, the isomeric shift, the quadrupole splitting and magnetic Zeeman interaction.

Infrared (IR) and Raman spectra result from dipolar transitions between vibrational energy states. Thus, vibrations of molecules, atomic groups and the crystal lattice can give structural information about the semi-range order of the atomic environment.

Finally, optical (UV-VIS) spectroscopy of transition metal ion bearing solids is a widespread experimental technique to investigate the coordination symmetry and crystal field strength of these transition metals.

In conclusion, spectroscopy is a powerful complementary method to X-ray structure analysis and to many other methods used in crystallography, probing short range structural effects rather than long range order.

MS07-T02

Application of group theory to resonance Raman spectra of relaxor ferroelectrics

G. de la Flor[1], A. Rohrbeck[2], B. Mihailova[2], E. Tasci[1], M. Aroyo[1]
[1]Universidad del País Vasco (UPV/EHU), Física de la Materia Condensada, Bilbao, Spain
[2]Universität Hamburg, Mineralogisch-Petrographisches Institut, Hamburg, Germany

Relaxor ferroelectrics are disordered crystals with peculiar structure and properties. These compounds are materials with broad, frequency dispersive maximum of the dielectric permitivity as a function of the temperature. The majority of relaxors belong to the family of perovskite (ABO_3) structures. The unique properties of relaxors are due to their complex nanoscale structure known as polar nanoregions (PNR). Different techniques have been used to characterize this kind of materials. Although there are many studies of these materials using Raman scattering, there are only few studies of these materials under resonance Raman scattering [1]. The resonance effect can be observed when the energy of the excited laser is close to the energy of an allowed electronic transition, an important enhancement of the Raman intensities is observed. The selection rules for this phenomenon are different from the classical Raman effect and hence, one may observed vibrational modes which are forbidden in Raman scattering under resonance conditions.

The purpose of the present contribution is to report on the determination of the selection rules for the resonance Raman effect by group-theoretical methods and the application of these selection rules in the analysis of the relaxors experimental data. A new shell with computer tools for the symmetry analysis of infrared, Raman and high-order Raman scattering phenomena has been developed in the *Bilbao Crystallographic Server* [2]. Using those tools the selection rules for the relaxors $PbSc_{1/2}Ta_{1/2}O_3$ (PST) and $PbSc_{1/2}Nb_{1/2}O_3$ (PSN) have been calculated. The theoretical results have been compared with the experimental data that have been obtained in collaboration of the crystallographic group of the Institute of Mineralogy and Petrography of the University of Hamburg. PST and PSN have been studied by resonance Raman scattering at room temperature and at different temperatures in the range of 100-800 K. The experimental results confirm that the collected data originate from the PNRs that exhibit polar rhombohedral symmetry. The interpretation of the resonance Raman data is supported by the predictions of the group theoretical analysis.

[1] B. Mihailova, M. Bastjan, B. Schulz, M. Rübhausen, M. Gospodinov, R. Stosch, B. Güttler, T. Malcherek, and U. Bismayer (2007) *Appl. Phy. Lett.* **90**, 042907.

[2] M. I. Aroyo, J. M. Perez-Mato, C. Capillas, E. Kroumova, S. Ivantchev, G. Madariaga, A. Kirov & H. Wondratschek. (2006). *Z. Kristallog.* **221**, 15-27.

MS07-T03

Raman spectroscopic Investigations of Monazite-type Ceramics used for Nuclear Waste Conditioning

J. Heuser[1], H. Schlenz[1], C. Babelot[1], T. Schuppik[1], S. Schmitz[1], D. Bosbach[1]
[1]Forschungszentrum Juelich GmbH, Nuclear Waste Management, Juelich, Germany

Lanthanide (*Ln*)-orthophosphate- and -phosphosilicate-ceramics represent promising materials for the immobilization of radionuclides like U, Pu and/or minor actinides resulting from the reprocessing of spent fuel. For the conditioning of radioactive waste, ceramics are a good alternative to the widely used borosilicate-glasses, especially for the conditioning of actinides. In terms of their crystal structures, e. g. monazite-type ceramics offer outstanding properties concerning chemical durability and radiation resistance which can also be confirmed by their natural analogues [1, 2, 3]. Monazite-type phases crystallize in the monoclinic space group $P\,2_1/n$ [4].

Therefore we are investigating different monazite-type phases as potential waste forms. Using different wet-chemical synthesis routes like hydrothermal synthesis (220 °C) and precipitation (room temperature) we prepared and characterized $Sm_{1-x}Ce_xPO_4$ and $La_{1-x}Eu_xPO_4$ in the range $0 \leq x \leq 1$. Raman data for the endmembers $SmPO_4$, $CePO_4$, $LaPO_4$ and $EuPO_4$, respectively are already available [5, 6, 7] and are in good agreement to our own data. [7] published the value for v_1 of the chemical composition $Sm_{0.5}Ce_{0.5}PO_4$that fits to our data in an excellent manner. New Raman data for the different solid solutions will be presented. Fig. 1 shows the Raman spectra of five different chemical compositions $Sm_{1-x}Ce_xPO_4$. Additionally we will present first results of a 400 keV Kr^{2+}-ion bombardment on $LaPO_4$-pellets analysed with Raman spectroscopy.

Beside this, we performed solid state reactions (1600 °C) to obtain Nd-monazite-cheralite ($NdPO_4$-$CaTh(PO_4)_2$) as well as Nd-monazite-huttonite ($NdPO_4$-$ThSiO_4$) solid solutions. We identified distortions of the PO_4-tetrahedra which could be observed by a change of the PO_4 modes in the Raman spectra, supported by corresponding Rietveld refinements. The Raman data show similar distortion effects for cheralite phases as described in literature [8, 9, 10].

[1] A. Meldrum et al., *Physical Review B* **56**, 13805 (1997)
[2] G. R. Lumpkin, *Elements* **2**, 365 (2006)
[3] Schlenz et al., *Zeitschrift für Kristallographie*, submitted (2012)
[4] Y. Ni et al., *American Mineralogist* **80**, 21-26 (1995)
[5] G. M. Begun et al., *Journal of Raman Spectroscopy* **11**, 273-278 (1981)
[6] E. N. Silva et al., *Optical Materials* **29**, 224-230 (2006)
[7] K. Ruschel et al., *Mineralogy and Petrology* **105**, 41-55 (2012)
[8] R. Podor, *European Journal of Mineralogy* **7**, 1353-1360 (1995)
[9] O. Terra et al., *Journal of the American Ceramic Society* **91**, 3673-3682 (2008)
[10] P. Raison et al., *Physics and Chemistry of Minerals* **39**, 685-692 (2008)

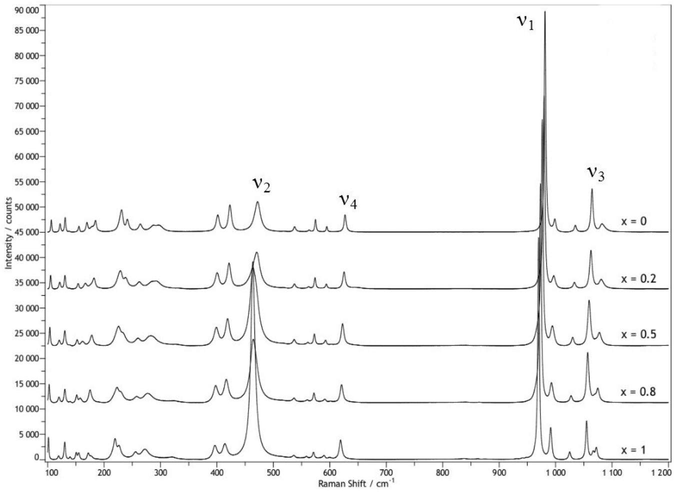

MS07-T04
Nonlinear deformation in GaN layers due to wafer curvature - simulation and Raman measurements

C. Röder[1], F. Beyer[2], G. Leibiger[3], F. Habel[3], M. Abendroth[4], C. Himcinschi[1], J. Kortus[1]
[1]*TU Bergakademie Freiberg, Institute of Theoretical Physics, Freiberg, Germany*
[2]*TU Bergakademie Freiberg, Institute of Applied Physics, Freiberg, Germany*
[3]*Freiberger Compound Materials GmbH, Freiberg, Germany*
[4]*TU Bergakademie Freiberg, Institute of Mechanics and Fluid Dynamics, Freiberg, Germany*

Group III-nitrides have emerged as important and promising materials for several electronic and optoelectronic applications. LEDs based on GaN and its ternary alloys with indium and aluminium exhibit green, blue and ultraviolet (UV) high brightness emission levels. In particular, blue laser diodes make high-density digital information storage systems affordable. In general, GaN based electronic devices take advantage of the superior electronic properties for high power, high frequency and high temperature applications. The lack of high-quality substrates for homoepitaxy is still a problem in GaN preparation. Owing to lattice mismatch and difference in the thermal expansion coefficients several deficiencies such as a large density of structural imperfections as well as the formation of strain that eventually leads to cracking are related to heteroepitaxial growth of GaN. In this work we present Raman scattering results on heteroepitaxially grown wurtzite GaN layers on sapphire substrates. The experiments were conducted in backscattering geometry investigating the stress distribution within the c-plane of GaN. Additionally, X-ray diffraction data were exploited to determine the wafer curvature of the specimens. Analysing the peak position of the non-polar E_2(high) phonon mode we found a wavenumber shift compared to the reference value of unstrained bulk GaN in dependence on the radius as well as the azimuthal angle. It is shown that the bending of the GaN/sapphire bilayer system can no longer be described by a single curvature. At some point bifurcation occurs, leading to a saddle point deformation which is correlated to the angular dependence of the phonon peak position. The experimental results are compared with numerical calculations by means of the finite element method (FEM) simulating all relevant deformation mechanisms across the substrate and the GaN film. The authors would like to thank the Cluster of Excellence "Structure Design of Novel High-Performance Materials via Atomic Design and Defect Engineering (ADDE)" which is financially supported by the European Union (European regional development fund) and by the Ministry of Science and Art of Saxony (SMWK).

MS07-T05
"$Li_7La_3Zr_2O_{12}$" Garnet Doped with Fe: Crystal Chemistry and Phase Stability of a Fast Li-Ion Conductor

G. Amthauer[1], D. Rettenwander[1], C. A. Geiger[1]
[1]*University of Salzburg, Department of Materials Engineering & Physics, Salzburg, Austria*

A flurry of recent research has shown that Li-oxide garnets with the general composition "$Li_7La_3Zr_2O_{12}$" are excellent fast ion conductors that could possibly be used in solid-state batteries (Murugan et al. (2007); Ramzy and Thangadurai, 2010; Cussen, 2010). Two crystal structure modifications have been found and the cubic high-temperature phase has better ion conductivity than the lower temperature tetragonal phase. It has also been demonstrated, importantly, that small amounts of Al, substituting at the Li positions in the garnet structure, stabilizes the cubic garnet structure at ambient conditions (Geiger et al. 2011). Though much research on "$Li_7La_3Zr_2O_{12}$" garnet has made in the past several years, there remain a number of open questions. This is especially true with regard to the role of substitutional cations (e.g. Al, Ga, Fe, etc.) and their effect on phase stability, ionic conductivity and crystal-chemical properties. To better understand these issues, we investigated a series of Fe^{3+}-containing "$Li_7La_3Zr_2O_{12}$" garnet. To begin, various composition $Fe^{3+}_xLi_{7-3X}La_3Zr_2O_{12}$ solid-solution garnets were synthesized at high temperatures using sintering techniques. The chemical composition of the garnets was determined by electron microprobe (La, Zr, Fe) and LA-ICP-MS measurements (Li). X-ray powder diffraction measurements and Rietveld refinements were made to characterize the synthetic products in terms of all phases present and to determine the symmetry of the garnet. Single-phase garnet with up 0.52 moles Fe could be synthesized. These results show that the incorporation of Fe^{3+} stabilizes the cubic garnet phase similar to the effect of Al^{3+} (Geiger et al. 2011). Scanning electron microscopy and EDX analyses were also undertaken to further characterize the polycrystalline samples. Finally, ^{57}Fe Mössbauer spectroscopic measurements, using enriched ^{57}Fe$_2$O3, were carried out in order to study the oxidation state and site distribution of Fe in "$Li_7La_3Zr_2O_{12}$", something that has not been done before. Preliminary spectra show a slightly asymmetric Fe^{3+} doublet probably indicating that Fe3+ substitutes for Li in a similar fashion as Al^{3+}, that is, on at least two different sites.

References:

Cussen, E.J.(2010) J. Mat. Chem. 20, 5167-5173.
Geiger C.A; Alekseev, E.; Lazic, B., Fisch, M.; Armbruster, T.; Langner, R.; Fechtelkord, M., Murugan, R.; Thangadurai, V., Weppner, W., Angew. Chem. (2007) 119, 7925-7928.
Ramzy, A.; Thangadurai, V., Am. Chem. Soc. (2010) 2, 385-390.

MS07-T06

Strontium Titanate Surface Modifications due to Nitrogen Implantation investigated by Grazing Incidence X-ray Absorption Near-Edge Spectroscopy

H. Stöcker[1], M. Zschornak[1], B. Abendroth[1], A. Lehmann[1], C. Richter[1], D. C. Meyer[1]
[1]*TU Bergakademie Freiberg, Institut für Experimentelle Physik, Freiberg, Germany*

Strontium titanate $SrTiO_3$ is an oxidic semiconductor and crystallizes in the perovskite-type of structure; however, several methods have been shown to induce distortions of this perfect cubic lattice. One of the key parameters is the oxygen stoichiometry that on the one hand acts as doping and has great influence on the electric conductivity but on the other hand also couples to the crystal structure. A common way to tune the real structure of surfaces is the implantation of ions. Therefore, we tested several species and found a strong impact of nitrogen implantation on the Ti-K absorption edge fine structure of $SrTiO_3$.

X-ray absorption near-edge spectroscopy (XANES) in grazing incidence geometry was used to characterize the nitrogen implanted samples and revealed a slight shift of the Ti-K edge position and a strong increase of the second pre-edge peak compared to pure $SrTiO_3$. As both of these observations showed a dependence on the angle of incidence, clear evidence of a distorted surface layer is given. This layer is characterized by a shift of the Ti-K edge from the Ti^{4+} state of $SrTiO_3$ towards Ti^{3+} in the layer phase, which may be related to an increased concentration of oxygen vacancies or the formation of Ti-N bonds. The strong increase of the second pre-edge feature in the distorted phase can be explained by a static displacement of the Ti atom relative to the surrounding oxygen octahedron.

Finally, the replacement of oxygen by implanted nitrogen may be the reason for both observations. This has been checked by comparing the measured spectra with simulations of the XANES region for different possible scenarios. Further electric and X-ray reflectometry measurements were carried out to verify the results.

MS08 - Non-ambient Conditions: Pressure, Temperature and Fields at Work III

MS08-T01

Chemically-induced renormalization phenomena in perovskite-type relaxor ferroelectrics under high pressure

B. Mihailova[1], N. Waeselmann[1], B. Maier[2], R. Angel[3], C. Paulmann[1], M. Gospodinov[4], U. Bismayer[1]
[1]*University of Hamburg, Earth Sciences, Hamburg, Germany*
[2]*LMU Munich, Earth Sciences , Munich, Germany*
[3]*University of Padova, Earth Sciences, Padova, Italy*
[4]*Bulgarian Academy of Sciences, Institute of solid state physics, Sofia, Bulgaria*

Relaxors are advanced ferroelectrics, exhibiting exceptional dielectric, elasto-electric and opto-electric properties. At ambient conditions, the average structure is rich in ferroic nanoregions too small to be directly studied by conventional diffraction analysis. Thus the complementary use of x-ray diffraction and phonon spectroscopy at different temperatures and/or high pressures is rather beneficial because of the different length and time scales of sensitivity of the two methods. The combined analysis of the pressure-induced long-range order and of the pressure-enhanced phonon anomalies can reveal the existence of ferroic species that exist at ambient conditions but are not enhanced at low temperatures and thus is vital for the better understanding of the relationship chemistry-nanoscale structure-properties. The pressure-induced phase-transition sequence in $PbSc_{0.5}Ta_{0.5}O_3$ (PST) and $PbSc_{0.5}Nb_{0.5}O_3$ (PSN) heavily doped with iso- and aliovalent cations on the A or B site of the perovskite-type structure (ABO_3) was analyzed by in-situ synchrotron x-ray diffraction and Raman spectroscopy up to pressures of 25 GPa. We have studied B-site Nb^{5+}- and Sn^{4+}-doped PST as well as A-site Ba^{2+}-, La^{3+}-, Sr^{2+}-doped PST and PSN, which allowed us to analyze the effect of local elastic stress, charge imbalance, and tolerance factor [1,2]. Similar to pure PST and PSN, all heavily doped relaxors exhibit two pressure-induced phase transitions at p_{c1} and p_{c2}, preceded by local structural transformations at characteristic pressures $p_1^* < p_{c1}$ and $p_2^* < p_{c2}$. At the first critical pressure the structure transforms from a relaxor cubic/pseudocubic state to a rhombhedral state containing BO_6 tilt order of type $a^-a^-a^-$, whereas the second transition involves the development of either antipolar Pb order and complimentary $a^+b^-b^-$ ordering of the octahedral tilts, or $a^-b^-b^-$ ($0 \leq a < b$) tilting alone. The effect of the type of the substitution cation on the critical and characteristic pressures, tilt pattern, correlation length of the anntipolar Pb order as well as on the dynamic compressibility of the high-pressure phases will be discussed in detail.

[1] B. Mihailova, R.J. Angel, B. J. Maier, A.-M. Welsch, J Zhao, M. Gospodinov, U Bismayer: *IEEE Transactions on Ultrasonics, Ferroelectrics and Frequency Control*, **58**, 1905 -1913 (2011) and references therein.

[2] B. Mihailova, N. Waeselmann, B. J. Maier, R. J. Angel, T. Prüßmann, C. Paulmann, M. Gospodinov and U. Bismayer, submitted.

MS08-T02

Crystalchemistry of silicate perovskite from single crystal X-ray diffraction at multimegabar pressures and high temperatures

L. Dubrovinsky[1], E. Bykova[1], K. Glazyrin[1], T. Boffa Ballaran[1], C. McCammon[1], A. Kantor[1], M. Merlini[2], M. Hanfland[2], N. Dubrovinskaia[3]
[1]*BGI, Bayreuth University, Bayreuth, Germany*
[2]*ESRF, Grenoble, France*
[3]*Bayreuth University, Bayreuth, Germany*

A comprehensive understanding of the iron- and aluminum-bearing magnesium silicate perovskite crystal structure and its evolution under pressure and temperature is vital for evaluating seismic data of the Earth's lower mantle. We investigate materials with different compositions and iron oxidation state by means of single crystal X-ray diffraction at pressures over 120 GPa and temperatures over 2200 K, and by Mössbauer spectroscopy. By tracking the changes of crystallographic parameters at extreme conditions, we find (a) no spin state crossover in ferric iron occupying the bicapped trigonal prism ("A") crystallographic site, and (b) ferric iron does not enter the octahedral ("B") site at any conditions of our experiments. We demonstrate that incorporation of ferric iron and aluminum significantly increases the compressibility of magnesium silicate perovskite (Pv). Based on experimental data we constrain the thermal equation of state for Pv with variable content of iron (ferrous and ferric) and aluminum. We report that for compositions of Pv relevant for Earth's lower mantle, variation of $Fe^{3+}/\Sigma Fe$ can lead to significant changes of Pv bulk sound velocity (over 1%), demonstrating that the oxidation state of iron is a critical parameter for interpretation of seismic tomography data.

MS08-T03

High-pressure structural behaviour of $CaIrO_3$ perovskite

T. Boffa Ballaran[1], K. Kularatne[1], A. Kurnosov[1], R. G. Trønnes[2]
[1]*Universitaet Bayreuth, Bayerisches Geoinstitut, Bayreuth, Germany*
[2]*University Oslo, Oslo, Norway*

The two known polymorphs of $CaIrO_3$ are isostructural analogues for $MgSiO_3$ perovskite and post-perovskite which are likely the dominant phases of the Earth's lower mantle. The structure of the $CaIrO_3$ phase stable at ambient conditions has been known since the late '60s and it has been renamed lately as post-perovskite structure at least in the geological community. This compound transforms at pressures above 2 GPa and temperatures above 1350 °C to an orthorhombic perovskite structure whose atomic positions are still unknown. However, without a correct knowledge of the atomic structure and its response to changes in pressure and temperature it is difficult to assess to what degree $CaIrO_3$ compounds can be used as analogues of the lower mantle phases. Aim of this study is therefore to obtain single-crystal structural data of $CaIrO_3$ both at ambient conditions and at high pressure and to compare them with high-pressure structural data of $MgSiO_3$ perovskite.

Single crystals of $CaIrO_3$ orthorhombic perovskite were synthesised with a piston cylinder apparatus at 1525 °C and 2.5 GPa using as starting material a mixture of high-purity $CaCO_3$ and IrO_2 decarbonated and sintered at 900-950 °C. A single-crystal of 0.06 x 0.08 x 0.09 mm has been measured using an Xcalibur diffractometer (Oxford Diffraction) operating with MoKa radiation at 50 kV and 40 mA and a CCD detector. From the structural refinements of these data it appears that the tilting of $CaIrO_3$ perovskite is only slightly larger than that reported for $MgSiO_3$ perovskite, however the octahedral site is much more distorted since all Ir-O bond distances are very different and the O-Ir-O angles deviate significantly from 90°.

A puzzling feature of the $CaIrO_3$ perovskite structure is that the octahedra are shortened along the *c*-axis, therefore one would expect such axis to be the least compressible. However, this is not the case since it has been reported that $b_a > b_c > b_b$. Moreover the behavior of $CaIrO_3$ perovskite clearly deviates from the relationship between bulk moduli and molar volume reported in the literature for Ca-oxide perovskites. Its larger incompressibility may be a result of the octahedral tilting approaching some limiting value, given that the tilting angles are already quite large at ambient conditions. Since it is generally accepted that the dominant compression mechanism of orthorhombic perovskites is volume reduction via tilting of relative rigid octahedral, high-pressure structural data which are at the moment collected from a single-crystal loaded in a diamond anvil cell with Ne as pressure transmitting medium will help to clarify this peculiar incompressibility.

MS08-T04

Coupling between Strain and Order Parameter: Distortion-Mode Refinement and Parametric Refinement of the Structural Phase Transitions in $LuF[SeO_3]$

O. V. Magdysyuk[1], R. E. Dinnebier[1], C. Lipp[2], T. Schleid[2]
[1]*Max Planck Institute for Solid State Research, Stuttgart, Germany*
[2]*University of Stuttgart, Institute for Inorganic Chemistry, Stuttgart, Germany*

$LuF[SeO_3]$ exhibits two independent phase transitions - one at 3 °C and one at 109 °C [1]. Depending upon its thermal history, the compound shows different structural behaviors during the phase transition at 109 °C from $P2_1/m$ to $P\text{-}1$. The simplified *Landau* theory for structural phase transitions in crystals can not provide an explanation of the unusual temperature dependence of lattice strains (Figure 1). It is necessary to include in the *Landau* model also the coupling between strain and order parameter [2, 3].

Powder diffraction data for $LuF[SeO_3]$ were collected at the high-resolution powder diffractometer I11 at Diamond, Great Britain. The sample was first cooled from room temperature (RT) to 100 K and then heated up to 300 °C before cooling down to RT again.

The phase transition from $P2_1/m$ to $P\text{-}1$ is associated with k= (0, 0, 0) with two irreducible representations corresponding to the phase transition: GM1+ (not active, responsible for non-symmetry-breaking strains) and GM2+ (active, responsible for symmetry-breaking strains). Strain/order parameter coupling dominates the properties and the thermal behavior of LuF[SeO$_3$]. The order of the phase transition depends on the coupling between order parameter and strain.

To understand the nature of the phase transition, it was necessary to develop the theory for biquadratic coupling before applying it to the experimental data for the phase transition from $P2_1/m$ to $P\text{-}1$ in LuF[SeO$_3$]. Parametric refinements [4] based on both *Le Bail* fit and *Rietveld* refinement of distortion modes [5] confirmed the description of the phase transition via strong coupling between strain and order parameter.

The preliminary cooling of the LuF[SeO$_3$] down to 100 K caused extensive strain in this material. The subsequent phase transition during heating from 25 up to 300°C is characterized by a critical temperature of 120 °C and a critical exponent of $\beta \approx 0.4$, close to a second order phase transition. Strong biquadratic coupling between strain and order parameter is responsible for the unusual shape of the lattice parameters and for the increasing of the temperature of the phase transition. The phase transition during cooling from 300 down to 25 °C is accompanied by much weaker strain (strain release at high temperature) and the strength of coupling is smaller. This phase transition is characterized by a critical temperature of 98 °C and a critical exponent $\beta \approx 0.25$, close to a tricritical phase transition.

[1] C. Lipp, PhD Thesis (2008),University of Stuttgart,Germany.

[2] M. A. Carpenter, E. K. H. Salje, A. Graeme-Barber, *Eur. J. Mineral.* **10** (1998)621-691.

[3] M. A. Carpenter, E. K. H. Salje, *Eur. J. Mineral.* **10** (1998) 693-812.

[4] G. W. Stinton, J. S. O. Evans, *J. Appl. Crystallogr.* **40** (2007) 87-95.

[5] B. J. Campbell, H. T. Stokes, D. E. Tanner, D. M. Hatch, *J. Appl. Crystallogr.* **39** (2006) 607-614.

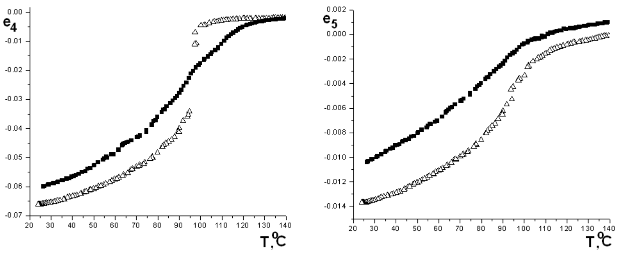

Figure 1. Dependence of symmetry-adapted strains from temperature; *left:* symmetry-breaking strain e_4 (corresponding to angle α), *right:* non-symmetry breaking strain e_5 (corresponding to angle β). Full squares: heating from 25 up to 300 °C, open triangles: cooling from 300 down to 25 °C.

MS08-T05

Detection of the magnetic phase transition of Cr$_2$O$_3$ at high pressure using second harmonic generation measurements

L. Bayarjargal[1], B. Winkler[1]
[1]*Institut für Geowissenschaften /Goethe-Universität, Abt. Kristallographie, Frankfurt, Germany*

The detection of magnetic phase transitions at high pressure is still a challenging task. Pressure-induced magnetic phase transitions have been studied using Mössbauer spectroscopy, neutron diffraction, electrical resistivity measurements or X-ray magnetic circular dichroism[1], but all these approaches have significant limitations and the development of complementary techniques is desirable. At ambient pressure, magnetic phase transitions have been detected with second harmonic generation (SHG) measurements[2]. Here, we demonstrate for the first time that SHG measurements can also be employed for the detection of a pressure-induced magnetic phase transition, using Cr$_2$O$_3$ as an example.

At ambient conditions Cr$_2$O$_3$ has a corundum-type crystal structure and is an antiferromagnetic insulator with an acentric magnetic structure[2]. The high pressure behavior of Cr$_2$O$_3$ has extensively been studied by x-ray diffraction experiments and Raman spectroscopy[3]. No indication of a structural phase transition was found up to 55 GPa[4]. A color change associated with a change in the c/a ratio at 15 GPa was suggested to be correlated with a change in magnetic ordering. The influence of pressure on the magnetic ordering has been discussed controversially[5,6].

Compacted powder samples of Cr$_2$O$_3$ and Ar were loaded in a diamond anvil cell. The pressure was determined using the ruby fluorescence method. Lasers with wavelengths of 1054 nm and 920 nm were used as a fundamental pump wave. The fundamental wave at 920 nm was generated with an Optical Parametric Oscillator from a Q-switched Nd:YAG laser system. The SHG signal was separated with a short pass filter and with a monochromator from the fundamental wave. The experimental setup of the 1054 nm wave has been described in detail elsewhere[7]. The SHG intensity was collected with a photomultiplier and photon counter at pressures up to 20 GPa.

Our measurements show that the SHG intensity at both wavelengths decreases continuously on increasing pressure and disappears around 10 GPa. This indicates a transition from the acentric magnetic order to a centrosymmetric arrangement of the magnetic order at this pressure.

The authors gratefully acknowledge financial support from the DFG within the SPP1236 (Ba-4020) and the FOKUS program of the Goethe University.

[1] A. M. Balagurov, *High-Pressure Crystallography* (Springer-Verlag, 2010)
[2] M. Fiebig, D. Fröhlich, B. B. Krichevtsov, R. V. Pisarev, Phys. Rev. Lett. **73**, 2127 (1994)
[3] S.-H. Shim, T. S. Duffy, R. Jeanloz, C.-S.Yoo, V. Iota, Phys. Rev. B **69**, 144107 (2004)

[4] P. Dera, B. Lavina, Y. Meng, V. B. Prakapenka, J. Solid State Chem. **184**, 3040 (2011)

[5] G. Gorodetsky, R. M. Hornreich, S. Shtrikman, Phys. Rev. Lett. **31**, 938 (1973)

[6] T. Worlton, R. Brugger, R. Bennion, J. Phys. Chem. Solids **29**, 435 (1968)

[7] L. Bayarjargal, B. Winkler, E. Haussühl, R. Boehler, Appl. Phys. Lett. **95**, 061907 (2009)

MS08-T06

Crystallographic studies of pressure-induced phase transitions in transition-metal oxychlorides.

M. Bykov[1], E. Bykova[1], L. Dubrovinsky[2], M. Hanfland[3], H.- P. Liermann[4], V. Prakapenka[5], S. van Smaalen[1]

[1]*University of Bayreuth, Laboratory of Crystallography, Bayreuth, Germany*

[2]*University of Bayreuth, Bayerisches Geoinstitut, Bayreuth, Germany*

[3]*European Synchrotron Radiation Facility, Grenoble, France*

[4]*PETRA III, FS-PE, DESY, Hamburg, Germany*

[5]*University of Chicago, Center for Advanced Radiation Sources, Chicago, United States*

The class of isostructural layered compounds MOX (M = Ti, V, Cr, Fe; X = Cl, Br) has been recently studied for their low-dimensional magnetic properties [1-3]. It was shown that the behavior at low temperatures strongly depends on the number of d electrons on the transition-metal atom. External pressure is an ideal tool to tune crystal lattice parameters and the interatomic distances and hence directly influence the material structure. Recently, high-pressure studies on TiOCl and TiOBr have demonstrated the high sensitivity of their electronic and structural properties regarding the application of pressure [4]. Two pressure-induced phase transitions were observed by Ebad-Allah *et al.* in TiOCl by means of powder X-ray diffraction experiments: at P_{c1} = 15 GPa with the formation of $2a \times 2b \times c$ superstructure having monoclinic symmetry, and at P_{c2} = 22 GPa, which was ascribed to an isostructural phase transition [5].

Here we present powder and single-crystal X-ray diffraction study of FeOCl and CrOCl at high pressures in diamond anvil cells. Both compounds reveal extremely anisotropic compression, however, the variation of the unit cell volume with pressure is found to be smooth up to 14 GPa, and can be described with third order Birch-Murnaghan equation of state. Bulk moduli of FeOCl and CrOCl are close to each other and they are defined by highly compressible c-direction, perpendicular to the layers. At pressures above 15 GPa both FeOCl and CrOCl undergo phase transitions of displacive type and form different superstructures, that are different from the low-temperature superstructures. Further increase of pressure leads to more complicated superstructures in CrOCl, and to magnetic ordering in FeOCl. Treatment of incomplete high-pressure singe-crystal data in superstructure analysis using the superspace formalism and the origin of phase transitions are discussed here.

[1] J. Zhang *et al.*, Phys. Rev. B **86**, 134428 (2012).

[2] J. Angelkort *et al.*, Phys. Rev. B **80**, 144416 (2009).

[3] A. Seidel *et al.* Phys. Rev. B **67**, 020405(R) (2003).

[4] C.A. Kuntscher *et al.*, Phys. Rev. B **74**, 184402 (2006).

[5] J. Ebad-Allah *et al.*, Phys. Rev. B **82**, 134117 (2010).

MS08-T07

Chemistry of Ammonothermal Nitride Growth

R. Niewa[1], S. Zhang[1], T. Richter[1]

[1]*Universität Stuttgart, Institut für Anorganische Chemie, Stuttgart, Germany*

Gallium Nitride crystals with highest quality for application mostly in optoelectronics are currently grown by ammonothermal synthesis [1]. This technique also bears large potential for crystal growth of further semiconducting nitrides [2, 3]. However, the whole process is not well understood due to lack of knowledge regarding the species present in solution and being responsible for the mass transport of the material depending on the process parameters temperature, temperature gradient and pressure, respectively filling rate of the autoclave [4].

We have characterized several novel amides and ammoniates of Ga and further relevant metals depending on the starting materials synthesized in liquid and supercritical ammonia in large ranges of technically accessible temperature and pressure conditions. These solid compounds are discussed in relation to the species most likely present in liquid/supercritical ammonia under ammonobasic or ammonoacidic conditions of nitride crystal growth.

References:

[1] R. Stevenson: The World's Best Gallium Nitride. *IEEE Spectrum*, July 2010, pp. 40.

[2] D. Peters, *J. Crystal Growth* **1990**, *104***,** 411.

[3] U. Zachwieja, H. Jacobs, *J. Less-Common Met*. **1990**, *16*, 175.

[4] Technology of Gallium Nitride Crystal Growth, D. Ehrentraut, E. Meissner, M. Bockowski (Eds.), Springer 2010.

MS08-T08

On the the transition mechanism between the pressure-induced zinc-blende- to- NaCl-type phase transition of InAs

N. Pukallus[1], H. Sowa[1], H. Klein[1]

[1]*Geowissenschaftliches Zentrum der Georg-August-Universität Göttingen, Abteilung Kristallographie, Göttingen, Germany*

Indium arsenide is a semi-conducting material used for photo diodes in infrared detectors. It crystallizes in the zinc-blende structure type with the space group F-43m. At a pressure of 7 GPa it transforms into the rocksalt structure with the space group Fm-3m and the coordination number of the atoms increases from 4 to 6 [1].

The pressure-induced phase transformation in InAs is of first order and considered to be reconstructive. The low and high pressure phases do not show a group-subgroup relation, but the transformation is assumed to happen via a common subgroup, so various energetically favoured transformation paths have been investigated via finding a common subgroup of the two phases to explain the phase transformation without the breaking of atomic bonds [2-5]. It is assumed that the orientation relations of the unit cells of both phases give clues about the actual transformation path.

The experiments were carried out in a "quadratic" high-pressure cell [6] that is equipped with laser-machined diamond anvils [7] without beryllium backing plates at the beamline BW5 at HASYLAB, Hamburg. A single crystal of indium arsenide transformed under pressure into a polycrystalline material with a highly preferred orientation [8]. After decreasing the pressure, the polycrystal transformed back into the low pressure phase again.

From these data the experimental pole figures were calculated. The comparison of the pole figures of the low pressure and the high pressure phase and the resulting orientation relations strongly suggest a transformation path via the common subgroup *Imm*2. For this transformation path an atomic shift by a distance of 1/8 of the unit cell length along the [001] direction of the zinc-blende type takes place. Cations and anions move in opposite directions [2]. This leads to the [100] direction of the ZnS type running parallel to the [1-10] direction of the NaCl type and the [001] direction of the ZnS type becoming the [-1-10] direction of the NaCl type. Likewise some of the {111} planes become {200} planes.

This corresponds to the theoretical orientation relations of the *Imm*2 transformation path.

After the phase transformation a significant decrease in the crystal size was observed. It amounted to 9% in the [110] direction and 6% in the [100] direction of the original zinc-blende type crystal. This is consistent with the theoretically predicted metrical changes. However, it is not possible to determine the changes in size in the direction perpendicular to the cleavage plane (110).

Literature:

[1] J. C. Jamieson: Science 139, 845 (1963)
[2] H. Sowa: Z. Krist. 215, 355 (2000)
[3] H. Sowa: Acta Cryst. A59, 266 (2003)
[4] D. M. Hatch, H. T. Stokes, J. Dong, J. Gunter, H. Wang and J. P. Lewis: Phys. Rev. B71, 184109 (2005)
[5] C. Capillas, J. M. Perez-Mato, M. I. Aroyo: J. Phys.: Condens. Matter 19, 275203 (2007)
[6] H. Ahsbahs, Z. Kristallogr. 219, 305 (2004)
[7] H. Sowa, H. Ahsbahs: J. Appl. Cryst. 39, 169 (2006)
[8] H. Sowa, H. Klein: Jahresbericht des Hasylab 2010 (2011)

MS09 - Crystallography in Materials Science: Real Structures II

MS09-T01

Structural characterization of thin epitaxial GaN films prepared by low-energy ion-beam nitridation of Ga droplets

J. Gerlach[1], T. Höche[1,2], D. Hirsch[1], B. Rauschenbach[1]
[1]Leibniz-Institut für Oberflächenmodifizierung, Leipzig, Germany
[2]Fraunhofer-Institut für Werkstoffmechanik IWM, Halle, Germany

Gallium nitride is well known as base material for optoelectronic devices emitting light in the blue, violet, or ultra-violet region of the optical spectrum. In order to study the influence of Ga droplets on the epitaxial GaN film growth by ion-beam assisted molecular beam epitaxy [1], the case of extremely Ga-rich growth conditions is investigated, i.e., the separate deposition of pure Ga at elevated substrate temperature and subsequent post-nitridation of the as-deposited liquid Ga by a hyperthermal nitrogen ion beam from a constricted glow- discharge source [2]. GaN films of up to 100 nm thickness were obtained on 6H-SiC(0001) and on other relevant substrates, depending on the amount of deposited Ga. *In situ* electron diffraction shows an epitaxial crystallization of GaN during the nitridation of liquid Ga [3]. The epitaxial nature of the formed GaN films is confirmed *ex situ* by x-ray diffraction structure and texture analysis. In order to comprehend the present mechanisms of epitaxial GaN formation from Ga droplets, the films were analyzed using scanning electron and transmission electron microscopy. The surface topography before and after the nitridation reveals a conversion of Ga droplets into densely arranged and almost coalesced epitaxial GaN crystallites of relatively homogeneous thickness forming a GaN film. As revealed by highly resolved cross-section transmission electron microscopy, the films are characterized by a distinct defect structure. The growth mechanisms of this alternative ion-beam based approach to form GaN films is discussed.

[1] L. Neumann, J.W. Gerlach, B. Rauschenbach, *Thin Solid Films* **520** (2012) 3936.

[2] A. Anders, M. Kühn, *Rev. Sci. Instrum.* **69** (1998) 1340.

[3] J.W. Gerlach, T. Ivanov, L. Neumann, Th. Höche, D. Hirsch, B. Rauschenbach, *J. Appl. Phys.* **111** (2012) 113521.

MS09-T02

Local order in intermetallic compounds investigated by *SMARTER* NMR spectroscopy

F. Haarmann[1], O. Pecher[1]
[1]RWTH Aachen University, Institute of Inorganic Chemistry, Aachen, Germany

Local ordering of the atoms is frequently observed in intermetallic compounds. Up to now the impact of disorder on the properties of this important class of materials is not known. Thus, basic research is of fundamental importance to analyze the relation of the atomic order and the properties of the materials.

The combination of NMR-spectroscopy, X-ray diffraction and density functional theory (DFT) calculations has been proven to be very useful for the investigation of the chemical bonding in intermetallic compounds. [1,2,3] This strategy is in line with the SMARTER approach of **S**tructure elucidation by co**M**bining m**A**gnetic **R**esonance, compu**T**ation mod**E**ling and diff**R**actions in an international cooperation among scientific groups in chemistry, physics and material sciences.

Especially nuclei possessing a nuclear quadrupole moment can be studied in detail with respect to chemical bonding since the results of the calculations can be decomposed into contributions of the orbital character of the electrons. The calculated coupling parameters have to be compared with those determined by line shape analysis of the NMR signal to probe the significance of the structure model.

The only drawback of this approach is the limited resolution of the wide line NMR signals of quadrupole nuclei. An enhancement of the data quality is necessary to deconvolute individual signal contributions. This is achieved by orientation dependent measurements on polycrystalline samples aligned in the magnetic field (Figure). Simultaneous refinement of NMR data obtained in various magnetic fields and orientations of the sample enable the determination of the coupling parameters of highly overlapping NMR signals. [4,5,6] The solid solutions of binary di- and tetragallides of the alkaline earth metals Ca, Sr and Ba, denoted as $Sr_{1-x}Ba_xGa_2$ (Figure) and $Ca_{1-x}Sr_xGa_4$ will be used to introduce the strategy.

[1] F. Haarmann, Quadrupolar NMR of Intermetallic Compounds. In: R. K. Harris and R. E. Wasylishen (Eds-in-chief), *Encyclopedia of Magnetic Resonance*. John Wiley & Sons, Ltd, Chichester (2011).

[2] F. Haarmann, K. Koch, P. Jeglič, O. Pecher, H. Rosner, Yu. Grin, *Chem. Eur. J.* **2011**, *17*, 7560.

[3] F. Haarmann, K. Koch, D. Grüner, W. Schnelle, O. Pecher, R. Cardoso-Gil, H. Borrmann, H. Rosner, Yu. Grin, *Chem. Eur. J.* **2009**, *15*, 1673.

[4] F. Haarmann, M. Armbrüster, Yu. Grin, *Chem. Mater.* **2007**, *19*, 1147.

[5] O. Pecher, F. Haarmann, *Z. anorg. allg. Chem.* **2010**, *636(11)*, 2089.

[6] O. Pecher, F. Haarmann, *Z. Kristallogr.* **2012**, *Suppl. 32*, 24.

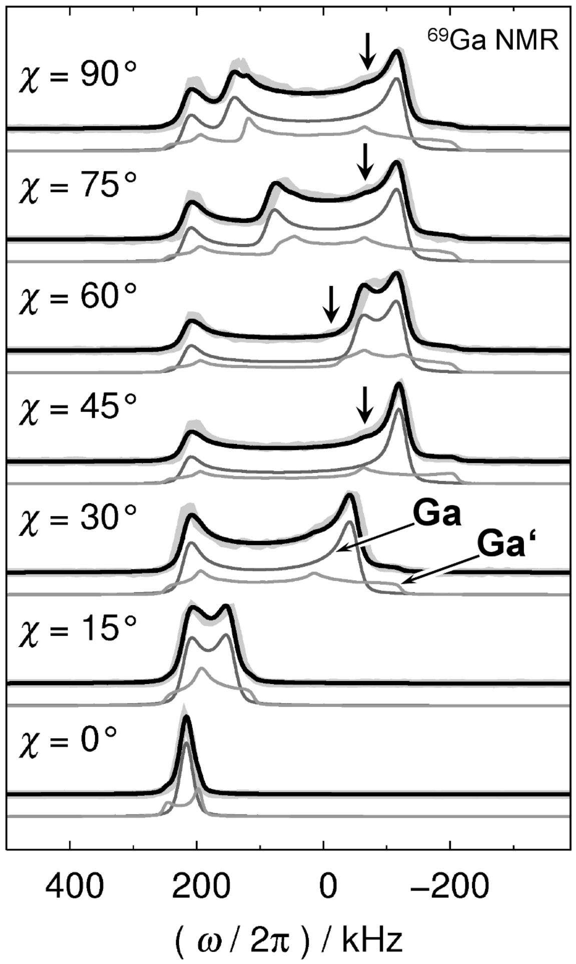

Figure: ^{69}Ga NMR signals of magnetically aligned crystallites of $Sr_{1-x}Ba_xGa_2$. Prominent features of the NMR signal line shape are marked by arrows.

MS09-T03

Real structure of ferritic-pearlitic steels from X-ray diffraction experiments and its effect on the mechanical properties

D. Simek[1], M. Motylenko[1], A. Oswald[2], R. Schmidtchen[2], G. Lehmann[2], D. Rafaja[1]
[1]*TU-Freiberg, Institute of Materials Science, Freiberg, Germany*
[2]*TU-Freiberg, Institute of Metal Forming, Freiberg, Germany*

A new method based on XRD is presented that is intended for a fast analysis of the microstructure changes during the rolling and drawing process. It should be employed in an on-line control and optimisation of the manufacture process of the F-P steels. A large series of ferritic-pearlitic (F-P) steel bars and wires were produced on an industrial type of rolling and drawing facility. The microstructure was studied by metallography with optical and scanning electron microscopy, and volume fraction of pearlite and its microstructure was determined. The X-ray diffraction (XRD) measurements were performed to characterize the real structure of the steels. In particular, residual stress and microstrain in the ferritic phase were analysed. Complementarily, transmission electron microscopy was employed to study the defects present in the material. The tensile tests were used to evaluate the mechanical parameters.

It was found that in the hot-rolled F-P steel, the prevailing structure defects are misfit dislocations located at the ferrite-cementite boundaries of pearlite. A correlation between the dislocation originated microstrain observed by XRD and the density of cementite lamellas was observed. The ultimate tensile strength (UTS) was found to be proportional both to the microstrain and to the lamellar density.

In cold-drawn F-P steel wires, additional dislocations appear first in the primary ferrite grains, and later then in the pearlite. The UTS of the steel still increases with increasing dislocation density and with increasing microstrain, but the residual stress in ferrite in the direction of drawing appears to be the parameter describing the tensile strength of the cold-drawn wire most reliably. Such parameter cannot be deduced from conventional metallography at all.

MS09-T04

Substitutional Disorder in Intermetallic Phases: Investigations of Chemical Bonding by XRD-NMR-QM

O. Pecher[1,2], F. Haarmann[1]
[1]*RWTH Aachen University, Institute of Inorganic Chemistry, Aachen, Germany*
[2]*Max Planck Institute for Chemical Physics of Solids, Dresden, Germany*

Intermetallic phases are widely used in industrial and technical applications. Until this day, the modification of properties is still based on empirics.[1,2] The lack of a precise knowledge of the chemical bonding in intermetallic phases limits the target oriented synthesis of materials with designated properties. Achieving detailed information about the structure-bonding-property relationships in intermetallic phases is one step to open new horizons in applications and to make existing materials more efficient. Substitutional disorder plays a prominent role concerning the properties of intermetallic phases.

Therefore we investigated the impact of increasing complexity of substitutional disorder on the local bonding situation in the solid solutions $Sr_{1-x}Ba_xGa_2$ and $M(Al_{1-x}Ga_x)_4$ with M = Sr, Ba as well as in the intermetallic phase $Ca_{1-x}Ga_{2+3x}$ possessing a homogeneity range (Figure). The combined application of X-ray diffraction (XRD), NMR spectroscopy and quantum mechanical (QM) calculations is well suited to study chemical bonding by an analysis of the electric field gradient (EFG).[3,4] We used orientation dependent ^{27}Al and $^{69;71}$Ga NMR experiments on aligned powder samples to analyse the local Al and Ga environments.[4,5]

The influence of alkaline earth metal substitution on the Ga atoms was investigated in the solid solution $Sr_{1-x}Ba_xGa_2$. NMR spectroscopy revealed two different species Ga and Ga' with similar values of the EFG. A local symmetry reduction for Ga' was proven (Figure, left). In $M(Al_{1-x}Ga_x)_4$ with M =Sr, Ba, a significant influence of group 13 elements substitution on the bonding situation with preferred occupancy of four (4b) and five bonded (5b) Al and Ga positions was studied, respectively (Figure, middle). Chemically different four bonded Al environments, Al(4b) and Al(4b'), were resolved on a microscopical scale of the crystal structure. In $Ca_{1-x}Ga_{2+3x}$ triangular Ga_3 units substitute the Ca atoms. Different three (3b) and four bonded (4b) Ga environments could be resolved and analysed by NMR experiments (Figure, right).

The local atomic environments were modelled in superstructures enabling ongoing quantum mechanical calculations of NMR coupling parameters. From that, a verification of experimental results as well as an analysis of the orbital characters of the electrons dominating the EFG will be possible.

[1] Yu. Grin, *Wiss. Z. Techn. Univers. Dresden* **2000**, *49*, 16.

[2] R. Nesper, *Angew. Chem.* **1991**, *103*, 805; *Angew. Chem. Int. Ed. Engl.* **1991**, *30*, 789.

[3] F. Haarmann, K. Koch, P. Jeglič, O. Pecher, H. Rosner, Yu. Grin, *Chem. Eur. J.* **2011**, *17*, 7560.

[4] F. Haarmann, Quadrupolar NMR of Intermetallic Compounds. In: R. K. Harris and R. E. Wasylishen (Eds-in-chief), *Encyclopedia of Magnetic Resonance*. John Wiley & Sons, Ltd, Chichester (2011).

[5] O. Pecher, F. Haarmann, *Z. Kristallogr.* **2012**, *Suppl. 32*, 24.

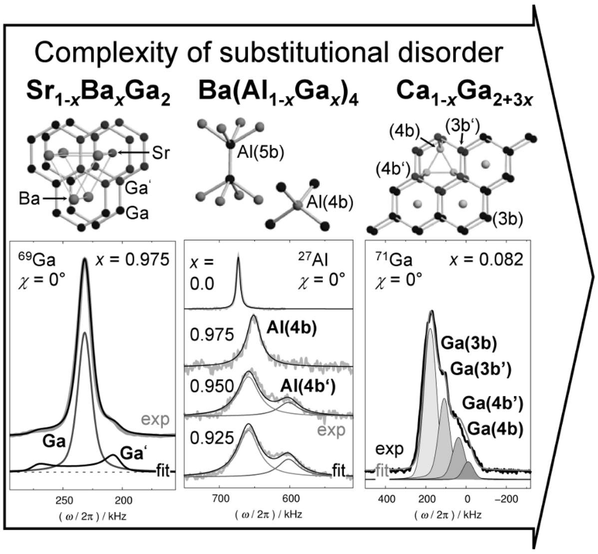

Figure: Static ^{69}Ga, ^{27}Al and ^{71}Ga NMR measurements of magnetically aligned powder samples of $Sr_{1-x}Ba_xGa_2$ (main transition), $Ba(Al_{1-x}Ga_x)_4$ (satellite transition) and $Ca_{1-x}Ga_{2+3x}$ (main transition) from left to right, respectively. Above the spectra cut-outs of the crystal structures are depicted. Different bonding situations of the Al and Ga atoms are labelled with (*n*b).

MS09-T05

Structural and Chemical Analysis of Shockwave-Synthesized Superhard γ - Si_3N_4 Materials

A. Köhler[1], C. Schimpf[1], T. Schlothauer[2], M. Schwarz[3], V. Klemm[1], G. Heide[2], E. Kroke[3], D. Rafaja[1]
[1]*TU Bergakademie Freiberg, Institute of Materials Science, Freiberg, Germany*

[2]*TU Bergakademie Freiberg, Institute of Mineralogy, Freiberg, Germany*
[3]*TU Bergakademie Freiberg, Institute of Inorganic Chemistry, Freiberg, Germany*

Spinel-type γ-Si_3N_4 is known as one of the hardest materials with a temperature stability of $T > 1250\,°C$ in air. It can be synthesized under high pressure only. Although γ-Si_3N_4 is thermodynamically stable above ~12 GPa, usually large overpressures are required for shock wave synthesis of this material.

The application of amorphous precursors and peak shock pressures of 31 GPa (shock duration 1.1 to 1.5 µs) enabled us to manufacture spinel-type material without detectable amount of the low pressure modifications (e.g. α- or β- Si_3N_4) with sample masses up to 1g per experiment.

Samples were comprehensively investigated by XRD, FT-IR, TEM including EELS and EDX, TG-MS and Elementary Analysis by Carrier Hot Gas Extraction (CHGE).

The shockwave-synthesis produces a nanopowder which consists of clusters of a size up to 500 nm containing nanocrystals of about 20 nm in diameter. XRD and high resolution TEM confirmed the expected spinel structure. However, they disclosed some extended crystal structure defects and defect structures. Also an additional amount of oxygen is found in the samples by EDX, EELS and CHGE. Analyses of the FT-IR spectra suggest Si-O bonds, too.

The etching of the as-received powders with hydrofluoric acid leads to a change in the structural parameters. Among others, the static Debye-Waller factor decreased. This reveals that the defect-rich rims of crystalites containing point defects were removed by etching. Simultaneously the overall oxygen content decreases. Thus we conclude that the point defects are related to the local oxygen excess. The incorporation of oxygen into the spinel-γ-Si_3N_4 lattice is discussed with respect to the existence of a metastable solid solution series $Si_{3-y}O_xN_{4-x}$.

MS09-T06
X-ray Grazing Incidence Diffraction from OTS-SAMs on Metal Oxides

H.- G. Steinrück[1], M. Klimczak[1], S. Gerth[1], M. Deutsch[2], B. Ocko[3], A. Magerl[1]
[1]*Universität Erlangen-Nürnberg, Kristallographie und Strukturphysik, Erlangen, Germany*
[2]*Bar-Ilan University, Ramat-Gan, Israel*
[3]*Brookhaven National Laboratory, Upton NY, United States*

The surface-parallel structure of octadecyltrichlorosilane ($C_{17}H_{37}Cl_3Si$, OTS) monolayers self-assembled on amorphous SiO_2, quartz (001) and sapphire (001) was studied by grazing incidence X-ray diffraction.

For all three substrates a powder-like diffraction ring was found at $q_r = 1.50$ Å^{-1}. The radial width of these peaks corresponds to a crystalline coherence length of about 4 OTS molecular diameters, in good agreement with earlier results for OTS monolayers on amorphous SiO_2 [1]. For OTS on sapphire, the peak found coincides with that of the hexagonal lattice of the sapphire surface. Moreover, azimuthal scans show that the intensity of the OTS peak gradually increases as the sapphire in-plane peak is approached [see fig. 1, azimuthal scan of an OTS-coated, and clean, sapphire wafer]. This suggests a significant epitaxy between the lattices of the OTS monolayer and the sapphire surface. The epitaxial behavior depends on the headgroup properties of the monolayer's molecules, as recently demonstrated in the study of octadecyl alcohol monolayers on sapphire, which shows a perfect commensurability [2]. No indication for this epitaxial behavior was found for the quartz substrate, which is due to the too large lattice mismatch of about 2%.

The temperature dependence of the lateral structure was also investigated, yielding a decreasing intensity and a decreasing q_r (i.e. an increasing lattice spacing) with increasing temperature for all three systems [see fig. 2, lattice parameter d assuming hexagonal packing as a function of temperature].

[1] Tidswell et al., J. Chem. Phys. 95, 2854 (1991)
[2] Ocko et al., Phys.Rev. Lett. 106, 137801 (2011)

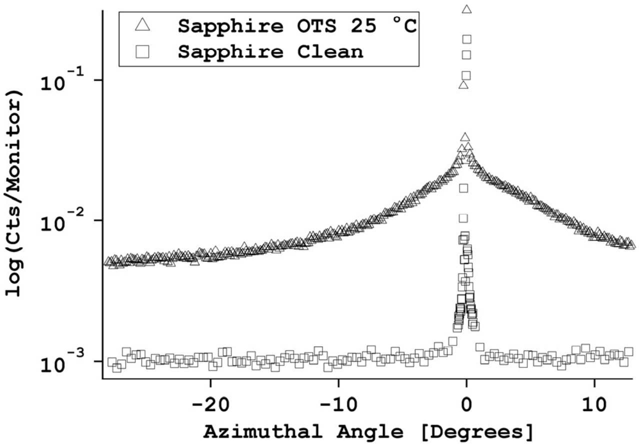

MS09-T07
Effect of Dislocation Array on Morphology and Photocatalytic Properties of Rutile TiO_2 Nanostructures

S. Cha[1], S. Seo[1], D.- Y. Lee[1]
[1]*Korea Electrotechnology Research Institute, Nano-hybrid technology Research Center, Changwon, Korea, Republic of*

TiO_2 nanocrystals are one of particular interests due to their promising applications for photocatalyst and electrodes of photoelectrochemical devices such as dye sensitized solar cell and water splitting to produce hydrogen from water.[1] As other types of nanocrystals, it is well known that the properties of TiO_2 nanocrystals are deeply dependent on their morphologies and there have been many studies to control the morphologies of TiO_2 nanostructures. In particular, hydrothermal synthesis of TiO_2 nanostructures in strong acidic solvents such as HF and HCl provides variety of morphologies including (001) facet- dominant anatase TiO_2 nano-plates and TiO_2 nano-rods and nano-belts, and 3-D dendritic structures.[2~4] However, the detail mechanisms for structural development and property control are not clear yet. In this study, the arrays of dislocations are observed in the TiO_2 one dimensional nanostructures prepared by hydrothermal synthesis with concentrated HCl. **(Figure 1)** The array of dislocations not only causes morphological changes by crystal splitting and also affects photocatalytic activities. The TiO_2 nanowires formed from TiO_2 nano-belts by continuous splitting mechanism owing to misorientation angle of about 6°, caused by dislocations array.**(Figure 2)** In addition, the array of dislocations generates strain field within the nanostructures and tunes the bend structures, which enhances photocatalytic activities under ultra-violet illumination.

Reference
[1] X. Chen, S. S. Mao, *Chem. Rev.*, 2007, **107**, *2891*
[2] H. G. Yang, C. H. Sun, S. Z. Qiao, J. Zhou, G. Liu, S. C. Smith, J. Zou, H. M. Cheng, G. Q. Lu, *Nature*, 2008, **453**, *638*
[3] Z. Sun, J. H. Kim, Y. Zhao, F. Bijarbooneh, V. Malgras, Y. Lee, Y. -M. Kang, S. X. Dou, *J. Am. Chem. Soc.*, 2011, **133**, *19314*
[4] B. Zhao, F. Chen, Q. Huang, J. Zhang, *Chem. Comm.*, 2009, **45**, *5115*

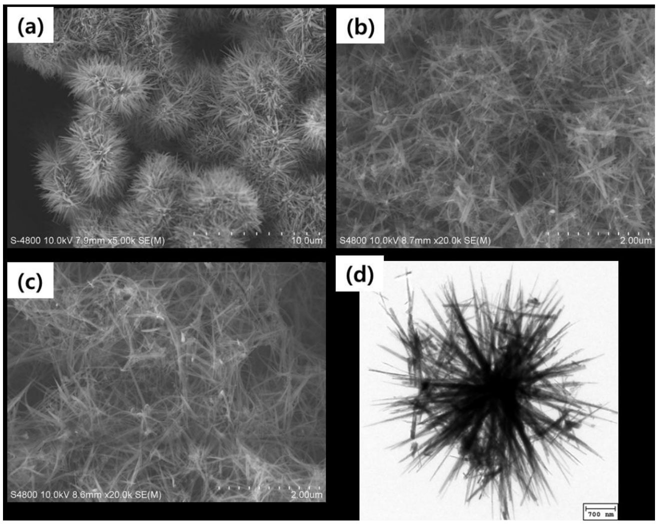

Figure 1. SEM micrographs of rutile TiO_2 (a) nano-flower, (b) nano-belt and (c) nano-wire. (d) TEM micrograph of rutile TiO_2 nano-flower

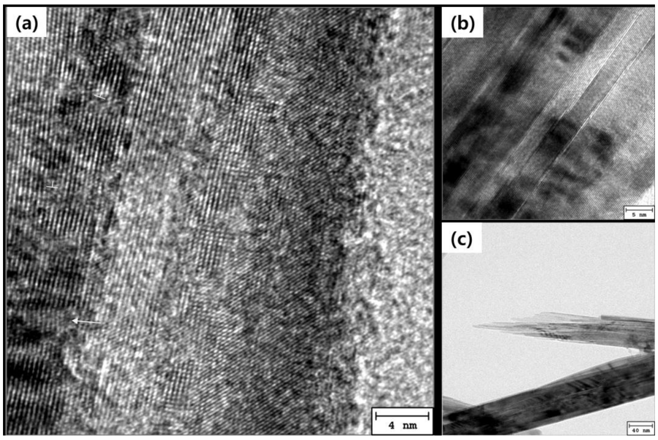

Figure 2. TEM micrographs showing (a) dislocation array, (b) cracks induced by dislocations and (c) crystal splitting near end of rutile TiO_2 nano-belts.

MS09-T08

X-ray scattering on turbostratic carbon structures

M. Dopita[1], M. Emmel[2], M. Rudolph[1], A. Salomon[1], D. Rafaja[1], C. G. Aneziris[2]
[1]*TU Bergakademie Freiberg, Institute of Materials Science, Freiberg, Germany*
[2]*TU Bergakademie Freiberg, Institute of Ceramics, Glass and Construction Materials, Freiberg, Germany*

The carbon binder phase, usually some of the high melting coal-tar pitch, is an important component of carbon bonded refractories. Since other constituents, i.e. refractory oxide and graphite exhibit exceptional thermal stability, the main materials changes or degradation, at elevated temperatures especially, depends upon the properties and microstructure of carbon binder phase. In our contribution we focused on modelling and estimation of microstructure of the binder phase using the X-ray scattering method.

The carbon binder phase is a turbostratic structure where the graphite layers are arranged parallel to each other however with random orientation about the normal to the layers. Such structure leads to the formation of *00l* peaks from the scattering on parallel layers groups and 2-dimensional asymmetric *hk* peaks from the scattering on individual layers, in the diffraction pattern. From measured diffraction *00l* and *hk* profiles one can estimate the mean cluster dimensions *Lc* and *La* (average number of disoriented graphite layers and its mean distance and average lateral size of individual layers) as well as the disorientation degree of individual parallel layers. In our work we simulated and refined the X-ray diffraction patterns to obtain the microstructural properties of those turbostratic structures. For the X-ray scattering patterns simulation we used the general Debye scattering equation in order to calculate the diffraction profiles corresponding to different shapes, sizes and disorientations of parallel layers. While for the measured diffraction patterns refinement the generalized Warren-Bodenstein approach, to obtain the mean microstructural parameters, *Lc* and *La,* was used.

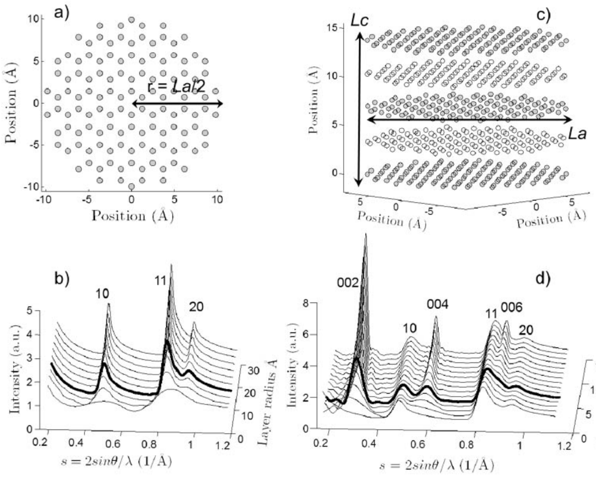

Fig. 1. Single carbon layer of radius 10 Å (a). Calculated diffraction patterns from the 2-dim carbon layers of different radius (b); thick curve corresponds to the scattering from layer shown in Fig 1a. Parallel layers cluster of dimensions *La* and *Lc* (c).

Calculated diffraction patterns from parallel layers groups with *La* = 10 Å; number of parallel layers varied between 1 and 15 (d). Thick curve corresponds to the scattering from parallel layers group shown in Fig 1c.

MS10 – Spectroscopy and other Tools for Analysis II

MS10-T01

Neuartige Auswertung von Mikrobeugungsaufnahmen mittels Fokalkurven

F. Henschel[1], S. Enghardt[2], J. Bauch[1]
[1]*TU Dresden, IfWW, Dresden, Germany*
[2]*TU Dresden, Institut Geometrie, Dresden, Germany*

Für die vorgestellte neuartige Auswertung kommen jene Mikrobeugungsverfahren in Betracht, deren Beugungsreflexe Kurven zweiter Ordnung sind. Neben der EBSD-Methode oder dem Röntgen-Dreh-Schwenk Verfahren trifft dies auch für die Kossel-Technik zu. Um deren hohe Präzision vollständig ausnutzen zu können, ist es notwendig, ein schnelles und hoch genaues Auswerteverfahren für digitalisierte Aufnahmen umzusetzen. Die vorgestellte Methode ermöglicht durch die Benutzung weitgehend automatisierter Prozesse und die Ausnutzung verschiedener Aussagen der Geometrie einen schnellen Zugang zu einer vielfältig auswertbaren Datenbank zahlreicher Röntgenbeugungsbilder. Dabei werden die Ergebnisse der in einem ersten Schritt eingelesenen Reflexlinien der verschiedenen Netzebenen durch eine anschließende kontrollierte Ausgleichung bezüglich der Genauigkeit weiter optimiert. Hierfür ist es erforderlich, die vollständige Aufnahmegeometrie zu ermitteln. Da die Scheitel aller im Probenraum liegenden Beugungskegel in einem Punkt inzidieren (Quelle der Röntgenstrahlung im Untersuchungspunkt der Probe), können die Parameter der inneren und äußeren Orientierung allein durch die Reflexlinien bestimmt werden. Alle Hauptachsen der in der Filmebene liegenden Kegelschnitte - unabhängig ihres Typs - inzidieren im Lotfußpunt des gemeinsamen Scheitels aller Beugungskegel, welcher dem Bildhauptpunkt der Aufnahme entspricht. Des Weiteren kann auch der Abstand der Filmebene zur Probe ohne Skalierungsfaktor aus den jeweiligen Fokalkurven der Reflexlinien bestimmt werden. Diese schneiden sich in einem gemeinsamen Punkt; der Spitze von allen Kossel-Beugungskegeln. Damit ist nicht nur die vollständige Orientierung berechenbar, sondern auch die Öffnungswinkel und Raumlage der Beugungskegel. Aus deren Geometrie lassen sich folgend auch Dehnungs- und Eigenspannungstensoren mit nunmehr noch höherer Genauigkeit ermitteln, da ein bisher notwendiges mechanisches Justiergestell mit den damit verbundenen Messfehlereinflüssen entfallen kann.

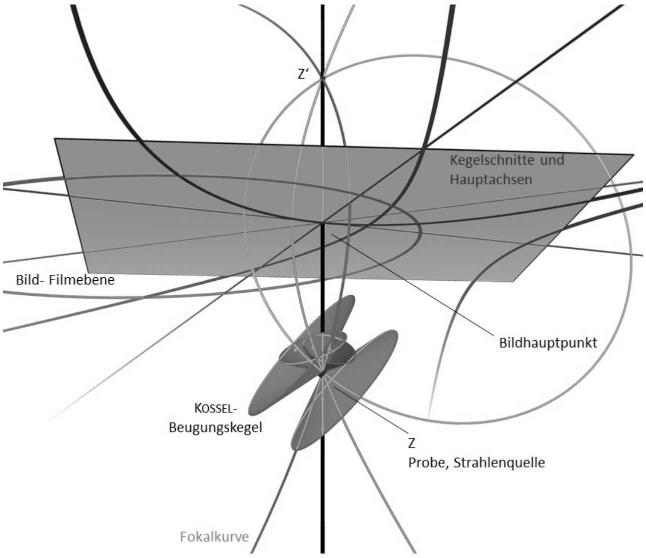

MS10-T02

Influence of polarization switching on the Diffraction Anomalous Fine Structure in ultra-thin, ferroelectric barium titanate films.

C. Richter[1,2], D. Novikov[2], M. Zschornak[1], E. Mehner[1], D. C. Meyer[1]
[1]*TU Bergakademie Freiberg, Experimentelle Physik, Freiberg, Germany*
[2]*DESY, photon science, Hamburg, Germany*

Barium titanate (BaTiO3) stays in focus of scientific and technological interest due to its unique combination of ferroelectric, pyrolectric and optical properties. The currently most common usage of the material is in the multiple billion market of BaTiO3-based capacitors and resistors. The behavior of bulk BaTiO3 being well known, an understanding of the physical properties of nano-scale effects is yet missing and stays in focus of many research groups. Ultra-thin barium titanate films are epitaxially grown on platinum-coated MgO substrates and on LaSrMn2O6 coated SrTiO3 substrates. The films are ferroelectric and polarized perpendicular to the sample surface[1]. Different samples which are polarized upwards or downwards or in a mixed state have been obtained. In contrast to conventional X-ray scattering, resonant X-ray scattering is dependent on the polarization direction and hence provides quantitative access on the polarization state as well as polarization switching dynamics[2]. We show how the measurement of Diffraction Anomalous Fine Structures (DAFS) of one or more Bragg reflections of the barium titanate films can be used to deduce the polarization state of the film. The X-ray wavelength was scanned in a region across the titanium K-absorption edge and the barium L-edges. For extraction of the fine structure of the dispersion correction an iterative Kramers-Kronig approach has been implemented. The result can be used to test the model against other reflections or fluorescence spectra (see Figure). For comparison the same experiments have been performed on bulk single-crystals of barium titanate where self-absorption effects display a challenge for the analysis. [1] A. Zenkevich et al. "Pulsed laser deposition of ultrathin BaTiO3/Fe bi-layers: Structural characterization and piezoelectric response", Thin Solid Films, Volume 520, Issue 14, 1 May 2012, Pages 4586–4589 [2] R. V. Wang et al., "Reversible Chemical Switching of a

Ferroelectric Film", Phys. Rev. Lett. 102, 047601 (2009) Figure Caption: Result of iterative Kramers-Kronig analysis of the DAFS measurement assuming either the 001 or $00bar{1}$ polarization state compared to fluorescence data.

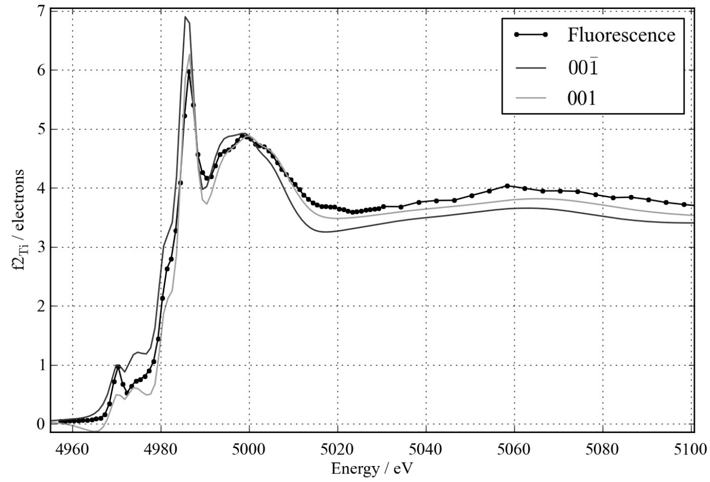

MS10-T03

Application of a Difference Electron Nanoscope (DEN): Correlation between 3D Magnetical Structures of Synthetic Fayalite with Synchrotron and Neutron Diffraction and Mössbauer Spectroscopy

W. Lottermoser[1], K. Steiner[2], G. Scharfetter[3], S.- U. Weber[4], M. Grodzicki[1], A. Kirfel[5], G. Amthauer[1]
[1]University of Salzburg, Dep. of Materials Engineering and Physics, Salzburg, Austria
[2]HBLA Ursprung, Salzburg, Austria
[3]University of Salzburg, Dep. of Computer Sciences, Salzburg, Austria
[4]Technical University of Braunschweig, Dep. of Physical and Theoretical Chemistry, Braunschweig, Germany
[5]University of Bonn, Inst. of Mineralogy and Palaeontology, Bonn, Germany

The evaluation of a 3-dimensional orientation of magnetic moments in solids is still a challenging problem in modern physics and crystallography. Common methods to arrive at this goal are neutron diffraction (in particular with polarised n.), magnetometry and Single Crystal Mössbauer Spectroscopy (SCMBS). However, each of these methods have their limitations, viz. antiphase domains, magnetical impurities, the confinement to special nuclides a.s.o. X-ray and synchrotron diffraction may provide valuable information on crystallographic structures, but the separation of the magnetically effective electrons (in our case: 3d) is hardly possible with the latter experiments.

However, we are in the favourite situation that in the case of synthetic fayalite we dispose of data sets of most of the methods mentioned above and can try to combine the collected physical informations of each one. By the recently presented Difference Electron Nanoscope (DEN) we dispose of a powerful tool to display the 3-dimensional distribution of very accurately determined difference electrons from synchrotron diffraction measurements and to correlate them to the size and direction of the electric field gradient (efg) of Mössbauer spectroscopy and DFT calculations. This has been demonstrated successfully elsewhere [1]. Since Mössbauer spectroscopy is also capable of providing informations on the size and direction of the internal magnetic field H(0) with respect to the efg, we can now correlate the diff. electron distribution mentioned above with H(0) and the magnetic moments orientation from neutron diffraction [2].

The results provide insights into the mechanisms of the orientation of the magnetic moments in synthetic fayalite at low temperatures. The vector of the internal magnetic field H(0) agrees well with the direction of the magnetic moments. Even the low residual amounts of magnetic electron density in the neighbourhood of special oxygens which are subject to superexchange coupling can be determined by our 3-dimensional display of the fayalite unit cell around the M1 and M2 position, respectively.

[1] W. Lottermoser, S,-U. Weber, M. Grodzicki, A. Kirfel, G. Amthauer. *Eur. J. Min*. **24**/5, 791-797 (2012).

[2] W. Lottermoser, K. Forcher, G.Amthauer, W. Treutmann, S. Hosoya. *Phys.Chem.Minerals* **23**, 432-438 (1996).

MS10-T04

A new high-performance small angle X-ray scattering instrument - Rigaku *NanoMax*™

Pennartz, P.U, Fan, L, Degen, M, Jiang, L, Grupido N.
Rigaku Innovative Technologies Inc., Auburn Hills, MI 48326, USA
P. U. Pennartz[1]
[1]Rigaku, Eschweiler, Germany

Rigaku's novel Small-Angle X-ray Scattering (SAXS) camera employs a 2-dimensionally focused monochromatic beam and a Kratky collimation system. Through optimized design, the camera offers two-dimensional capability at exceptionally high intensity and resolution.

The traditional Kratky system, limited by its one-dimensional nature and resultant data smearing, is best for the study of isotropic samples. Rigaku's new SAXS instrument utilizes a focusing Confocal Max-Flux® Optic providing focused beam at the detector plane that eliminates the need for data desmearing and the instrument can be used to investigate both isotropic and anisotropic samples. The integrated solid-state photon counting pixel detector, a Pilatus 100K, has 99% efficiency for Cu Kα radiation. With a Point Spread Function of a single pixel, the detector is well suited for research requiring high sensitivity and high resolution.

Compared to traditional two-dimensional SAXS pinhole cameras, the new camera offers a smaller footprint, higher intensity and wider Q coverage.

NanoMax is optimized for SAXS studies of material science samples. The straight version has a fixed detector that allows a Q range up to $7nm^{-1}$ in a single measurement. In the extended version, the detector can be moved out to $2\theta=60°$ which allows an even larger Q_{max} and offers Wide-Angle X-ray Scattering capability. Rigaku's new platform is designed to work with microfocusing sources such as MM007HF, FR-E+, MM003 and MM002+. The NanoMax is applicable to various forms of samples including solid, liquid, powder, gel and film. Rigaku's NanoMax cameras are capable of *in situ* characterization of a large variety of materials ranging from biological macromolecules and complexes, colloids of all types, cements, oils, polymers, plastics, surfactants, foods and pharmaceuticals. In this presentation, we demonstrate the comparison between NanoMax and a three-pinhole SAXS system and show the characterization of nanomaterials using this instrument.

MS11 - Along the Innovation Chain: From Minerals and Crystals via Natural Sciences to Functional Materials

MS11-T01

Biocalcite architectures - from nanoscale primary particles to functionalized cm-sized multiplex composite crystals

W. W. Schmahl[1], E. Grießhaber[1], A. Ziegler[2], K. Kelm[3], G. Jordan[1], B. Maier[1]
[1]*LMU Munich, Earth- and Environmental Sciences, München, Germany*
[2]*Universität Ulm, Zentrum für Elektronenmikroskopie, Ulm, Germany*
[3]*DLR, Institut für Werkstoffforschung, Köln, Germany*

Biocalcite is an abundant and biodiverse component of biologic hard tissue. It occurs in mollusk and brachiopod shells, echinoderm endoskeleton, teeth and spines, vertebrate egg shells, trilobite eyes, to name but a few examples. Biocalcite is always a hybrid composite including intra- and intercrystalline organic matrix with a hierarchical architecture. The organic matrix directs the morphology and fabric of the mineral and improves mechanical performance. Biocalcite occurs in a range of crystallographic constitutions, where axially textured polycrystalline fabrics [1] and whole "single-crystal" functional entities [2, 3] are most common. With an increasing number of materials investigated in detail by TEM and electron backscatter diffraction, we can now establish systematics of calcite biocrystal architectures. Ubiquitous in calcite produced by multicellular organisms are primary particles in the 20-80 nm range. These primary particles are usually crystallographically co-oriented and compose *mesocrystal* units, with sizes in the range of a few micrometers; they may form *mesocrystal* fibres which reach lengths of hundreds of micrometers, e.g. in brachiopod or mollusk shells. Morphologically similar *mesocrystals* are frequently combined to aggregates to form submillimeter-to-millimeter-sized hybrid *composite crystals*, in which the *mesocrystal* subunits are separated by organic membranes but are crystallographically co-oriented. If *mesocrystal* subunits of different sizes and shapes are combined and display a "single-crystal"-like 3D crystallographic co-orientation, a *multiplex composite crystal* architecture [3] is present, e.g. in sea urchin teeth where this architecture is essential for self-sharpening.

[1] Schmahl WW, Griesshaber E, Kelm K, Goetz A, Jordan G, Ball A, Xu D, Merkel C, Brand U (2012) Hierarchical structure of marine shell biomaterials: biomechanical functionalization of calcite by brachiopods.- Zeitschr. Kristallogr. 227, 793-804.

[2] Kelm K, Goetz A, Sehrbrock A, Irsen S, Hoffmann R, Schmahl WW, Griesshaber E (2012) Mosaic structure in the spines ofHolopneustes porossisimus.- Zeitschr. Kristallogr. 227, 758-765

[2] Schmahl WW, Griesshaber E, Kelm K, Ball, A, Goetz A, Xu DY, Kreitmeier L, Jordan G (2012) Towards systematics of calcite biocrystals: insight from the inside.- Zeitschr. Kristallogr. 227, 604-611

MS11-T03

Growth and Characterization of $Sn_{1-x}Pb_xS$ thin films

S. Lobe[1], G. Wagner[1], K. Bente[1]
[1]*Leipzig University, Leipzig, Germany*

The minerals herzenbergite (SnS) and teallite ($Sn_{0.5}Pb_{0.5}S$) form the $Sn_{1-x}Pb_xS$ solid solution ($0 \leq x \leq 0.5$). This series shows an α-SnS structure (Space group: Pbnm) below 600°C [1]. While SnS is well studied due to its physical properties and potential application as solar cell absorber, there is little known about the physical properties of the solid solution and the end member teallite ($Sn_{0.5}Pb_{0.5}S$).

In order to investigate the physical properties of the solid solution regarding its application as solar cell absorber material, $Sn_{1-x}Pb_xS$ thin films are synthesized via a hot-wall co-evaporation of the binary sulfides. SnS and PbS are evaporated simultaneously at different temperatures based on data calculated by the CVTrans software which uses the G_{min} method [2]. As substrates, which were heated also independently, as well, silica glass, soda-lime glass and gold-coated silica glass were used. The thin films were characterized by x-ray diffraction, electron microscopy and UV-Vis spectroscopy.

Thin films on silica glass substrates show low heterogeneities and nearly smooth thin films with small pinholes. The UV-Vis transmission spectra reveal increasing band gap energies for direct allowed transitions with increasing x from 1.25 eV for x=0.25 to 1.31 eV for x=0.43 and decreasing band gap energies for indirect allowed transitions at the same conditions from 1.05 for x=0.25 to 0.97 for x=0.43 eV. Time-dependent growth show linearly thin film growth and a marked increase of both band gap energies (for x=0.23 and 500µm thickness $E_{g,ind}\approx 1.1$ eV, $E_{g,dir.}\approx 1.7$eV) for smaller thin films. If thin films are deposited on soda-lime glass they show a similar behavior as the films deposited on silica glass substrates.

Silica glass substrates were modified by depositing a gold film on the glass by thermal evaporation. The gold film showed a strong (111) texture. Thin films deposited on this kind of substrates are homogeneous, have a smooth surface and are pinhole-free. X-ray diffraction also reveals a strong (0k0) texture.

[1] A. A. Volykhov, V. I. Shtanov, and L. V. Yashina, Inorg. Mat. 44, 345 (2008)

[2] Glaum et al., Program CVTrans, University Gießen 1997

MS11-T04
On ordering in bixbyite-structured oxide films

M. Niehle[1], A. Trampert[1], X. Kong[1], O. Bierwagen[1]
[1]*Paul-Drude-Institut, Mikrostruktur, Berlin, Germany*

Rare-earth sesquioxides and indium sesquioxide belong to two different categories of functional materials. The former oxides are considered for electronical applications due to their high dielectric constant and as buffer material for the integration of alternative semiconductors in silicon technology. The latter is under investigation as transparent electrode material used in displays and photovoltaic devices.

These two materials have the cubic bixbyite crystal structure in common. It belongs to space group Ia-3 (No. 206). An illustrative way to describe the unit cell, relates bixbyite to calcium fluoride structure where all tetrahedral gaps of the face centered cubic metal sublattice are occupied by anions. In bixbyite, two of these tetrahedral gaps along the space diagonal are empty. Putting together eight of these calcium fluoride-like subunits with the oxygen vacancies on the four different space diagonal results in the bixbyite structure with approximately twice the lattice constant (Fig. 1a).

The bixbyite structure has been identified in thin films of rare-earth oxides by high-resolution transmission electron microscopy (HREM) imaging. Alongside, superstructure reflections of {110}, {330} and {550} type that are kinematically forbidden in the body centered cubic bixbyite structure, occur in electron diffractograms (Fig. 1b). Furthermore, there are parts in such oxide films that exhibit a modulation along {110} planes in phase contrast of bixbyite lattice corresponding to an ordered structure (Fig. 2).

Spatially resolved electron energy-loss spectroscopy reveals fluctuations in oxygen content on a scale of several nanometers. Therefore, we attribute the observed superstructure to an ordering of additional, i.e. extrinsic, oxygen vacancies affecting the metal sublattice, too. We discuss different structure models by means of phase contrast simulation in comparison to experimental images. Additional results are obtained by lattice resolved high-angle annular dark field imaging allowing an access to chemically sensitive information.

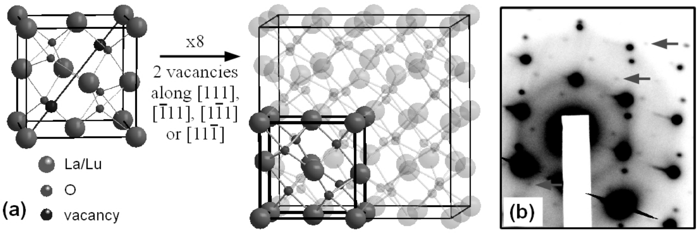

Figure 1: (a) Model representing the bixbyite structure. (b) Diffraction pattern of Lu2O3/Si heterostructure (arrows: superstructure reflections)

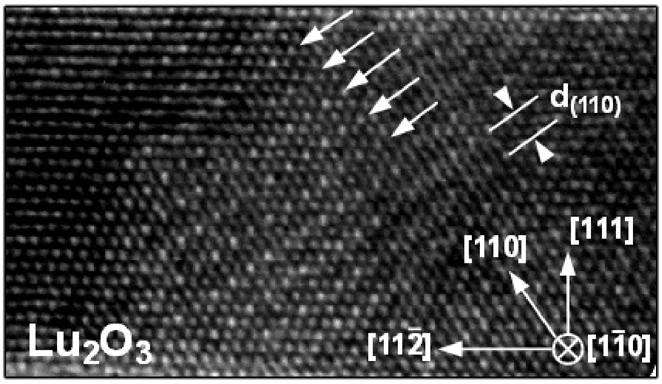

Figure 2: HREM image of ordered structure in Lu2O3

MS12 – Biocrystallography: Synthesis, Structure and Function I

MS12-T01
The Bifunctional Kinase and Methyltransferase WbdD Regulates the Polymerization of Lipopolysaccharide O Antigen in *Escherichia coli* O9a

G. Hagelueken[1,2], H. Huang[2], B. R. Clarke[3], T. Lebl[4], C. Whitfield[3], J. H. Naismith[2]
[1]*Universität Bonn, Institute for Physical and Theoretical Chemistry, Bonn, Germany*
[2]*University of St Andrews, Biomolecular Sciences Research Complex, St Andrews, United Kingdom*
[3]*University of Guelph, Department of Molecular and Cellular Biology, Guelph, Canada*
[4]*University of St Andrews, School of Chemistry, St Andrews, United Kingdom*

The O-antigen polysaccharide (O-PS) of *Escherichia coli* serotype O9a is a model system for glycan biosynthesis and export by the ATP-binding cassette (ABC) transporter-dependent pathway. Mannosyltransferase enzymes located at the cytoplasmic membrane synthesise the polymannose O9a O-PS from polyprenol-linked building blocks. An ABC-transporter subsequently exports the polymer to the periplasm where it is assembled into lipopolysaccharide prior to translocation of the completed molecule to the cell surface. During this process, the WbdD enzyme tightly regulates the chain length of the O9a O-PS. WbdD first stops polymerisation by phosphorylating the terminal non-reducing mannose of the O-PS. The methyltransferase domain of WbdD then methylates the phosphate group. Modification of the non-reducing terminus of the glycan is essential for export.

Solving the crystal structure of WbdD proved to be a challenge because the available crystals belonging to space group I23 only diffracted to low resolution (>95% of the crystals diffracted to resolution lower than 4 Å and most only to 8 Å) and were non-isomorphous, with changes in unit-cell dimensions of greater than 10%. After the initial structure had been solved, a novel crystal dehydration protocol was devised to routinely improve the resolution of WbdD crystals to better than 2.5 Å (Hagelueken et al. 2012a).

Our 2.2 Å resolution crystal structure of WbdD reveals a conventional bacterial methyltransferase domain, fused to a kinase domain that is very similar to eukaryotic kinases. Our results show that WbdD is specific to a number of D-mannose based sugars but works most efficiently with mimics of the natural polymer such as 2-α-D-mannosyl-D-mannose (mannobiose). Further, we have determined the co-complex structure of two known Src-like kinase inhibitors that inhibit WbdD *in vitro* (Hagelueken et al. 2012a). Our structure reveals a C-terminal coiled-coil (Figure 1) which provides new insights into how the tight chain length control is achieved in this important model system.

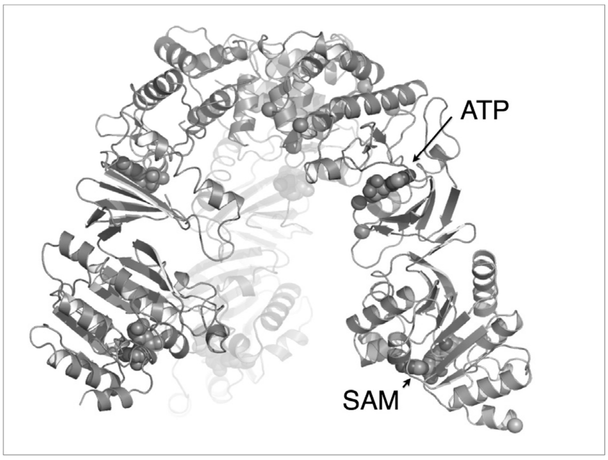

Figure 1: The crystal structure of trimeric WbdD. The protein is shown as a cartoon model with a colour gradient running form blue (N-terminus) to purple (C-terminus). The cofactors ATP and SAM are depicted as spheres.

Hagelueken, G., Huang, H., Harlos, K., Clarke, B.R., Whitfield, C., and Naismith, J.H. (2012a). Crystallization, dehydration and experimental phasing of WbdD, a bifunctional kinase and methyltransferase from Escherichia coli O9a. Acta Crystallogr. D Biol. Crystallogr. *68*, 1371-1379.

Hagelueken, G., Huang, H., Clarke, B.R., Lebl, T., Whitfield, C., and Naismith, J.H. (2012b). Structure of WbdD; a bifunctional kinase and methyltransferase that regulates the chain length of the O antigen in Escherichia coli O9a. Mol. Microbiol.

MS12-T02

Ring-size determination and substrate recognition in the amylomaltase-CA34 complex

C. Roth[1], T. Maier[2], N. Weizenmann[3], N. Bexten[4], W. Sänger[4], W. Zimmermann[3], N. Sträter[1]
[1]*University Leipzig, Center for Biomedicine and Biotechnology, Leipzig, Germany*
[2]*University Basel, Biocenter, Basel, Switzerland*
[3]*University Leipzig, Institue for Biochemistry, Leipzig, Germany*
[4]*Free University Berlin, Institute for Chemistry, Berlin, Germany*

Insoluble polysaccharides such as starch in plants and glycogen in animals and prokaryotes are the major carbon and energy source of life. The mobilization of these polymeric substrates is achieved by numerous enzymes, which either belong to the superfamilies of glycosyl-hydrolases or -transferases. Amylomaltases (AMs) are bacterial intracellular hydrolases of glycosylhydrolase family 77 (GH 77). They are involved in glycogen mobilisation, maltose metabolism and are related to the disproportionating enzymes of plants. AMs catalyse the transfer of one α-1,4-glucan to another, to glucose or to water, resulting in hydrolysis. If the nonreducing end of the bound sugar chain acts as acceptor, an intramolecular transfer results in a cyclization yielding cycloamyloses (CAs), a larger variant of cyclodextrins (CDs) with a degree of polymerization (dp) of 20 and higher.

Amylomaltases comprise a catalytic TIM barrel domain (A), three inserted subdomains (B1,B2, B3) and a loop shielding the active centre, as revealed by crystallographic structure determination of the *Thermus aquaticus* AM (TaqAM) [1]. The catalytic mechanism of AMs was revealed by crystallographic snapshots obtained for the *Thermus thermophilus* AM with a covalently bound intermediate and an acceptor analogue in subsite -1 and subsite +1, respectively [2]. Amylomaltases do not comprise classical carbohydrate binding domains or motifs, but a cocrystal structure with the inhibitor acarbose indicated a secondary carbohydrate-binding site between the unique B2 domain and the core barrel. However, a detailed knowledge how such enzymes interact with their polymeric substrate is still missing.

We obtained a structure of amylomaltase with a bound 34meric CA, mimicking the substrate bound form of amylomaltase, representing the first structure of a carbohydrate interacting enzyme with its polymeric substrate. The structure reveals the binding mode of the substrate in an extended crevice with up to 14 interacting glucose moieties. Together with mutational studies we could explain the role of selected structural features in the catalytic cycle. Furthermore an unsusual posttranslational imide, part of the acceptor subsites were identified to be critical for the proper function of the enzyme with the polymeric substrate. This is, to the best of our knowledge, the first prove of the functional relevance of this type of backbone modification in enzymes.

[1] Przylas,I. *et al.* Crystal structure of amylomaltase from T*hermus aquaticus*, a glycosyltransferase catalysing the production of large cyclic glucans. *J. Mol. Biol.* **296**, 873-886 (2000).

[2] Barends,T.R. *et al.* Three-way stabilization of the covalent intermediate in amylomaltase, an α-amylase-like transglycosylase. *J. Biol. Chem.* **282**, 17242-17249 (2007).

MS12-T03

Forward and reverse peptide binding modes and conformational changes of the Hsp70 chaperone DnaK

M. Zahn[1], N. Berthold[1], D. Knappe[1], B. Kieslich[1], R. Hoffmann[1], N. Sträter[1]
[1]*University of Leipzig, Institute of Bioanalytical Chemistry, Leipzig, Germany*

Hsp70 chaperones interact with short polypeptide stretches in an extended conformation. They are involved in protein folding and trafficking in essentially all organisms, both at normal as well as stress conditions. In *E. coli*, DnaK consists of two functional domains, a 42 kDa nucleotide binding domain (NBD) and a 27 kDa substrate binding domain (SBD). The SBD is further subdivided into a 12 kDa β-subdomain, which contains the substrate binding site and a 15 kDa α-helical subdomain, which forms a lid that covers the substrate binding cleft and stabilizes the loop regions of the β-subdomain. The last 30 amino acids of the helical domain are unstructured. NBD and SBD are connected by a short conserved interdomain linker, which is involved in the interdomain communication. In general, DnaK binds to hydrophobic sequences, which are flanked by basic residues[1-8].

We elucidated the binding mode of proline-rich antimicrobial peptides to the SBD of DnaK. Interestingly, peptides bind either in a forward or reverse direction to the SBD. These studies reveal the structural basis for the ability of DnaK to bind peptides in the forward as well as reverse orientation and the sequence-specific properties that determine the binding mode. In addition, we obtained a near full length crystal structure with a bound peptide which gives new insights into the influence of nucleotide binding on the DnaK chaperone cycle.

1. Czihal, P., Knappe, D., Fritsche, S., Zahn, M., Berthold, N., Piantavigna, S., Muller, U., Van, D. S., Herth, N., Binas, A., Kohler, G., De, S. B., Martin, L. L., Nolte, O., Strater, N., Alber, G. & Hoffmann, R. (2012). Api88 Is a Novel Antibacterial Designer Peptide To Treat Systemic Infections with Multidrug-Resistant Gram-Negative Pathogens. *ACS Chem. Biol.* Ref Type: Journal

2. Gragerov, A., Zeng, L., Zhao, X., Burkholder, W. & Gottesman, M. E. (1994). Specificity of DnaK-peptide binding. *J. Mol. Biol.* **235**, 848-854. Ref Type: Journal

3. Knappe, D., Zahn, M., Sauer, U., Schiffer, G., Strater, N. & Hoffmann, R. (2011). Rational design of oncocin derivatives with superior protease stabilities and antibacterial activities based on the high-resolution structure of the oncocin-DnaK complex. *Chembiochem.* **12**, 874-876. Ref Type: Journal

4. Liebscher, M. & Roujeinikova, A. (2009). Allosteric coupling between the lid and interdomain linker in DnaK revealed by inhibitor binding studies. *J. Bacteriol.* **191**, 1456-1462. Ref Type: Journal

5. Rudiger, S., Germeroth, L., Schneider-Mergener, J. & Bukau, B. (1997). Substrate specificity of the DnaK chaperone determined by screening cellulose-bound peptide libraries. *EMBO J.* **16**, 1501-1507. Ref Type: Journal

6. Van, D. J., Maurer-Stroh, S., Gallardo, R., Wilkinson, H., Rousseau, F. & Schymkowitz, J. (2009). Accurate prediction of DnaK-peptide binding via homology modelling and experimental data. *PLoS. Comput. Biol.* **5**, e1000475. Ref Type: Journal

7. Zhu, X., Zhao, X., Burkholder, W. F., Gragerov, A., Ogata, C. M., Gottesman, M. E. & Hendrickson, W. A. (1996). Structural analysis of substrate binding by the molecular chaperone DnaK. *Science* **272**, 1606-1614. Ref Type: Journal

MS12-T04

The nanoscale and composite nature of biological materials

P. Alexa[1], G. Jordan[1], E. Griesshaber[1], W. W. Schmahl[1]
[1]*LMU, Department of Earth and Environmental Sciences, München, Germany*

In order to highlight the composite nature and nanoscale internal structure of carbonate biomaterials we performed dissolution experiments and monitored the changes with AFM. The investigated samples were skeletons of modern calcitic brachiopods, sea urchin teeth and sea urchin spines. By using different solutions in the AFM cell, both components, the organic and the inorganic component present within the skeletons could be dissolved selectively. The mineral phase was dissolved by using destilled water, the organic polymers within the skeletons were digested with the enzymes tripsin and chitinase. The resulting morphology highlighted the dissolved and the remaining undissolved components. Thus the nanoscale nanoscale structure of both, the inorganic and the organic components (Figures 1 and 2) as well as their dissolution behavior and distribution pattern in the skeleton (Figure 3) could be resolved in-situ.

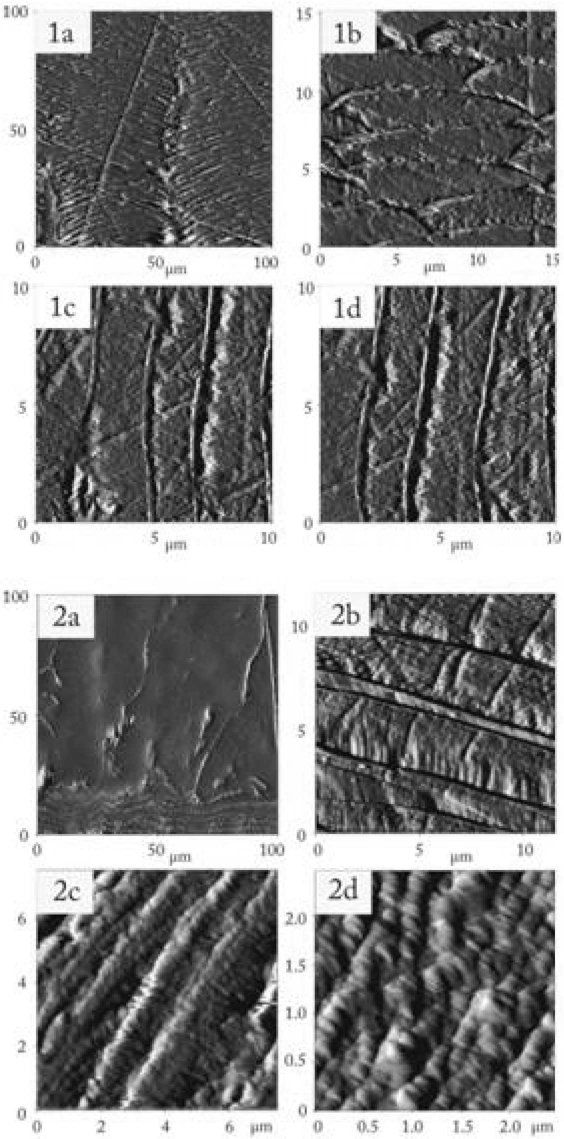

Figures 1 and 2. Arrays of brachiopod fibres in the shell of the modern brachiopod *Magellania venosa.* The fibres are lined by organic sheaths (e.g. Figs. 1c, 1d, 2b) and have an internal granular nanostructure (Figs. 2b, 2c, 2d).

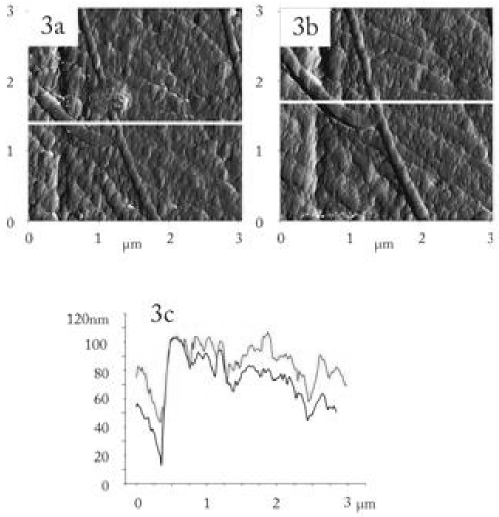

Figure 3. Dissolution of brachiopod calcite for 1 hour by destilled water. Figs. 3a and 3b show in AFM images brachiopod fibre structures before and after water was used to leach the calcite component. Fig. 3c shows the height of the sample at the position of the white line in Figs. 3a and 3b before (red graph in 3c) and after (black grach in 3c) the dissolution experiment. The difference in height shows that calcite has been dissolved in contrast to the organic sheaths around the fibres.

MS12-T05

Composite crystal misorientation and homoepitaxial meso- and microscale co-orientation across matrix membranes in Mytilus edulis nacre

B. J. Maier[1], F. Nindiyasari[1], E. Griesshaber[1], H. Singh Ubhi[2], A. Ziegler[3], W. W. Schmahl[1]
[1]*Ludwig-Maximilians Universität München, Department für Geo- und Umweltwissenschaften, München, Germany*
[2]*Oxford Instruments, High Wycombe, United Kingdom*
[3]*Freie Universität Berlin, Institut für Biologie, Berlin, Germany*

Nacre is a hybrid composite biomaterial which exhibits extraordinary strength and toughness due to its complex nanostructure consisting of c-axis-oriented aragonite tablets embedded in an organic matrix. The co-orientation of nanocrystals within the aragonite tablets could be resolved and quantified for the first time applying new developments in high-resolution electron backscatter diffraction which allow for a step resolution of 125 nm. A mosaic structure with 2° FWHM misorientation distribution is revealed within the nacre tablets, and this mosaic structure spans across tablet boundaries to form composite crystals comprised of up to 20 stacked co-oriented tablets. Small-angle misorientations (< 20°) in the mosaic structure and between the tablets within a composite crystal stack are typically rotations around the a-axis. The different composite crystal stacks are typically misoriented by a rotation larger than 20° around the c-axis. Here {110} twin boundaries are frequent as the probability distribution of mesoscale grain boundary misorientations has a dominant peak near 64°. We attribute the formation of the mesoscale composite crystals to growth by accretion of amorphous calcium carbonate particles followed by semicoherent homoepitaxial crystallization. The crystallization percolates between the tablets through mineral bridges across matrix membranes to form the stacked-tablet crystals. We attribute the low-angle misorientations (rotations around the a-axis) to the disturbance of coherent crystal growth by the 3D network of organic matrix within the tablets and the membranes between the tablets. Each composite crystal of stacked co-oriented of tablets nucleates independently, i.e. no mineral bridge exists between two adjacent crystals.

MS12-T06

The intra- and inter-grain crystallographic nano- and microstructure of nacre

E. Griesshaber[1], H. S. Ubhi[2], W. W. Schmahl[1]
[1]*LMU Munich, GeoBioCenter, Department of Earth- and Environmental Sciences, München, Germany*
[2]*Oxford Instruments, High Wycombe, United Kingdom*

We measured the crystallographic aspects of the microstructure of mollusk nacre for the species *Mytilus edulis* and a cultured pearl of *Hyriopsis cummingii* with high-resolution electron backscatter diffraction (EBSD). A low acceleration voltage was applied to limit penetration depth in order to achieve a resolution sufficient to map individual nacre tablets. For *M. edulis* the aragonite tablets are irregular convex polygons with typically 900 nm thickness and 4-5 micrometer diameter. Within the aragonite tablets the crystallographic orientation has a mosaic spread of typically 2.5° FWHM (compared to the experimental accuracy of +/- 0.3°) with the c-axis generally perpendicular to the tablet (unit cell setting a = 4.97 Å, b = 7.97 Å, c = 5.75 Å). We attribute this mosaic spread to a mesocrystal architecture within the tablets. If "crystal grains" in the EBSD map of the nacre are identified as connected volumes of aragonite with crystallographic misorientations no larger than 3.5° (small angle boundaries), then the "crystals" composing the *M. edulis* nacre emerge on a higher hierarchical level than individual tablets: crystals typically comprise several neighboring aragonite tablets. We observe such *composite crystal grains* forming tower-like stacks of up to 20 tablets along the c-axis and covering the area of 1-2 tablets in the a-b-plane. Thus the tablet boundaries are defined only by the organic matrix membranes which have been occluded into the growing *composite crystal*, and these boundaries do not necessarily imply large-angle grain boundaries. In a scanned area of 20 x 40 micrometers squared containing several hundreds of platelets, the overall crystallographic texture is axial along the c-direction, with a 2D near-Gaussian orientation spread of the c-axes of 25° (+/- 2°) FWHM. In the a-b- plane many different discrete orientations are present (corresponding to the composite crystal grains), which may merge to a continuous cylindrical distribution with increasing scan area.

For the cultured pearl nacre of the mussel *Hyriopsis cummingii* the irregular convex polygonal tablets of 400 nm thickness and 2-4 micrometer diameter form concentric layers in accordance with the spherical shape of the pearl. Grains usually comprise several platelets as described above, and for single platelets the mosaic spread is only in the order of 1.1-2.2° FWHM in 3D. For an ensemble of several hundred grains the overall near-Gaussian 2D orientation spread of the c-axes shows a FWHM in the order of 11° (+/-1°). Moreover, there is also preferred orientation in the a-b plane. Thus the investigated cultured pearl has a structural perfection much higher than the nacre of *M. edulis*.

The quality of our maps allows detailed investigations of grain boundary arrangements. Between neighboring *composite crystal grains* in the nacre the most frequent large-angle misorientation is the common {110} aragonite twin orientation system (which creates the classical pseudohexagonal triplets in abiotic aragonite). However, the nacre tablets are not pseudohexagonal and we observe twinning within a tablet only in very rare instances.

(A) EBSD map of a cross-section through the shell of *Mytilus edulis* and corresponding pole figures. The colours code for crystallographic orientation in the inverse pole figure colouring mode defined in the insert: the colour indicates which axis of the crystal is parallel to the horizontal direction in the map (reference direction x_0). Superimposed on the colour in the map is the EBSD band contrast (Kikuchi band signal strength) as a grey scale component. From this contrast the distribution of the organic matrix membranes between the aragonite tablets becomes visible as dark lines. (B) Misorientation profiles along two trajectories in the map. Note the co-orientation of clusters of stacked tablets along the profiles.

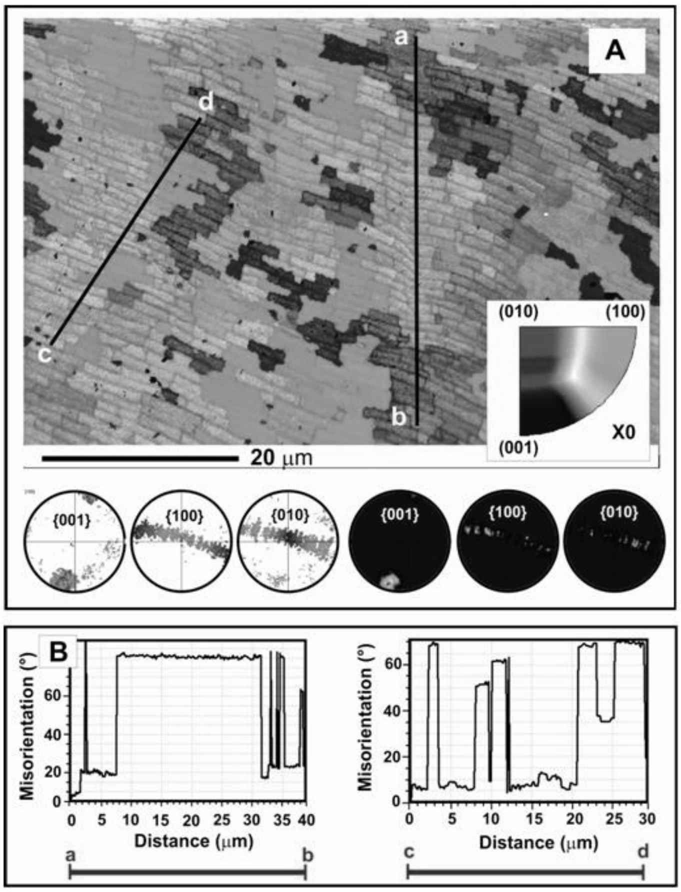

MS13 – Crystal Physics, Crystal Chemistry: Synthesis and New Crystal Structures I

MS13-T01

Structure prediction as a guide in synthesis planning: Identification of promising chemical systems for the synthesis of the "5-5" structure type using an *ab initio* minimization structure extrapolation procedure

D. Zagorac[1], C. J. Schoen[1], M. Jansen[1]
[1]*Max Planck Institute, Solid State Research, Stuttgart, Germany*

In this research we present our *ab initio* minimization structure extrapolation procedure applied to one specific theoretical structure type, the "5-5" structure (see Fig. 1 and Ref. [1]), an ionic analog of the h-BN structure with five fold cation-anion coordination. The goal was to identify chemical systems where this recently proposed "5-5" structure type might be experimentally accessible. [2,3] In the first stage we have constructed the 5-5 type for more then 50 different binary compounds with elements from groups V, IV - VI, and III - VII. From among these, only about half passed the first selection criterion which consisted of experimentally known compounds being available with coordination 4 or 6. This selection was necessary in order to compare experimentally observed structures with hypothetical ones and make conclusions about thermodynamic stability. Therefore, TlF, SnO, SnS, SnSe, GeS, GeSe, PbO, PbS, ZnO and ZnS, were chosen for further study.

In the next step, for each of these systems a local optimization on *ab initio* level with the LDA functional was performed for the 5-5 structure type plus other experimentally observed and theoretically proposed structure types, for comparison. Afterwards, the energy difference between the ground state and the 5-5 modification was correlated with ionic radii and transition pressures. In addition, the results were combined with earlier theoretical work involving the 5-5 structure in the earth alkaline metal oxides [4] and the alkali metal halides [5]. As a final result, we suggest the GeSe and the ZnO systems as the most suitable ones for synthesizing the 5-5 structure type.

[1] J. C. Schön , M. Jansen, *Comp. Mater. Sci.* **4**, 43 (1995)
[2] C. L. Pueyo, et al., *Chem. Mater.* **22**, 4263 (2010)
[3] C. Tusche, H. L.Meyerheim, and J. Kirschner, *PRL* **99**, 026102 (2007)
[4] J. C. Schön, *Z. Anorg. Allg. Chem.* **630**, 2354 (2004)
[5] Z. Cancarevic, J. C. Schön , and M. Jansen, *Chem. Asian J.* **3**, 561 (2008)

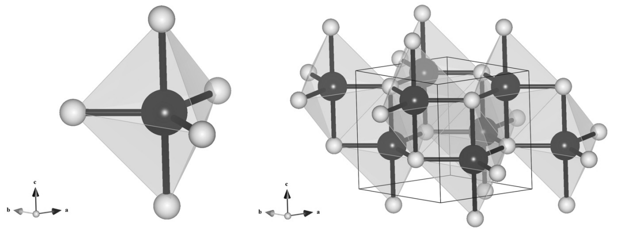

Figure 1. Visualization of the "5-5" structure type. Pictures show coordination polyhedron (left) and periodically repeated unit cell (right). Note that the darker larger spheres and smaller lighter spheres correspond to the A and B atoms of the investigated AB compound, respectively.

MS13-T02

$M(CH_3SO_3)_2(CH_3SO_3H)_2$ (M = Cd, Zn, Co): Syntheses, crystal structures, and thermal decomposition

S. Gagelmann[1], M. S. Wickleder[1]
[1]*Institute of Pure and Applied Chemistry, Oldenburg, Germany*

Despite of their relevance in technical processes, e.g. electroplating [1, 2], methanesulfonates are only characterized for few metals [3-7]. In the course of our ongoing research evaluating the reaction potential of highly concentrated acids we took also a closer look at methanesulfonic acid. Here we present the results of the reactions of anhydrous methansulfonic acid with elemental Cd, Zn and Co in sealed glass ampoules at elevated temperatures. The structure elucidation was accomplished via single crystal X-ray diffraction and the thermal decomposition of the compounds was monitored via TGA/DSC measurements. Intermediates of the thermal decomposition have been identified by X-ray powder diffraction. $Cd(CH_3SO_3)_2(CH_3SO_3H)_2$ crystallizes triclinically (P-1, $Z = 2$, a = 847.79(9), b = 849.2(1), c = 1068.1(1) pm, α = 89.53(1)°, β = 86.23(1)° and γ = 79.88(1)° and V = 755.4(1) Å³, the Cd^{2+} ion is octahedrally coordinated by six oxygen atoms belonging two $CH_3SO_3^-$ ions and two methanesulfonic acid molecules. Each $CH_3SO_3^-$ ion connects two Cd^{2+}, resulting in a chain structure (Fig. 1) which can be described by the Niggli formula $^{\infty}_{1}\{Cd(CH_3SO_3)_{4/2}(CH_3SO_3H)_{2/1}\}$. The isotypic compounds $M(CH_3SO_3)_2(CH_3SO_3H)_2$ (M = Zn, Co) are orthorhombic ($Pccn$, Z = 4, (Zn/Co) a = 1066.69(4)/1070.9(2), b = 1283.87(5)/1286.4(2), c = 1043.20(4)/1049.1(1) pm and V = 1428.65(9)/1445.2(3) Å³. Each M^{2+} ion is coordinated by six oxygen atoms in a distorted octahedral fashion. Two M^{2+} ions are linked by the $CH_3SO_3^-$ ions and coordinated by two methanesulfonic acid molecules, leading to the same motif as found for $Cd(CH_3SO_3)_2(CH_3SO_3H)_2$. The first step of the thermal decomposition of the compounds is the release of the two methanesulfonic acid molecules leading to the binary phases $M(CH_3SO_3)_2$ (M = Cd, Zn, Co). The next step is the formation of sulfidic (M = Cd and Co) or oxidic intermediates (M = Zn). Finally only the Zn-compound yields a mixture of ZnO and ZnS. For the other two compounds the thermal decomposition ends with CdS and Co_9S_8, respectively.

Figure 1.: Crystal structure of $Cd(CH_3SO_3)_2(CH_3SO_3H)_2$ viewed along the c-axis

References:
[1]: M. D. Gernon, M. Wu, T. Buszta, P. Janney, *Green Chem.*, **1999**, 1, 127-140.
[2]: N. M. Martyak, R. Seefeldt, *Galvanotechnik*, **2004**, 10, 2372.
[3]: U. Betke, M. S. Wickleder, *Chemistry - A European Journal*, **2011**, 17, 12784 - 12801.
[4]: C. H. Wei, B.E. Hingerty, *Acta Crystallogr. B*, 1981, 37, 1992-1997.
[5]: J. K. Brandon, I.D. Brown, *Can. J. Chem.*, **1947**, 45, 1385-1390.
[6]: F. Charbonnier, R. Faure, H. Loiseleur, *Acta. Crystallogr. B*, **1977**, 33,2824-2826.

[7]: M. S. Wickleder, *Z. Anorg. Allg. Chem.*, **2002**, 628, 1848-1852.

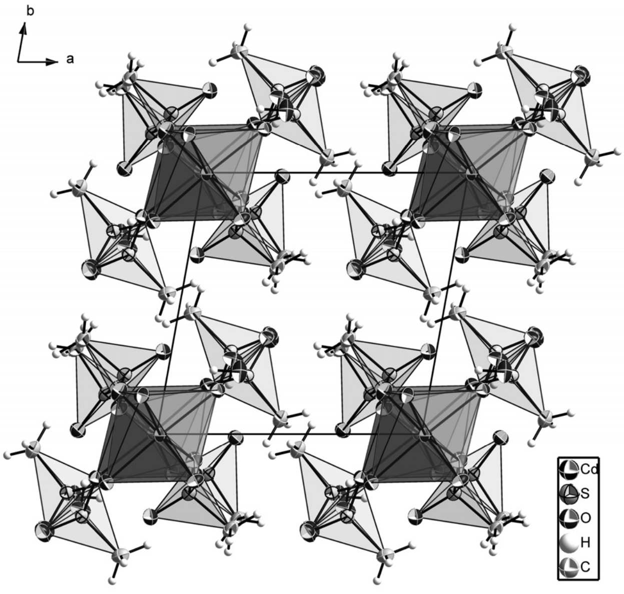

MS13-T03

$Sr_3Gd_2[BO_3]_4$ - growth, thermal behavior and structure

C. Reuther[1], H. Schmidt[2], C. Paulmann[3], M. Hengst[1], R. Möckel[1], G. Heide[1]
[1]*TU Bergakamdemie Freiberg, Mineralogie, Freiberg, Germany*
[2]*TU Bergakademie Freiberg, Chemie, Freiberg, Germany*
[3]*DESY, HASYLAB, Hamburg, Germany*

1968 Dzhurinskii *et al.* [1] synthesized a new borate, $Dy_3Sm_2[BO_3]_4$. They did not know the wide chemical variation of the system, but grew the first single crystal of it. Today borate crystals like the mentioned are of high interest in optics and sensor research due to its wide chemical variation and interesting properties.

The material $Sr_3Gd_2[BO_3]_4$ was sintered in stoichiometric composition. DTA-measurements offer a congruent melting behavior at 1461 °C ± 5K and crystallization temperature 1388 °C ± 5 K. Single crystals were grown in multiple directions using the Czochralski-method. X-ray data of the single crystal show two possible solutions due to the systematic extinction. The possible space groups are P*nma* and P*na2*$_1$. Both structures could be found in literature (e.g. Pan *et al.* [2] or Palkina *et al.* and Bambauer *et al.* [3-4]). For space group P*nam* or P*na*2_1 the cell parameters are a=0.71450 nm, b=0.87555 nm and c=1.60547 nm. The question concerning the correct space group is not answered finally. Both solutions are discussed in the literature (e. g. Bambauer et al. [4] or Mill et al. [5]). The structure shows that one of the boron triangles has two conformations. Dilatation experiments show tow effects (maybe phase transition of higher order) at 450-700 °C and 800-1000 °C. As a possible reasons an structure distortion for the first and an order-disorder transition between Gd and Sr or a domain building (twinnig/BO3-domains) for the second effect could be approved.

Literature:

[1] Dzhurinskii, B. F., Tananev, I. V. and Aliev, O. A.: Synthesis of single crystals of double borats in the system Ln_2O_3-SrO-B_2O_3, In: Neorganiceskie Materialy 4 (1968), p. 1972-1974

[2] Pan, S.-K., Wang, G. and Huang, Z.-X.: Synthesis and Structure of $Ba_3La_2(BO_3)_4$ Crystal, In: Chinese Journal of Structural Chemistry 21. 4 (2002), p. 382-384.

[3] Palkina, K. K., Kuznetsov, V. G. und Moruga, L. G.: Crystal structure of $Pr_2Sr_3(BO_3)_4$, In: Journal of Structural Chemistry 14. 6 (1974), p. 988-992

[4] Bambauer, H. U. and Kindermann, B.: Darstellung und kristallographische Daten von Orthoboraten $(SE)_2Ca_3[BO_3]_4$, In: Zeitschrift für Kristallographie 147 (1978), p. 63-74

[5] Mill, B. V.; Tkachuk, A. M.; Belokoneva, E. L.; Ershova, G. I.; Mironov, D. I. & Razumova, I. K.:Growth, Structure and Intensities of Spectra of $Ln_2Ca_3B_4O_{12}$:Nd^{3+} Crystals (Ln= Y, La, Gd), In: Optics and Spectrocopy 84 (1998), p. 74-81

MS13-T04

Kristallisationsverhalten von Tobermorit unter Einfluss von $CaCl_2x2H_2O$

A. Hartmann[1], D. Schulenberg[1], J.- C. Buhl[1]
[1]*Institut für Mineralogie, Universität Hannover, Hannover, Germany*

Im Rahmen dieser Arbeit wurden Experimente zur Tobermoritsynthese mit dem Additiv $CaCl_2x2H_2O$ durchgeführt [1]. Ziel der Untersuchung war die Fragestellung, welchen Einfluss das Additiv auf das Kristallisationsverhalten von Tobermorit hat. In vorherigen Untersuchungen wurde bereits der Einfluss der Additive Sucrose [2] und Ca-Format [3] auf die Bildung von CSH-Phasen, bzw. Tobermorit, untersucht. Hier konnte jeweils ein Verzögerungseffekt der Tobermoritbildung beobachtet werden.

Als Edukte für die Synthese von Tobermorit wurden Quarzpulver und Quarzsand ausgewählt, um neben der Zugabe von $CaCl_2x2H_2O$ auch den Einfluss der Korngröße der Siliziumquellen auf das Kristallisationsverhalten von Tobermort zu prüfen. In Anlehnung an unsere bisherigen Experimente wurden auch unterschiedliche C/S-Verhältnisse (C/S= 0,53 und C/S= 0,83) ausgewählt. Das Additiv $CaCl_2x2H_2O$ wurde entsprechend der molaren Verhältnisse A/C (Additiv/Calciumoxid) von 0,25 und 0.50 hinzugefügt. Das C/S-Verhältnis erhöhte sich dadurch entsprechend.

Die Reaktionsedukte wurden in Stahlautoklaven bei 200°C für 40,5 h einer Hydrothermalbehandlung unterzogen. Die Charakterisierung der CSH-Phasen erfolgte anhand röntgenographischer (XRD), elektronenmikroskopischer (REM und EDX) und IR-spektroskopischer (MIR) Methoden.

Die Ergebnisse zeigen bei den Synthesen mit Quarzpulver eine ausgiebige Bildung von 11 Å Tobermorit und weiteren CSH Phasen. Bei den Synthesen mit Quarzsand wurde dagegen vorwiegend Portlandit gebildet. Bei einem C/S Verhältnis von 0,75 (mit Additiv) konnte allerdings auch bei Verwendung von Quarzsand als Siliziumquelle eine beginnende Bildung von 11 Å Tobermorit nachgewiesen werden, siehe Abb. 1 und 2. Somit führte in diesem Fall die Verwendung des Additivs $CaCl_2x2H_2O$ zu einer beschleunigten CSH-Phasen Bildung, im Gegensatz zu vorherigen Synthesen ohne Verwendung eines Additivs [4].

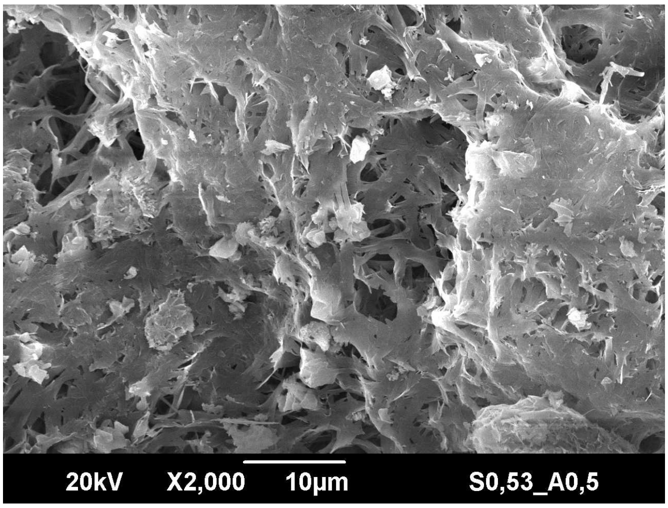

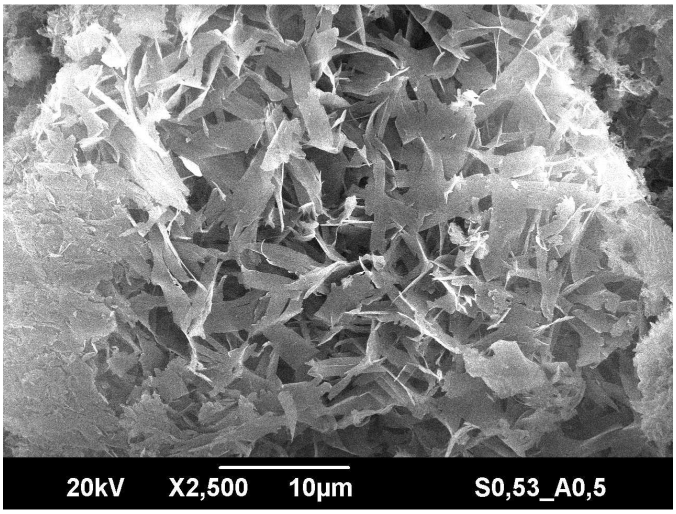

Abb. 1: REM-Abbildung der Synthese mit Abb. 2: REM-Abbildung der Synthese mit Quarzsand und Additiv (C/S=0.75) Quarzsand und Additiv (C/S= 0,75)

[1] Schulenberg, D.: Bachelorarbeit. Institut für Mineralogie, Leibniz Universität Hannover, Hannover 2012

[2] Hartmann, A., Buhl, J.-C.: Materials Research Bulletin 45 (2010), 396-402

[3] Khakhutov, M.: Diplomarbeit. Institut für Mineralogie, Leibniz Universität Hannover, Hannover 2011

[4] Hartmann, A.: Dissertation. Institut für Mineralogie, Leibniz Universität Hannover, Hannover 2004

MS13-T05

Growth and characterization of Ce^{3+} doped $CaSc_2O_4$ single crystal fibers

J. Philippen[1], C. Guguschev[1], D. Klimm[1]
[1]*Leibniz Institute for Crystal Growth, Berlin, Germany*

Ce^{3+} ions in an oxide environment show optical emission in the green spectral range resulting from its $5d$-$4f$ transition. However, only Ce(III) halides are stable under ambient conditions, whereas Ce(IV) oxide CeO_2 is the most stable oxide. Only at very high temperature $T \approx 2000°C$ and under sufficiently low oxygen fugacity f_{O2} Ce(III) oxide Ce_2O_3 is stable; in between several Ce(III,IV) oxides are formed (Fig. 1). $CaSc_2O_4$ ($CaFe_2O_4$ structure type, *Pnam*) is known as host material for Ce^{3+} doping, and incorporation of trivalent cerium is typically obtained by co-doping with alkalines, e.g. Na^+, $Ce^{3+} \leftrightarrow 2\ Ca^{2+}$. Unfortunately, this way is feasible only for ceramic samples: At the very high melting point of $CaSc_2O_4$ (Fig. 1) alkali atoms evaporate: Consequently charge compensation does not work.

In this study Laser Heated Pedestal Growth (LHPG) is used to melt ceramic Ce:$CaSc_2O_4$ feed rods locally. The molten zone travels through the sample, and crystallizes as single crystal of ca. 1 mm diameter (Fig. 2). The fiber length was up to 50 mm. As the melt during growth process is not in contact to any container, a wide variety of atmospheres can be used. In this study gases ranging from strongly oxidizing (20% O_2 in Ar) to strongly reducing (5% H_2 in N_2) were used.

It turned out that especially calcium and to a smaller degree cerium evaporate partially from the melt. This evaporation became obvious visually during LHPG growth under strongly reducing atmosphere, and was measured by quadrupole mass spectrometry. These experimental findings are in agreement with thermodynamic equilibrium calculations. The fibers where characterized by photoluminescence (337 nm and 450 nm excitation) and a clear dependence of the 515 nm emission peak on growth atmosphere was found, revealing the efficiency of Ce^{3+} formation. First Differential Thermal Analysis (DTA) measurements up to the melting point of $CaSc_2O_4$ gave information on the CaO-Sc_2O_3 phase diagram that is not yet published.

Literature: Philippen et al., J. Crystal Growth, *in press*.

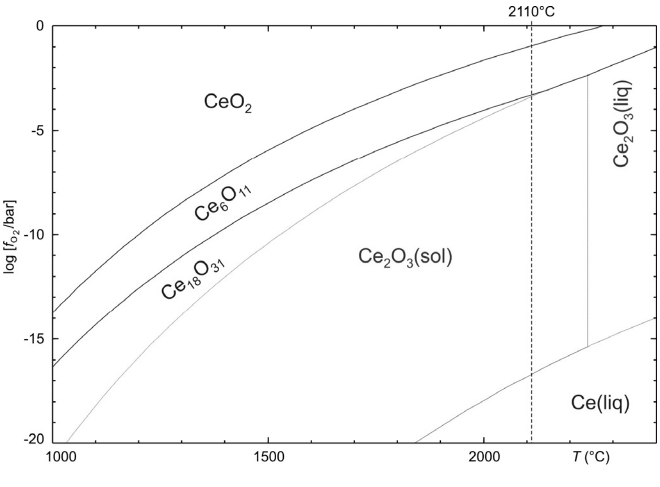

Fig. 1: Predominance diagram $f_{O2}(T)$ for the system Ce-O_2. The vertical line at $T = 2110$°C marks the melting point of $CaSc_2O_4$.

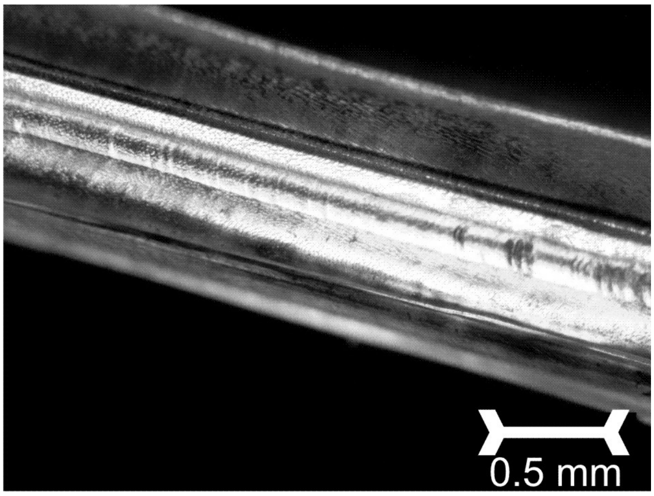

Fig. 2: Ce^{3+}:$CaSc_2O_4$ LHPG fiber.

MS13-T06

Oxygen-driven competition between structural types in Sr_3CoRuO_{6+x} and Sr_3CoIrO_{6+x} systems

D. Mikhailova[1], P. Reichel[1], A. A. Tsirlin[1], M. P. Schmidt[1], L. H. Tjeng[1]
[1]*MPI CPfS, Dresden, Germany*

Two different structural types exist in the Sr_3CoMO_{6+x} systems (M = Ru, Ir) depending on the oxygen stoichiometry: the one-dimensional K_4CdCl_6-type structure with the Co, M cation ordering at low x (denoted as 1D-Sr_3CoMO_{6+x}), and the Ruddlesden-Popper-type structure $A_{n+1}B_nO_{3n+1}$ (n = 2) with a random distribution of Co and M cations (denoted as RP-Sr_3CoMO_{6+x}). The driving force for the formation of one or the other structure is the difference in the ionic radii of Co and M. In the one-dimensional structures (Fig.1), the size difference between Co^{2+} (HS) and M^{4+} (LS) leads to the cation ordering. The Co ions have an unusual prismatic coordination of oxygen atoms; whereas M ions occupy the oxygen octahedra. Additional oxygen atoms presumably oxidize Co atoms toward Co^{3+}, thus resulting in the smaller size difference between Co^{3+} and M^{4+} and, therefore, in the mixed occupancy of both cation sites. In the Ruddlesden-Popper-type structures, both cations, Co and M, have the octahedral oxygen coordination, see Fig.2.

One-dimensional compounds have a very complicated magnetic behavior. For example, 1D-Sr_3CoIrO_{6+x} has two characteristic temperatures, $T_1 = 90$ K and $T_2 = 25$ K, that correspond to the spin freezing below T_2, an intermediate temperature region ($T_2 < T < T_1$) with field-induced magnetic transitions, and the paramagnetic region above T_1 [1]. The Ruddlesden-Popper-type compounds are antiferromagnetic: Sr_3CoIrO_{6+x} and Sr_3CoRuO_{6+x} order below 50 K and 150 K, respectively.

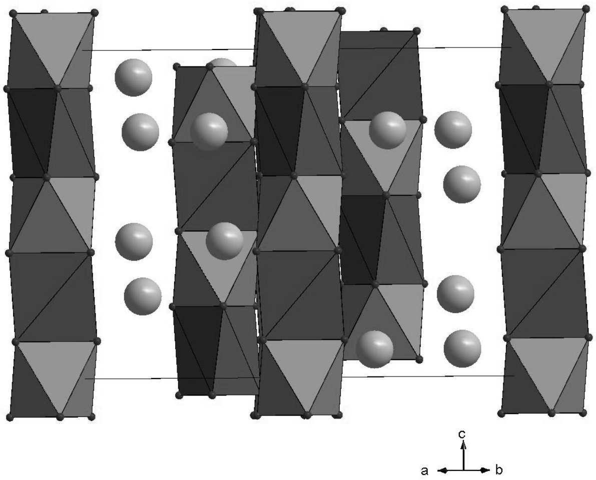

Figure 1. Crystalstructure of 1D-Sr_3CoIrO_{6+x} (R-3c). One-dimensional chains along the c-direction consist of alternating face-sharing CoO_6 trigonal prisms and IrO_6 octahedra (left). Grey spheres are Sr atoms.

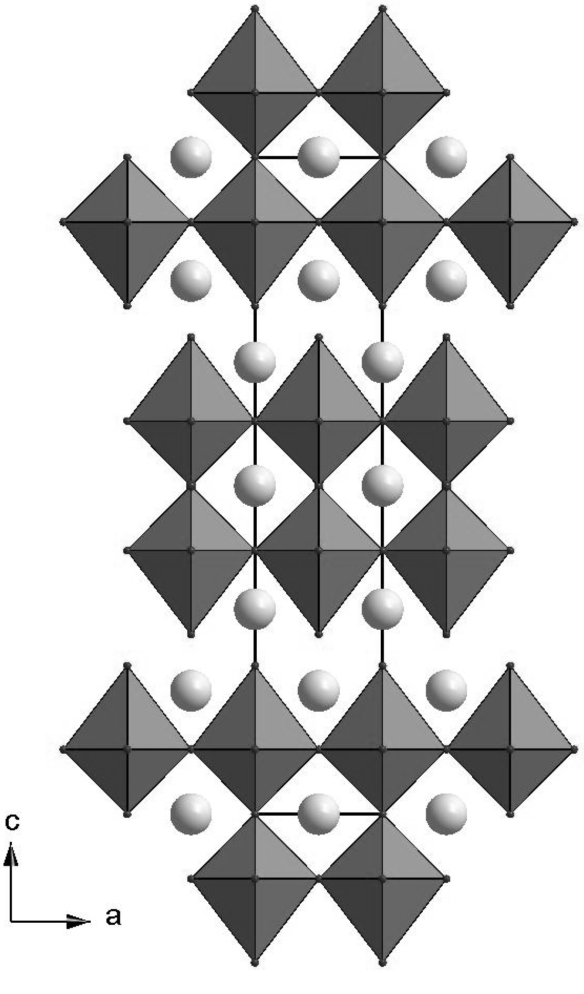

Figure 2. Crystalstructure of RP-Sr_3CoIrO_{6+x} (*I*4/*mmm*). $(Co,Ir)O_6$ octahedra are corner-sharing. Grey spheres are Sr atoms.

[1] D. Mikhailova, B. Schwarz, A. Senyshyn, A. M. T. Bell, Y. Skourski, H. Ehrenberg, A. A. Tsirlin, S. Agrestini, M. Rotter, P. Reichel, J. M. Chen, Z. Hu, Z. M. Li, Z. F. Li, L. H. Tjeng, *Phys. Rev. B.* **86** (2012) 134409.

MS14 – Crystallography: History, Art, Cultural Heritage, Teaching and Public Communication

MS14-T01

Non-destructive elemental analysis of Mughal silver coins without using X-ray Fluorescence

P. Dasgupta[1], A. Dutta[2]
[1]*Indian Association for the Cultivation of Science, Central Scientific Services, Kolkata, India*
[2]*Chandernagore Govt. College, Economics, Chandarnagore, India*

Aurangzeb was the last mighty Mughal (a dynasty that ruled India between 1526-1857 AD.) emperor ,who ruled India during 1658-1707 AD. Chemical constituents of two silver coins struck from Surat mint during the 24th and 41st reginal year of Aurangzeb were first qualitatively identified from their respective XRD diagrams. Phases identified were metallic silver(Ag),α-Ag-Cd (solid solution of silver and cadmium), traces of metallic cadmium (precipitated) and silver oxide(Ag_2O). The elemental composition of the coins were obtained from EDX studies. Quantitative phase analysis of coins using Rietveld refinement (taking only silver and cadmium into consideration) [1] reveal that only a small amount of metallic cadmium has precipitated from the solid solution of Ag and Cd. The elemental compositions of these two coins were further corroborated from the measurement of densitiy, electrical resistivity and Rockwell hardness of these two coins. Both the coins were found to be made of an alloy of ~ 5 weight % of cadmium and ~ 95 weight % of silver.

Authors also tried to trace the origin of silver used in Surat mint in terms impurities present or absent.

Comparison of minting techniques used to strike these two coins was done in terms of relative broadening of instrumental contribution corrected XRD lines of silver.

Photograph of obverse side of two coins under study.

Reference:

[1]B.L.Bish & S.A. Howard , J.Appl.Cryst.(1988),vol-21,p-86-91

Fig 1a

MS14-T02

Colouring agents in medieval glazes characterized by μ-XRD^2 and electron microprobe

R. Gradmann[1], C. Berthold[2], J. Badr[3], U. Schuessler[1]
[1]*Institute for Geography and Geology, Geodynamic and Geomaterialscience, Wuerzburg, Germany*
[2]*Applied Mineralogy, Geoscience, Tuebingen, Germany*
[3]*Institute of Conservation Science, Bamberg, Germany*

The monuments of medieval Islamic culture impress with their lavish tile decoration and brilliant colours of tiles glazing. The technique of colouring glazes combines on the one hand integrating transition metal oxides into the silicate network and on the other hand crystalline particles, which are either added as small grained agents or recrystallized in the cooling melt (1, 2). It is still a big challenge to determine not only the chemical composition but also the phase content of the very fine particles in the glaze to get therefore more information about the ancient colouring methods. Typically this is done by electron microprobe analysis to characterize the local chemical composition of the glaze and also the particles. But from only this chemical information a mineral identification is often hindered. Locally resolved X-ray diffraction with a 2-dimensional detector (μ-XRD^2) is nowadays a tool to characterize the phase content of samples with a local resolution down to several 10μm.

The locally resolved mean elementary concentration in the glazes is measured with a wavelength dispersive electron microprobe as far down as about 500 ppm depending on the element with a local resolution in the μm-range. The problem of sodium migration in electron microprobe analysis of glasses can be tackled with a defocused electron beam and an enhanced scan area (3). In contrast, the measurement of the pigment particles, especially when partially molten or recrystallized is difficult with respect to the very small grain size in the μm-range, even with a highly focussed electron beam. Again μ-XRD^2 is the appropriate method to yield this information: It is able to detect crystalline particles of less than 200 nm size and is sensitive only close to the surface, which is essential for glaze analysis by excluding the influence of underlying ceramics. The large 2-dimensional Bruker VÅNTEC500 detector in our actual setup covering app. 40° 2θ and 40°ψ allows us to distinguish directly between fine dispersed particles with their typical diffraction rings and large isolated single crystal particles, showing single crystal spots in the detector image (Fig. 1). Additionally, a modern μ-XRD^2-setup with a combination of focussing X-ray optics and 2D-detector gives nowadays the opportunity to characterize crystalline phases with spot sizes down to app. 50μm in a laboratory setup (4).

We will show in our presentation that μ-XRD equipped with a large 2-dimensional detector (μ-XRD^2) meanwhile is an easy to handle and non-destructive method which complements the electron microprobe analysis and gives further important information about the mineralogy and also the distribution of the colouring particles. Together with electron microprobe analyses and the BSE-pictures, we receive a comprehensive picture of the glazes composition.

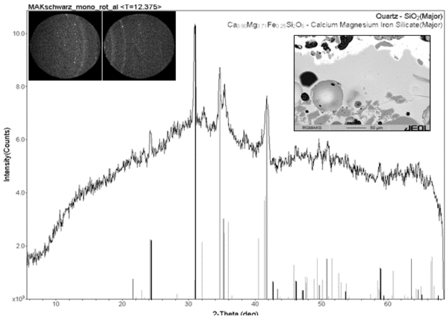

Figure 1: *Diffraction pattern of a black glaze from the Madrasa Abdul Aziz Khan in Bukhara, Uzbekistan. The left picture shows the two detector frames with the diffraction rings of fine dispersed agents and the intense spots of single crystal signals. The single crystal spots are from the coarser quartz grains, which are used as whitening or stabilization material (5), and diffraction rings are from fine dispersed clinopyroxene crystallites. The background curve is dominated by diffuse scattering of the glassy matrix of the glaze. The intensities of the Quartz reflections in the calculated pattern from the detector images are influenced by the bad crystallite statistics of the coarse crystallites in the analysed area (X-ray beam diameter app. 300µm) and therefore not representative. The right picture shows the back-scattered-electron image of electron microprobe with the different µm-scaled particles.*

Literature:
(1) Henderson, J. *The Raw Materials of early Glass Production.* Oxford Journal of Archaeology, 1985. **4**(3): p.267-291
(2) Molera, J., Pradell T., Salvado N., Vendrell-Saz M., *Evidence of Tin Oxide Recrystallization in Opacified Lead Glazes*, Journal of the American Ceramic Society, 1999 **82**(10): p.2871–75
(3) Shugar, A., Rehren, T., *Formation and composition of glass as a function of firing temperature*, Glass Technology, (2002) **43C:** p.145-50
(4) Berthold, C., A. Bjeoumikhov, and L. Brügemann, *Fast XRD² Microdiffraction with Focusing X-Ray Microlenses.* Particle & Particle Systems Characterization, 2009. **26**(3): p. 107-111.
(5) Vandiver P.B., Vandiver A., Rakhimov Ak., Rakhimov Al., *Ishkor glazes of Usbekistan,* Conservation of Ancient Sites on the Silk Road: Proceedings of the Second International Conference of Grotto Sites (2004) p. 234-248

MS14-T03

Warum heißt Bunsenit Bunsenit - Kristallographie und Mineralogie von einst im Licht heutiger Nanoforschung

M. Petrik[1]
[1]Philipps-University Marburg, Chemistry, Marburg, Germany

Das Typmineral Bunsenit (NiO) von 1858 wird bis heute im Freiberger mineralogischen Museum aufbewahrt. Außer in Sachsen ist natürlicher Bunsenit nur noch in Südafrika vereinzelt aufgefunden worden. Wie kam dieses seltene Mineral zu seinem großen Namen? Wir beschäftigen uns in Marburg mit den besonderen magnetischen [1a], strukturellen [1b] und chemischen [1c] Eigenschaften von nanoskaligem NiO. Robert Wilhelm Bunsen (1811-1899) wirkte etwa ein Jahrzehnt lang ebenfalls in Marburg - ein historischer Zufall, der uns interessieren musste. Aber eine Durchsicht der alten Literatur ergab, dass Bunsen selbst wohl weder Bunsenit noch synthetisches NiO jemals in Händen hielt. Vielmehr war es ein außergewöhnlicher Doktorand und Habilitand von ihm, der in Marburg kristallines NiO zum ersten mal beobachtete [2]: Friedrich August Genth.

Friedrich August Genth (1820-1893) studierte in Heidelberg u.a. unter Leopold Gmelin und in Gießen bei Justus Liebig, promovierte und habilitierte sich in Marburg bei Robert Wilhelm Bunsen in der analytischen Chemie, um anschließend in die USA auszuwandern, wo er als angesehener Chemiker und Mineraloge nicht nur Gründungsmitglied, sondern auch der fünfte Präsident der „American Chemical Society“ wurde. Er entdeckte in seinem Leben über zehn neue Minerale und analysierte kristalline Kobalt-Amminkomplexe, als es die Komplexchemie noch gar nicht gab. Er war angesehener Professor für analytische Chemie an der *University of Pennsylvania* in Philadelphia, sein Wirken war aber nicht unumstritten und er wurde unter kontroversen Umständen entlassen [3].

Wir werden in diesem Beitrag neueste historische Erkenntnisse mitteilen [4], nicht nur zur Namensgebung von Bunsenit, sondern vor allem zu der Entdeckung von kristallinem NiO, kristallinen Kobalt(III)-Amminkomplexen und sogar von nanoskaligen Kobaltoxiden, welche heute wieder hochaktuell sind [5]. Auf Probleme der modernen Nano-Kristallographie [1b] und des Nano-Antiferromagnetismus (Abb. 1) [1a] wird im historischen Kontext eingegangen. Schließlich wird an unvermuteter Stelle ein Jugendbildnis von Genth neu endeckt: In der berühmten Zeichnung des Gießener Liebig-Laboratoriums von Wilhelm Trautschold (1815-1876) aus dem Jahr 1841 (Abb. 2).

[1] a) M. Petrik, B. Harbrecht, *Solid State Phenomena* **2011**, *170*, 244-247; b) M. Petrik, B. Harbrecht, *Z. Kristallogr. Proc.* **2011**, *1*, 253-258; c) M. Petrik, B. Harbrecht, *Z. Anorg. Allg. Chem.* **2012**, *638*, 1622.
[2] F. A. Genth, *Eur. J. Org. Chem.* (früher *Liebigs Annalen*) **1845**, *53*, 139-141.
[3] a) G. Jahn, B. Brill, M. Preuschoff, *Sammlungen z. Gesch. v. Wächtersbach* **1993**, *21*, Nr. 134 (100 Seiten); b) G. Jahn, *Gießener Universitätsblätter* **1994**, 47-60.
[4] M. Petrik, *Sammlungen z. Gesch. v. Wächtersbach*, **2012**, zur Publikation angenommen (34 Seiten).
[5] C. Nethravathi, S. Sen, N. Ravishankar, M. Rajamathi, C. Pietzonka, B. Harbrecht, *J. Phys. Chem. B* **2005**, *109*, 11468-11472.

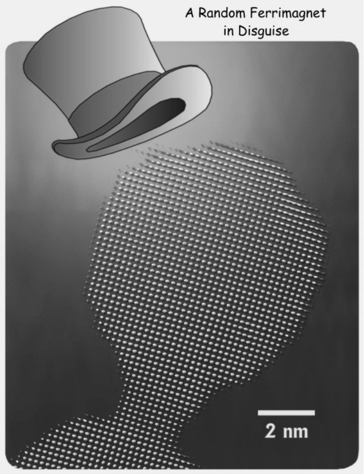

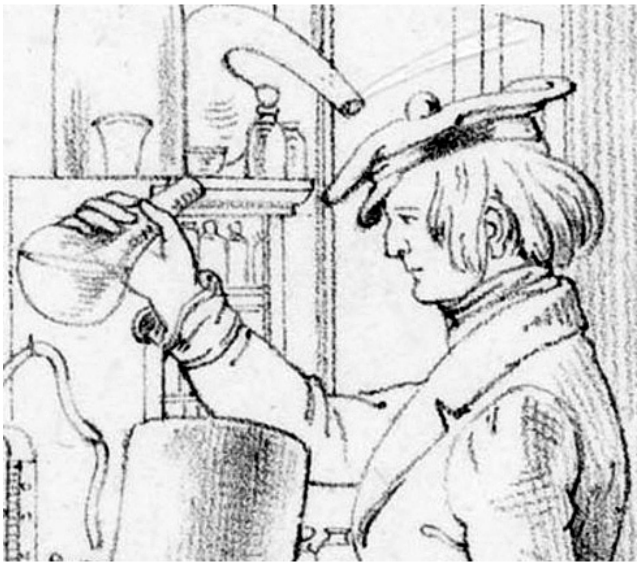

MS14-T04

Making crystallography understandable

A. Dziwetzki[1]

[1]*terra mineralia, TU Bergakademie Freiberg, Freiberg, Germany*

The terra mineralia is a permanent exhibition displaying a collection of 3500 rare and beautiful minerals, precious stones and meteorites in Freiberg/Saxony.

The exhibits are part of one of the world´s largest private collections of minerals and have been given to the TU Bergakademie Freiberg on permanent loan by Dr. Erika Pohl-Ströher. The exquisite pieces stem from sites on every continent, and as such, allow the visitor to virtually journey around the world to the world´s most beautiful minerals.

There is a special area at the exhibition dedicated to young visitors and school classes - the so called “research expedition”, where first experiences with scientific methods of mineralogy, geology and even crystallography can be made. It is here, where students of the TU Bergakademie introduce young visitors to exciting aspects of these sciences.

There is a huge range of programmes for all types of schools and classes according to the Saxonian Curriculum. Interestingly, mineralogy is fully integrated into different school subjects like geography, chemistry, astronomy or mathematics.

“Fire, Earth, Water, Air - Plato’s Solids” is for example a programme, which combines crystallography with mathematics. While learning something about special polyhedra, students discover “mathematics” not only in their classroom, but also in nature. The fascinating crystals of minerals like pyrite, fluorite, tetraedrite or even diamonds make the complicated aspects of Plato’s solids visible. With experiments and minerals to touch, mathematics and crystallography are no longer abstract subjects for the students.

The school programmes are completed by holiday activities taking place regularly. During the winter holidays we proved that even snowflakes are crystals. Crystal growing experiments like salt growing processes under the microscope were offered as well. Other examples for crystal growing were brought by experiments with melted acetylsalicylic acid which ended in wonderful little hedgehog crystals. On experiments with potash alum grown around wood we found out how the mineralisation of fossils possibly works. On the other hand the raising of 850 blue copper(II)sulphate crystals for the 850 jubilee of Freiberg was a huge fun for all guests taking part in the city celebrations.

In our new exhibition, the Mineralogical Collection Germany at the KRÜGERHAUS, a lot of space has been given to crystallography, which has a long tradition at the TU Bergakademie Freiberg. The new collection near Freudenstein Castle offers a trip to Germany´s most famous mineral localities. In the first place the exhibition targets mineral collectors and scientists, like mineralogists, geologists and even crystallographers. Experts are immediately impressed by the “gallery of crystals” because of its immense number of different crystal mock-ups on show. Their systematic order reveals itself to the visitor only at the second glance. Historical specimens witness the history of crystallography in Freiberg.

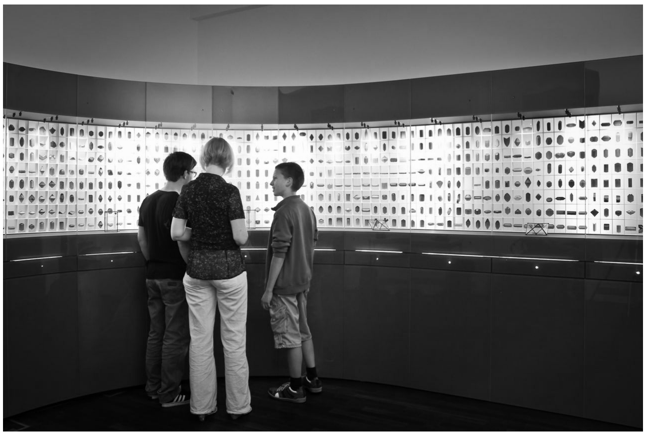

MS14-T05

Color-coded cubes: an effective and inexpensive way to display point group symmetries in 3D

G. Nolze[1]
[1]*BAM, Berlin, Germany*

The representation of crystal classes in 3D is usually linked to crystal models which either show theoretical polyeder formed by one or more {hkl} or copy the (rarely ideal) habit of single crystals of some selected minerals. Although valuable as a reflection of natural objects (not to mention aesthetically pleasing), widespread use of such models is limited by the high price of a set displaying the symmetries of all crystal classes. Moreover, the influence of the crystal metric on a crystal form distracts from the importance of the symmetry as the only true criterion for size and distribution of the asymmetric unit. A simple consequence is the confusion of cause and effect, e.g. the general definition of the cubic crystal system by the metric of the unit cell parameters in literature, which is actually a result of the symmetry and not the origin.

The presentation will demonstrate that all point group symmetries can be displayed using a cube as the projection surface, except those of the hexagonal system. The latter require a simple adaptation of cube planes so that a stacking and a space-saving storage of all polyhedra are still possible.

The asymmetric unit is demonstrated as continuous color variation, which is already applied in similar applications for inverse pole figure representations, e.g. for the crystallographic interpretation of single orientation measurements using electron diffraction.

MS15 – Biocrystallography: Synthesis, Structure and Function II

MS15-T01

Structural Basis of Assembly Chaperone-Mediated snRNP Formation

C. Grimm[1], J. Pelz[1], U. Fischer[1], N. n/a[1], N. n/a[1], N. n/a[1]
[1]*Institut für Biochemie, Würzburg, Bosnia and Herzegovina*

Small nuclear ribonucleoproteins (snRNPs) represent key constituents of major and minor spliceosomes. SnRNPs contain a common core, composed of seven Sm proteins bound to snRNA, which forms in a step-wise and factor mediated reaction. The assembly chaperone pICln initially mediates the formation of an otherwise unstable pentameric Sm-protein unit. This so-called 6S complex docks subsequently onto the SMN-complex, which removes pICln and enables the transfer of pre-assembled Sm proteins onto snRNA. We present two crystal structures that allow a glimpse into the mode of action of the snRNP assemby line. The 6S complex structure identifies pICln as an Sm-protein mimic, which enables the topological organization of the Sm pentamer in a closed ring. A second structure of 6S bound to the SMN-complex components SMN and Gemin2 uncovers a plausible mechanism of pICln elimination and Sm protein activation for snRNA binding.

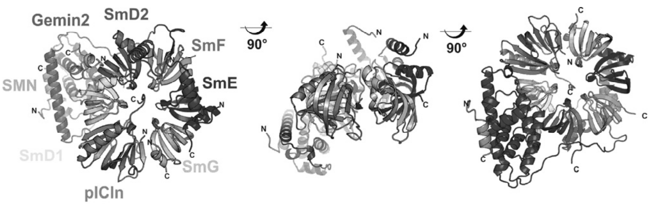

Structure of the 8S Spliceosomal Assembly Intermediate

MS15-T02

Structure of the viral effector protein IE1 from cytomegalovirus

S. Klingl[1], M. Scherer[2], T. Stamminger[2], Y. A. Muller[1]
[1]*FAU Erlangen-Nürnberg, Lehrstuhl für Biotechnik, Erlangen, Germany*
[2]*FAU Erlangen-Nürnberg, Klinische und Molekulare Virologie, Erlangen, Germany*

Human cytomegalovirus (HCMV) infections are a threat to immunocompromised patients and prenatal or postnatal infected infants. One of the first and strongly expressed proteins of HCMV is the immediate-early protein 1 (IE1), which is primarily detectable in the nucleus of the host cell. [1]

Besides a transactivation activity, IE1 is an antagonist of the antiviral functions mediated by a cellular subnuclear structure referred to as nuclear domain 10 (ND10). IE1 is able to induce disruption and dislocation of the ND10 structures upon binding. However the molecular mechanisms of this process remain so far elusive. [2, 3, 4] (Figure 1)

Structural information for the IE1 protein has not been available so far. We purified IE1 protein from different species and identified stably folded core fragments suitable for crystallization. After chemical modification we obtained crystals of IE1 from rhesus macaque CMV that initially diffracted to ~ 3 Å. The resolution was enhanced to 2.3 Å by controlled dehydration using the HC1c crystal humidifier at the BESSY-II synchrotron facility.

The crystal structure reveals a dimer of two elongated mainly alpha-helical molecules. Now we attempt to elucidate the structure-function relations of the protein by structure-guided mutations and bioinformatics to get insights into the molecular mechanism that drive ND10 disruption.

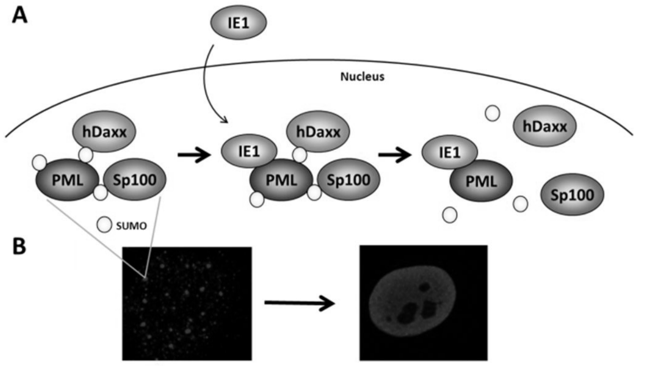

Figure 1 - Disruption of ND10 domains by CMV IE1. (A) Four of the main components of ND10 domains are depicted. The interaction of IE1 with PML leads to de-SUMOylation of PML and disruption of the ND10 structure. (B) Immunofluorescence microscopy images stained against PML illustrate intact ND10s inside the nucleus (left image) and dispersed ones after IE1 expression (right image).

References

- Castillo, J. P. at al. “Human cytomegalovirus immediate early proteins and cell growth control.” Gene, 2002, 290, 19-34
- Korioth, F. et al. (1996) "The nuclear domain 10 (ND10) is disrupted by the human cytomegalovirus gene product IE1." Exp Cell Res, 1996, 229, 155-158
- ADDIN EN.REFLIST Ahn, J. H et al. (1998) "Disruption of PML subnuclear domains by the acidic IE1 protein of human cytomegalovirus is mediated through interaction with PML and may modulate a RING finger-dependent cryptic transactivator function of PML." Mol Cell Biol, 1998, 18, 4899-4913
- Tavalai, N. & Stamminger, T. "Intrinsic cellular defense mechanisms targeting human cytomegalovirus." Virus Res, 2011, 157, 128-133

MS15-T03

Structure of ADP•AlF_3-Stabilized Dark-Operative Protochlorophyllide Oxidoreductase Complex

J. Krausze[1], C. Lange[2], J. Moser[2], D. Heinz[1]
[1]*Helmholtz Center for Infection Research, Molecular Structural Biology, Braunschweig, Germany*
[2]*Technische Universität Braunschweig, Institut für Mikrobiologie, Braunschweig, Gabon*

The capture of the global energy demand vitally depends on the bio-synthesis of chlorophylls, a process yielding six billion metric tons of these compounds annually. The second-last step of this process is the stereo-specific reduction of the C17-C18 double bond in ring D of protochlorophyllide *a* (Pchlide), which results the architecture of the central ring system common to all chlorophylls. This reduction goes along with a change of the absorption properties that provides the basis for light harvesting and energy transduction processes of photosynthesis. Two completely unrelated enzymes have evolved for the two-electron reduction of Pchlide: a monomeric, light-dependent system and the dark operative protochlorophyllide oxidoreductase (DPOR). The latter is found in photosynthetic bacteria, cyanobacteria, algae, and gymnosperms and shows an architecture and mechanism similar to that of nitrogenase. Like nitrogenase, DPOR is a metalloprotein composed of three subunits, termed L, N, and B, and assembles as a transient octamer of the form $(L_2)_2(NB)_2$. The homodimeric L_2 sub-complex shares about 30% amino acid sequence identity with the Fe-protein NifH of nitrogenase. Like NifH, it contains a [4Fe-4S] cluster and exhibits ATPase activity. Driven through ATP hydrolysis, L_2 transfers one electron per hydrolyzed ATP to the heterotetrameric sub-complex $(NB)_2$, which constitutes the actual oxidoreductase. $(NB)_2$ shares about 15% sequence identity with the nitrogenase proteins NifD and NifK and, in contrast to its nitrogenase counterpart, contains two [4Fe-4S] instead of [8Fe-7S]clusters.

We crystallized and solved the structure of the DPOR octamer from *Prochlorococcus marinus* in complex with Pchlide with DPOR being trapped in the intermediate state of ATP hydrolysis through the presence of ADP•AlF_3 [1]. Our analysis permits a thorough investigation of the dynamic interplay between L_2 and $(NB)_2$. Upon complex formation, substantial ATP-dependent conformational rearrangements of L_2 trigger the protein-protein interactions with $(NB)_2$ as well as the electron transduction between the two redox-active [4Fe-4S] clusters and the substrate. The catalytic differences and similarities between DPOR and nitrogenase have broad implications for the mechanism of energy transduction of related multi-protein complexes that are involved in the reduction of chemically stable double- or triple-bonds.

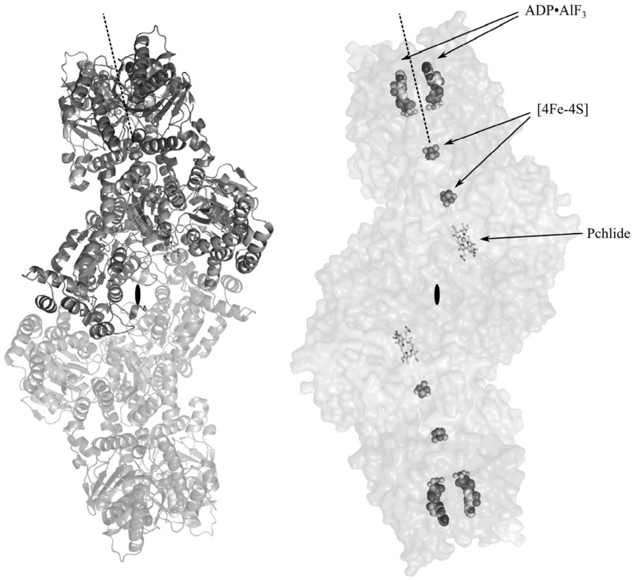

Fig. 1: Quarternary structure of the quarternary DPOR complex $(L_2)_2(NB)_2$ with ADP•AlF3 and Pchlide bound,

[1] J. Moser, C. Lange, J. Krausze, J. Rebelein, W.-D. Schubert, M.W. Ribbe, D.W. Heinz, D. Jahn. Structure of ADP•AlF_3-Stabilized Protochlorophyllide Oxidoreductase Complex. PNAS. In press.

MS15-T04

Structure of a *Helicobacter pylori* type IV secretion protein with an unusual RGD motif

S. Barden[1], H. Niemann[1]
[1]*Universität Bielefeld, Fak. für Chemie, Bielefeld, Germany*

Helicobacter pylori, a Gram-negative human pathogen, can cause gastric ulcers and stomach cancer and was rated a class I carcinogen by the World Health Organization (WHO). The virulence of *H. pylori* is closely linked to a type IV secretion system (T4SS).

Type IV secretion systems are macromolecular assemblies resembling a syringe for the transport of cargo, e.g. effector proteins, across the bacterial envelope. They consist of a core complex spanning both membranes, associated ATP-ases that provide the energy for translocation, and an extracellular pilus that makes contact with the host cell. The pilus, consists of a major component polymerizing into a hollow tube and a minor component associated with the pilus surface and thought to establish contact with the target cell. In the case of *H. pylori*, the protein CagL represents this minor component.

On the host cell side, integrins were shown to be important for effector translocation. CagL is the only *H. plyori* T4SS protein that contains an Arg-Gly-Asp (RGD) tripeptide, which is a widespread integrin-binding motif. RGD motifs are present in proteins of the extracellular matrix but also employed by pathogens. Therefore, CagL was suspected and also shown to bind to α5β1 integrins in an RGD dependent manner [1]. While the importance of both CagL and integrins for effector translocation is commonly accepted, the RGD-dependent binding of CagL to integrins is heavily disputed [2].

In order to illuminate the molecular function of CagL and also its evolutionary relation to other T4SS proteins, we determined its crystal structure. Strategies to overcome problems of crystallization and structure determination will be discussed. We find that the structure of CagL is apparently not related to that of the minor pilus component in other T4SSs. Thus, CagL appears to be a protein specific to *H. pylori*.

All integrin-binding RGD motifs that have been structurally characterized so far are located in an extended or flexible loop. In contrast, the RGD motif of CagL is embedded in a long helix. Using cellular assays we could confirm that the RGD motif of CagL is required for cell adhesion, suggesting that most likely it will be involved in binding of integrins. Functional implications of this unexpected finding will be discussed.

References

1. Kwok T., Zabler D., Urman S., Rohde M., Hartig R., Wessler S., Misselwitz R., Berger J., Sewald N., König W., Backert S. (2007) Nature 449(7164), 862

2. Jiménez-Soto L.F., Kutter S., Sewald X., Ertl C., Weiss E., Kapp U., Rohde M., Pirch T., Jung K., Retta S.F., Terradot L., Fischer W., Haas R. (2009) PLoS Pathog. 5(12):e1000684

MS16 - Biocrystallography: Biomimetic Materials, Drug Design, Processes and Functions

MS16-T01

Lattice energy calculation - a quick tool for screening of stability and relative solubility of cocrystals.

L. Kuleshova[1,2], D. Hofmann[1,2]
[1]*CRS4, Biomedicine, Pula, Italy*
[2]*FlexCryst, Uttenreuth, Germany, Italy*

Cocrystals (or multicomponent crystals) have other physico-chemical properties, than pure crystals of one of the components. This is of large interest for drug developments, since the desired properties, e.g. solubility, stability, bioavailability, can be tailored by binding of two substances in a single crystal without chemical modification of an active component (API). Here, with the aim to find a feasible approach for *in silico* screening of pharmaceutical cocrystals, *FlexCryst* program suit, implemented with Data Mining Force Field have been used. The very quick algorithm of *FlexCryst* allows to predict correctly the typical hydrogen bonded motives (synthons) and to estimate properly (within +/- 2 kJ) the free energy of crystal lattice. The approach for a screening of cocrystals bases on the simple thermodynamic arguments that a cocrystal can be formed, if its total free lattice energy (G_{CC}) is lower than the sum of lattice energies of pure components: $-G_{CC} > -(G_{API}+G_{CF})$.

The free energy of cocrystals G_{CC} and the pure components G_{API} and G_{CF} have been calculated for two class of cocrystals: cocrystals of flavonoids and cocrystals of caffeine. Both substances are able to form extended systems of intermolecular hydrogen bonds. This ability is recognizedcurrently as one of the most important prerequisite for co-crystal formation. In the same time the flavonoids are known for the reason of difficulties in experimental formulation of their cocrystals The caffeine, vice versa, forms cocrystals relatively easily: for the moment the large amount of cocrystals is formulated and their crystal structures are known. The reasons of different behavior are discussed in terms of stability and solubility of pure components.

The analysis of experimental and calculated data were performed. It was found that present state of art of energy function of *FlexCryst* allows a very good correlation between free energy of experimental and predicted crystal energy for both class of cocrystals (Fig.1) and results in 80- 85% of successful predictions. The values $\Delta G = G_{cryst\_API} + G_{cryst\_CF} - G_{cryst\_CC}$, can be used as indication for probability of cocrystal formation. Taking into account that for the case of simple dissolution, solubility constant, Ks, depends on the balance between two kinds of interactions: G_{hydr} (how strongly the molecule associates with the solvent) and G_{cryst} (how tightly the molecule is bound to its own crystal lattice) , the values ΔG open the excellent opportunity to estimate also the relative solubility of cocrystals. These findings will allow to restrict experimental trials for cocrystallisation only with the "best" coformers admitting better probability of cocrystal formation with improved API solubility.

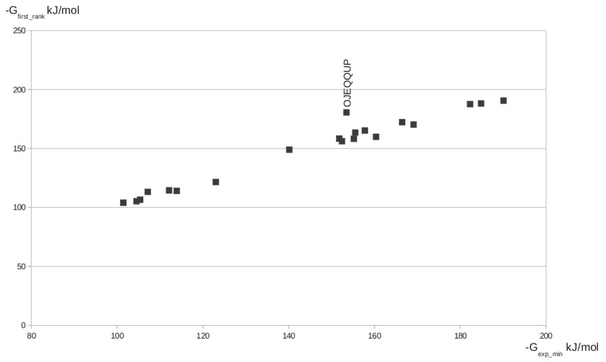

Figure 1. The correlation between experimental and calculated values of free energy of crystal lattices.

MS16-T02

Solubility Prediction by Crystal Structure Prediction with Force Fields obtained by Data Mining on experimental Crystal Structures

D. W. M. Hofmann[1,2], L. N. Kuleshova[1,2]
[1]*CRS4, Biomedicine, Pula, Italy*
[2]*FlexCryst, Uttenreuth, Italy*

The solubility is one of the crucial properties of drugs. From the thermodynamic point of view the prediction of the solubility is simple. The free energy of the drug must be equal in the crystal and in the solution. In fact it is a tremendous theoretical problem. The free energy includes effects of temperature and pressure. However, quantum-mechanics gives a priori the enthalpy and the effect of temperature and pressure has to be added in elaborated calculations.

Here we would like to show a simple way for the prediction of the free energy for the crystal and the prediction of the solubility, if the hydration energy is known. Data Mining Force Fields (DMFF) can fulfil this task very quickly and accurate. The basic idea of data mining on crystal structures is that any crystal structure is a global minimum in the free energy. The force field is obtained by optimization of the parameters, till it assigns always to the experimental structure lower energy as to virtual crystal structures produced during crystal structure prediction. A general description about the method can be found in the recently published textbook "Data mining in Crystallography" [1] and more specific for the investigation of the isotopic effect in a recent publication [2].

The free energy of the molecule in the crystal can be easily estimated by a crystal structure prediction with the data mining force field. The lowest energy of the predicted polymorphs corresponds to the free energy. This is even true, if the predicted crystal structure does not coincide with the experimental crystal structure. In this case commonly another polymorph is predicted with a very similar energy and the error in prediction of the free energy is small. We performed a crystal structure prediction for all 30 drugs, where we did find accurate values for the free energy of hydration. A plot of the free reaction energy ΔG versus the solubility log(S) shows a very high correlation with a coefficient of determination of 0.92. The linear regression holds over a range of 14 magnitudes of solubility.

References
[1] Data Mining in Crystallography, ed. D.W.M. Hofmann and L.N. Kuleshova, Structure & Bonding, Vol. 134, Springer Verlag 2010.
[2] A. Kupka, V. Vasylyeva, D. W. M. Hofmann, K. Merz, Crystal Growth & Design, 2012

Figure Legends

- Correlation between predicted reaction energy and experimental solubility

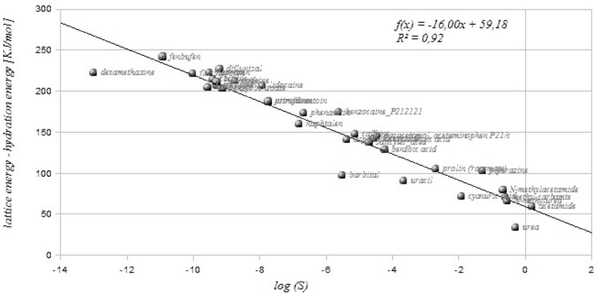

MS16-T03

Electron Densities of Bexarotene and Disila-Bexarotene from Invariom Application: A Comparative Study.

P. Luger[1], M. Weber[1], C. Hübschle[1], R. Tacke[1]
[1]*Institute for Chemistry FU Berlin, Bio-Che-Pha, Berlin, Germany*

From an application of the invariom formalism, which provides aspherical atomic scattering factors, the electron densities of the RXR-selective retinoid agonists bexarotene (**1a**) and disila-bexarotene (**1b**) were derived from their known low resolution (d=0.76 Å) crystal structures. The density distributions allowed a comparison of the electronic properties of these pharmacologically relevant compounds. Differences were found to be restricted to relatively small regions in the terminal six-membered rings of the tetrahydronaphthalene and tetrahydrodisilanaphthalene fragments, which is clearly indicated by the electrostatic difference potential. In total, the replacement of two carbon atoms in **1a** by silicon atoms (→ **1b**) does neither influence the electronic structures nor the pharmacological properties (RXR receptor activation) significantly. It should be noted that the almost completely software supported invariom formalism can yield electronic information for biologically interacting systems with moderate effort. This offers interesting possibilities for drug research, in that steric and electronic information can be combined for the analysis of intermolecular recognition and interaction on an atomic scale. This approach is also valuable for the design and development of silicon-containing drugs using the carbon/silicon switch strategy.

[1] C. B. Hübschle, P. Luger, *J. Appl. Crystallogr.*, **2006**, *39*, 901-904.

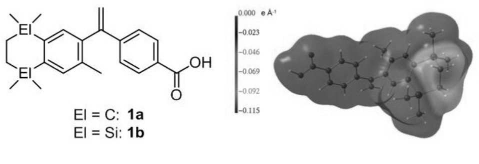

Fig. 1. Formulae of the title compounds and electrostatic difference potential disila-bexarotene/bexarotene, MOLISO representation [1]

MS16-T04

Gypsum - cellulose composites with improved material properties leading to a new low-cost building material

F. NINDIYASARI[1], E. GRIESSHABER[1], T. ZIMMERMAN[2], T. BECHTOLD[3], C. RANDOW[4], L. FERNANDEZ-DIAZ[5], C. FLECK[4], W. W. SCHMAHL[1]
[1]*Ludwig-Maximilians-Universität, Department für Geo- und Umweltwissenschaften, München, Germany*
[2]*Swiss Federal laboratories for Material Testing and Research (Empa), Dübendorf, Switzerland*
[3]*University of Innsbruck, Laboratory for Textile and Fibre Chemistry in Cellulosics, Research Institute for Textil Chemistry and Textile Physics, Dornbirn, Austria*
[4]*Technische Universität Berlin, Department of Material Engineering, Berlin, Germany*
[5]*Universidad Complutense, Department of Crystallography and Mineralogy, Madrid, Spain*

We synthesized cellulose - gypsum - alginate composites and investigated their interlinkeage as well as material quality with mechanical testing experiments, SEM, TEM and X-ray diffractometry. We used five different cellulose materials characterised by distinct particle sizes and morphology. A water/hemihydrate ratio of 0.5 produced the composites. The total amount of organics (the mixture of cellulose/alginate) was 2.5 wt. %.

Pure gypsum was used as the reference (Fig.1). While pure gypsum has a compressive and bending strength and E-modulus of 9.60±0.96 MPa, 4.77±0.93 MPa, 4.02±0.56 GPa, respectively, composites with the cellulose arbocel UFC100 and alginate give slightly higher bending and compressive strength values whereas the composites of nanofibril cellulose and alginate are decreased in bending and compressive strength (Figs.1a, 1b). In comparison to the pure gypsum end-member the composite gypsum-alginate-lyocell shows an increased E-modulus, whereas nanofibril cellulose - alginate composites have a lower E-modulus (Fig.1c). We observed thatgypsum crystals grew on arbocel cellulose B400 and lyocell cellulose fibre surfaces but not on nanofibril cellulose fibres and particles. Thus, since lyocell fibres are characterized by a high tensile strength, their addition increased the E-modulus of the composites. We found that cellulose acts as a retarding agent by absorbing the surface of the growing gypsum crystals. The crystal growth mechanism of gypsum in the presence of cellulose follows the Ostwald-ripening process.

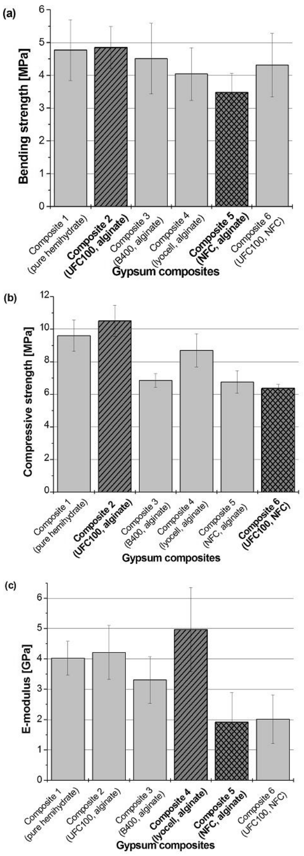

Figure 1. Material properties of the pure gypsum end-member and the investigated cellulose - gypsum composites.

MS17 - Materials for Electronics: Energy and Data Storage through the Eyes of Crystallographers

MS17-T02

A high time resolved and flexible synchrotron powder diffraction setup for the *in situ* structural investigation of electrode materials in rechargeable batteries.

M. Herklotz[1,2], F. Scheiba[3,1], M. Hinterstein[2,4], A.- C. Dippel[4], J. Eckert[1,2], H. Ehrenberg[3,1]
[1]*IFW Dresden, IKM, Chemie komplexer Materialien, Dresden, Germany*
[2]*TU Dresden, Institut für Werkstoffwissenschaft, Dresden, Germany*
[3]*KIT Karlsruhe, Institut für Angewandte Materialien (IAM), Karlsruhe, Germany*
[4]*DESY Hamburg, Hasylab, Hamburg, Germany*

In situ or also called *in operando* techniques are indispensable for the characterization of energy storage systems like lithium ion batteries. A large number of *in situ* spectroscopic, *in situ* microscopic and *in situ* diffraction setups have been developed and offer a detailed surface or bulk analysis of the involved materials [1].

In situ powder diffraction studies using synchrotron radiation sources in combination with 2D detectors enable a detailed and time resolved investigation of structural phenomena. It has been reported that diffraction patterns with markedly good statistics can be obtained from an *in situ* cell within two minutes [2]. In dependence on the used electrode material and the set current hundreds of patterns per charge or discharge cycle respectively can be observed. The evolution of lattice parameters, microstructure, phase transformations and atomic positions can be determined which makes the analysis of limiting or fatigue processes of battery materials possible.

The research development in a wide field of new electrode materials [3] raises the need for more flexible and faster *in situ* techniques. Even a time resolution in the range of minutes can become insufficient if high current experiments are carried out, where a full charge or discharge cycle takes less than half an hour.

A new *in situ* setup at P02.1 - a 60 keV beamline at the storage ring PETRA III in Hamburg, Germany is presented [4]. An overview about crucial parameters like signal to noise ratio, background contributions of different cell parts and time per diffraction pattern is given. The latter can be reduced to the region of seconds which offers the possibility of high throughput experiments by the use of multiple cell holders. By varying the distance of the 2D Perkin Elmer detector either high q-range or high instrumental resolution can be achieved (figure 1).

The outstanding performance of P02.1 is exemplified by *in situ* powder diffraction results of the high voltage cathode material $Li_3Cr_2(PO_4)_3$ with a low symmetric monoclinic structure [5] .The limitations of the electrochemical performance are related to structural phenomena like anisotropic lattice parameter changes (figure 2) or distortions of the atomic structure.

The Bundesministerium für Bildung und Forschung is gratefully acknowledged for financially supporting this work within the HE-Lion consortium and grant no. 05K10ODA.

[1] Amalraj, S. F. & Aurbach, D., *Journal of Solid State Electrochemistry* **15**, 877-890 (2011).
[2] Conry, T., Mehta, A., Cabana, J. & Doeff, M., *Chem. Mater.* **24**, 3307-3317 (2012).
[3] Whittingham, M. S., *Proceedings of the IEEE* **100**, 1518-1534 (2012).
[4] Herklotz, M., Scheiba, F., Nikolowski, K., *et al.*, *to be published in Journal of Synchrotron Radiation* (2013).
[5] Herklotz, M., Scheiba, F., Mosymow, E., *et al.*, *in preperation*

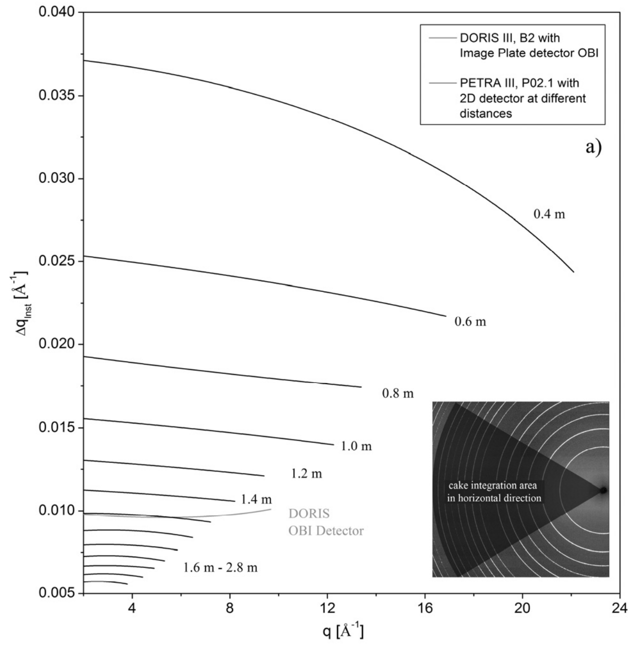

Figure 1: instrumental resolution, quantified by a refinement of Caglioti parameters

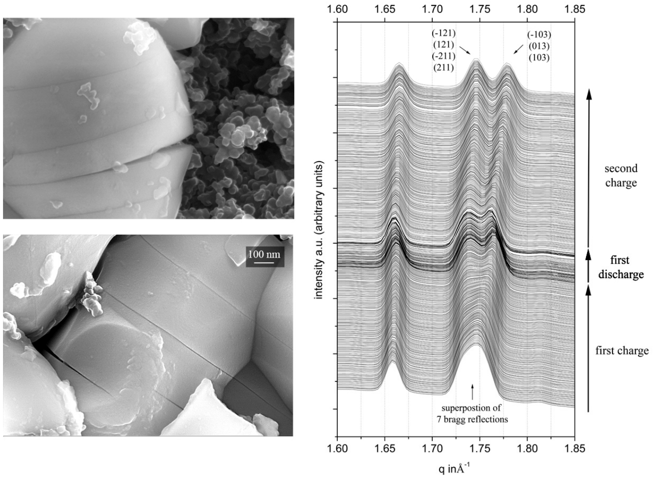

Figure 2: *ex situ* SEM images of the $Li_3Cr_2(PO_4)_3$ cathode composite after charging, where characteristic crack propagation is visible, right: chosen region of the *in situ* diffraction patterns - a separation of bragg reflections is visible

MS17-T03
Structural and magnetic properties of compounds $(Ge_{1-x}TM_xTe)_nSb_2Te_3$ (TM = Cr, Mn, Fe)

S. Welzmiller[1], A. Dorn[1], P. Huth[1], T. Faske[1], F. Schleife[1], B. Kersting[1], O. Oeckler[1]
[1]*Leipzig University, Chemistry and Mineralogy, Leipzig, Germany*

Most phase-change materials (PCMs) for data storage, e. g. GST (Ge/Sb/Te) or AIST (Ag/In/Sb/Te) contain no transition metals (TM). The metastable crystalline phase of GST materials corresponds to a rocksalt-type high temperature phase. The stable ambient-temperature phase is layered and contains rocksalt-type blocks divided by van der Waals gaps. Quenching bulk material of the high-temperature phase yields pseudocubic domain crystals with partial defect ordering which also have interesting thermoelectric properties.[1] Doping PCMs with TM may yield materials where the phase-change is associated with a change of the magnetic properties as shown for Fe-doped GST thin films.[2,3] First principle calculations suggest that various substitutions with 3d TM should be possible and may be used to tune the properties in a wide range.[4] However, there are very few crystallographic data for TM containing PCMs. Their thermoelectric properties might further be influenced by the so-called magneto-Seebeck effect if the magnetic ordering changes.[5]

Fe-Se-Te compounds, on the other hand, have raised attention because of their magnetic and superconducting properties. We prepared TM containing GST phases by melting stoichiometric mixtures of elements and obtained $Ge_{0.9}Cr_{0.1}Sb_2Te_4$, $Ge_3MnSb_2Te_7$ and $Ge_{0.9}Fe_{0.1}Sb_2Te_2Se_2$. The compositions were confirmed by EDX.

$Ge_{0.9}Cr_{0.1}Sb_2Te_4$ forms a 21*R-type* structure (*R*-3*m*, a = 4.23569(6) Å, c = 41.1058(11) Å) with 3 cation and 4 anion layers per rocksalt-type slab. The Cr atoms thus formally exhibit the unusual valence state +II. SQUID measurements show ferromagnetic ordering at low temperatures (~22 K). At 2 K, there is a hysteresis with a coercitive field of ~150 Oe and a remanence of ~ 0.11 emu/cm^3.

Pseudocubic metastable $Ge_3MnSb_2Te_7$ was obtained as single-phase bulk by quenching (a = 5.97119(17) Å, broadened reflections). Annealing yields a disordered rhombohedral modification with a predominantly 39*R*-type stacking sequence (13 layers per slab; *R*-3*m,* a = 4.20891(13) Å, c = 72.583(5) Å). The formally divalent Mn atoms might lead to interesting magnetic features.

$Ge_{0.9}Fe_{0.1}Sb_2Te_2Se_2$ forms a 21*R*-type structure (*R*-3*m*, a = 4.12549(4) Å, c = 40.1046(7) Å). A Rietveld refinement shows that one anion position is predominantly occupied by Te the other by Se. The compound is a member of a hypothetical solid solution between Ge(Te,Se), Fe(Se,Te), and $Sb_2(Te,Se)_3$.

[1] T. Rosenthal, M. N. Schneider, C. Stiewe, M. Döblinger, O. Oeckler, *Chem. Mater.* **2011**, *23*, 4349.
[2] W.-D. Song, L.-P. Shi, C.-T. Chong, *J. Nanosci. Nanotechnol.* **2011**, *11*, 2648.
[3] W.-D. Song, L.-P. Shi, X.-S. Miao, C.-T. Chong, *Adv. Mater.* **2008**, *20*, 2394.
[4] W. Zhang , I. Ronneberger , Y. Li , R. Mazzarello, *Adv. Mater.* **2012**, *24*, 4387.
[5] M. Walter, J. Walkowski, V. Zbarsky, M. Münzberg, M. Schäfers, D. Ebke, G. Reis, A. Thomas, P. Peretzki, M. Seibt, J. S. Moodera, M. Czerner , M. Bachmann, C. Heiliger, *Nat. Mater.* **2011**, *10*, 742.

MS17-T04

How Ca/Ba ratio affects the relaxor behavior of $Ca_xBa_{1-x}Nb_2O_6$?

C. S. Pandey[1], J. Schreuer[1], M. Burianek [2], M. Mühlberg[2]
[1]*Ruhr-Universität Bochum, Bochum, Germany*
[2]*Universität zu Köln, Köln, Germany*

The relaxor behavior of incompletely filled tetragonal tungsten bronze uniaxial relaxor ferroelectric calcium barium niobate ($Ca_xBa_{1-x}Nb_2O_6$, CBN-*x*) was studied on large single crystals with *x* = 0.24 and 0.32 grown by the Czochralski method. To this end the elastic constants and the coefficients of thermal expansion were derived using resonant ultrasound spectroscopy and dilatometry, respectively, in the temperature range 300 K - 1503 K. In this present work, we show that the relaxor behavior strongly varies with the Ca/Ba ratio. Evidence is found for a decrease of the size of the polar nanodomains above the transition temperature with increasing *x*. The Curie temperature and the Burns temperature are also very sensitive to the compositione whereas the intermediate temperature T^* appears nearly unaffected from the Ca/Ba ratio.

MS17-T05

Anatase and Rutile formation in atomic layer deposition of TiO_2

B. Abendroth[1], S. Rentrop[1], T. Moebus[1], R. Strohmeyer[1], F. Hanzig[2], H. Stöcker[1], D. C. Meyer[1]
[1]*TU Bergakademie Freiberg, Institut f. Experimentelle Physik, Freiberg, Germany*
[2]*TU Bergakademie Freiberg, Institut für Werkstoffwissenschaften, Freiberg, Germany*

Titanium dioxide is a wide gap semiconductor, which is, based on its optical and electronic properties, widely used as renewable energy material and in the emerging technology of resistive switching non-volatile memories. The band gap is above 3 eV and the visible light refractive index ranges from 2.5 to 2.9, depending on the structural modification. Many properties relevant for the specific application rely on the presence of a specific crystalline phase of TiO_2: in microelectronic applications such as high k dielectric in metal-insulator-metal capacitor structures, amorphous TiO_2 or rutile are preferred due to a higher dielectric constant and lower leakage currents as compared to anatase [1,2]. Photocatalysis on the other hand is more effective in the anatase polymorph [3].

Atomic layer deposition (ALD) is a well-known technique used for the fabrication of thin oxide layers for high-k-dielectrics or resistive switching memory applications.

Here, we present our studies on the atomic layer deposition of TiO_2 from Tetrakis(dimethylamino)titanium (TDMAT) and H_20 precursors in the substrate temperature range from 120 °C to 350 °C. The effects of the deposition temperature *Ts* and layer thickness *d* on the resulting anatase and rutile phase composition are investigated by grazing incidence x-ray diffraction and are summarized in a *Ts-d* phase diagram.

The effect of the presence of crystalline phases on resistance switching performance is investigated for metal-TiO_2-metal (MIM) capacitor structures. For this the current-voltage characteristics of MIM cells with 10 - 30 nm thick insulator layers with either amorphous, partially or fully crystalline ALD TiO_2 are measured.

References

1. H. Mähne, S. Slesazeck, S. Jakschik, I. Dirnstorfer, T. Mikolaijick, Microelectronic Engineering 88 (2011) 1148.

2. S.K. Kim, W. Kim, K.M. Kim, C.S. Hwang, J. Jeong, Appl. Phys. Lett. 85 (2004) 4112.

3. M.L. Kääriäninen, D.C. Cameron, Surface Science 606 (2012) L22.

MS17-T06
The BaTiO$_3$(001)-(2x1) reconstruction: Structure and magnetism

H. L. Meyerheim[1], A. Ernst[1], K. Mohseni[1], I. V. Maznichenko[2], S. Ostanin[1], F. Klimenta[1], N. Jedrecy[3], W. Feng[1], I. Mertig[1,2], R. Felici[4], J. Kirschner[1,2]
[1]*Max-Planck-Institut für Mikrostrukturphysik, Halle, Germany*
[2]*Martin-Luther-Universität Halle-Wittenberg, Institut für Physik, Halle, Germany*
[3]*UPMC-Sorbonne Universite´s, Institut des Nano Sciences de Paris, Paris, France*
[4]*ESRF, Grenoble Cedex, France*

Though BaTiO$_3$ (BTO) is the prototype perovskite type ferroelectric and its (2x1) reconstruction has been observed more than 30 years ago [1] no detailed analysis of its atomic geometry has been reported so far. We have carried out a surface x-ray diffraction (SXRD) analysis of the BTO(001)-(2×1) reconstructed surface [2] using a 2D pixel detector allowing the fast and precise collection of SXRD reflection intensities.

The structure model is shown in perspective view in Fig. 1. The crystal is terminated by two TiO$_2$ layers. Within the top TiO$_2$ layer one Ti atom (5) resides in a tetragonal pyramidal oxygen environment. The Ti-atom (5) is located 0.53 Å below the bulk truncated surface to bind to four second layer O-atoms (7,8 and equivalent ones labelled by primed numbers) at a distance of 2.29 (0.15) Å. The fifth O-atom (4) is located 2.30 (15) Å above Ti(5).

Ab initio calculations based on this structure model suggest that the surface is metallic and magnetic involving local magnetic moments up to 2 Bohr magnetons in magnitude located at surface Ti and O atoms.

References:
[1] R. Courths, Phys. Status Solidi B 100, 135 (1980)
[2] H. L. Meyerheim, A. Ernst, K. Mohseni, I. V. Maznichenko, S. Ostanin, F. Klimenta, N. Jedrecy, W. Feng, I. Mertig, R. Felici, and J. Kirschner, Phys. Rev. Lett. 108, 215502 (2012)

Fig. 1

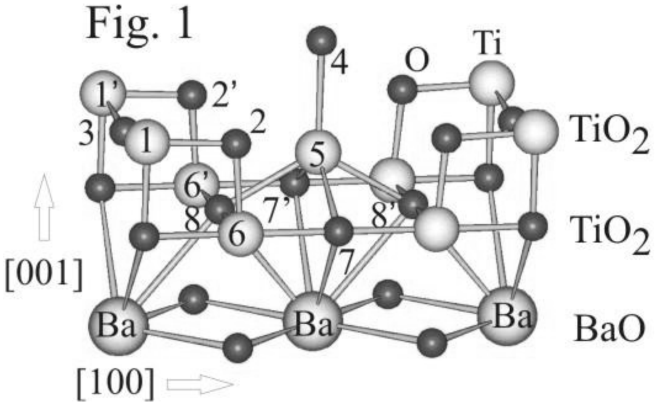

MS17-T07
Residual stress and defect density determination in HVPE grown GaN layers.

M. Barchuk[1], C. Röder[2], G. Lukin[3], J. Kortus[2], O. Pätzold[3], D. Rafaja[1]
[1]*TU Bergakademie Freiberg, Institute of Materials Science, Freiberg, Germany*
[2]*TU Bergakademie Freiberg, Institute of Theoretical Physics, Freiberg, Germany*
[3]*TU Bergakademie Freiberg, Institute of Nonferrous Metallurgy and Purest Materials, Freiberg, Germany*

Gallium nitride is nowadays a promising semiconductor material for the development of light emitting diodes, blue lasers, solar cells etc. As GaN is typically grown on foreign substrates [1], the GaN [0001]-oriented layers grown by hydride vapor phase epitaxy (HVPE) on sapphire possess non-zero residual stress and large number of threading dislocations (TDs) with dislocation lines perpendicular to their surface. [2].

In-situ stress determination by wafer curvature measurements is not always applicable, especially for very thick HVPE films. Therefore, an accurate ex-situ residual stress determination is of great importance for characterization of the GaN layers. We suggest using two complementary techniques for residual stress values determination based on high-resolution x-ray diffraction (HRXRD) and micro-Raman spectroscopy.

The $\sin^2\psi$-method applied to the HRXRD data determines the residual stress from the changes of interplanar distances in different macroscopic and crystallographic directions. It allows the residual stresses to be determined accurately, but the (integral) experimental information is obtained from the near-surface region, which extent is limited by the penetration depth of x-rays. On the contrary, m-Raman equipment enables to perform measurements at fixed depth below the sample surface. However, the excited phonon vibrations can be affected not only by the residual stress but also by the structure defects within the crystal lattice. The separation of these two contributions is not a trivial task. In general, it can affect the determined values of the residual stress. The results obtained with these two methods are compared and referred to the growth conditions and to the thickness of the respective GaN layer.

One of the relevant structure defects observed in the HVPE GaN layers are threading dislocations. The reliably determined densities of particular types of TDs were correlated with the stress values. Both quantities, i.e. the residual stress and the TD density were found to characterize the attainment of the respective growth technique well. For calculation of the dislocation density, we applied the Monte Carlo simulation developed recently [3], which is based on the comparison of the simulated and measured x-ray reciprocal-space maps as well as the q_x and q_z cuts. Furthermore, this method allowed the densities of the screw and edge threading dislocations to be determined independently. In our contribution, the densities of screw and edge TDs are related to the determined residual stress and to the thicknesses of the GaN layers.

References.

- S. Nakamura, G. Fasol, The Blue Laser Diode, *Springer*, New York, 1997.
- G. Lukin, C. Röder, E. Niederschlag, Y. Shashev, U. Mühle, O. Pätzold , J. Kortus, D. Rafaja, and M. Stelter, *Cryst. Res. Technol.* **47**, No. 2, 121 - 130 (2012)
- M. Barchuk, V. Holý, B. Miljevic, B. Krause, T. Baumbach, J. Hertkorn, and F. Scholz, J. Appl. Phys., **108**, 4 (2010).

MS19 - Biocrystallography Other

MS19-T01

Synchrotron based fragment screening

U. Mueller[1], A. Heine[1], M. Ühlein[1], M. S. Weiss[1], G. Klebe[1]

[1]*Helmholtz Zentrum Berlin, Macromolecular Crystallography, Berlin, Germany*

Within the last decade, the fragment-based screening approach has been matured to a reliable and powerful instrument of pharmaceutical drug discovery. The success of fragment screening strongly depends on the quality of the chosen fragment library (100-200 Da) as well as the possibility to use high throughput methods for the screen application. A thorough crystallographic analysis of many protein-fragment complex structures and their binding modes has the perspective to result in the development of new potential lead structures. Within this project we designed and have tested a small fragment library consisting of 364 compounds [1] against endothiapepsin, a model protease for pepsin-like aspartic proteases. In a biochemical assay 55 compounds were identified as screening hits and were subjected to further crystallographic investigation. The resulting 11 crystal structures showed diverse binding modes, addressing directly the catalytic dyad aspartates and water-mediated interaction or no interaction to the catalytic dyad.

Furthermore we started with the development of a dedicated experimental station for high throughput fragment screening at the BESSY II storage ring. This will comprise the high throughput data collection and its automatic evaluation [3].

References:

[1] H. Köster, T. Craan, S. Brass, C. Herhaus, M. Zentgraf, L. Neumann, A. Heine, G. Klebe; A Small Nonrule of 3 Compatible Fragment Library Provides High Hit Rate of Endothiapepsin Crystal Structures with Various Fragment Chemotypes, J. Med. Chem. 54, 2011, 7784-7796.

[2] U. Mueller, N. Darowski, M.R. Fuchs, R. Förster, M. Hellmig, K.S. Paithankar, S. Pühringer, M. Steffien, G. Zocher, M.S. Weiss, 2012. Facilities for Macromolecular Crystallography at the Helmholtz-Zentrum Berlin. J. Syn. Rad., 19, 442-449

[3] M. Krug, M. S. Weiss, U. Heinemann and U. Mueller, 2012, XDSAPP: a graphical user interface for the convenient processing of diffraction data using XDS, J. Appl. Cryst. 45, 568-572

MS19-T02

Towards automated high-throughput sample evaluation and diffraction data collection in Structural Biology at the European Synchrotron Radiation Facility

Christoph Mueller-Dieckmann on behalf of the Structural Biology group.

C. MUELLER-DIECKMANN[1]

[1]*European Synchrotron Radiation Facility, Structural Biology, Grenoble, France*

As part of the ESRF's upgrade programme (http://www.esrf.fr/AboutUs/Upgrade) for Structural Biology, the new bioSAXS beam line BM29 has been opened to users since June 2012. Efforts have now turned to the installation and commissioning of the *MASSIF* (*M*assively *A*utomated *S*ample *S*election *I*ntegrate *F*acility) suite of beam lines. This new core facility for Macromolecular Crystallography sample evaluation will address more challenging projects such as multi-protein complexes and membrane assemblies which often require the evaluation of more samples before the actual diffraction experiment takes place and often require experimenters to exploit the fact that macromolecular crystals can show considerable inter- and intra- crystal variability with respect to diffraction quality. Fundamental for *MASSIF* will be a very high degree of automation based on robotic systems thus enabling users to evaluate their samples and allow them to choose only the best suited for full diffraction experiments.

Here, the ESRF's Structural Biology Group's Upgrade Project will be presented. The particular emphasis will be on *MASSIF* plans for currently existing beam lines such as ID23 and ID29 will also be addressed.

MS19-T03

New Tools for Biological Crystallography : Low Multiplicity Sulfur-SAD Phasing in the Home lab

S. Freisz[1], M. Benning[2], V. Smith[3]

[1]*Bruker AXS, application , Karlsruhe, Germany*

[2]*Bruker AXS, Madison, United States*

[3]*Bruker AXS, Karlsruhe, Germany*

Advances in crystallographic hardware and software have enabled structural biologists to investigate more challenging projects. Recent developments have greatly increased the capabilities of in-house diffraction systems and made it easier to obtain de novo structural information in the home lab.

Single-wavelength anomalous diffraction (SAD) techniques with Cu radiation are now widely used for structure solution even in cases involving weak anomalous scatterers, like sulfur.

The combination of a brighter, more stable X-ray source with a high sensitivity low noise detector have greatly improved the quality of data collected in-house. The high quality allows successful SAD measurements even far away from the absorption edge.

Higher multiplicity data sets are typically necessary for successful in-house SAD trials. This requires software which optimizes the collection strategy, for example with respect to overall data collection time to minimize radiation damage.

We have now introduced the new D8 VENTURE solution for structural biology with the PHOTON 100 detector featuring the first CMOS active pixel sensor in X-ray crystallography. The new microfocus X-ray sources, METALJET,TXS and IμS now deliver beam intensities comparable to those of typical bending-magnet beamlines.

Here we present a low multiplicity sulfur-SAD phasing experiment on a small Thaumatin crystal as well as other examples of data collected from chalenging crystals on the D8 VENTURE that allowed us to obtain nice structures of the concerned proteins.

MS19-T04

A generalized mechanism for X-ray radiation damage on the atomic level

D. Heintz[1], A. Burkhardt[1], R. Raghunandan[1], M. Gutmann[2], A. Wagner[3], M. Nachtegaal[4], E. Weckert[1], A. Meents[1]
[1]*DESY, Hasylab, Hamburg, Germany*
[2]*ISIS Neutron Source, Oxfordshire, United Kingdom*
[3]*Diamond Light Source, Oxfordshire, United Kingdom*
[4]*Paul Scherrer Institut, Villigen, Switzerland*

Single crystal X-ray diffraction at 3rd generation synchrotron sources is an important tool for structure determination of large biological molecules, such as proteins or viruses. Unfortunately, the high doses of radiation absorbed by the crystals cause a fast deterioration of the molecule under investigation, often within a few images[1]. Effects such as loss in diffraction power, increase in unit cell volume or mosaicity, changes in bond lengths and oxidation state of the samples have been observed[2,3].

In order to reduce radiation damage experiments are routinely carried out at 100 K [4]. Although many studies have addressed f X-ray radiation damage to crystals, a consistent model involving all effects has not been found so far[1,2,4-6].

Recent investigations performed by our group have shown that site-specific changes such as X-ray induced hydrogen abstraction[7,8] or X-ray induced photoreduction have a strong influence on X-ray radiation damage. X-ray and neutron diffraction as well as X-ray absorption spectroscopy were applied on model compounds in order to follow X-ray radiation damage on the atomic level.

Based on this work, a consistent generalized mechanism for X-ray radiation damage could be proposed. It could be shown that X-ray induced hydrogen abstraction and subsequent gas generation is the main contributor to X-ray radiation damage. It is possible to divide the damage process into different steps: The susceptibility of a compound to X-ray radiation damage is clearly dependent on the susceptibility to selective hydrogen abstraction. The more hydrogen is abstracted in the compound, the more gas is formed within the crystal. This gas exerts a stress on the crystal lattice. Crystals have anisotropic elasticity properties which leads to different expansion/contraction behavior of each cell axis as a result of irradiation. At a certain point, the stress exceeds the tensile strength of the crystal and the crystal starts to break, leading to an increase in mosaicity.

[1] Burmeister, W.P. **(2000)**, *Acta Cryst. D* **(56)**, 328 - 341.
[2] Ravelli, R.B.G.; Theveneau, P.; McSweeney, S.; Caffrey, M. **(2002)**, *J. Sychrotron Rad.* **9**, 355 - 360.
[3] Champloy, F.; Gruber, K.; Jogl, G.; Kratky, C. **(2000)**, *J. Synchrotron Rad.* **7**, 267 - 273.
[4] Garman, E.F.; Nave, C. **(2002)**, *J. Synchrotron Rad.* **9**, 327 - 328.
[5] Meents, A.; Wagner, A.; Schneider, R.; Pradervand, C.; Pohl, E.; Schulze-Briese, C. **(2007)**, *Acta Cryst. D* **63**, 302 - 306.
[6] Nave, C.; Garman, E.F. **(2005)**, *J. Synchrotron Rad.* **12**, 257 - 260.
[7] Ravelli, R.B.G.; Garman, E.F. **(2006)**, *Curr. Op. Struct. Biol.* **16**, 624 - 629.
[8] Meents, A.; Dittrich, B.; Gutmann, S. **(2009)**, *J. Synchrotron Rad.* **16**, 183 - 190.
[9] Meents, A.; Gutmann, S.; Wagner, A.; Schulze-Briese, C. **(2010)**, *PNAS* **107**(3), 1094 - 1099.

MS19-T05

Structural and energetic basis of folded protein transport by the FimD usher

S. Geibel[1], E. Procko[2], S. J. Hultgren[3], D. Baker[2], G. Waksman[1]
[1]*Institute of Structural and Molecular Biology, University College and Birkbeck College, London, United Kingdom*
[2]*Howard Hughes Medical Institute and Department of Biochemistry, University of Washington, Seattle, United States*
[3]*Center for Women's Infectious Disease Research and Department of Molecular Microbiology, Washington University School of Medicine, St. Louis, United States*

Type 1 pili, produced by most strains of uropathogenic Escherichia coli (UPEC), are multi-subunit fibers that play crucial roles in recognition of and adhesion to host tissues[1]. During pilus biogenesis, subunits are recruited to an outer membrane assembly platform, the FimD usher, which catalyzes their polymerization and mediates pilus secretion[2]. The recent crystal structure of an initiation complex provided insights into the initiation step of pilus biogenesis resulting in pore activation[3], but very little is known about the elongation steps that follow. Here we present the crystal structure of FimD bound to the FimC:FimF:FimG:FimH pilus tip assembly complex, whereby the FimD pore is fully traversed by the protein polymer. This structure reveals the conformational changes required to prevent backsliding of the nascent pilus through the FimD pore and also reveals unexpected properties of the usher pore. By computational analysis we show that the usher pore is energetically designed to facilitate substrate passage within the pore and that the circular binding interface between the pore lumen and the folded substrate plays an active role in transport by defining a low energy pathway along which the nascent pilus polymer is guided during secretion.

References

1. Mulvey, M. A. et *al.* Induction and evasion of host defenses by type 1-piliated uropathogenic Escherichia coli. *Science* **282** 1494-7 (1998).

2. Allen, W. J. et *al.* Pilus biogenesis at the outer membrane of Gram-negative bacterial pathogens. *Curr Opin Struct Biol* (2012).

3. Phan, G. *et al.* Crystal structure of the FimD usher bound to its cognate FimC-FimH substrate. *Nature* **474**, 49-53 (2011).

MS19-T06

New sample environment options at the neutron diffractometer “BioDiff”

T. Schrader[1], A. Ostermann[2], M. Monkenbusch[3], B. Laatsch[4], P. Jüttner[2], W. Petry[2], D. Richter[3,5]
[1]*Forschungszentrum Jülich GmbH, Outstation in Garching, Jülich Centre for Neutron Science, Garching, Germany*
[2]*Technische Universität München, Forschungs-Neutronenquelle Heinz Maier-Leibnitz (FRMII), Garching, Germany*
[3]*Forschungszentrum Jülich GmbH, Jülich Centre for Neutron Science, Jülich, Germany*
[4]*Forschungszentrum Jülich GmbH, Zentralinstitut für Technologie, Jülich, Germany*
[5]*Forschungszentrum Jülich GmbH, Institute for Complex Systems, Jülich, Germany*

The neutron diffractometer BioDiff is a joint project of the Forschungszentrum Jülich (FZJ/JCNS) and the Forschungs-Neutronenquelle Heinz Maier-Leibnitz (FRM II). BioDiff is especially designed to collect data from crystals with large unit cells (for a schematic overview see Fig. 1). The main field of application is the structure analysis of proteins, especially the determination of hydrogen atom positions. Typical scientific questions addressed are the determination of protonation states of amino acid side chains and the characterization of the hydrogen bonding network between the protein and an inhibitor or substrate. The orientation of water molecules in the active centre of the protein can also be determined. To first solve the structure of the protein using x-rays is a prerequisite for a successful experiment at BioDiff because we use the x-ray structure to solve the phase problem of crystallography. In some cases it is desirable to record the neutron data set at the same temperature as the x-ray data set. Especially this enables a joint neutron/x-ray refinement. Since the x-ray data at synchrotrons are often measured at cryogenic temperatures of 100 K we integrated a standard Oxford Cryosystems “Cryostream 700 Plus” as a new sample environment option to the instrument BioDiff (for a picture see Fig. 2). Recording data sets at low temperatures also facilitates measurements of frozen intermediate states of the protein or protein substrate complexes where the substrate is not digested by the protein due to the low mobility at cryogenic temperatures. The main advantage of the monochromatic instrument BioDiff is the possibility to adapt the wavelength between 2.4 Å and 5.6 Å to obtain a compromise between higher scattering yields at longer wavelengths and better resolution at smaller wavelengths. The main detector of BioDiff consists of a neutron imaging plate system in a cylindrical geometry in order to cover a large solid angle. A Li/ZnS scintillator imaged onto a CCD-chip is available for additional detection purposes (see scheme Fig. 1). Applications of the BioDiff instrument as a powder diffractometer are also discussed.

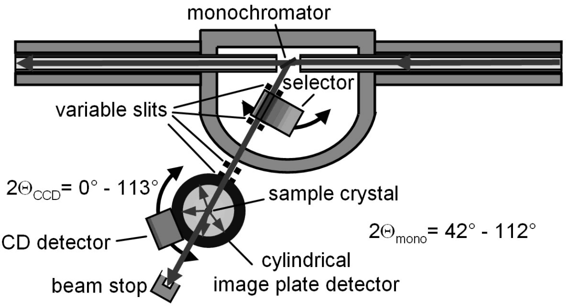

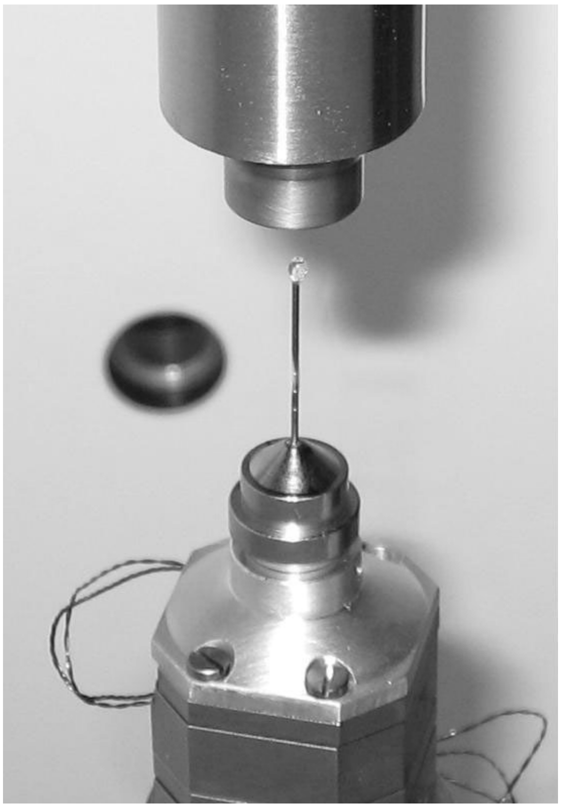

MS20 - Crystal Physics, Crystal Chemistry: Synthesis and New Crystal Structures II

MS20-T01

Symmetry and Chemistry of Complex Intermetallics

J. Dshemuchadse[1], W. Steurer[1]
[1]*ETH Zurich, Laboratory of Crystallography, Department of Materials, Zurich, Switzerland*

Complex structures with giant unit cells can be found in many different intermetallic systems. They feature a number of peculiar properties, but until recently, no unifying approach has been applied to describe their structures.

To achieve a deeper understanding of their building principles, we are examining the structures of complex intermetallics on three different levels. For a generalized definition, we are statistically comparing the distribution of complex intermetallics over the entirety of intermetallic structures. Secondly, we have picked out highly symmetric Bravais lattices (*e.g.*, the face-centered cubic lattice [1]), which feature a large number of complex structures. Within these groups we then analyze the distribution of different structure types, as well as their interrelations. The third step focuses on specific intermetallic systems featuring multiple complex compounds and describes their special geometries in a comparative way to reveal similarities and distinctions.

Until now, no significant effect in the distribution of complex structures over the lattices and space group symmetries could be found [2]. There are some tendencies towards the prevalent occurrence of some elements as major components in complex intermetallics, but apart from this, the compositions seem to be quite diverse. These predominant metallic elements are mainly Zn, Al, Ge, Sn, Cd, Ga, and Mg, most of which are also main constituents of quasicrystals. Among these complex intermetallics, quasicrystal approximants can be found, but most compounds were never assigned to any aperiodic structure, although they occur in very similar systems.

As a means to describe these large unit cells, we choose a similar approach as is applied to quasiperiodic structures: the cluster description. This renders good results for large groups of these complex intermetallics, but its application fails with a number of structures that should not be ignored, either. Other approaches for structure description are utilized in order to reveal the principles of building such complex structures. By trying to better understand complex intermetallic structures, we hope to be able to gain more profound knowledge on the formation of metallic matter in general.

[1] J. Dshemuchadse, D. Y. Jung, W. Steurer, Acta Cryst. B67, 269-292 (2011).

[2] J. Dshemuchadse, W. Steurer, MRS Proceedings 1517, *accepted* (2012).

MS20-T02

How complicated can a lillianite homologue become? - the case of jasrouxite

E. Makovicky[1], D. Topa[2]
[1]*University of Copenhagen, University of Copenhagen, Denmark*
[2]*Museum of Natural History, Wien, Austria*

Since its first solved structure, $Pb_3Bi_2S_6$ (Otto & Strunz 1968), the lillianite homologous series (Makovicky & Karup-Møller 1977) underwent steady growth, which reflected both the spectrum of incremental thickness variations in the basic lillianite-like *Cmcm* motif and the steadily more complicated superstructures of it (e.g., gustavite $PbAgBi_3S_6$, $P2_1/c$). In modular description, lillianite homologues are composed of $(311)_{PbS}$ slabs of galena-like structure, unit-cell twinned via trigonal coordination prisms of lead. Typical for the series is a complex substitution 2Pb ↔ Ag + (Bi,Sb). In gustavite (and its Sb analog andorite) the only Pb left untouched by the Ag+Bi (or Ag+Sb) substitution is situated in these prisms, a case we define as '100% substitution'.

Jasrouxite, $Ag_{16}Pb_4(Sb_{25}As_{15})_{\Sigma 40}S_{72}$, is triclinic, space group *P*-1; lattice parameters are *a* = 8.2917(5), *b* = 19.101(1), *c* = 19.487(1) Å, a = 89.731(1)^o, b = 83.446(1)^o, and g = 89.944(1). Z = 1 for the title formula. The structure contains 30 independent cation sites, from which 12 are mixed sites, and 36 independent sulfur sites (a sextuple of the sites in the lillianite-like subcell). Only the *c* parameter copies that of lillianite, the *a* parameter is doubled and *b* is about 3/2 of a cell diagonal in (001) of lillianite. According to the above scheme, jasrouxite is heavily 'oversubstituted'. On the composition planes there are two distinct rows of alternating Pb and Sb sites and these are in alternation with one row of pure Sb. As a consequence, the slabs contain a surplus of Ag sites. Unlike the simple lillianite scheme, the alternating $(311)_{PbS}$ slabs are non-equivalent and each of them has two types of differently occupied diagonal $(100)_{PbS}$ planes of atoms, always present in a 2:1 ratio. All this produces triclinic symmetry of the structure, with only small distortions from monoclinic metrics. Lone electron pairs of As and Sb congregate in large micelles with elliptic cross-section, situated along the median planes of the $(311)_{PbS}$ slabs.

Jasrouxite, and at least two Sb-Bi members of the lillianite homologous series currently under investigation exhibit hitherto unexpected complications of cation ordering and supercell formation. This results from the presence of two distinct metalloids in the structure, from the oversubstitution by (Ag + M^{3+}), and from highly expressed lone electron pair activity of trivalent cations.
Makovicky, E. & Karup-Møller, S. (1977): N. Jb. Mineral. Abh. 130, 264-287.
Otto, H.H. & Strunz, H. (1968): N. Jb. Mineral. Abh. 108, 1-19.

MS20-T03

Dissolution Kinetics of Nanocrystals: New Insights

M. Petrik[1], B. Harbrecht[1]
[1]*Philipps-University Marburg, Chemistry, Marburg, Germany*

Crystal dissolution is closely related to crystal growth. Ideally, the two processes follow the same microscopic path, only in reverse. From an understanding of the one, one may gain an insight into the other. Obviously, crystal growth is more important in practice, but crystal dissolution is not less challenging intellectually. Herein, we shall demonstrate, theoretically and by experiment, that for small nanocrystals the specific rate of dissolution (per unit surface area) is markedly dependent on the crystal size. This novel nanoeffect [1] will, for the first time, be rationalized in terms of a frustrated multiple nucleation of surface steps and kinks.

Like crystal growth, crystal dissolution is known to proceed at the atomic level via the propagation of surface steps. Depending on conditions, e.g. undersaturation, the moving steps follow each other at a certain distance D_S (step spacing). The movement results from kinks receding at constant speed, on average a distance D_K apart. In general, $D_K < D_S$. Thus, at fixed experimental conditions, a change, or crossover, in the kinetics of dissolution should occur when 1. the crystal size D_P ('particle size') gets smaller than D_S, and 2. when $D_P < D_K$. In regime 1, each facet of the crystal may accommodate only a single atomic step at a time (frustrated nucleation of additional steps because $D_S > D_P$), though the step may still contain a sufficient number of kinks so as to advance at a constant speed. Similarly, in regime 2, only one kink may be accommodated, therefore the step advances at a speed proportional to its reciprocal length (~ D_P^{-1}).

Size-dependent dissolution rate data on nanocrystals of NiO (bunsenite) corroborate these predictions [1, 2]. Thus, although for nanocrystals the specific dissolution rate is enhanced by orders of magnitude (depending on size) [1], it is not necessary to invoke fundamental changes, say, in surface free energy [3] to explain this pronounced nanoeffect - it follows straightforwardly from the established microscopic model of crystal growth and dissolution.

[1] M. Petrik, B. Harbrecht, *Z. Anorg. Allg. Chem.* **2012**, *638*, 1622.
[2] M. Petrik, B. Harbrecht, in preparation.
[3] J. Liu et al., M. F. Hochella Jr., *Geochim. Cosmochim. Acta* **2008**, *72*, 5984.

MS20-T04
Properties and crystal structure of B-mullite

H. Lührs[1], A. Senyshyn[2], S. P. King[3], J. V. Hanna[3], H. Schneider[1,4], R. X. Fischer[1]
[1]*Universität Bremen, Fachbereich Geowissenschaften, Bremen, Germany*
[2]*Technische Universität München, Forschungsneutronenquelle Heinz-Maier-Leibnitz (FRM II), Garching, Germany*
[3]*University of Warwick, Department of Physics, Coventry, United Kingdom*
[4]*Universität Köln, Institute for Crystallography, Köln, Germany*

The technical importance of mullite ceramics is due to the outstanding properties of mullite: high thermal stability, low thermal expansion and conductivity, high creep resistance and corrosion stability. The chemical composition of mullite is given by the solid-solution series $Al_2Al_{2+2x}Si_{2-2x}O_{10-x}$, $0.2 < x < 0.9$ [1]. Depending on the synthesis temperature and atmosphere the crystal strucuture of mullite is able to incorporate a large variety of cations [2, 3 and references therein]. B-doping of mullite results in significant changes of lattice parameters *b* and *c* as reported by several authors [4-6]. Furthermore the incorporation of B results in a strong reduction of the mean thermal expansion coefficient of 15% [5].

A series of samples doped with different amounts of boron were prepared at 1200°C. Single-phase gels consisting of aluminum nitrate nonahydrate, tetraethoxysilane, and boric acid were used as precursor phases. The crystal structure of boron-doped mullite (B-mullite) was studied by means of neutron powder diffraction and ^{11}B solid state, magic-angle-spinning (MAS) NMR spectroscopy.

The MAS NMR results clearly show that the ^{11}B isotropic chemical shift (δ_{iso}) and quadrupolar coupling constant and asymmetry paramater (C_Q, η) describe that of three-coordinated B in a near-trigonal planar environment. The B position was derived from a combination of Rietveld refinements with difference Fourier calculations and gridsearch analyses applied to a series of samples with varying B contents. This BO_3 group connects the octahedral chains perpendicular to the **c**-axis (Fig. 1). The indices of distortion indicate that the incorporation of boron leads to more regular polyhedra and a rotation of the AlO_6 octahedra. Nevertheless, distance least squares refinements (DLS) were necessary to determine the local BO_3 configuration. The DLS calculations yielded split positions for the oxygen atoms directly linked to B leading to a local distortion of the octahedral geometry verified in the crystal-structure refinements. This crystallographic model including the split positions for the oxygen atoms of the AlO_6 octahedron provides an explanation for the anisotropic behavior of the lattice parameters upon B-incorporation.

References:
1. Fischer, R.X., et al. (1996) J Eur Ceram Soc, **16**(2), 109-113.
2. Schneider, H., in *Mullite*, H. Schneider and S. Komarneni, Editors. 2005, WILEY-VCH: Weinheim. p. 70-93.
3. Schneider, H., et al. (2008) J Eur Ceram Soc, **28**(2), 329-344.
4. Griesser, K.J., et al. (2008) Mineralogy and Petrology, **92**(3-4), 309-320.
5. Lührs, H., et al. (2012) Mater Res Bull, **47**, 4031-4042.
6. Zhang, G.M., et al. (2010) J Eur Ceram Soc, **30**(12), 2435-2441.
7. Fischer, R.X., et al. (2012) Int J Mater Res, **103**(4), 402-407.

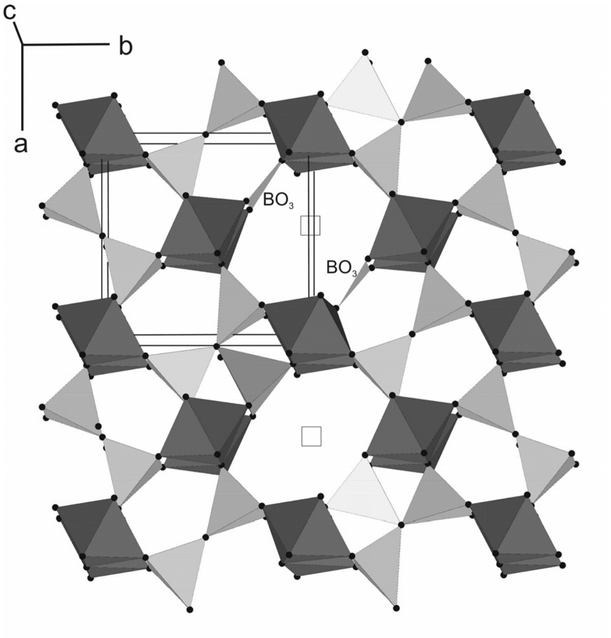

Fig. 1: crystal structure of B-mullite. Oxygen vacancies are indicated by squares. Only one out of many possible distributions [7] of oxygen vacancies, T_3O groups and BO_3 groups is shown.

MS20-T05
Structural Characterisation of shocked AlN-powders

K. Keller[1,2], T. Schlothauer[1,2], M. Schwarz[2,3], E. Brendler[4], E. Kroke[2,3], G. Heide[1,2]
[1]*TU Mining Academy, Institute for Mineralogy, Freiberg, Germany*
[2]*TU Mining Academy, Freiberg High-Pressure Research Centre, Freiberg, Germany*
[3]*TU Mining Academy, Institute for Inorganic Chemistry, Freiberg, Germany*
[4]*TU Mining Academy, Institute for Analytical Chemistry, Freiberg, Germany*

Aluminium nitride, which has a wurtzite structure (w-AlN), undergoes a phase transition to the rocksalt structure (rs-AlN) at pressures of about 14-23 GPa in static experiments [1-3]. Shock wave experiments have been performed with subsequently sample recovery to investigate the high-pressure phase [4].

The powders were characterised with X-ray diffraction and Rietveld full-pattern fitting. However, no pure rs-AlN phase was produced, but a phase mixture of w-AlN, rs-AlN and different Al-O-N phase. The oxygen-bearing phases, espγ-AlON with spinel structure and the 27R polytypoid of Al(O)N, gives a rough estimation of the shock temperature. We observe a sluggish phase transition caused by the kinetic barrier and a temperature-activated re-conversion.

The Rietveld-refinement of the lattice constant of rs-AlN gives a value of a = 4,044Å, which is in good agreement with the HRTEM results. The crystallite size of the starting w-AlN and the synthesised rs-AlN was determined with XRD and TEM. We come to the conclusion, that the phase transition has a crystallite size dependence.

A vibration band in the IR-spectrum at about 490 cm^{-1} is assigned to the rs-AlN. Furthermore, solid state ^{27}Al-NMR studies were conducted, showing a chemical shift of 2 ppm for the sixfold Al-N coordination.

References

[1]I. Gorczyca, N.E. Christensen, P. Perlin, P. I. Grzegory, J. Jun, M. Bockowski, Solid State Commun. 1991, **79**, 1033.

[2] M. Ueno, A. Onodera, O. Shimomura, K. Takemura, Phys. Rev. B 1992, **45**, 10123.

[3] Q. Xia, H. Xia, A.L. Ruoff, J. Appl. Phys. 1993, **73**, 8198.

[4] K. Keller, T. Schlothauer, M. Schwarz, G. Heide, E. Kroke, High Pressure Res. 2012, **32**, 23.

MS20-T06
Structural and electrochemical studies of the Li-In alloys

I. Chumak[1], M. Knapp[1], H. Ehrenberg[1,2]
[1]*Karlsruhe Institute of Technology, Institute for Applied Materials - Energy Storage Systems, Karlsruhe, Germany*
[2]*Karlsruhe Institute of Technology, Institute of Inorganic Chemistry, Karlsruhe, Germany*

Two new binary Li-In phases are detected during galvanostatic Li-extraction from the alloy $Li_{13}In_3$ ($Li_{4.33}In$). The crystal structures of new compounds were determined by single-crystal X-ray diffraction. The compositions obtained after structure refinements were: $Li_{9.95}In_{5.05}$ (trigonal crystal system, Pearson symbol *hP15*, space group *P-3m1* (No. 164), a = 4.7480(7) Å, c = 14.283(3) Å) and $Li_{8.37}In_{3.63}$ (hexagonal, *hP12*, *P6/mmm* (No. 191), a = 4.6975(7) Å, c = 11.526(2) Å). The structure of $Li_{9.95}In_{5.05}$ can be described as derivative from the CdI_2 typ. $Li_{8.37}In_{3.63}$ can by derived from the Li_2Pt structure.

The electrochemical tests were performed in Swagelok-type cells assembled in an argon-filled dry box with electrolyte 1M $LiPF_6$ in a 1:1 mixture of dimethylcarbonate and ethylencarbonate and the Li metal foil as the negative electrode. The electrode material was prepared by grinding the powders of 80 wt. % $Li_{4.33}In$ (acting as active material), 10 wt. % carbon black (electronically conductive additive) and 10 wt. % PVDF (binder) in an agate mortar. The structural changes in $Li_{13}In_3$ electrode during electrochemical lithium extraction-insertion were studied by *ex situ* XRD (STOE STADI/P powder diffractometer, Mo-Kα_1 radiation). *In situ* diffraction during galvanostatic charging was performed at beamline B2 (DESY, Hamburg, Germany).

MS20-T07
POLYMORPHISM OF MONOMERIC NICKEL ACETATE WITH 2-PYRIDINEETHANOL

M. Trdin[1], N. Lah [1], I. Leban[1]
[1]*University of Ljubljana, Faculty of Chemistry and Chemical Technology, Ljubljana, Slovenia*

The investigation of the coordination chemistry of simple pyridine alcohols in combination with different carboxylate ligands resulted in the preparation and characterization of three polymorphic forms of mononuclear Ni(II) acetate with 2-pyridineethanol, $Ni_2(ac)_2(2\text{-}pyEtOH)_2$: two of them concomitantly crystallize from the mixture of nickel acetate and 2-pyEtOH in acetonitrile (triclinic and monoclinic form), while a third polymorph (another monoclinic form) was obtained from the mixture of nickel acetate, 2-pyEtOH and potassium oxalate in methanol.

The coordination geometry and the overall molecular structures are similar in all three polymorphs. Ni(II) atom is located on an inversion center and is surrounded by two 2-pyEtOH ligands coordinated in a chelating manner and two acetates coordinated as monodentate ligands through one of the two carboxylate O atoms. Thus, almost perfect octahedral N_2O_4 geometry is achieved. Noncoordinated carboxylate oxygen enhances the stability of the complex through a strong intramolecular H-bond with the hydroxy group of the 2-pyEtOH ligand.

The three polymorphs differ primarily in their packing arrangement which is governed by weak intermolecular interactions. The three crystal structures will presented and compared.

MS20-T08
High temperature elastic properties of a pseudo-single crystal of the nickel-base superalloy CMSX-4

K. Demtröder[1], H. Buck[2], P. Wollgramm[2], G. Eggeler[2], J. Schreuer[1]
[1]*Ruhr-Universität Bochum, Kristallographie, Bochum, Germany*
[2]*Ruhr-Universität Bochum, Lehrstuhl für Werkstoffwissenschaften, Bochum, Germany*

Today composite pseudo-single crystals of nickel-base superalloys are widely used in gas turbines and jet engines. The extreme operation conditions of high temperatures, corrosive atmosphere and high mechanical stresses may result in microstructural changes of the turbine blades. The characteristic microstructure consists of a coherent arrangement of γ' precipitates with an ordered Ni_3Al-structure embedded in a matrix of γ-phase [1,2]. This exsolution structure enables extraordinary high mechanical strength at high temperatures [3]. In order to improve the superalloys for high temperature applications a better understanding of the correlations between their mechanical properties and their microstructure as a function of temperature, mechanical stresses and composition is crucial.

To this end we studied the elastic and anelastic properties of pseudo-cubic as cast and heat treated nickel-base superalloy CMSX-4 using the innovative technique of resonant ultrasound spectroscopy (RUS) between room temperature and 1250°C. In addition, the thermal expansion was investigated with the aid of a commercial dilatometer. Microstructural characterization was performed using a combination of atomic force microscope (AFM), optical microscope, electron microprobe analysis and scanning electron (SEM) microscopy.

The elastic behavior of the pseudo-single crystals of CMSX-4 show a pronounced pseudo-cubic anisotropy at room temperature (Fig. 1). Between room temperature and 1000°C the elastic constants soften non-linearly by about 28% (Fig. 1). At higher temperatures strong ultrasound dissipation effects develop indicating an increasing number of point defects or increasing mobility of defects or grain boundaries. This coincides with the dissolution of the γ'-phase which also starts at around 1000°C.

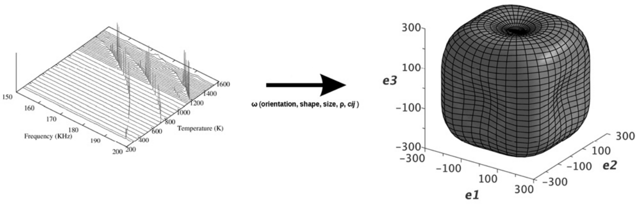

Fig.1: Section of experimental resonance spectra of CMSX-4 (left); Representation surfaces of the longitudinal elastic stiffness at room temperature (right).

References:

[1] R. C. Reed, *The Superalloys*, 2006.

[2] T. M. Pollock, *et al., Acta Metall. Mater*, **1992**, 40, 1-30.

[3] S. Kaciulis *et al., Surf. Interface Anal.*, **2012**, 44, 982-985

MS21 – Cutting Edge Techniques in Analysis and Preparation

MS21-T01

Current Status of the Liquid-Metal-Jet X-ray Source Technology

B. Hansson[1], O. Hemberg[1], T. Tuohimaa[1], M. Otendal[1], P. Takman[1]
[1]*Excillum AB, Kista, Sweden*

High-end x-ray diffraction and scattering techniques such as high-resolution XRD, protein crystallography, and SAXS rely heavily on the x-ray source brightness for resolution and exposure time. Traditional solid or rotating anode x-ray tubes are typically limited in brightness by when the e-beam power density melts the anode. The liquid-metal-jet technology has overcome this limitation by using an anode that is already in the molten state.

We have previously demonstrated prototype performance of a metal-jet anode x-ray source concept [1-3] with unprecedented brightness in the range of one order of magnitude above current state-of-the art sources. The technology has since been developed into a stable and reliable source for home-lab systems.

This presentation will review the current status of the technology specifically in terms of stability, lifetime, flux and brightness. It will also discuss details of the liquid-metal-jet technology with a focus on the fundamental limitations of the technology. It will furthermore refer to some recent data from applications within x-ray diffraction and SAXS.

[1] O. Hemberg, M. Otendal, and H. M. Hertz, *Appl. Phys. Lett.*, **2003**, 83, 1483.

[2] M. Otendal, T. Tuohimaa, U. Vogt, and H. M. Hertz, *Rev. Sci. Instr.*, **2008**, 79, 016102.

[3] T. Tuohimaa, M. Otendal, and H. M. Hertz, *Appl. Phys. Lett.*, **2007**, 91, 074104

MS21-T02

Beam Conditioning in Cutting Edge X-ray Analytical Equipment

J. Graf[1], A. Kleine[1], B. Hasse[1], J. Wiesmann[1], C. Michaelsen[1], J. Lange[2], C. Ollinger[2]
[1]*Incoatec GmbH, Geesthacht, Germany*
[2]*Bruker AXS GmbH, Karlsruhe, Germany*

Nowadays, X-ray optical components, such as multilayer mirrors or scatterless apertures, are used as beam conditioning devices in nearly all state-of-the-art X-ray analytical equipment to improve its performance. Scatterless apertures, such as the scatterfree pinholes SCATEX, are usually made of oriented single crystals, and enable a beam conditioning that is free of parasitic scattering commonly associated with conventional metal apertures. Therefore, such pinholes allow a significant improvement of small angle scattering instruments as the number of necessary pinholes can be reduced while simultaneously enlarging the beam defining pinhole size. This leads to an increased flux on the sample.

Multilayer X-ray mirrors are widely used as monochromators and beam shaping devices in protein and small molecule crystallography, powder diffraction and small angle scattering. Beam shaping with multilayer mirrors includes the optimization of the flux on the sample and the control over the beam shape and divergence. The mirrors comprise multilayer coatings with a typical double-layer thickness d in the range of 20 to 60 Å. The coating is usually deposited by physical vapor deposition techniques with a precision within ± 1-2% on elliptically or parabolically shaped substrates. Very low shape tolerances below 100 nm and figure errors below 5 arcsec are required for multilayer mirrors to ensure a superb flux density of more than 4×10^{11} phts/s/mm^2 in combination with very high-brightness microfocus X-ray sources, such as the novel liquid metal jet X-ray source.

In this contribution, we will give an overview of current developments in multilayer optics and scatterless beam components, showing their benefit for typical applications in combination with high-brightness microfocus X-ray sources. We will be presenting selected results for protein crystallography and small angle scattering obtained with the novel METALJET X-ray source.

MS21-T03

A X-ray Color Camera for spatially resolved XRF and XRD at once and fast chemical mapping of 3-dimensional Objects in a Laboratory Setup

C. Berthold[1], O. Scharf[2], K. Bente[3], A. Bjeoumikhov[4], I. Ordavo[5]
[1]*University of Tuebingen, Applied Mineralogy, Tuebingen, Germany*
[2]*IAP-Institut für angewandte Photonik e.V., Berlin, Germany*
[3]*University of Leipzig, Institute for Mineralogy, Crystallography & Material Science, Lepzig, Germany*
[4]*IfG-Institute for Scientific Instruments GmbH, Berlin, Germany*
[5]*PNSensor GmbH, München, Germany*

Spatially resolved X-ray fluorescence (XRF) and X-ray diffraction (XRD) mappings in a combined setup are till now only possible by using X-ray setups which combine microfocus X-ray sources with X-ray optics to decrease the spotsize down to the 10µm-range. The X-ray spectrum of each location is then analyzed by a classical EDX-detector separating the chemical information (XRF) from the structural information by energy dispersive X-ray diffraction (EDXRD) in the spectrum. Therefore, a chemical and structural mapping of a whole object is typically done measuring each point separately by moving the sample step by step which is a time consuming procedure.

The actual development of modern detectors gives nowadays the opportunity to overcome this limitation of spatially resolved XRF and XRD. Especially the new pnCCD detector (developed by PNSensor GmbH, Munich) with its image area of 12,7mm x 12,7mm and a 264x264 pixel resolution in the X-ray color camera “SLcam” of the IFG Institute for Scientific Instruments GmbH, Berlin allows for the first time to measure locally resolved energy spectra for each pixel (1,2). A unique advantage of this novel X-ray color camera is thus the possibility to perform a direct high resolution full-field energy-resolved X-ray imaging of the sample surface (FF-XRF) if a X-ray optic is mounted in front of the detector. Using different types of such X-ray polycapillary optics with varying magnification it is also possible to simply change the magnification of the camera setup to increase or decrease the local resolution or vice versa the area, which is measured. Details regarding this setup are given in (1,2).

In our presentation we will give insights into combined chemical and phase mappings of heterogeneous material systems performed in a laboratory setup with a common Mo-sealed tube (Fig. 1).

Additionally we will demonstrate the possibility to get directly highly local resolved “pictures“ of the elemental distribution of 3-dimensional objects, which demonstrates another unique advantage of the SL-camâ: the almost infinite depth of sharpness, when using a 1:1 polycapillary optic. This gives now the opportunity to perform a chemical analysis of 3-dimensional objects without any focusing effort. On the other hand it is also possible to change the area of interest or the local resolution by simply exchanging the polycapillary optics.

This capabilities of the SLcam setup will open completely new possibilities for an efficient chemical and structural characterization of all kinds of materials in all fields of e.g. materials sciences, raw materials, recycling materials and in archaeometrie.

(1) Scharf, O. et al., (2011) *Compact pnCCD-Based X-ray Camera with High Spatial and Energy Resolution: A Color X-ray Camera*, Anal. Chem., Vol. 83(7), pp. 2532-2538

(2) Ordavo, I, et al., (2011) *A new pnCCD-based color X-ray camera for fast spatial and energy-resolved measurements,* Nucl. Instrum. Methods Phys. Res. Sec. A 654(1) pp. 250 - 257.

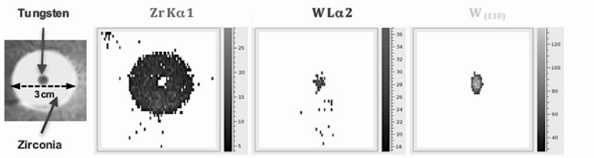

Fig. 1 A typical SLcam® picture from material science (an embedded tungsten wire in a zirconia matrix) after 4min exposure time with a 1:1 capillary optic, unfiltered Mo-sealed tube as X-ray source running at 40kV/50mA. Only 80pixel x 40pixel resolution due to mounted 1:1 optic => only inner part of the detector (12,7x12,7mm, 264x264Pixel) is used.
On one hand, the chemical information is visible in the spectra from each pixel of the camera, but on the other hand also the (110)-Laue-reflection from the cubic tungsten could be detected in each spectra if the goniometer angles are known. For the first time it is now possible to get local highly resolved chemical and structural distribution maps simultaneously from the same camera pixel.

MS21-T04

Fast quantitative determination of crystallite size distributions from 2D diffraction data

M. Chaouachi[1], S. Neher[1], S. Stracke[1], A. Falenty[1], H. Klein[1], W. F. Kuhs[1]
[1]*Universität Göttingen, GZG Abt. Kristallographie, Göttingen, Germany*

Crystallite sizes and crystallite size distributions (CSDs) of polycrystalline materials are of primary importance for their physical properties. Particularly important are the CSDs for the mechanical behaviour, e.g. the dependency of yield strength on the grain diameter via the Hall-Petch equation. Moreover, many transport properties depend on the grain-boundary network (GBN) which is determined also by the CSDs. As the manufacturing process strongly influences the CSDs (and GBNs) it is often necessary to control these quantities in fields reaching from metallurgy over ceramics to pharmaceutical products. Likewise, in natural samples much can be learned from CSDs about the formation process. Optical and electron microscopy on polished and etched surfaces are routinely used methods to measure CSDs. However, the latter methods are time-consuming (and generally only give 2D information), and in certain cases are unsuitable, in particular for unstable samples or *in-situ* investigations of changing CSDs. Here we propose a new fast diffractometric method for establishing CSDs of powders or polycrystalline aggregates using a 2D detector, a method which we like to call *fast diffraction CSD analysis*.

Our method uses 2D diffraction data with spotty Debye-Scherrer rings, usually (but not necessarily) measured in transmission. The individual Bragg spots are identified and their intensity is extracted from the diffraction data by a program written in the interpreter language Python (1). Details of this procedure are given in an accompanying paper (2). We demonstrate the capabilities of our *fast diffraction CSD analysis* in a study of the CSD of cryogenic polycrystalline materials (gas hydrates, ice), which are inaccessible to standard (electron-) optical methods. Information on the growth mechanism of these materials are obtained from the CSD analysis. The determination of CSDs using our fast quantitative method needs little sample preparation and could also be applied for time-resolved work with a resolution of a few minutes, in particular at synchrotron sources. For gas hydrates the method works almost two orders of magnitude faster than a slit-scanning method used earlier (3,4,5) for the price of an isotropic averaging over the crystallite sizes.

1. available at http://www.python.org/
2. S Neher, M Chaouachi, H Klein, and WF Kuhs (this conference)
3. SA Klapp, H Klein, and WF Kuhs (2007). *Geophys. Res. Lett.*, 34:L13608.
4. SA Klapp, S Hemes, H Klein, G Bohrmann, and WF Kuhs (2009) In: *Sediment-hosted Gas Hydrates* (Eds. D. Long, J. Rees, and C. A. Rochelle), Geological Society Publishing House, London, Special Publications 319, 161-170.
5. SA Klapp, S Hemes, H Klein, I MacDonald, and WF Kuhs (2010) *Mar. Geol.* 274: 85-94.

MS21-T05

Absorb7 and Absorb-GUI for single-crystal absorption corrections under non-ambient conditions

R. Angel[1], J. Gonzalez-Platas[2]
[1]*University of Padova, Geosciences, Padova, Italy*
[2]*Univeristy of La Laguna, Dept Fundamental Physics II, La Laguna, Spain*

Intensity data collected from single crystals held under non-ambient conditions in devices such as furnaces or diamond-anvil pressure cells has to be corrected for the absorption of X-rays as they pass through the device. Such devices often cause either rapidly-changing absorption corrections as a function of crystal rotation, or different correction factors for the same beam to different points on the crystal, situations for which empirical absorption corrections are inappropriate. Empirical approaches based solely on the minimization of Rint also will not necessarily correct absorption that has a strong 2theta dependence, for example as generated by the anvils of a diamond-anvil cell. In these cases the absorption corrections may be more accurate if they are based on a physical representation of the experiment (diffractometer, crystal and environmental device) from which path lengths of the incident and diffracted beams in the various materials can be calculated, and the absorption corrections thus determined.

ABSORB [1,2] is a program to calculate and apply absorption corrections to single-crystal X-ray intensity data from any source, any detector type, and any instrument configuration. A new version, ABSORB-7 [3], contains several significant new features. ABSORB-GUI has been developed to allow much easier specification of standard experiments, and to import experimental information from diffractometer software. The program that calculates the absorption calculations has been re-configured to allow it to be called directly from other commercial and non-commercial software packages. In addition, a number of new features have been introduced to allow more flexibility in the way the experimental configuration is described, and to correct synchrotron diffraction data collected with beams smaller than the sample crystal. Prospects for future developments will also be discussed.

[1] Burnham, C. W. (1966). *American Mineralogist* **51**, 159-167. [2] Angel, R. J. (2004). *Journal of Applied Crystallography* **37**, 486-492. [3] Angel, R. J. & Gonzalez-Platas, J. (2013). *Journal of Applied Crystallography, in press.*

MS21-T07

A Bench Top Solution for Challenging Crystal Structures

A. Gerisch[1], M. Adam[1], R. Glaum[2], M. Ruck[3]
[1]*Bruker AXS, Karlsruhe, Germany*
[2]*University of Bonn, Department of Inorganic Chemistry, Bonn, Germany*
[3]*Technical University of Dresden, Department of Inorganic Chemistry II, Dresden, Germany*

Up-to-now crystallographically challenging samples, such as twinned or modulates samples, have been measured using floor-standing instruments. The SMART X2S is a table top single crystal instrument, which has a proven record of providing high quality structures from thoroughly single crystalline organic and organometallic samples at the push of a button[1]. In addition to that, the system is also very capable of handling samples as challenging as those mentioned above. For illustration, we present here two crystals structures. In both cases the data collection was carried out fully automatically. As anticipated, the standard automated indexing, data processing and structure solution routines failed due to the crystallographic challenges presented by the samples. Consequently, after data collection all further steps required the expertise of a crystallographer exploring the sophisticated features of the APEX2 software package, shipped with each instrument. Between 285 K and 345 K chromium(II) diphosphate forms an incommensurately modulated structure[2]. The measurement of a Cr2P2O7 crystal at ambient temperature on the SMART X2S nicely confirms the structure. Additionally, the detailed investigation reveals a second domain of a non-crystallographic twin. The resulting data set was processed with Jana2006[3]. As a second example we present Bi14.33IrI12. In solid state chemistry, subvalent bismuth compounds are notoriously well known to give crystallographic problems, such as multiple twinning, pseudo symmetry, disordering, and superstructures. Even combinations of these effects have been frequently reported[4]. We will demonstrate how challenges such as the extremely high absorption coefficient, and the six fold twinning were successfully overcome and the strongly disordered structure was processed using a TWINABS corrected HKLF 5 file.

1 S. Lawrence; Analytical Chemistry, University College Cork, Cork, Ireland.
2 L. Palatinus, M. Dusek, R. Glaum, B. El Bali; Acta Cryst. (2006), B62, 556-566.
3 V. Petricek, M. Dusek, L. Palatinus; (2000), JANA2000, Institute of Physics, Praha, Czech Republic.
4 A. Gerisch, M. Ruck, Z. Krist., (2011), 226, 613-618.

MS21-T08

In-situ characterizationof the growth mechanism in the TiN/(Ti,Al)N/AlN multilayers

U. Ratayski[1], C. Baehtz[2], D. Rafaja[1]
[1]TU Bergakademie Freiberg, Institut of Materials Science, Freiberg, Germany
[2]Helmholtz-Zentrum Dresden-Rossendorf, Institute of Ion Beam Physics and Materials Research, Dresden, Germany

Titanium aluminum nitride thin films are commonly used for high temperature application such as machining at high cutting speeds or for dry cutting. Due to their excellent properties such as high oxidation resistance and increase of the hardness at elevated temperatures, (Ti,Al)N monolayer coatings are subject of many investigations since the 1980's. The characterization of (Ti,Al)N monolayer coatings revealed the complex 3D microstructure containing not only the stable fcc-TiN and w-AlN phases but also the metastable supersaturated fcc-(Ti,Al) and fcc-AlN. The main task of this study was the investigation of the growth mechanism of the metastable fcc-(Ti,Al)N and fcc-AlN inTiN/(Ti,Al)N/AlN multilayers at different ad-atom mobilities.

The in-situ characterization of the growth mechanism during the deposition of TiN/(Ti,Al)N/AlN multilayer coatings were carried out by in-situ X-ray scattering at the BM20 beamline at the ESRF. The TiN/(Ti,Al)N/AlN multilayer coatings were reactively deposited in Ar/N_2 atmosphere by magnetron sputtering from pure Ti and Al targets with an applied bias voltage of -30 V. The target power at the Ti and Al targets was varied between 20 and 60 W that affected primarily the ad-atom density. The growth of TiN/(Ti,Al)N/AlN multilayers was monitored by the small-angle scattering performed as time-resolved 2θ scans at a constant angle of incidence of the primary beam. These scans yield information about the growth rate, about the evolution of interface roughness and about the formation of the correlated interface roughness during the deposition process of the multilayer stack. The in-situ X-ray scattering showed a significant increase of the interface roughness during the deposition of the AlN layers, which is related to a lower ad-atom mobility of the Al atoms as compared to the Ti atoms. The time-resolved 2θ scans in the small angle region were accompanied by X-ray reflectivity measurements and reciprocal space mapping in the small angel region as well as by glancing angle X-ray diffraction (GAXRD) after the deposition process.

MS21-T09

Hard x-ray scanning microscopy with diverse contrast mechanisms at P06, PETRA III.

R. Hoppe[1]
[1]TU Dresden, Institut fuer Strukturphysik, Dresden, Germany

A hard x-ray microscope at the nanoprobe endstation of P06, PETRA III, DESY has now been running in user operation for more than a year. The instrument supports a variety of contrast mechanisms like x-ray absorption spectroscopy, fluorescence spectroscopy, small/wide angle x-ray scattering, and coherent diffraction contrast, retrieving chemical, elemental and complimentary structural information from inside the specimen [1]. The microscope routinely uses nanofocusing refractive lenses (NFLs)[2] to generate an intense x-ray nanobeam with a size of 50 nm to 100 nm. The spatial resolution of conventional scanning x-ray imaging techniques are limited by the numerical aperture of the x-ray optics. To overcome this limitation ptychography combines coherent x-ray diffraction imaging (CXDI) with raster scanning [3,4]. The ptychography has been invented in the late 1960s to solve the phase problem in electron crystallography [5]. Recent developments on this method allow to investigate nonperiodic samples and, in addition, to obtain the full information of the complex illumination wave field [6,7,8]. Ptychography joins the advantages of the high resolution of coherent diffraction imaging with the large field of view of scanning based methods. The spatial resolution of diffraction imaging is limited by the largest measured diffraction angle [9].Nevertheless all the methods mentioned before, do only provide a projection of the sample. To obtain a three-dimensional contrast map throughout the sample without dismantling it, a combination with tomography is possible. In my talk I will address the instrumental framework at the nanoprobe endstation as well as the theoretical background of the microscopy methods. I will introduce all the contrast mechanisms with an example experiment.

[1] C. G. Schroer, P. Boye, J. M. Feldkamp, J. Patommel, D. Samberg, A. Schropp, A. Schwab, S. Stephan, G. Falkenberg, G. Wellenreuter, N. Reimers, Nucl. Instrum. Meth. A 606, 93 (2010)
[2] P.Boye, urn:nbn:de:bsz:14-qucosa-27137 (2010)
[3] J. M. Rodenburg and H. M. L. Faulkner, Appl. Phys. Lett. 85(20), 4795 (2004).
[4] A. Schropp, P. Boye, A. Goldschmidt, S. Hönig, R. Hoppe, J. Patommel, C. Rakete, D. Samberg, S. Stephan, S. Schöder, M. Burghammer, and C. G. Schroer, J. Microscopy 241, 9 (2011).
[5] W.Hoppe, Acta Cryst. A25, 495 (1969)
[6] A. M. Maiden and J. M. Rodenburg, Ultramicroscopy 109, 1256 (2009).
[7] P. Thibault, M. Dierolf, O. Bunk, A. Menzel, and F. Pfeiffer, Ultramicroscopy 109, 338 (2009).
[8] A. Schropp, P. Boye, J. M. Feldkamp, R. Hoppe, J. Patommel, D. Samberg, S. Stephan, K. Giewekemeyer, R. N. Wilke, T. Salditt, J. Gulden, A. P. Mancuso, I. A. Vartanyants, E. Weckert, S. Schöder, M. Burghammer, and C. G. Schroer, Appl. Phys. Lett. 96, 091102 (2010).
[9] A. Schropp and C. G. Schroer, New Journal of Physics 12, 035016 (2010)

PS01 - Along the Innovation Chain: From Minerals and Crystals via Natural Sciences to Functional Materials

PS01-P01

Ordered defects in Hydrous Layer Silicates (HLSs) containing Ferrierite-type layers

B. Marler[1], H. Gies[1]
[1]Ruhr University Bochum, Geoscience, Bochum, Germany

Hydrous Layer Silicates (**HLSs)** are characterized by cations of low charge density (mainly organic cations) intercalated between silicate layers [1]. In many cases the topology of the layer of a HLS is identical to the layer-like building unit of a known zeolite. HLSs are used as precursors to form microporous 3D framework materials by either condensing the layers (this generates zeolites) or by introducing pillars between layers (Interlayer Expanded Zeolites).

Five different HLSs containing Ferrierite-type layers were obtained by hydrothermal synthesis from mixtures of silicic acid, water and specific organic cations. The materials were characterized by SEM, DTA/TG, solid state NMR spectroscopy and were structurally analyzed by Rietveld refinements. Unprecedented among the known HLSs, two of these materials are made up by layers with a significant amount of ordered defects. These silicates, RUB-20 and RUB-40 are monoclinic and crystallized with the smallest cations used in this study, tetramethylammonium and tetramethylphosphonium, respectively. The defects are not randomly distributed within the layer but involve a certain Si-O-Si bridge which is - to a fraction of ca. 50% - hydrolyzed into two -Si-OH groups. The regular, terminal silanol groups which are part of the idealized, non-interrupted layer and the additional silanol groups related to the defects generate a hydrogen bonding system which interconnects neighboring silicate layers (see Fig.). The results of the structure analysis are confirmed by ^{1}H and ^{29}Si NMR spectra. The other three HLSs synthesized with larger cations possess orthorhombic symmetry and are constructred from non-interrupted layers.

If RUB-20 and RUB-40 are transformed into framework structures by condensing the layers, the defects cause the formation of materials with low structural order and very limited porosity. The defects, however, may be very valuable - acting as weak acidic sites in catalytic processes - if RUB-20 and RUB-40 are transformed into Interlayer Expanded Zeolites.

[1] Marler, B. and Gies, H.: Hydrous layer silicates as precursors for zeolites obtained through topotactic condensation, Eur. J. Mineral **24**, 405, 2012.

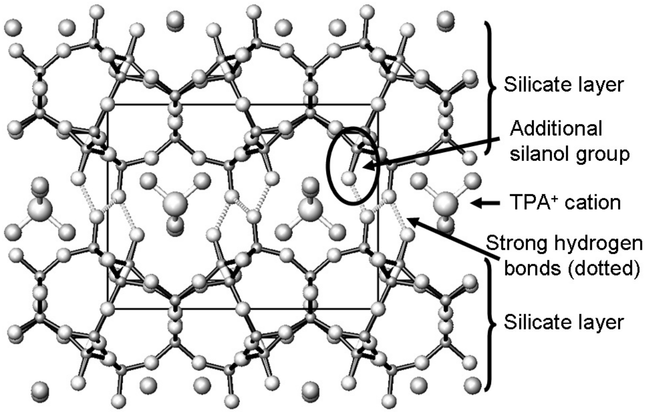

Fig.: The structure of RUB-40 ($P2_1/m$ with a = 10.763 Å, b= 14.001Å, c = 7.407 Å, β = 99.337°) projected on (001).

PS01-P02

Native Indium from a quartz-cassiterite-sulfide-paragenesis in the Erzgebirge - an electron microscopy study

M. Trinkler[1], U. Kempe[2]
[1]Erz&Stein - Gesellschaft für Lagerstätten u. Rohstoffberatung, Bobritzsch / OT Niederbobritzsch, Germany
[2]TU Bergakademie Freiberg, Institute of Mineralogy, Freiberg, Germany

Several rare minerals were recently found in the gneiss quarry of Dörfel near Annaberg-Buchholz in the westernErzgebirge. This includes stokesite, the beryllium minerals beryl, bertrandite, and bavenite, and native indium too.

Sulfides occur in veins and quartz bodies representing a late stage of a high temperature rare metal mineralization that was formerly called ‘pneumatolytic’. Sphalerite with high contents of Cd and In is part of this paragenesis. The sphalerit was leached partially together with other minerals during later metasomatic processes. One result of metasomatic leaching is the formation of native indium at the surface of sphalerite grains. The indium forms perfect pseudocubic crystals with diameters of about one micrometer. The metasomatic leaching produced intense corrosion structures on other minerals.

PS02 - Aperiodic and Modulated Structures: Potential in Higher Dimensions

PS02-P01

Incommensurate Phase of the Molecular Crystal p-$C_6F_4Br_2$ at T=15 K

L. Noohinejad[1], S. van Smaalen[1]
[1]University of Bayreuth, Laboratory of crystallogarphy, Bayreuth, Germany

Phase transitions may occur by variation of temperature or pressure. They are common in molecular systems, and the study of phase transitions can give information about the intermolecular forces. An example of a molecular compound is p-Dibromotetrafluorobenzene. The crystal structure at T= 150 K has been reported as a classic periodic structure [1]. Pawley *et. al* found that the crystal symmetry is $P2_1/c$ by using single crystal x-ray photographs and neutron powder diffraction. According to the quasi-elastic neutron scattering [2], the scattering pattern indicates a three dimensional periodic structure at T= 300 K, and at T= 4.2 K, an incommensurate phase with wavevector **q** = 0.24 along the b* direction was reported. The crystal structure was not reported.

According to our single-crystal X-ray diffraction measurement at in house diffractometer with Mo radiation at T= 248K, it is classical three-dimensional periodic crystal, the crystal system is monoclinic and space group belongs to $P2_1$ / c. To explore the nature, physical properties, and structure of p-$C_6F_4Br_2$ at low temperatures, we have done a single-crystal X-ray diffraction experiment at T = 15 K at the synchrotron Hasylab/DESY (Hamburg, Germany). At lower temperatures, we observed the appearance of additional Bragg spots indicative of superlattice formation and transformation to an incommensurate phase. Our initial analysis shows that at T= 15 K, the corresponding spots appeared at **q** = 0.1395 along a* direction which is in contrast to Overell *et. al* report [2].

[1] Pawley, G. S., Mackenzie, G. A., Dietrich, O. W., Acta Crystallogr, A 33 (1977) 142-145.

[2] Overell, J.S. W., Pawley, G. S., Mackenzie, G. A., Fitzgerald, W. J., Kirin, D., Chemical Physics letters 74 (1980) 373- 375.

PS02-P02

The commensurately modulated structure of trimethyltin hydroxide at 220 K

S. Dey[1], A. Schönleber[1], S. van Smaalen[1]
[1]*University of Bayreuth, Laboratory of Crystallography, Bayreuth, Germany*

At room temperature the structure of trimethyltin hydroxide is reported to crystallize in a (2**a** × 2**b** × 8**c**) superstructure with monoclinic **b**-unique symmetry, space group *Pn* [1]. At *T* = 176 K the structure undergoes a phase transition, at *T* = 120 K the structure is reported to be a disordered (1**a** × 1**b** × 2**c**) superstructure in space group $P2_1/c$ [2].

Temperature dependent single crystal X-ray diffraction experiment at the Hasylab/DESY (Hamburg, Germany) were performed to search for weak superstructure reflections, to perform full data collection and to explore crystal structures between room temperature and *T* = 100 K. At *T* = 220 K superstructure reflections along **a*** and **b*** are not observed and superstructure reflections up to fourth order are found along **c***, indexed with a **q**-vector (σ_1,0,σ_3) with σ_1 = 0 and σ_3 = 3/8. Strong diffuse scattering is present in the (**a***,**b***) planes defined by main reflections which reflects strong disorder in the crystal structure.

The eight-fold superstructure at *T* = 220 K is described in superspace with monoclinic symmetry $P2_1/m(\sigma_1,0,\sigma_3)0s$, the disorder can be interpreted with a hypothetical mirror plane perpendicular to **a**.

[1] N. Kasai, K. Yasuda, R. Okawara, *J. Organomet.Chem.* **3** (1965) 172-173.

[2] K. M. Anderson, S. E. Tallentire, M. R. Probert, A. E. Goeta, B. G. Mendis, J. W. Steed, *Cryst. Growth Des.* **11** (2011) 820-826.

PS02-P03

Modulated structure of $CeCuGa_3$

K. Sparta[1], Y. J. Sohn[1], G. Roth[1], D. A. Joshi[2], P. Burger[2], P. Adelmann[2], D. Ernst[2], T. Wolf[2], K. Grube[2], C. Meingast[2], H. V. Löhneysen[2,3]
[1]*RWTH Aachen University, Institut für Kristallographie, Aachen, Germany*
[2]*Karlsruhe Institute of Technology, Institut für Festkörperphysik, Karlsruhe, Germany*
[3]*Karlsruhe Institute of Technology, Physikalisches Institut, Karlsruhe, Germany*

The rare-earth intermetallic compounds CeM_xX_{4-x}, where M is a transition metal, have been shown to exhibit various interesting physical properties. Recently, superconductivity has been discovered in $CeMSi_3$ and $CeMGe_3$ (M=Co,Rh,Ir), leading to renewed efforts in the investigation of $CeMX_3$ [1]. Among those heavy-fermion systems, $CeCuGa_3$ stands out because of the contradicting magnetic properties reported in the literature, which could be related to different Cu/Ga ordering degrees [2]. The completely disordered polymorph of $CeCuGa_3$ crystallizes in the $BaAl_4$ structure type with 4/mmm site symmetry for Ce^{3+}, while an ordered phase with $BaNiSn_3$ structure type and non-centrosymmetric 4mm site symmetry for Ce^{3+} is also possible. We report a new modulated structure for $CeCuGa_3$, with the approximate propagation vector (0,0,1/3), exhibiting ferromagnetic properties.

[1] N. Kimura and I. Bonalde, in Non-Centrosymmetric Superconductors: Introduction and Overview, edited by E. Bauer and M. Sigrist, Lecture Notes in Physics Vol. 847 (Springer-Verlag, Berlin, 2012), pp. 35-79

[2] D.A. Joshi et al., PRB 86, 035144 (2012)

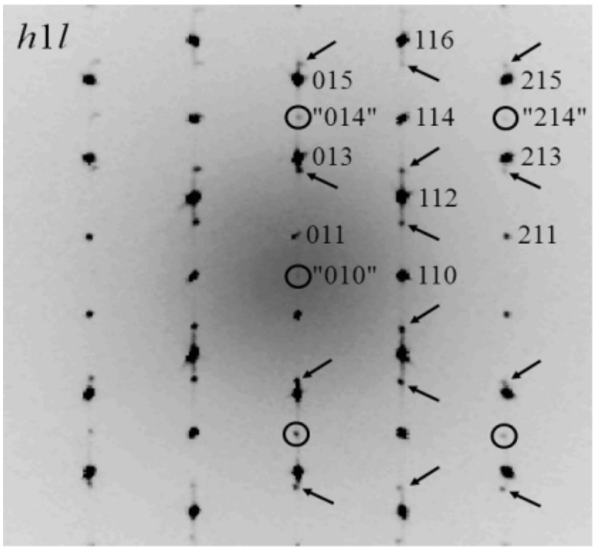

Abb. 1: *h*1*l* plane of the reconstructed reciprocal space from our single crystal X-ray diffraction data. The arrows point to the first- and second-order satellite reflections. The circles show the third-order satellites on the positions of forbidden reflections from the body-centered lattice.

PS02-P04

Local electronic structure studies of Ho_2PdSi_3 using Diffraction Anomalous Fine Structure

M. Nentwich[1], M. Zschornak[1], C. Richter[1,2], D. C. Meyer[1]
[1]*TU Bergakademie Freiberg, Institut für Experimentelle Physik, Freiberg, Germany*
[2]*DESY/ HASYLAB, Hamburg, Germany*

Diffraction Anomalous Fine Structure (DAFS) is a site-selective X-ray diffraction method for studying local electronic structures. Relying on an energy scan, the DAFS method is applied at absorption edges like *X-ray Absorption Fine Structure* (XAFS). But as an advantage over XAFS it is possible to differentiate between atoms of the same kind but different Wyckoff positions. The reason for this site-selectivity is the varying the momentum transfer of dffierent reflections. Here, this method is applied to study the atomic structure of the intermetallic compound Ho_2PdSi_3. A (2x┐ 2x┐ 8)-super structure model as proposed by Tang et al. [1] is used to determine the *c*-ordering of Pd substitutes on Si sites. This super structure model could be confirmed in comparison to a high symmetric *c*-stacking. The measurements of the experimental data have been carried out at beamline E2 and BW1 of DESY/ HASYLAB in Hamburg. The experiment is compared with theoretical data modeled with the FDMNES code [2].

[1] F. Tang et al., Phys. Rev. B 84, 104105 (2011).

[2] Y. Joly, Phys. Rev. B 63, 125120-125129 (2001).

PS03 - Biocrystallography I: Synthesis, Structure and Function

PS03-P01

Structural Basis of Assembly Chaperone-Mediated snRNP Formation

C. Grimm[1], J. Pelz[1], U. Fischer[1]
[1]*Institut für Biochemie, Würzburg, Germany*

Small nuclear ribonucleoproteins (snRNPs) represent key constituents of major and minor spliceosomes. SnRNPs contain a common core, composed of seven Sm proteins bound to snRNA, which forms in a step-wise and factor mediated reaction. The assembly chaperone pICln initially mediates the formation of an otherwise unstable pentameric Sm-protein unit. This so-called 6S complex docks subsequently onto the SMN-complex, which removes pICln and enables the transfer of pre-assembled Sm proteins onto snRNA. We present two crystal structures that allow a glimpse into the mode of action of the snRNP assembly line. The 6S complex structure identifies pICln as an Sm-protein mimic, which enables the topological organization of the Sm pentamer in a closed ring. A second structure of 6S bound to the SMN-complex components SMN and Gemin2 uncovers a plausible mechanism of pICln elimination and Sm protein activation for snRNA binding.

PS03-P02

Fluorinated Boron-dipyrromethene (BODIPY) Structures for Surface Analysis

W. Kraus[1], M. Hecht[1], T. Fischer[1], K. Rurack[1]
[1]*BAM Federal Institut of Materials Research, FB 1.3, Berlin, Germany*

A family of bright boron-dipyrromethene-type fluorophores with a high number of fluorine atoms (F-BODIPYs) has been developed and characterized by X-ray crystallography and optical spectroscopy. The introduction of 3,5-bis(trifluoromethyl)phenyl and pentafluorophenyl moieties significantly enhances the photo-stability of such dyes, yielding for instance photo-stable NIR (near-infrared) fluorophores that show emission maxima >750 nm.

F-BODIPYs can be used as potent dual labels for the quantification of primary amino groups on surfaces by X-ray photoelectron spectroscopy (XPS) and fluorescence, two powerful yet complementary tools for the analysis of organic surface functional groups[1-5].

The work presented here describes a family of BODIPY dyes containing various fluorinated substituents. Whereas the spectral features of the dyes are typical for such type of BODIPYs, these dyes show an exceptional brightness and an improved photo stability[6-8].

The BODIPY skeleton formed by three conjugated heterocyclic rings is almost planar, with an rms deviation ranging from 0.0126 Å to 0.0659 Å. In all the cases, the boron atom has a slightly distorted tetrahedral coordination with the two fluorine atoms being perpendicularly oriented with respect to the dipyrrin plane. This overall higher planarity of the bis-styryl-BODIPY skeleton leads to a propeller-like distortion of the BODIPY core, entailing the observed differences. Due to steric repulsion from the methyl groups attached to C1 and C7, the phenyl ring appended to C8 is strongly twisted out of the BODIPY mean plane.

Interestingly, control of the conformation and planarity of the styryl extensions in red/NIR emitting BODIPYs by choice of the styryl's aromatic unit allows a tailoring of the Stokes shifts of such dyes to a significant extent[9].

[1] Y. Xing, E. Borguet, *Langmuir* **2007**, *23*, 684-688.
[2] G. Ulrich, R. Ziessel, A. Harriman, *Angew. Chem., Int. Ed.* **2008**, *47*, 1184-1201.
[3] H. Kobayashi, M. Ogawa, R. Alford, P. L. Choyke, Y. Urano, *Chem. Rev.* **2010**, *110*, 2620-2640.
[4] S. Suzuki, M. Kozaki, K. Nozaki, K. Okada, *J. Photochem. Photobiol., C* **2011**, *12*, 269-292.
[5] N. Boens, V. Leen, W. Dehaen, *Chem. Soc. Rev.* **2012**, *41*, 1130-1172.
[6] C. L. Picou, E. D. Stevens, M. Shah, J. H. Boyer, *Acta Crystallogr., Sect. C: Cryst. Struct. Commun.* **1990**, *46*, 1148-1150.
[7] D.-C. Wang, C. He, J.-L. Fan, W.-W. Huang, X.-J. Peng, *Acta Crystallogr., Sect. E: Struct. Rep. Online* **2007**, *63*, o2900.
[8] X. Zhou, *Acta Crystallogr., Sect. E: Struct. Rep. Online* **2010**, *66*, o757.
[9] M. Hecht, T. Fischer, P. Dietrich, W. Kraus, A.Descalzo, W. Unger, K. Rurack, *ChemistryOpen*, accepted

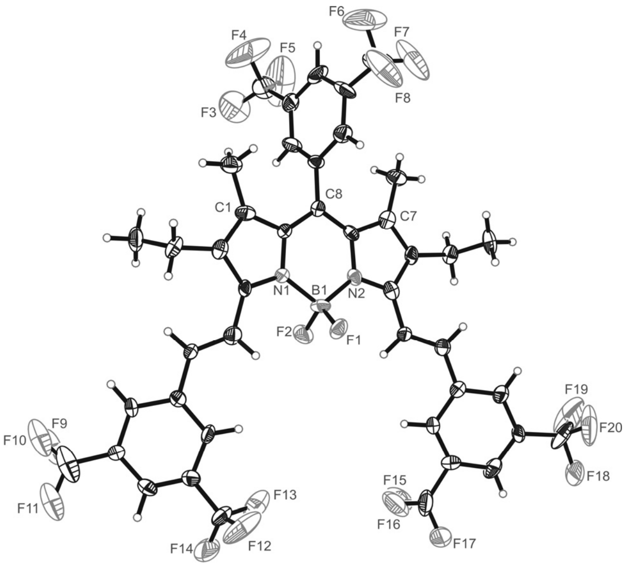

PS03-P03

P450 BM3 crystal structures reveal the role of the charged surface residue Lys/Arg184 in inversion of enantioselective styrene epoxidation

S. Panneerselvam[1], A. Shehzad[2], M. Linow[3], M. Bocola[2], D. Roccaatano[3], J. Mueller-Dieckmann[4], M. Wilmanns[5], U. Schwaneberg[2]
[1]*DESY, Hamburg, Germany*
[2]*RWTH Aachen University, Aachen, Germany*
[3]*Jacobs University, Bremen, Germany*
[4]*University of Hamburg, Biocenter Klein Flottbek, Hamburg, Germany*
[5]*EMBL, Hamburg, Germany*

Styrene oxide and its derivatives are versatile intermediates in the synthesis of valuable chemicals such as antidiabetic agents and dopamine agonists.[1] P450 BM3 is a 119-kDa water-soluble heme monooxygenase originating from *Bacillus megaterium*.[2] Interestingly, an exchange of a single amino acid to a positively charged residue at position 184 in P450 BM3 variant 5F5 inverts the enantioselectivity of styrene epoxidation towards *S*-styrene oxide;[3] even though Ala184 is located far from the active site (~18 Å). The latter findings, combined with excellent catalytic properties, make P450 BM3 a prime candidate to explore how a single charged surface residue inverts the enantioselectivity in the P450 BM3 variants 5F5 A184K (*S* selectivity 27.3% *ee*) and 5F5 A184R (*S* selectivity 26.5% *ee*) as compared to 5F5 variant (*R* selectivity 26.6% *ee*).[3]

High-resolution crystal structures of P450 BM3 variants in complex with styrene have been successfully determined which are the first crystal structures of P450 BM3 in the presence of a non-natural substrate, and illustrate the bound styrene in hitherto unobserved productive and non-productive substrate binding modes in the active site of P450 BM3.The backbone architecture of *S*-selective variants is similar to wild-type substrate-bound forms, whereas an overlay of *R*-selective variants with that of wild-type substrate-free forms shows a high degree of similarity.

The structural data reveal the formation of a new inter-helical salt bridge at the surface in *S*-selective variants which causes that key structural elements adjacent to the active site are repositioned in a concerted manner and, as a consequence, styrene binding geometries are altered. Solved crystal structures provide on the molecular level a first explanation how a positively charged surface residue (at position 184) inverts the enantiopreference of styrene epoxidation in P450 BM3. The obtained knowledge in understanding the enantioselective styrene epoxidation in P450 BM3 variants can very likely be generalized to structurally related monooxygenases and substrates.

1 J. D. Bloom, M. D. Dutia, B. D. Johnson, A. Wissner, M. G. Burns, E. E. Largis, J. A. Dolan and T. H. Claus, *J Med Chem*, 1992, 35, 3081-3084; F. R. Pfeiffer, J. W. Wilson, J. Weinstock, G. Y. Kuo, P. A. Chambers, K. G. Holden, R. A. Hahn, J. R. Wardell, Jr., A. J. Tobia, P. E. Setler and H. M. Sarau, *J Med Chem*, 1982, 25, 352-358.

2 L. O. Narhi and A. J. Fulco, *J Biol Chem*, 1986, 261, 7160-7169; L. O. Narhi and A. J. Fulco, *J Biol Chem*, 1987, 262, 6683-6690.

3 K. L. Tee and U. Schwaneberg, *Angew Chem Int Ed Engl*, 2006, 45, 5380-5383.

PS03-P04

DegQ - deciphering protein quality control in *Legionella*

W. Robert[1], H. Scott[1], A. Schubert[1], R. Hilgenfeld[1], G. Hansen[1]
[1]*University of Lübeck, Institute of Biochemistry, Lübeck, Germany*

Protein quality control is crucial for all living cells and sophisticated molecular mechanisms have evolved to combat the excessive accumulation of unfolded proteins. High-temperature requirement A (HtrA) proteases are important ATP-independent quality-control factors in most prokaryotic species. One distinctive property of HtrAs is their ability to assemble into complex oligomers ranging from pyramidal 3-mers to higher-order complexes consisting of up to 24 molecules. Tight control of chaperone and protease function is of pivotal importance to prevent deleterious HtrA-protease activity [1, 2].

Employing x-ray crystallography, we determined the structure of the DegQ, a major chaperone-protease of the periplasm and important virulence protein in *Legionella* species [3,4]. To understand how protease activity of DegQ is controlled, we probed its functional properties with the help of designed protein variants. Combining crystallographic, biochemical, and mutagenic data, a model for the intrinsic regulation of protease activity was developed. The 2.15-Å resolution structure of DegQ from *Legionella fallonii* revealed that the protein assembles into large, cage-like 12-mers [4]. We provide evidence that 12-mer formation is essential for the degradation of substrate proteins but not for the chaperone activity of DegQ. Interestingly, DegQ is unable to form 6-meric assemblies, which represent an important protease resting state in the homologous DegP chaperone-protease [4]. We present a mechanistic model that suggests how protease activity of DegQ 12-mers is intrinsically regulated and how deleterious proteolysis by free DegQ 3-mers is shut down. Our study sheds light on a previously uncharacterized component of the prokaryotic stress-response system with implications for other members of the HtrA family.

[1] G. Hansen & R. Hilgenfeld (2012): Architecture and regulation of HtrA-family proteins involved in protein quality control and stress response . Cell Mol Life Sci. 10.1007/s00018-012-1076-4 [Epub ahead of print].

[2] T. Clausen , M. Kaiser, R. Huber, M. Ehrmann (2011) HtrA proteases: regulated proteolysis in protein quality control. Nat RevMol Cell Biol **12**, 152-162.

[3] G. Hansen & R. Hilgenfeld (2012): Recent structures of virulence proteins of *Legionella* establish targets for new antibacterials. J. Microbes Infect. **7**, 2-12.

[4] R. Wrase, H. Scott, R. Hilgenfeld & G. Hansen (2011): The *Legionella* HtrA homologue DegQ is a self-compartmentizing protease that forms large 12-meric assemblies. Proc. Natl. Acad. Sci. USA **108**, 10490-10495.

PS03-P05
Conformational polymorphism in Atg8 family proteins

P. Ma[1], O. Olubiyi[2], B. Strodel[2], O. H. Weiergräber[2]
[1]*Institut de Biologie Structurale, Grenoble, France*
[2]*ICS-6, Forschungszentrum Jülich, Jülich, Germany*

Autophagy is a fundamental homeostatic process in eukaryotic organisms, fulfilling essential roles in development and stress adaptation. These functions involve either the removal of potentially harmful structures, such as damaged organelles, aggregates or pathogens, or the degradation of dispensable material to compensate for nutrient or energy deprivation. The hallmark of macroautophagy is the formation of double-walled vesicles called autophagosomes, which enclose target structures and later fuse with the lysosoamal compartment, leading to degradation of their cargo. Formation of these organelles critically depends on the Atg8 family of small adaptor proteins. While all members are composed of a ubiquitin-type β-grasp domain and an N-terminal helical extension, available data point to considerable conformational polymorphism involving both the N-terminal and the C-terminal segments of these proteins. We have taken a multi-disciplinary approach to investigate the conformational dynamics of GATE-16, representing one of the mammalian Atg8 subfamilies. First of all, crystallization of GATE-16 under near-physiological conditions yielded a structure with a closed conformation of the C-terminus, which is at variance with the more extended conformations observed previously [1]. Indeed, this new crystal structure is more likely to represent the prevailing conformer in solution, as indicated by comparison of observed and calculated NMR correlation times. While GATE-16 appears to be quite rigid overall, lower NMR order parameters were observed for the N and C termini, as well as for certain loop regions (residues 40-43 and 81-87), which is in good agreement with the distribution of crystallographic temperature factors. Finally, molecular dynamics simulations were applied to explore the underlying trajectories. The most significant finding was a fluctuation of the C-terminus between open and closed conformations, which are stabilized by unique patterns of salt bridges. Together, these complementary methods have provided new insight into a structural transition centered on the C-terminus of Atg8 homologs, which is crucial for the biological function of these proteins.

[1] Paz et al. (2000) J. Biol. Chem. 275, 25445ff.

PS03-P06
Studies on FKBP38 activation by Ca^{2+}-calmodulin

M. Michel[1], A. Stadler[2], O. H. Weiergräber[1]
[1]*ICS-6, Forschungszentrum Jülich, Jülich, Germany*
[2]*ICS-1, Forschungszentrum Jülich, Jülich, Germany*

FKBP38 is a non-canonical member of the human FK506-binding protein (FKBP) family which is distinguished by a unique domain structure and peculiar functional properties. In addition to a large N-terminal stretch with unknown structure and function, it is composed of a single FKBP-type segment, a tetratricopeptide repeat (TPR) domain and a C-terminal membrane anchor. While the FKBP domain *per se* is devoid of peptidylprolyl cis-trans isomerase (PPIase) activity, it has been shown to be activated by Ca^{2+}-loaded calmodulin [1]. This interaction has been studied by biochemical and biophysical methods, including NMR spectroscopy, but the three-dimensional structure of the complex as well as the mechanism of PPIase activation are still not understood. Another intriguing property of FKBP38 is its interference with Bcl-2-regulated apoptosis pathways, which has been proposed to underly the neuroprotective effect of FKBP38 inhibitors [2,3]. Again, the nature of the interaction with Bcl-2 and the structure of the complex have remained elusive. We therefore set out to reconstitute those assemblies with recombinant proteins and characterize them using X-ray crystallography. Preliminary data indicate that the complex formed between soluble FKBP38 and calmodulin is stable in the presence of > 50 µM Ca^{2+}. In addition to crystallization trials, we are currently performing small angle X-ray scattering measurements (Figure 1) to obtain the shapes and sizes of individual components as well as of the heterodimer. Unexpectedly, the affinity of Bcl-2 for FKBP38 turned out to be rather weak with rapid dissociation kinetics, pointing to a transient character of this interaction.

[1] Edlich et al. (2007) J. Biol. Chem. 282, 36496ff
[2] Edlich et al. (2006) J. Biol. Chem. 281, 14961ff
[3] Choi & Yoon (2011) Curr. Opin. Pharmacol. 11, 354ff.

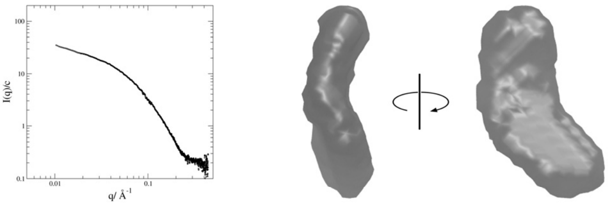

Scattering curve

Low-resolution model

Soluble FKBP38 was expressed in E. coli, purified under native conditions to crystallization grade quality and subjected to small angle X-ray scattering (BM29, ESRF).

PS03-P07

Structure of the Fe(II)/2-Oxoglutarate Dependent Dioxygenase RdpA in Complex with Substrate and Co-Substrate

J. Krausze[1,2], R. Müller[3], N. Sträter[2]
[1]*Helmholtz Center for Infection Research, Molecular Structural Biology, Braunschweig, Germany*
[2]*Universität Leipzig, Institut für Bioanalytische Chemie, Leipzig, Germany*
[3]*Helmholtz-Zentrum für Umweltforschung, Umweltmikrobiologie, Leipzig, Germany*

The Fe(II)/2-oxoglutarate (2-OG) dependent dioxygenase RdpA was originally isolated from the soil bacterium *Delftia acidovorans*, an organism that is capable of utilizing chlorinated aromatic compounds as sole carbon source [1]. RdpA catalyzes the cleavage of the ether bond of 2,4-dichlorophenoxy alkanoates, which is the initial step of the degradative pathway of chlorinated aromates. Despite the fact that RdpA accepts various 2,4-dichlorophenoxy alkanoates as substrates, it shows its highest activity for the turnover of *R*-2-(2,4-dichlorophenoxy) propionate (R-DP). RdpA exhibits a strong enantioselectivity and does not convert the S-form of the substrate [2]. Here, we present the X-ray structure of RdpA in complex with R-DP and 2-OG [3]. Whereas the binding of the 2-OG is similar to that seen in homologous structures, the binding of R-DP above the equatorial plane of the metal ion is unique to RdpA. The main free energy gain upon substrate binding comes from hydrophobic interactions of R-DP's aromatic ring with a hydrophobic pocket of the enzyme. The substrate's correct orientation, which brings the hydrogen atom of the asymmetric carbon atom close to the metal ion and thus allows for the cleavage of the substrate, is realized through hydrogen bonds with the amino acids S114 and Y221. Moreover, these hydrogen bonds guarantee RdpA's enantioselectivity: the binding of *S*-2,4-dichlorophenoxy propionate would result in an orientation in which the hydrogen atom points away from the metal ion and thus cannot be subtracted.

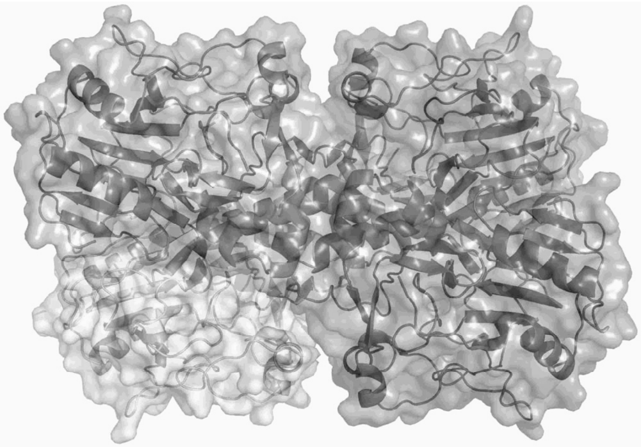

Fig. 1: Quarternary structure of RdpA.

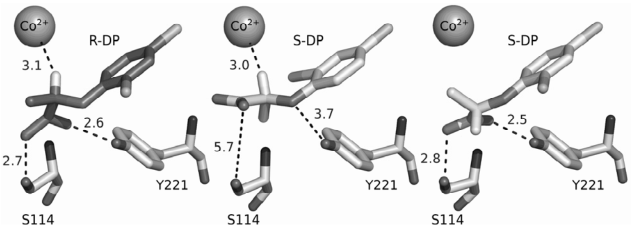

Fig. 2: Substrate binding to RdpA. Left: Binding of R-DP with the to-be-attacked hydrogen atom close to the catalytic metal ion (here replaced by cobalt). Middle: Binding of S-DP that would allow turnover but is not favored because of lacking hydrogen bonds. Right: Favored binding of S-DP that does not allow for turnover.

[1] A. Ehrig, R. H. Müller, W. Babel. Isolation of phenoxy herbicide-degrading *Rhodoferax* species from contaminated building material. Acta Biotechnol 17 (4) (1997) 351-356.

[2] A. Westendorf, D. Benndorf, T. Pribyl, H. Harms, R. H. Müller. Kinetic traits and enzyme form patterns of *R*-2-(2,4-dichlorophenoxy)propionate/α-ketoglutarate dioxygenase (RdpA) after expression in different bacterial strains. Engin Life Sci 6 (6) (2006) 552-559.

[3] J. Krausze, R. H. Müller., N. Sträter. Structure Determination of the 2-Oxoglutarate Dependent Dioxygenase RdpA in Complex with Substrate and Co-Substrate. In preparation.

PS03-P08

The hierarchical composite crystal architecture of sea urchin teeth: A crystallographic, chemical and mechanical characterization

B. J. Maier[1], A. J. Götz[2], E. Griesshaber[1], J. Deuschle[3], R. Abel[4], L. Howard[4], K. T. Fehr[1], B. Ruthensteiner[5], W. W. Schmahl[1]
[1]*Ludwig-Maximilians Universität München, Department für Geo- und Umweltwissenschaften, München, Germany*
[2]*Ludwig-Maximilians Universität München, GeoBio-Center, München, Germany*
[3]*Max-Planck-Institut für Metallforschung, Stuttgart, Germany*
[4]*Natural History Museum, London, United Kingdom*
[5]*Zoologische Staatssammlung München, München, Germany*

The crystallographic orientation of the crystalline elements constituting the hierarchical composite crystal of the tooth of the sea urchin Paracentrotus lividus was investigated together with variations in chemical composition and nanomechanical properties by computed micro- and nano-tomography, scanning-electron-microscopy, electron-backscatter-diffraction (EBSD), X-ray diffraction (XRD), energy dispersive x-ray spectroscopy, electron-probe-micro-analysis, and nanoindentation testing. In addition, the crystallographic orientation of the tooth of several other sea urchin species was determined by in-house XRD. Modern sea urchin teeth are Mg dominated calcite composite materials distinctly harder than inorganic calcite and even dolomite. We found that the hardness of the tooth is positively correlated to its magnesium content. The nanohardness of the tooth scatters between 3.5 GPa and over 8 GPa, showing a consistently higher hardness in comparison to non-biological calcite and dolomite and almost reaching the hardness of magnesite. Tomographical imaging revealed that the tooth of Paracentrotus lividus is composed of distinct structural elements, i.e the primary, secondary and the carinarr process plates regions. These regions constitute of stacks of curved platelets and surround bundles of channels and needles that are located in the centre portion of the mature tooth. Our EBSD results show that the mean crystallographic orientation of crystals composing these major structural elements are tilted to each other by 3-5°. Furthermore, even within each structural element the orientation of the constituting subunits such as single platelets varies by 1-2°. In addition, synchrotron XRD rocking curves measured along a sagittal cut reveal that the intrinsic mosaic spread is reduced towards the tip. We regard the tooth of the sea urchin Paracentrotus lividus as a hierarchically assembled mesocrystal with a mosaic texture. The mosaic spread varies between different species.

PS03-P09

Structural and functional characterization of Bacterial MDR-transporters

P. Simeonov[1], S. Werner[2], F. Jaenecke[1], C. Haupt[1], K. Bacia[2], M. Tanabe[1]
[1]*Martin-Luther-Universität Halle-Wittenberg, ZIK HALOmem, Memrbane Protein Biochemistry, Halle, Germany*
[2]*Martin-Luther-Universität Halle-Wittenberg, Biophysical Chemistry of Membranes, Halle, Germany*

Nowadays an increasing number of pathogens show clinically relevant resistance against multiple antimicrobial agents. A major contribution to this ability is conferred by a number of multidrug resistance (MDR) transporters. These multidrug efflux pumps are ubiquitously conserved in many pathogens' genomes and have function as the exporters of natural substances produced by the host as well as structurally dissimilar harmful compounds such as antibiotics, dyes or detergents crucial for the host cell survival. Furthermore the natural functions of these multidrug efflux systems are largely unknown and nearly no specific structural information is available. Due to these characteristics, the studies of MDRs may be able to provide an important link between bacterial pathogenesis and antibiotic resistance, making them attractive targets for future therapeutic studies.

The main aim of our research is to establish a work flow towards structural and functional characterization of MDRs. We use a GFP fusion protein expression system (Drew et al. 2006) to improve the monitoring on protein expression levels and solubility. In addition the MDR-GFP fusion proteins can be used for the reconstitution into phospholipid environment and the efficiency of reconstitution is easily measured via fluorescence technique. The MDR integrated proteoliposomes are used for specific transport assays and functional characterizations. The purified GFP cleaved MDRs are submitted to Lipid Cubic Phase (LCP) or conventional vapor diffusion crystallization trials. Combining these techniques makes us utilize the resource efficiently and the results can produce a detailed structural and functional characterization of MDRs.

David Drew, Mirjam Lerch, Edmund Kunji, Dirk-Jan Slotboom & Jan-Willem de Gier (2006) Nature Methods - 3, 303 - 313

PS04 - Biocrystallography: Other

PS04-P01

Facilities for Macromolecular Crystallography at the Helmholtz-Zentrum Berlin

M. Weiss[1], M. Bommer[1], R. Förster[1], M. Hellmig[1], M. Krug[1], S. Pühringer[1], M. Steffien[1], M. Ühlein[1], U. Mueller[1]
[1]*Helmholtz-Zentrum Berlin, Macromolecular Crystallography, Berlin, Germany*

The Macromolecular Crystallography (MX) group at the Helmholtz-Zentrum Berlin (HZB) has been in operation since 2003. Since then, three state-of-the-art synchrotron beam lines (BL14.1-3) for MX have been built up on a 7T-wavelength shifter source [1,2]. Currently, the three beam lines represent the most productive MX-stations inGermany, with more than 800 PDB depositions. BLs14.1 and 14.2 are energy tunable in the range 5.5-15.5 keV, while BL14.3 is a fixed-energy side station (13.8 keV). All three beam lines are equipped with CCD-detectors. Beam lines BL14.1 and BL14.2 are in regular user operation providing about 200 beam days per year and about 600 user shifts to approximately 50 research groups acrossEurope. BL14.3 has been equipped with a HC1 crystal dehydration device and has been set back to user operation as a screening and test beam line in 2010. BL14.1 has recently been upgraded with an MD2-microdiffractometer including a kappa-geometry option and an automated sample changer. In January 2013, a PILATUS 6M-detector will be installed on this beamline. Additional user facilities include office space adjacent to the beam lines, a sample preparation laboratory, a biology laboratory (safety level 1) and high-end computing resources. On the poster, a summary on the experimental possibilities of the beam lines and the provided ancillary equipment for the user community will be given.

[1] Heinemann U., Büssow K., Mueller, U. & Umbach, P. (2003). Acc. Chem. Res. 36, 157-163.

[2] U. Mueller, N. Darowski, M. R. Fuchs, R. Förster, M. Hellmig, K. S. Paithankar, S. Pühringer, M. Steffien, G. Zocher & M. S. Weiss (2012). J. Synchr. Rad. 19, 442-449.

PS04-P03

Ultraviolet laser radiation damage induced phasing as an efficiently applicable method to solve the crystallographic phase problem of death receptor six (DR6)

S. Kemmerzehl[1], M. Krug[2], U. Mueller[2], M. E. Than[1]
[1]*Leibniz-Institute for Age Research , Proteincrystallography Group, Jena, Germany*
[2]*Helmholtz-Zentrum Berlin, Macromolecular Crystallography, Berlin, Germany*

Tumor necrosis factor receptor superfamily members and their ligands regulate apoptosis and inflammation. The death receptor 6 (DR6) is a member of this superfamily and represents nine characteristically arranged disulfide bridges within its cysteine-rich region[1] DR6 has been an orphan receptor until the Amyloid precursor protein (APP) was identified as a potential DR6 ligand and so DR6 was associated with Alzheimer´s disease[2]. For a better understanding of the molecular mode of this interaction, the structure of the potential ligand-binding domain of DR6 was solved[1].

Here we employed the hexagonal crystals of space group $P6_122$ comprising the cysteine-rich region of DR6 to characterize the utility, versatility and adaptability of solving the phase problem by ultra-violet radiation damage induced phasing (UV-RIP) at beamline Bl14.1 of BESSY II[3]. Two distinct crystals were used for the measurements where at first a native dataset was measured and then the crystals were exposed to two times to UV light laser radiation while rotating. After analyzing the effect of UV (and X-ray) radiation on the structural integrity and on the disulfide bridges, we demonstrated the suitability of UV-RIP for experimental phasing. Therefore we set up a pseudo single isomorphous replacement approach, considering the dataset before UV irradiation as the one carrying the heavy atoms (the sulfur atoms e.g. of the disulfide bridges) and the datasets after irradiation as the native ones. A key step was to identify the sulfur atom positions using ShelX C, D[4] as implemented in the CCP4i suite. SHARP was used for experimental phasing performing a single isomorphous replacement with anomalous scattering approach based on X-ray data not optimized for sulfur anomalous dispersion[5] followed by solvent flattening resulting in experimental electron density maps of very high quality. One must conclude that it is not necessary to identify all sulfur sites for phasing, but that rather the correct identification of a few sulfur-sites strongly affected by UV-RIP is sufficient.

References:

[1] Kuester M, Kemmerzehl S, Dahms SO, Roeser D, Than ME (2011). *J Mol Biol*, 409, 189-201.

[2] Nikolaev, A., McLaughlin, T., O'Leary, D. D. & Tessier-Lavigne, M. (2009) *Nature* **457**, 981-9.

[3] Mueller, U., Darowski, N., Fuchs, M.R., Förster, R., Hellmig, M., Paithankar, K.S., Pühringer, S., Steffien, M., Zocher, G., Weiss, M.S. (2012). J. Syn. Rad., 19, 442-449

[4] Sheldrick, G. M. (2008). Acta Crystallogr A 64, 112-122.

[5] Bricogne, G., Vonrhein, C., Flensburg, C., Schiltz, M. & Paciorek, W. (2003). Acta Crystallogr D Biol Crystallogr 59, 2023-2030.

PS04-P04

Applications with the New, Brighter X-ray Source from Agilent Technologies.

Z. Gal[1]
[1]Agilent Technologies, Marketing, Yarnton, United Kingdom

Zoltán Gál,[a] Tadeusz Skarzynski,[a] Fraser White,[a] Oliver Presly,[a] , Adrian Jones,[b] Damian Kucharczyk,[b] and Mathias Meyer,[b]

[a]Agilent Technologies UK Ltd, 10 Mead Road, Oxford Industrial Park, Yarnton, Oxfordshire, OX5 1QU, UK, [b]Agilent Technologies Sp. z o.o., Szarskiego 3, PL-54-610 Wroclaw, Poland E-mail:Zoltan.Gal@agilent.com

While a majority of macromolecular X-ray data are currently collected using highly efficient beam-lines on an increasing number of synchrotrons, there is still a need for low-maintenance, reliable systems for in-house experiments.

Agilent Technologies develop and supply X-ray systems for single-crystal diffraction research, including the SuperNova; a compact, highly reliable and very low maintenance instrument providing X-ray data of the highest quality; and the PX Scanner for testing and characterization of protein crystals in their original crystallization drops (in-situ). The SuperNova and PX Scanner are constantly improving, with recent enhancements including the introduction of the second generation Nova sealed-tube micro-focus X-ray source, which results in over 2x stronger diffraction from protein crystals with significantly improved signal to noise ratio.

We have also developed a completely new micro-focus X-ray source based on Gradient Vacuum technology, with novel filament and target designs. This novel source is an integral part of the new Agilent GV1000 X-ray diffractometer, which has been designed for applications that require even higher brightness of the X-ray beam.

As part of our ongoing research and development effort we have evaluated currently available CCD and CMOS imaging technologies used in the production of modern electronic 2D area detectors. Results of this evaluation show that for currently available large-area chips, CCD-based detectors are significantly more sensitive, with an increased signal-to-noise ratio resulting from much lower readout noise.

PS04-P05

XDSAPP - A graphical user interface for the convenient processing of diffraction data using XDS

M. Krug[1]
[1]HZB Berlin, MX, Berlin, Germany

XDS (1-3) is a software for processing single-crystal monochromatic diffraction data of (protein)-crystals recorded by the rotation method. It is a textbased software: the user provides XDS with a textfile (XDS.INP) containing instructions and XDS produces textfiles with output data. Setting up a correct input textfile for XDS can be tricky and time consuming as well as evaluating the text output of the software, especially for novice users.

XDSAPP is a Tcl/Tk GUI that combines the software packages XDS, POINTLESS of the CCP4 software suite (2) and XDSSTAT (3), allowing the user to process one or multiple diffraction image datasets with minimum input effort. Plots of all the important statistics within the XDS output files are generated. These plots offer the possibility to easily estimate the quality of the processed datasets. The statistical output produced by XDSSTAT is also plotted. XDSAPP is available at beamlines 14.1-14.3 at BESSY II and downloadable from our website.

For remote data collection we will offer a python-based tool (XDSIT), that processes all collected datasets automatically and stores important information for each dataset within a MySQL-database. The user will then be able to check the processing results remotely via a webbrowser interface.

We are currently developing a Qt-based Graphical User Interface for XDSIT that will in some future replace the XDSAPP application. Finally XDSIT will than be usable as a command-line script, a GUI application and a fully automated background data processing/database tool.

References
1. Kabsch, W. (1993). J. Appl. Cryst. 26, 795-800.
2. Kabsch, W. (2010a). Acta Cryst. D66, 125-132.
3. Kabsch, W. (2010b). Acta Cryst. D66, 133-144.
4. CollaborativeComputationalProject(1994).Acta *Cryst. D50*760-763
5. Diederichs,K.(2006).Acta Cryst. D62, 96-101

PS05 - Crystal Physics, Crystal Chemistry: Synthesis and New Crystal Structures

PS05-P01
Aminkomplexe des Gold(I)-cyanids

C. Döring[1], P. G. Jones[1]
[1]*Technische Universität Braunschweig, Institut für Anorganische und Analytische Chemie, Braunschweig, Germany*

Es wurden Cyanogold(I)-Komplexe in der linearen Form L-Au-CN dargestellt (L = primäres oder sekundäres Amin). Darüber hinaus wurden Verbindungen mit den Azaaromaten 3,5-Lutidin (zwei Polymorphe), 2,4-Lutidin und 4-Picolin (beide isotyp) synthetisiert. Mit Ethylendiamin wurde ein Komplex der Stöchiometrie 2:1 erhalten. Es wurden keine Komplexe mit tertiären Aminen erhalten.

Die Verbindungen wurden durch das Lösen und Auskristallisieren von Gold(I)-cyanid im jeweiligen Amin dargestellt, röntgenographisch untersucht und ihr Packungsaufbau bezüglich Wasserstoffbrücken und aurophilen Wechselwirkungen analysiert. Es bilden sich bei allen Strukturen mit N-H-Gruppen hauptsächlich klassische Wasserstoffbrücken zwischen den Amin-*H*-Atomen und den Cyanid-*N*-Atomen aus. In den meisten Fällen treten kurze Gold-Gold-Kontakte um 3,3 Å auf, die häufig Ketten ausbilden und ein zentrales Element des Packungsaufbaus sind. Diese werden durch Wasserstoffbrücken und seltener durch Gold-Wasserstoff-Kontakte zu Strängen, Schichten oder dreidimensionalen Netzwerken verknüpft. Bei einigen Strukturen tritt Pseudosymmetrie auf.

Bis auf Dipyrrolidingold(I)-dicyanoaurat(I) liegen alle Komplexe in der ungeladenen molekularen Form L-Au-CN vor. Im Gegensatz zu Amin(chloro)gold(I)-Komplexen[1,2], die z. T. auch in der ionischen Form [L_2Au^+ Cl^-] auftreten, enthalten die Amin(cyano)gold(I)-Komplexe keine „freien" Cyanidionen.

Primäre Amine	**Sekundäre Amine**
Cyano(cyclohexylamin)gold(I):Cyclohexylamin (1:1) [$P2_1$]	Cyano(diethylamin)gold(I) [$Fdd2$]
Cyano(cyclohexylamin)gold(I) [$P2_1$]	Cyano(morpholin)gold(I) [$Pca2_1$]
Cyano(isobutylamin)gold(I) [$Pca2_1$]	Cyano(piperidin)gold(I) [$P2/c$]
Cyano(isopropylamin)gold(I) [$R3c$]	Cyano(pyrrolidin)gold(I) [P-1]
Azaaromaten	Dipyrrolidingold(I)-dicyanoaurat(I) [P-1]
Cyano(2,4-lutidin)gold(I) [$Pbcm$]	**Diamine**
Cyano(3,5-lutidin)gold(I) [$P2_1/n$ und $C2/c$]	Ethylendiamin[bis(cyanogold(I))] [$P4_32_12$]
Cyano(4-picolin)gold(I) [$Pbcm$]	

Tabelle 1 Röntgenographisch charakterisierte Cyanogold(I)-Komplexe [Raumgruppe]

Vorläufige Versuche an Systemen Amin/Gold(I)-thiocyanat führten zu Komplexen der ionischen Form [L_2Au^+ $Au(SCN)_2^-$].

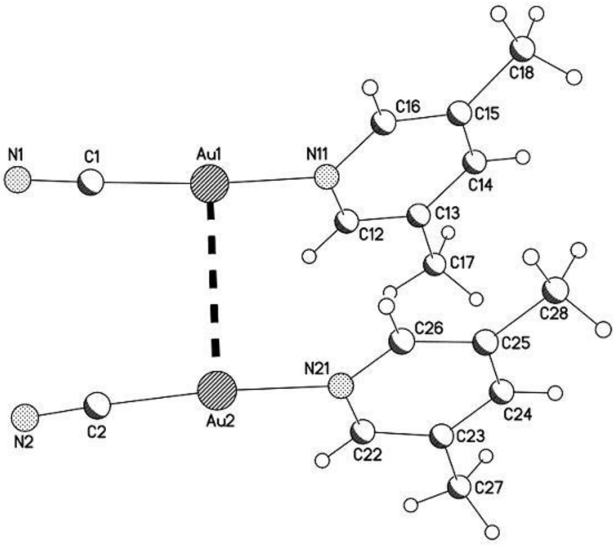

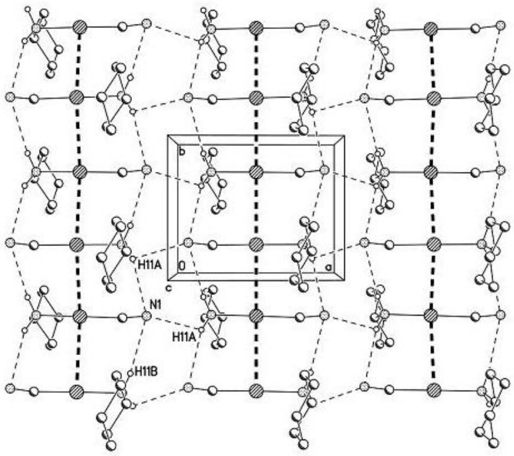

Abbildung 1. Asymmetrische Einheit von Cyano(3,5-lutidin)gold(I) in $P2_1/n$ mit eingezeichnetem Gold-Gold-Kontakt (Länge 3,32 Å).

Abbildung 2. Packung des Cyano(cyclohexylamin)gold(I). Parallele Ketten aus Gold-Gold-Kontakten (dick gestrichelt, Länge 3,40 Å, Winkel 142,14°) durch Wasserstoffbrücken zur Schicht verknüpft (dünn gestrichelt, N11-H11A…N1 2,62 Å, 148,7° und 2,64 Å, 115,6°, N11-H11B…N1 2,63 Å, 172,2°).

Literatur
[1] P. G. Jones, B. Ahrens, *Chem. Ber./Recueil*, **1998**, *130*, 1813-1814
[2] P. G. Jones, B. Ahrens, *New J. Chem.* **1998**, *22*, 1041-1042

PS05-P02

$Zr_2Fe_{12}As_7$: A New Iron Arsenide with Structural Relations to LiFeAs

M. Bischoff[1], L. Shlyk[1], R. Niewa[1]
[1] *University of Stuttgart, Institute of Inorganic Chemistry, Stuttgart, Germany*

Crystals of $Zr_2Fe_{12}As_7$ were originally obtained as minority byproduct during the synthesis of LiFeAs crystals with variable substituents [1-4]. Dark black needle-shaped crystals of $Zr_2Fe_{12}As_7$ with sizes up to several mm in length (Fig. 1) were intentionally obtained from the reaction of the elements. $Zr_2Fe_{12}As_7$ crystallizes in the hexagonal $Zr_2Fe_{12}P_7$ structure type [5] (P-6, $Z = 2$, $a = 952.10(7)$ pm, $c = 373.24(2)$ pm, $V = 293.01 \cdot 10^6$ pm^3, $R_1 = 0.033$, $wR_2 = 0.077$).

Figure 2 shows a projection of the crystal structure along [001], depicting the interconnection of trigonal prisms surrounding the As atoms. As(3) is exclusively coordinated by Fe atoms in a trigonal prism, the further As sites are coordinated in distorted prisms by four Fe and two Zr. All of these prisms are capped by three Fe (CN(As) = 9). The surroundings of Fe(1), Fe(2) and Fe(4) can be described as distorted tetrahedra, which each form infinite chains via vertex-sharing. Those three chains constitute a band running along [001] by edge-sharing. Fe(3) is situated in square pyramidal coordination forming chains along [001] via edge-sharing, with three of the chains forming a windmill like motif. Between the windmill sails the above mentioned bands of tetrahedra are located. The resulting framework provides channels filled with Zr, leading to a trigonal prismatic coordination by As. This regular prism is surrounded by a second trigonal prism rotated by 60° formed by Fe. These two trigonal prisms result in a hexagonal prismatic coordination of Zr.

Striking are the similarities of the Fe-As-frameworks in $Zr_2Fe_{12}As_7$ and the new iron pnictide superconductors as, e.g., LiFeAs [6] or LaFeAsO [7], which all contain flat layers of edge-connected $FeAs_{4/4}$ tetrahedra. In $Zr_2Fe_{12}As_7$ tetrahedral and square pyramidal coordinated Fe form a 3D framework, which partly shows the same motif of flat bands of edge-connected tetrahedra intersecting within 60° angle.

Electric resistivity measurements taken on one selected crystal display metallic temperature dependence of the resistivity with no significant magnetic field dependence (1.8 K to 320 K; 0 T to 9 T). $Zr_2Fe_{12}As_7$ crystals show paramagnetic behavior. The effective magnetic moment results in $\mu_{\mathrm{eff}} = 5.8\ \mu_B$.

[1] M. Bischoff, L. Shlyk, E. Rose, S. Zapf, M. Dressel, R. Niewa, *Z. Anorg. Allg. Chem.* **2012**, *638*, 1628.

[2] L. Shlyk, M. Bischoff, E. Rose, R. Niewa, *J. Supercond. Novel Magn.* **in press**.

[3] L. Shlyk, M. Bischoff, E. Rose, R. Niewa, *J. Appl. Phys.* **2012**, *112*, 053914.

[4] L. Shlyk, M. Bischoff, R. Niewa, *Supercond. Sci. Technol.* **2012**, *25*, 125006.

[5] E. Ganglberger, *Monatsh. Chem.* **1968**, *99*, 557.

[6] Pitcher *et al.*, *Chem. Commun.* **2008**, *45*, 5918.

[7] Kamihara *et al.*, *J. Am. Chem. Soc.* **2008**, *130*, 3296.

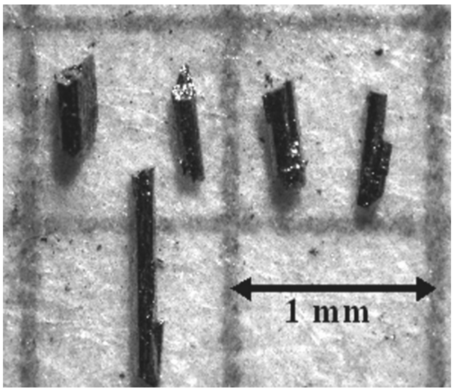

Figure 1: Needle-like crystals of $Zr_2Fe_{12}As_7$ with hexagonal basis.

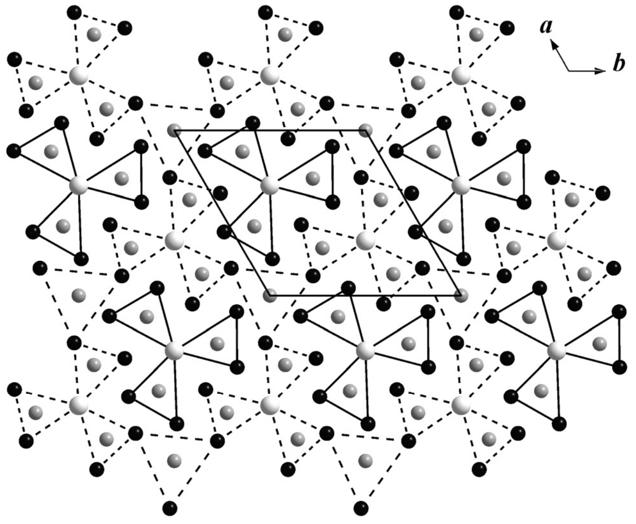

Figure 2: $Zr_2Fe_{12}As_7$: Projection in [001] (Zr: light grey; Fe: black; As: grey). Black lines indicate trigonal prisms surrounding As (dashed at the level of c/2).

PS05-P03

The crystal structure of the potassium-trisulphidometallate double salts $K_3[MOS_3]Y$ (M = Mo, W; = Cl^-, SH^-) and $K_6[WOS_3]_2(S_2O_3)$ and the first crystal structure of $K_2(S_2O_3)$

A. J. Lehner[1], L. V. Schindler[1], C. Röhr[1]
[1] *Albert-Ludwigs-Universität Freiburg, Freiburg im Breisgau, Germany*

Oxidosulfido-ortho-molybdates(VI) and tungstates(VI) were synthesized more than 150 years ago [1] and were intensely investigated spectroscopically [2]. Still, there were only basic studies concerning the structures of the NH_4^+ and alkali salts, before we recently presented the first systematic examinations of the crystal structures and properties of these compounds [3,4]. In additon to the pure metallate salts, the double salts $A_3[MOS_3]Y$ (A = K: M = Mo, W; Y = Cl, Br, SH [5,6]; A = Rb: M = W; Y = Cl [7]) were characterized by vibrational spectroscopy and powder X-ray diffraction. The compounds crystallize with two new structure types, for $Y = SH^-$ in spacegroup $Pca2_1$, for Y = Cl, Br in s.g. $Pmn2_1$. Only for $K_3[WOS_3]Cl$ the crystal structure has been solved [8]. Here we present the first crystal structures of the salts $K_3[MoOS_3]Cl$, $K_3[(Mo/W)OS_3]SH$ and the new compound $K_6[WOS_3]_2(S_2O_3)$. The structural relationship between $K_3[MoOS_3]Cl$ ($Pca2_1$, Z = 4, a = 1246.27(12), b = 623.20(4), c= 1230.44(8) pm) and $K_3[(Mo/W)OS_3]SH$ ($Pmn2_1$, Z = 2, M = Mo: a = 957.7(2), b = 636.2(2), c= 812.4(2) pm) can be rationalized by symmetry reduction from the common perovskite aristotype. The new thiosulfate double salt was obtained by methanothermal decomposition of $K_2[WO_2S_2]$ at 110 °C. In the crystal structure of $K_6[WOS_3]_2(S_2O_3)$ ($P6_3mc$, new structure type, Z = 2, a = 980.16(12), c= 1219.4(2) pm) the thiosulfate anion was refined to be disordered between two sites (fig. a). All crystal structures contain metallate anions which are 12-fold coordinated by K^+. The anions Cl^- and SH^- are 6-fold coordinated by K^+, while the $(S_2O_3)^{2-}$-anions are surrounded by 9 cations. The coordination of the thiosulfate's chalkogenido ligands (CN(S): S + 6K, CN(O): S + 3K) is similar to the coordination environment of the monosulfidometallates [3]. Fittingly, in addition to the new thiosulfate salt, we report the first crystal structure of anhydrous potassium thiosulfate. $K_2(S_2O_3)$ crystallizes with a - to our knowlege - new structure type ($P2_1/c$, Z = 4, a = 1010.4(1), b = 909.4(1), c = 1334.1(2) pm, β=112.253(4)°). The $(S_2O_3)^{2-}$ tetrahedra are arranged to corrugated hexagonal layers (fig. b). The sulfido ligands are 6 to 7-fold coordinated (S + 5K; S + 6K), while the oxido ligands are 4 to 6-fold coordinated (4(S + 3K); 1(S + 4K); 1(S + 5K)). Thus, the overall coordination number of the $(S_2O_3)^{2-}$ tetrahedra by K^+ is 9 to 10, similar to the thiosulfate tungstate salt. The crystal chemistry of all these closely related compounds is discussed based on packing and coordination considerations.

[1] J. J. Berzelius, *Ann. Phys.* **1826**, 83, 261-288; 84, 267-282. [2] A. Müller *et. al.*, *Angew. Chem.* **1981**, 93, 957-977. [3] A. Lehner, M. Braitsch, C. Röhr, *Z. Kristallogr.* **2012**, *227*, 557-568. [4] A. J. Lehner, K. Kraut, C. Röhr, *Z. Naturforsch.* **2012**, *67b*, 127-148. [5] A. Müller *et. al.*, *Z. Naturforsch.* **1972**, *27b*, 702-722. [6] E. Königer-Ahlborn *et. al.*, *Z. Anorg. Allg. Chem.* **1977**, *428*, 5-15. [7] A. Müller *et. al.*, *Z. Anorg. Allg. Chem.* **1974**, *403*, 310-318. [8] B. Krebs *et. al.*, *Z. Anorg. Allg. Chem.* **1972**, *387*, 142-153.

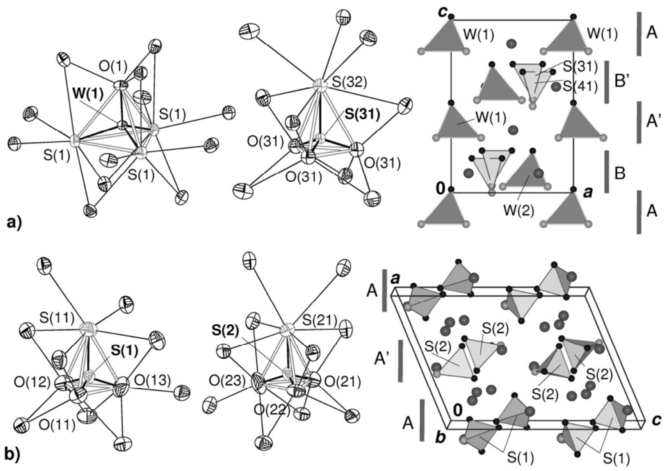

Figure: Crystal structures and Ortep plots (ellips. 70%) of the anion coordination environments: **a)** $K_6[WOS_3]_2(S_2O_3)$ ($P6_3mc$); **b)** $K_2(S_2O_3)$ ($P2_1/c$).

PS05-P04

A mononuclear rhenium(III) product obtained in a solvothermal process with catalytic reactions

A. Kochel[1], M. Hołyńska[2]
[1]*Poland, Faculty of Chemistry, Wrocław, Poland*
[2]*Philipps-Universitat Marburg, Fachbereich Chemie, Marburg, Germany*

Solvothermal conditions lead to a cleavage of a C-C bond in 2,2'-bipyridine-3,3',6,6'-tetracarboxylic acid, apparently catalyzed by the starting rhenium salt, ammonium hexachloridorhenate(IV) [1]. The resulting product (**1**) is a rhenium(III) complex. Coordination environment of the Re^{3+} ion includes one tetradentate 2,2'-bipyridine-6,6'-(dicarboxylic acid)-3,3'-dicarboxylato ligand (L^1), one bidentate pyridine-2,5-dicarboxylato ligand (L^2) and one chlorido ligand (Fig. 1). **1** is characterized by X-ray diffraction, magnetic and spectroscopic, as well as TGA properties measurements.

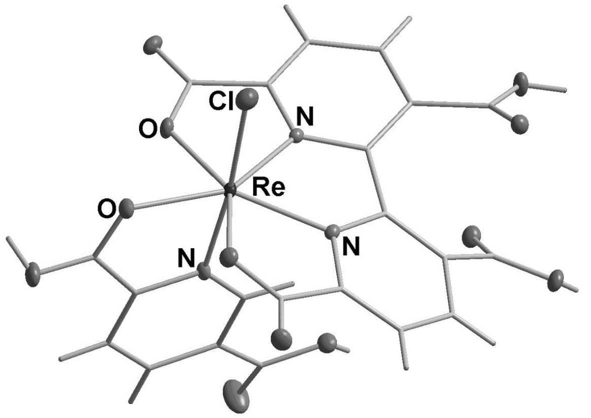

Fig. 1. Molecular structure of **1**.

[1] Kochel A., Hołyńska M., Twaróg K., *Inorg. Chem. Commun.* **2012**, *24*, 47-49.

PS05-P05
The crystal structure of $Cs_{10}Al_6S_{14}$

V. Winkler[1], M. Schlosser[1], A. Pfitzner[1]
[1]*Universität Regensburg, Anorganische Chemie I, Regensburg, Germany*

Single crystals of highly air sensitive $Cs_{10}Al_6S_{14}$ were obtained by reaction of non-stoichiometric amounts of aluminum, sulfur and cesium azide. After melting CsN_3 to a homogenous, transparent flux, a controlled thermal decomposition of cesium azide was carried out at 543 K in the presence of elemental aluminum and sulfur. After heat treating the dark red melt for 10 days, the raw product was homogenized under an argon atmosphere and annealed for further 7 days in a dry and evacuated silica tube at 893 K.

$Cs_{10}Al_6S_{14}$ crystallizes in pale red blocks. The crystal structure of this new solid was determined by single crystal X-ray diffraction at 123 K. $Cs_{10}Al_6S_{14}$ crystallizes in the space group $C2/m$ (No. 12) with the unit cell dimensions: a = 17.3136(7) Å, b = 12.4726(4) Å, c = 9.1688(4) Å and β = 106.405(4)° with Z = 2 and V = 1899.4(1) $Å^3$.

$Cs_{10}Al_6S_{14}$ crystallizes isotypic to $Cs_{10}Ga_6Se_{14}$[1,2]. Both structures consist of linear, hexameric $[T_6Q_{14}]^{10-}$ (T: Al, Ga; Q: S, Se) anions which are surrounded by a cesium matrix (Figure 1a). Six tetrahedra $[AlS_4]^{5-}$ are condensed via edges to built up an oligomeric anion $[Al_6S_{14}]^{10-}$ of 14.820(3) Å length (Figure 1b).

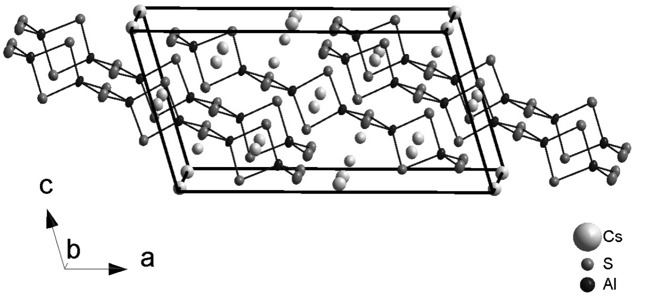

Figure 1a) Section of the crystal structure of $Cs_{10}Al_6S_{14}$ (ellipsoids represent 95% probability).

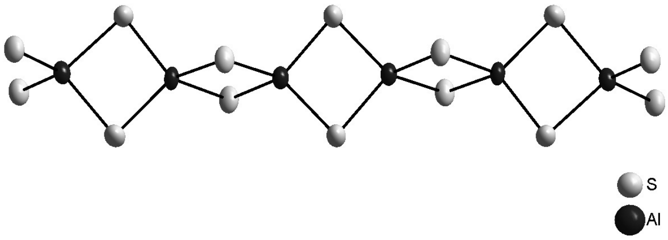

Figure 1b) Linear, hexameric $[Al_6S_{14}]^{10-}$ anion in $Cs_{10}Al_6S_{14}$ (ellipsoids represent 95% probability)

References:

[1] H. J. Deiseroth, H. Fu-Son, *Angew. Chem.* **1981**, *93*, 1011-1012.

[2] H.J. Deiseroth, *Z. Kristallogr.* **1984**, *166*, 283-295.

PS05-P06
Series of pentanuclear $[Co^{III}_4Ln^{III}]$ complexes (Ln = La, Sm, Gd) with a tripodal oxime ligand

D. Premužić[1], M. Hołyńska[1]
[1]*Philipps-Universität Marburg, Fachbereich Chemie, Marburg, Germany*

Single Molecule Magnets (SMMs) are subject to growing interest. They are molecules displaying a barrier for the spin reversal below a blocking temperature T_B.[1] The first examples were dodecanuclear mixed-valence Mn-Clusters with acetate as a bridging ligand.[2,3] Until today many efforts have been made in understanding the design of such complexes and it was shown, that not only the choice of metals, ligands and nuclearity, but also molecular symmetry plays an important role.[4] The presence of threefold symmetry in a complex molecule suppresses relaxation of the magnetization via Quantum Tunneling Mechanism[5] and prevents spin reversal below the blocking temperature. Among the groups linking metal centers oxime functionalities are very promising candidates.[6] Inducing the presence of threefold symmetry by the use of tripodal ligands combined with oxime functionality could yield new potential SMMs with good properties. Utilizing a heterometallic approach we report the synthesis and characterization of a novel series of pentanuclear cationic $[Co^{III}_4Ln^{III}]$ complexes (Ln = La, Sm, Gd) with tris(2-hydroxyiminopropyl)amine (Ox_3H_3). The compounds were synthesized in a self-assembly process by combining $Co(ClO_4)_2$, $Ln(NO_3)_3$, Ox_3H_3 and CH_3ONa in methanol. The amount of added base plays an important role. The title compounds are isolated as perchlorate salts. In the complex cation four Co^{III}-ions are linked together and further to a central lanthanide ion by oxime bridges/μ_3-oxido ligand. Preliminary studies of magnetic properties will also be presented.

References: [1] R. Sessoli, A. Powell, *Coord. Chem. Rev,* **2009**, *253*, 2328-2341; [2] T. Lis, *Acta Cryst.*, **1980**, *B36*, 2042-2046; [3] A. Caneschi, D. Gatteschi, R. Sessoli, A.-L. Barra, L. C. Brunel, M. Guillot, *J. Am. Chem. Soc.,* **1991**, *113*, 5873-5874; [4] T. Glaser, *Chem. Commun.*, **2011**, *47*, 116; [5] R. Sessoli, D. Gatteschi, *Angew. Chem. Int. Ed.*, **2003**, *42*, 268_297; [6] M. Hołyńska, D. Premužić, I.-R. Jeon, W. Wernsdorfer, R. Clérac, S. Dehnen, *Chem. Eur. J.* **2011**, *17*, 9605-9610.

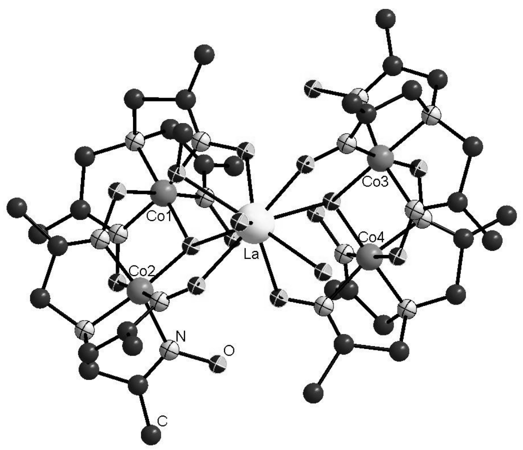

Figure 1: The $Co_4^{III}La^{III}$-Compound; Hydrogen, solvent-molecules and perchlorate-anions are not shown

PS05-P07

Synthesis, characterization and phase transition of $Li_{0.4}WO_3$ bronze

M. S. Rahman[1], M. M. Murshed[1], T. M. Gesing[1]
[1]*Institut für Anorganische Chemie, Universität Bremen, Chemische Kristallographie fester Stoffe, Bremen, Germany*

Alkali metal tungsten bronzes (A_xWO_3: A = alkali metals, 0 < x < 1) are of great interest because of their interesting electrical [1-3] and optical properties [1,4,5] including a wide range of chemical homogeneity [6] and crystal chemistry [1,7,8]. Here we investigated crystalline lithium containing phases with a nominal composition of $Li_{0.4}WO_3$. Samples were synthesized by solid state reactions using Li_2WO_4, WO_2 and WO_3 in a sealed quartz tube at 973 K and low pressure for 24 h, 48 h, 72 h and 168 h. Products were characterized by powder and single crystal X-ray diffraction as well as Raman spectroscopy. The investigations demonstrate that the air pressure in the sealed tubes play an important role for the formation of different cubic perovskite-type bronze (PTB_c) phases. At a pressure of 10^{-7} MPa, a body centered cubic $Li_{0.4}WO_3$ phase (*I*m-3, *a* = 744.9(2) pm) was formed. Using a pressure of 10^{-6} MPa two different PTB-phases were observed; *I*m-3: *a* = 744.2(4) pm and *P*m-3m: *a* = 373.1(2) pm with 92(2) wt.-% and 8(2) wt.-%, respectively. This phase fraction remains more or less constant irrespective of the reaction time between 24 h and 168 h. Pure body centered $Li_{0.4}WO_3$ bronze powder samples slowly transform into a tetragonal perovskite tungsten bronze (PTB_T; *P*4/nmm: a = 520.5(2) pm, c = 383.0(3) pm) while keeping the products under open atmospheric conditions. Using a mixed phase (92 wt.-% *I*m-3 phase and 8 wt.-% *P*m-3m phase) only the body centered bronze gradually transforms into PTB_T whereas the primitive phase remains unchanged. Different *I*m-3 to *P*4/nmm phase transition kinetics is observed for the pure body centered and mixed phase system. On the other hand, if the mixed phase sample (92 % *I*m-3 / 8 % *P*m-3m) is kept in a capillary sealed under atmospheric pressure, a transformation of the *I*m-3 phase to *P*m-3m symmetry is observed. The kinetic behavior of the phase transition *I*m-3 → *P*4/nmm at open conditions is almost similar to that of *I*m-3 → *P*m-3m at closed conditions. In all three investigated cases ((i) body centered exposed into air, (ii) mixed phase exposed into air, (iii) mixed phase kept in a sealed capillary) only the body centered phase transformed. Since the investigated $Li_{0.4}WO_3$ bronzes were rapid quenched down to room-temperature after the reaction period, the body centered $Li_{0.4}WO_3$ might form due to kinetic reason, which transformed into thermodynamic stable phase at room-temperature conditions, thus showed a kind of metastability.

References

[1] P. G. Dickens, M. S. Whittingham, Q. Rev. Chem. Soc. 22 (1968) 30-44. [2]. D. R. Wanlass, M. J. Sienko, J. Solid State Chem. 12 (1975) 362-369. [3]. A. R. Sweedler, Ch. J. Raub, B. T. Matthias, Phys. Lett. 15 (1965) 108-109. [4] A. Simon, J. Ravez, C. R. Chimi, 9 (2006) 1268-1276. [5] J. P. Doumerc, F. Kabbaj, G. Campet, J. Claverie, M. Pouchard, Solid State Commun. 39 (1981) 1045-1048. [6] W. Ostertag, Inorg. Chem. 5 (1996) 758-760. [7] R. J. D. Tilley, Int. J. Refractory Metals & Hard Materials 13 (1995) 93-109. [8] F. Takusagawa, R. A. Jacobson, J. Solid State Chem. 18 (1976) 163-174.

PS05-P08

Molecular Zinc Dihydrides

T. P. Spaniol[1], A. Rit[1], J. Okuda[1]
[1]*RWTH Aachen, Department of Inorganic Chemistry, Aachen, Germany*

Zinc dihydride is known since 1947 [1] and used in organic chemistry as reducing agent, but has never been structurally characterized. Its low solubility suggest a polymeric structure [2]. We report here that ZnH_2 can be stabilized with the N-heterocyclic carbene 1,3-bis-(2,6-diisopropylphenyl)imidazol-2-ylidene (IPr). The dimeric molecule $[(IPr)ZnH_2]_2$ (**1**) is thermally robust and can be considered as adduct of the parent binary ZnH_2. Despite the pronounced Lewis acidity of the metal centre, simple Lewis base adducts of ZnH_2 have never been described. **1** crystallizes in space group $P2_1/c$ and shows crystallographic inversion symmetry around the centroid of the Zn_2H_2 ring. Each metal atom is tetrahedrally coordinated by two μ-hydrides, one terminal hydride and the carbene C atom of the IPr ligand. The Zn···Zn separation of 2.4980(4) Å is close to the distance of 2.4513(9) Å found in $[LZn(\mu\text{-}H)]_2$ with L = $HC\{CMeN(2,6\text{-}Me_2C_6H_3)\}$ [3]. In both systems a Zn-Zn interaction is unlikely. The structure of **1** may be compared to the closely related structure of $[(IMes)ZnR_2]_2$ (IMes = 1,3-bis-(2,4,6-trimethylphenyl)imidazol-2-ylidene, R = $PhCH_2O$) which reveals a similar $Zn_2(\mu\text{-}O)_2$ core structure and an equal zinc-carbene bond distance of 2.054(2) Å [4].

[1] A. E. Finholt, A. C. Bond Jr., H. I. Schlesinger, J. Am. Chem. Soc. 69 (1947) 1199.

[2] M. P. Coles, S. M. El-Hamruni, J. D. Smith, P. B. Hitchcock, Angew. Chem. Int. Ed. 47 (2008) 10147.

[3] H. Hao, C. Cui, H. W. Roesky, G. Bai, H.-G. Schmidt, M. Noltemeyer, Chem. Commun. (2001) 1118.

[4] T. R. Jensen, L. E. Breyfogle, M. A. Hillmyer, W. B. Tolman, Chem. Commun. (2004) 2504.

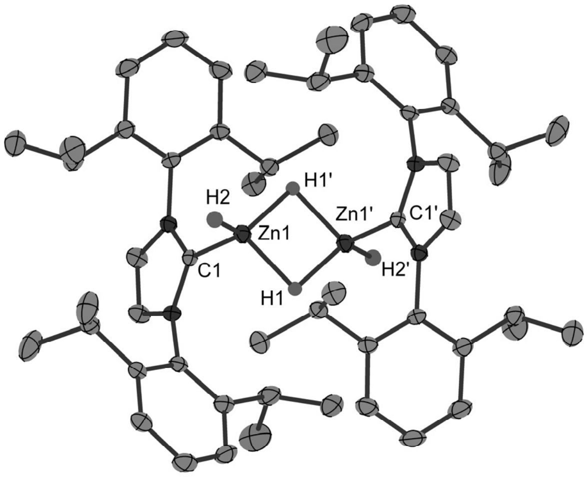

Figure 1: Molecular structure of $[(IPr)ZnH_2]_2$ in the crystal. Selected bond lengths (Å) and angles (°): Zn1-H1 1.73(2), Zn1-H1' 1.70(2), Zn1-H2 1.53(2), Zn1-C1 2.0573(17), H1-Zn1-H2 120.0(11), H1-Zn1-H1' 86.2(11).

PS05-P09

A systematic crystal chemical study of alkaline earth rich mixed stannides/germanides

M. Jehle[1], C. Röhr[1]
[1]*Universität Freiburg, Freiburg, Germany*

In this work, the systematic investigation of ternary alkaline earth (*A*=Ca, Sr, Ba; La see [1]) rich stannides/germanides (*M*=Ge, Sn) is presented. Therefore, the corresponding binary phases of the compositions 1:1, 31:20, 5:3 and 2:1 have been taken as starting points.

1:1: The monotetrelides [2,3] all crystallize in the CrB structure type (e.g. $BaSn_{0.65}Ge_{0.35}$, *Cmcm*, *a*=522.3(1), *b*=1228.9(3), *c*=451.6(1) pm, *R*1=0.024) and show continuous phase widths without any indications of superstructures present.

31:20: The stoichiometrically and structurally closely related tetragonal phases $Ca_{31}Sn_{20}$ and $Ca_{36}Sn_{23}$ have been described much earlier, in which crystallographic problems have been reported [4,5].
Our reinvestigation of $Ca_{31}Sn_{20}$ showed pronounced diffuse scattering along *c**. The features of the diffraction patterns can be simulated by separating the building blocks of both structures along the tetragonal *c*-axis and arrange them in a statistical stacking sequence.
A clear conclusion about the Ge content can't be made under these circumstances, so far. The phases $Ca_{31}Sn_{20}$ and $Ca_{36}Sn_{23}$ only obey Zintl's rule not considering the linear coordination of Sn.

5:3: Nearly all alkaline earth stannides/germanides A_5M_3 [2,3,6] crystallize in the Cr_5B_3 structure type (*I*4/*mcm*). The only exception is Ba_5Ge_3 crystallizing in the Ba_5Si_3 structure type (*P*4/*ncc*), which can be understood as distorted Cr_5B_3 structure type. Therefore, it is not astonishing, that the phases containing Ca or Sn show continuous phase widths $A_5[Sn_xGe_{3-x}]$ (e.g. $Sr_5Sn_{2.19}Ge_{0.81}$, *I*4/*mcm*, *a*=845.7(1), *c*=1604.2(2) pm, *R*1=0.036), whereas the ternary system Ba-Sn-Ge shows a change from the Cr_5B_3 type to its slightly distorted variant, however at relatively high Ge contents. The symmetry reduction from *I*4/*mcm* to *P*4/*ncc* can be rationalized by a Bärnighausen tree (k2, 1/4 1/4 1/4). It can clearly be shown, that the distortion can both be induced by a change of the ratio (v.e.c./*M* atom) (e.g. *A* gallides, not part of this work) and by changes of the electronegativity of *M.*

2:1: The phases $A_2Sn_xGe_{1-x}$ crystallize in the well known Co_2Si structure type [2]. The Sn and Ge positions, accordingly, are substituted in a statistical manner without forming any kind of superstructure.

The extensive study of the systems *A*-Sn-Ge mainly showed, that a statistical substitution of the tetrel atoms is preferred. Only in few cases, the formation of corresponding superstructures have been observed.

[1] I. Dürr, C. Röhr, *Z. Naturforsch.*, 66b, 1015-1028 (2011).

[2] A. Palezona, P. Manfrinetti, M.L. Fornasini, *J. Alloys Compd.*, 312, 165-171 (2000).

[3] A. Palezona, P. Manfrinetti, M.L. Fornasini, *J. Alloys Compd.*, 345, 144-147 (2002).

[4] M.L. Fornasini, E. Franceschi, *Acta Cryst.*, B33, 3476-3479 (1977).

[5] A.K. Ganguli, A.M. Guloy, E.A. Leon-Escamilla, J.D. Corbett, *Inorg. Chem.*, 32, 4349-4353 (1993).

[6] A.-V. Mudring, J.D. Corbett, *J. Am. Chem. Soc.*, 126, 5277-5281 (2004).

PS05-P10

Growth and morphology of Sillenite crystals synthesized in hydrothermal solutions.

E. Marina[1], A. Marin[1], I. Mahina[1]
[1]*Institute of Experimental Mineralogy RAS, LSMM, Chernogolovka, Moscow Distr., Russian Federation*

Crystals of Sillenites ($Bi_{12}M_XO_{20\,\pm\,\delta}$, where M - the elements of groups II-VIII) has a combination of important physical properties - piezo-, photo- and electro-optical effects, which allows their uses in piezotechnology and optoelectronics. The bringing in Sillenite structure of various elements to exert an impact on their properties and morphology, so getting the crystals of various compositions and their study is very important.

The main method of Sillenite crystal growth is crystallization from the melt by the Czochralski method. However, using to this method is difficult to obtain incongruently melting Sillenites, such asGa-, Al-, Fe - containing Sillenites with better specifications than congruently melting sillenites.

In recent years one of the most important innovative achievements in the field of laser materials is the development of laser ceramics, which by its spectral and lasing characteristics are none the worse of single crystals. Production of optical quality ceramic is mainly be realized by sintering the powder of starting oxide components. However, current research indicates that ceramics obtained by sintering of nano- or micro- crystals has better mechanical and optical characteristics.

Nanoparticles are often showing the dependence of the properties from the form. At present, various functional materials with desired morphology of nanoparticles synthesized: Pt tetrahexahedrons, Nb_2O_5 nanotubes, CdS-Ag_2S superlattices, CuO spheres, $LiNbO_3$ nanosticks etc. So the study of synthetic Sillenite crystals morphology is a topical problem.

In alkaline hydrothermal solutions were synthesized by spontaneous crystallization of Zn-, Ga-, Fe-, Si-, P- and Cr-containing Sillenite crystals. We carried out experimental researches at temperature 260º C and pressure 50 MPa in the solution of 10 wt. % NaOH. In addition, Sillenite crystals in ammonium fluoride NH_4F (5 wt.%) and hydrogen peroxide H_2O_2 (10% vol.) solutions was successful grown in a first time in the world. Synthesis was carried out in PTFE ampoules (volume 5 - 8 ml). Six ampoules were placed in a heat-resistant autoclave also has contact Teflon fettle. The autoclave was filled with the same solution to the same filling factor as the ampoules. Starting material was Bi_2O_3 or $NaBiO_3$. In addition, in the starting material was placed various additives: $C_4H_{10}O_6Zn$, Ga_2O_3, Fe_2O_3, SiO_2, $Na_3PO_4 \cdot 12H_2O$, K_2CrO_3, $Al(OH)_3$. The main components (Bi_2O_3 or $NaBiO_3$) was 95 wt. % of the total mass and one of the above additives was 5 wt. %. Experiment duration was 5 to 10 days.

The research of obtained crystals by means of electronic-scanning and optical microscopes has showed that Zn-, Ga-, Fe- and Cr-containing crystals grown as a tetrahedron, and silicon and phosphorus Sillenites - as cubes (Fig. 1).

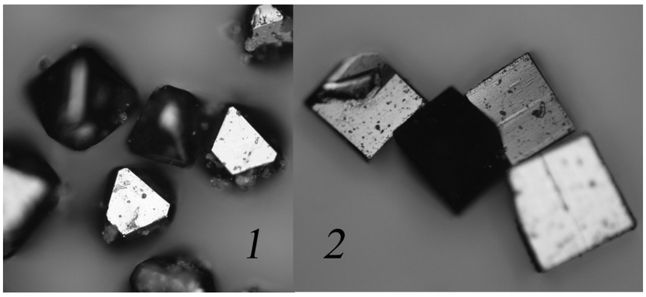

PS05-P11

A new mixed metal cluster of platinum and silver

W. Raven[1], U. Englert[1], I. Kalf[1]
[1]*RWTH Aachen, Institute for inorganic chemistry , Aachen, Germany*

In an attempt to synthesize a derivative from a previously published and patented orthoplatinated primary amine [1], a new crystal including an exciting structure has been obtained. The crystal structure of the compound with the chemical Formula $[C_{32}H_{46}Ag_3N_4O_4Pt_2(ClO_4)_2] \cdot 3ClO_4 \cdot 2H_2O$ was found: A discrete cluster of three silver and two platinum atoms has been obtained, in which the platinum atoms are in a square planar geometry with a water molecule and two primary amines of which one underwent cycloplatination. The silver atoms are bonded to the platinum in an almost perpendicular geometry.Thus provides a rather uncommon dative platinum-silver bond with a length of 2.85(5) A. Few cases are previously reported [2] with such a short unbridged intermetallic Ag-Pt bond length. The trication is accompanied by three perchlorate and two water molecules, the whole structure crystallises with Z = 2 in the space group ***P***2_1.

The addressed issues (dative bond, geometry) and further crystallographic issues, such as twinning, disorder and hydrogen bonds, shall be discussed and visualised in the poster.

[1] B. Calmuschi-Cula and U. Englert, *Organometallics* 27, 3124-3130, **2008**

[2] T. Yamaguchi, F. Yamazaki, T. Ito *J. Am. Chem. Soc.*, 123, 743-744, **2001**

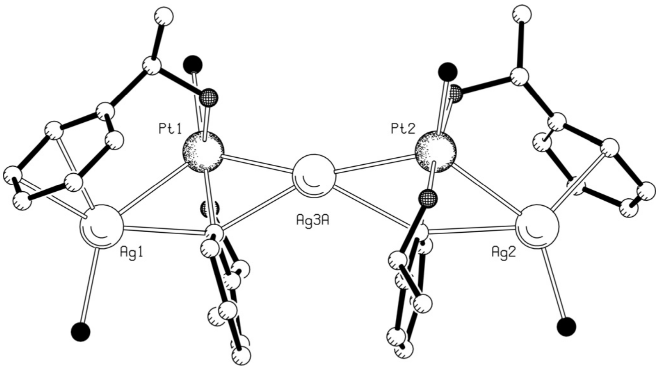

PS05-P12

Racemic and chiral form of the two-dimensional $CaCl_2(proline)_2$ networks

K. Lamberts[1], U. Englert[1]
[1]*RWTH Aachen University, Inorganic Chemistry, Aachen, Germany*

The research on coordination polymers has been very active over the past decades and led to promising results with respect to materials science and possible applications [1]. However, in academic research toxic substances are often employed, making the transfer to industrial use difficult. Thus exploring the chemistry of essential metals and amino acids, calcium has been chosen as versatile cation and has been reacted with proline in enantiopure and racemic form. This opens up the investigation on the possible influence of chirality.

Two closely related structures have been found with the formal composition of $CaCl_2(proline)_2$, one from the enantiopure and the other from the racemic ligand. Both are structurally related and can be synthesised phase pure from aqueous solution. Stoichiometry-changes in the reaction yields two other products, pointing out the diversity in this system.

The few structures known from calcium and amino acids [2, 3] are molecular or one-dimensional complexes with coordination number 7 and 8. In all structures the amino acid is deprotonated and acts as chelating and sometimes bridging ligiand. Additionally, water is always incorporated, as calcium is very oxophilic.

In contrast, the calcium atom in the two new structures is found in an octahedral geometry coordinated by four zwitterionic proline molecules and two chlorides. Besides the rather unusual geometry and chloride-calcium coordination the structures are anhydrous and form two-dimensional networks. The characteristics of the structures will be presented in detail on this poster and their relationship will be outlined. Investigations on the influence of chirality as well as water content during synthesis will be discussed.

[1] See for example: The pervasive chemistry of metal-organic frameworks, *Chem. Soc. Rev., 5*, **2009**

[2] H. Schmidbaur, I. Bach, D. L. Wilkinson, G. Muller, *Chem. Ber.*, *122*, **1989**, 1439

[3] S. Fox, I. Busching, W. Barklage, H. Strasdeit, *Inorg. Chem.*, *46*, **2007**, 818

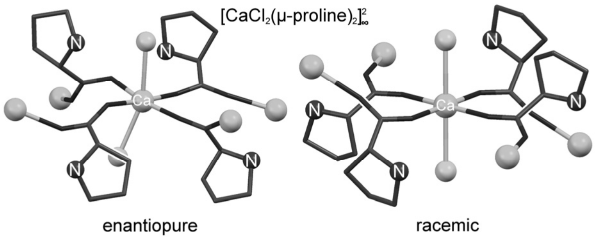

PS05-P13

The New Potassium Amalgam KHg_6

F. Tambornino[1], C. Hoch[1]
[1]*Ludwig-Maximilians-Universität München, Department Chemie, München, Germany*

Single crystals of the new mercury-rich amalgam KHg_6 were the result of a combination of isothermal preparative eletrolysis and thermochemical methods, similar to the preparation method described for $Na_{11}Hg_{52}$ [1]. A saturated solution of KI in absolute N,N-dimethylformamide was electrolysed under Ar atmosphere with a single Hg drop suspended in an amalgamated copper spoon as cathode and a Pt foil as anode. At 85°C a mixture of KHg_{11} [2] and the new amalgam KHg_6 in the approximate ratio of 4 : 6 according to Rietveld refinement was yielded. The lumps of bright silver luster were of low crystal quality, insufficient for X-ray structure investigations. In order to improve both crystal quality and sample purity, pure KHg_{11} was prepared by electrolysis at room temperature and subsequently mixed with metallic potassium to give the desired sample stoichiometry KHg_6. After adding a small quantity of KHg_6 seed crystals from the electrolysis experiments, the mixture was heated to a temperature right below the peritectic decomposition temperature of KHg_6 (ca. 80 - 85°C, according to Hg droplet formation seen in a Thiele melting point determination apparatus) for 72 h. The resulting product was phase-pure KHg_6 in form of single crystals with quality sufficient for X-ray structure investigations.

KHg_6 is sensitive towards air and moisture and crystallizes isotypic with $BaHg_6$ [3] in the orthorhombic space group *Pnma*(a = 13.394 Å, b= 5.270 Å, c= 10.463 Å, Z= 4) with 6 crystallographically independent Hg and one K site in the asymmetric unit. The structure can be subdivided into planar nets parallel to the *ab* plane on z=1/4 and 3/4 and consisting from five- and eight-membered rings of Hg atoms. The nets are arranged in a ...ABAB... stacking, leading to the formation of large coordination polyhedra $[KHg_{18}]$ which share pentagonal faces to form columns $[KHg_{13}]$ along *b*.The K-Hg distances ranging from 3.457(7) to 4.235(11) pm are in good agreement with those found in KHg_{11} [2] and K_3Hg_{11} [4].

Other than many Hg-rich amalgams, KHg_6 shows good metallic behaviour and becomes superconducting at T_C= 3.45 K.

References:

[1] Hoch, C.; Simon, A., *Angew. Chem. Int. Ed.* **51**, 3262 (2012).

[2] Biehl, E.; Deiseroth, H. J. *Z. Anorg. Allg. Chem.* **625**, 1073 (1999).

[3] Wendorff, M.; Rőhr, C.; *J. Alloys Compd.* (in print).

[4] Todorov, E.; Sevov, S. C.J. *Solid State Chem.* **149**, 419 (2000).

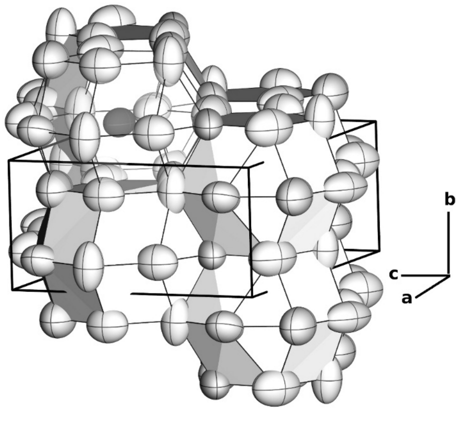

Figure 1: Crystal structure of KHg_6. Ellipsoids for all atoms are drawn at a propability level of 90% (black: K, light grey: Hg).

Empirical formula	KHg_6
M_W (g·mol^{-1})	1242.64
ρ_{calc} (g·cm^{-3})	11.167
Radiation/λ (Å)	Ag-Kα/0.56083
μ (cm^{-1})	68.154
Crystal system	orthorhombic
Space group	$Pnma$ (No. 62)
a (Å)	13.410(8)
b (Å)	5.269(3)
c (Å)	10.459(7)
Volume (Å^3)	739.1(8)
Z	4
Temperature (K)	295(2)
max. 2 ϑ (°)	45
Refl. with $I \geq 2\sigma$ (I)	466
L.s. parameters	44
R_{int}/R_σ	0.2568/0.1437
R_1/wR_2 ($I \geq 2\sigma$ (I))	0.0618/0.1119

Table 1: Selected crystallographic data for KHg_6.

PS05-P14
The Hg-Richest Europium Amalgam, $Eu_{10}Hg_{55}$

F. Tambornino[1], C. Hoch[1]
[1]*Ludwig-Maximilians-Universität München, Department Chemie, München, Germany*

The Eu - Hg phase diagram published in 1993 by Guminski [1] depicts the most mercury-rich phase as $EuHg_{3.6}$, corresponding to $Eu_{14}Hg_{51}$ [2] which already was assigned to the $Gd_{14}Ag_{51}$ structure type [3] on the base of powder diffraction patterns. However, Tkachuk and Mar [4] could show that the corresponding phases in the systems Ca - Hg and Sr - Hg were of a new structure type with very similar metrics, $A_{11-x}Hg_{54+x}$, and therefore suggested a reinvestigation of all the numerous amalgam crystal structures assigned to the $Gd_{14}Ag_{51}$ structure type. Structural analyses on $Eu_{10}Hg_{55}$ now show a structure closely related to the model suggested by Tkachuk and Mar but with additional, partially occupied Hg sites.

Single crystals of $Eu_{10}Hg_{55}$ were prepared by isothermic electrolysis at room temperature or below. A saturated EuI_3 solution in DMF was reduced on a cathode consisting of a single mercury drop under inert conditions. This method has been used as a new snythetic access towards mercury-rich compounds [5] which suffer from low peritectic decomposition temperatures combined with high reaction enthalpies. The hexagonal unit cell (P-6, a= 13.6165(13) Å, c= 9.7074(10) Å, Z= 1) exhibits structural elements from closest sphere packings, Frank-Kasper polyhedra, ionic coordination polyhedra and Hg clusters reminding of the multi-center-bond clusters from early p metal chemistry as a sign for the complex interplay of ionic, metallic and covalent bonding present in many polar amalgams. The atomic coordination polyhedra consist of capped prisms or Frank-Kasper polyhedra and are known from the structures of $A_{11-x}Hg_{54+x}$ and the closely related $Na_{11}Hg_{52}$ structure [5c]. However, the crystal structure of $Eu_{10}Hg_{55}$ constitutes yet another structure type in this family and shows as a main difference to the $A_{11-x}Hg_{54+x}$ structure additional atomic positions forming a chain of six Hg atoms along 2/3, 1/3, z, with almost identical distances. Their occupation factors form pairs with 1/3:2/3, resulting in statistical pairings of Hg atoms with sensible interatomic distances.

References
[1] Guminski, C. *J. Phase Equilibria* **14,** 97 (1993).
[2] Merlo, F.; Fornasini, M. L. *J. Less Common Met.* **64**, 221 (1979).
[3] Steeb, S., Godel, D., Lohr, C., *J. Less Common Met.* **15**, 137 (1968); McMasters, O. D., Gschneider, K. A., Venteicher, R. F., *Acta Cryst.* **B26**, 1224 (1970).
[4] Tkachuk, A. V., Mar, A., *Inorg. Chem.* **47**, 1313 (2008).
[5] a) Hoch, C., Simon, A., *Z. Anorg. Allg. Chem.* **632**, 2288 (2006); b) Hoch, C., Simon, A., *Z. Anorg. Allg. Chem.* **634**, 853 (2008); c) Hoch, C.; Simon, A., *Angew. Chem. Int. Ed.* **51**, 3262 (2012).

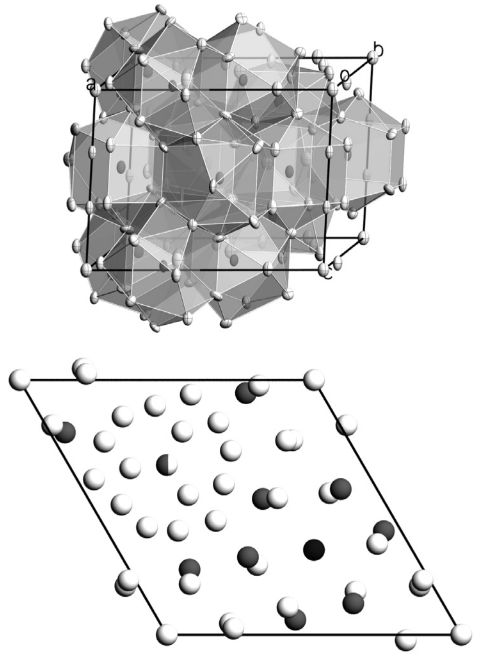

Figure 1: Crystal structure of $Eu_{10}Hg_{55}$. Top: Polyhedra around Eu atoms, (ellipsoids drawn at 90% propability level), bottom: Projection along 001 (half black/white sphere: mixed occupation Eu/Hg, dark grey: Eu atoms, light grey: Hg atoms, black: Hg atoms with partial occupation).

Empirical formula	$Eu_{9.9(1)}Hg_{55.0(1)}$
M_W (g·mol^{-1})	12849.90
ρ_{calc} (g·cm^{-3})	13.00
Radiation/λ (Å)	Mo-Kα/0.71073
μ (cm^{-1})	141.28
Crystal system	hexagonal
Space group	$P\bar{6}$, (No. 174)
a (Å)	13.595(5)
c (Å)	9.735(4)
Volume (Å^3)	1558(1)
Z	1
Temperature (K)	295(2)
max. 2ϑ (°)	30.0
Refl. with $I \geq 2\sigma$ (I)	1527
L.s. parameters	119
R_{int}/R_σ	0.3735/0.0788
R_1/wR_2 ($I \geq 2\sigma$ (I))	0.0492/0.1247

Table 1: Crystallographic data for $Eu_{10}Hg_{55}$.

PS05-P15

Lattice thermal expansion of some bismuth based complex oxides with mullite-type structures

M. M. Murshed[1], R. X. Fischer[2], T. M. Gesing[1]
[1]*Universität Bremen, chemische Kristallographie fester Stoffe, Bremen, Germany*
[2]*Universität Bremen, Kristallographie, Bremen, Germany*

The lattice thermal expansion of $Bi_2Al_4O_9$, $Bi_2Ga_4O_9$ and their strontium substituted analogues $(Bi_{1-x}Sr_x)_2Al_4O_{9-x}$ and $(Bi_{1-x}Sr_x)_2Ga_4O_{9-x}$ were studied between 298 K and 1300 K. Each sample was synthesized using glycerin method [1], and the lattice parameters (a, b, c and V) were determined from the X-ray powder data Rietveld refinements in the space group *Pbam*. Throughout the investigated temperature range the metric parameters of $Bi_2Al_4O_9$ and $Bi_2Ga_4O_9$ lied close to each other in the respective heating and cooling temperatures. In contrast, the cell parameters of both $(Bi_{1-x}Sr_x)_2Al_4O_{9-x}$ and $(Bi_{1-x}Sr_x)_2Ga_4O_{9-x}$ significantly differ between the heating and the cooling curves. Almost all the cell parameters in the cooling cycle were smaller than those of the heating cycles. Of particular exceptions, the a parameter of $(Bi_{1-x}Sr_x)_2Ga_4O_{9-x}$ increased in the cooling cycle. Moreover, whereas the b and c parameter of all investigated compounds showed a quadratic expansion trend, the a cell parameter fits well with a cubic polynomial. As a consequence, the thermal expansion coefficients $\alpha(b)$, $\alpha(c)$ and $\alpha(V)$ showed a linear and that of $\alpha(a)$ a non-linear behavior with increasing temperature between 298 K and 1300 K. Each V-value contracted about 1.0×10^{-6} pm^3, and 0.5×10^{-6} pm^3 for $(Bi_{1-x}Sr_x)_2Al_4O_{9-x}$ and $(Bi_{1-x}Sr_x)_2Ga_4O_{9-x}$, respectively, during cooling at the respective temperatures. The $\alpha(V)$ of $Bi_2Al_4O_9$ and $(Bi_{1-x}Sr_x)_2Al_4O_{9-x}$, and, $Bi_2Ga_4O_9$ and $(Bi_{1-x}Sr_x)_2Ga_4O_{9-x}$ in the cooling curves stayed close to each other throughout the whole temperature range. Both the intrinsic and extrinsic parameters were considered for the description of the observed features. We also include the decomposition, average crystal size, microstrain, possible formation of triclusters [2] in the strontium-doped samples and their role for changing the vibrational Eigenvectors. The bond lengths and the bond angles were calculated, and the conventional bond valence analysis was performed. Due to the stereochemical activity of the $6s^2$ lone electron pair (LEP) of Bi^{3+} cations, the BiO_6 octahedra show a high distortion index (mean quadratic elongation). The Liebau [3] vector term eccentricity parameter $\mathbf{\Phi}_i$ was calculated, which decreased, in some cases, with increasing temperature, thus showing the decrease of the stereoactivity of LEP of Bi^{3+} cation.

References

[1] Th.M. Gesing, R.X. Fischer, M. Burianek, M. Mühlberg, T. Debnath, C.H. Rüscher, J. Ottinger, J.C. Buhl, H. Schneider, J. Eur. Ceram. Soc. 31 (2011) 3055.

[2] Th.M. Gesing, M. Schowalter, C. Weidenthaler, M.M. Murshed, G. Nénert, M. Curti, C.B. Mendive, A. Rosenauer, J.-Ch. Buhl, H. Schneider, R.X. Fischer, J. Mater. Chem. 22 (2012) 18814.

[3] X. Wang, F. Liebau, Z. Kristallogr. 211 (1996) 437.

PS05-P16

Strukturelle, spektroskopische and DFT-Untersuchungen an einem neuen mikroporösen Thalliumsilikat

V. Kahlenberg[1], L. Perfler[1], J. Konzett[1], P. Blaha[2]
[1]*Universität Innsbruck, Mineralogie & Petrographie, Innsbruck, Austria*
[2]*TU Wien, Institut für Materialchemie, Wien, Austria*

Die Strukturchemie von Silikaten des einwertigen Thalliums ist nur in Ansätzen bekannt. Bislang wurde im System Tl_2O-SiO_2 mit der Verbindung $Tl_6Si_2O_7$ nur eine kristalline Phase beschrieben [1].

Im Rahmen von Rekristallisationsexperimenten an Gläsern mit einem Tl_2O:SiO_2 Verhältnis von 1:2 konnten Einkristalle eines neuen Thalliumsilikates der Zusammensetzung $Tl_4Si_5O_{12}$ erhalten werden. Aus Einkristallbeugungsexperimenten ergaben sich die folgenden kristallographischen Basisdaten: monokline Symmetrie, Raumgruppentyp *C*2/*c*, a= 9.2059(5), b=11.5796(6), c=13.0963(7) Å, b=94.534(5)°. Die im Anschluss durchgeführte Kristallstrukturanalyse zeigte, dass es sich bei diesem Material um ein unterbrochenes Gerüstsilikat handelt, bei dem die Q^3- bzw.Q^4-Tetraeder im Verhältnis 2:1 vorliegen. Wie aus der die Konnektivität der Si-Atome darstellenden Abbildung (s.u.) hervorgeht, können innerhalb des Gerüstes vier-, sechs- bzw. zwölfzählige Tetraederringe unterschieden werden. Die Gerüstdichte beträgt 14.4 T-Atome/1000 Å^3 und ist somit vergleichbar mit Werten, wie sie z.B. im Zeolith Linde Typ A beobachtet worden sind.

Die poröse Struktur enthält kanalartige Hohlräume parallel zu [110] bzw. [-110], in denen die Tl^+-Kationen zum Ladungsausgleich eingebaut werden. Diese zeigen eine für Kationen mit einem stereochemisch aktiven $6s^2$ Elektronenpaar typische einseitige Koordination und besetzten die Spitzen von verzerrten trigonalen [TlO_3]-Pyramiden. Aus der Verknüpfung benachbarter Pyramiden über gemeinsame Kanten resultieren zickzack förmige Doppelketten, die auch im schon bekannten Pyrosilikat $Tl_6Si_2O_7$ als Strukturelement auftauchen.

Eine theoretische Strukturoptimierung mittels DFT-basierenden WIEN2k [2] Rechnungen liefert eine Struktur in sehr guter Übereinstimmung mit dem Experiment. Die elektronische Struktur der nichtäquivalenten Tl-atome ist sehr ähnlich und dominiert durch eine bindende Wechselwirkung von Tl-s Zuständen mit den benachbarten O-atomen, während am Valenzbandmaximum eine O-p Tl-p antibindende Wechselwirkung zu einem ausgeprägten „lone pair“ am Tl führt. Auch die elektronische Struktur aller Si Atome ist sehr ähnlich, während die verschiedenen O Atome mit und ohne Tl-Nachbarn doch signifikante Unterschiede aufweisen und der ionischen Bindungscharakter der Si-O Wechselwirkung ist stärker als von Tl-O. Die aus DFT-Rechungen für den Γ-Punkt resultierenden Phononen zeigen in ihren Bandenlagen eine sehr gute Übereinstimmung mit den Ergebnissen von ramanspektroskopischen Messungen.

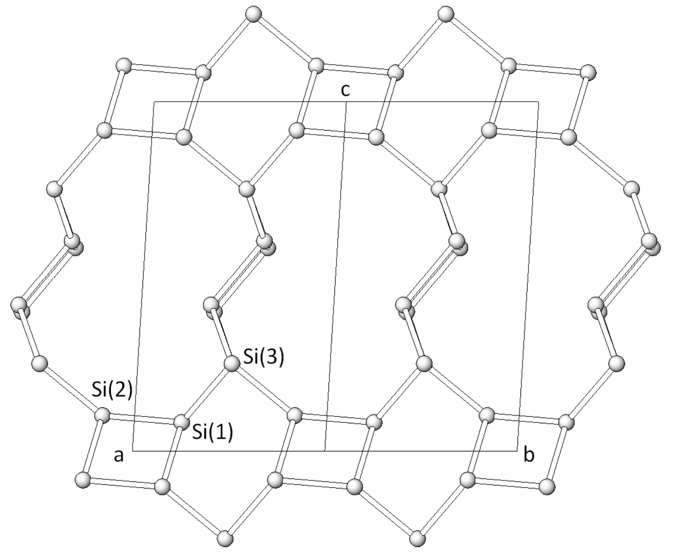

Abbildung: Konnektivität der Si-Atome in der Kristallstruktur des Tl4Si5O12

[1] Piffard, Y., Marchand, R., Tournoux, M. Rev. Chim. Min, 1975, 12, 210-217.

[2] Blaha, P., Schwarz, K., Madsen, G., Kvasnicka, D., Luitz, J. Software package WIEN2k, 2001, www.wien2k.at

PS05-P17

Extended Network Construction *via* Non-Covalent N···I Halogen Bonding

C. Merkens[1], U. Englert[1]
[1]*RWTH Aachen University, Institute of Inorganic Chemistry, Aachen, Germany*

The construction of extended network structures represents an area of very active research in crystal engineering. Networks featuring two different cations in predictable order can be synthesized based on ditopic ligands. For this purpose *N*-substituted acetylacetonates have attracted particular interest.[1-4] The synthesis of the network is based on a stepwise approach. In the first step a **s**econdary **b**uilding **u**nit, consisting of one metal center and the organic linker, is constructed. The SBU has free coordination sites for further crosslinking reactions in the second step. The architecture of the resulting network depends on the interactions in the solid state including metal coordination by organic ligands, classical and non-classical hydrogen bonds, and π-π stacking.

Additionally, non-covalent halogen bonding has proven an efficient tool for the tailoring of complex network structures.[5,6] This Lewis acid-base interaction results in relatively strong non-covalent bonding in which lone pair electrons of heteroatoms interact with electron-poor halogens. Electron-poor halogen atoms with a so called “sigma hole” are designed by introducing electron withdrawing fluorinated hydrocarbons.

A combination of the two concepts - synthesis of SBUs and crosslinking reactions using halogen bonding - offers interesting opportunities for crystal engineering of extended networks. We present the organic ligand 3-(4-pyridyl)-acetylaceton (HacacPy)[7] as ditopic ligand for the stepwise construction of networks. The hard oxygen-based chelating site is used for the synthesis of SBUs based on oxophilic cations. The lone pair electrons of the pyridine moiety serve as electron donors for non-covalent N···I halogen bonding combined with diiodo-tetrafluorobenzene (TFDIB).

[1] V. D. Vreshch, A. B. Lysenko, A. N. Chernega, J. A. K. Howard, H. Krautscheid, J. Sieler and K. V. Domasevitch, *Dalton Trans*., **2004**,2899-2903.
[2] A. D. Burrows, K. Cassar, M. F. Mahon and J. E. Warren, *Dalton Trans*.,**2007**, 2499-2509.
[3] M. Kondracka, U. Englert, *Inorg. Chem*., **2008**, *47*, 10246-10257.
[4] C. Merkens, U. Englert, *Dalton Trans*., **2012**, *41*, 4664-4673.
[5] D. Cincic, T. Friscic, W. Jones, CrystEngComm, **2011**, *13*, 3224-3231 and references cited therein
[6] L. Russo, S. Biella, M. Lahtinen, R. Liantonio, P. Metrangolo, G. Resnati, K. Rissanen, *CrystEngComm*, **2007**, *9*, 341-344.
[7] L.G. Mackay, H.L. Anderson, J.K.M. Sanders, *J. Chem. Soc. Perkin Trans. 1*, **1995**, 2269-2273.

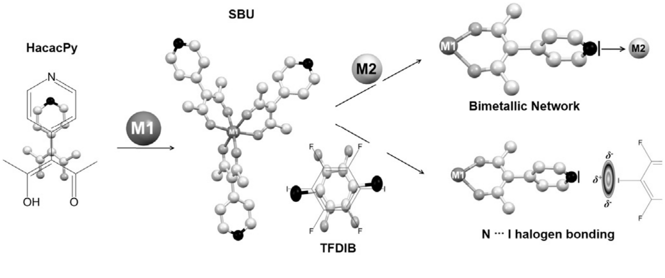

PS05-P18

Ammonothermal Synthesis of a New Modification of $K_2[Zn(NH_2)_4]$

T. Richter[1], S. Zhang[1], R. Niewa[1]
[1]*Universität Stuttgart, Institut für Anorganische Chemie, Stuttgart-Vaihingen, Germany*

Potassium tetraamidozincate ($K_2[Zn(NH_2)_4]$) was first obtained as early as 1907 [1, 2] but not structurally characterized. A triclinic form was described by Brisseau and Rouxel in 1969 [3] prepared from zinc and potassium in liquid ammonia at ambient temperature. Possible hydrogen positions were subsequently determined by Fröhling and Jacobs [4]. No isotypic triclinic ternary amide is known up to now. Recently, we have obtained a monoclinic modification of $K_2[Zn(NH_2)_4]$ ($P2_1/c$, a = 746.54(8) pm, b = 700.7(6) pm, c = 1327.6(2) pm and β = 106.07(1)°) under ammonothermal conditions (ammonobasic, 520 - 720 K, 92 - 228 MPa) from zinc and potassium amide. There are several isotypic monoclinic ternary alkali metal amides of manganese, zinc and magnesium reported [5-⊥ 7]. The crystal structure can be described with a $[Zn(NH_2)]_2^{4-}$ substructure, realizing a distorted hexagonal closed packing with stacking direction in [010]. Zinc is tetrahedrally coordinated by four amide ions. The potassium cations are coordinated by seven amide ions. The surrounding of K^+ ions may be described as a trigonal prism with one single capped rectangular face of amide ions. Thermal analysis was employed to study the thermal behavior and decomposition of the title compound. Prior to the decomposition at 563 K, two endothermal signals at about 463 K and 495 K can be observed. The second signal was assigned to the melting of the sample, the first one may represent the onset of a thermally induced free rotation of the amide ions. During cooling two exothermal signals appear at 478 K and 463 K. The first signal was assigned to the solidification. After cooling (slow or rapid) only the monoclinic modification was obtained. Thus, there is no clear indication for solid-solid phase transition so far. Furthermore, the calculated density of the monoclinic modification (2.067 g/cm^3) is slightly higher than the density of the triclinic modification (2.015 g/cm^3). Those results indicate that the triclinic modification may be a metastable phase and the monoclinic modification is the stable phase at ambient conditions.

References
[1] F. Fitzgerald, *J. Am. Chem. Soc.* **29** (1907) 656-665.
[2] W. Fernelius, F. Bergstrom, *J. Phys. Chem.* **35** (1931) 740⊥ -755.
[3] L. Brisseau, J. Rouxel, *C. R. Hebd. Seances Acad. Sci. C* **268** (1969) 2308⊥ -2311.
[4] B. Fröhling, H. Jacobs, *Z. Anorg. Allg. Chem.* **623** (1997) 1103⊥ -1107.
[5] M. Drew, L. Guémas, P. Chevalier, P. Palvadeau, J. Rouxel, *Rev. Chim. Min.* **12** (1975) 419-⊥ 426.
[6] H. Jacobs, J. Birkenbeul, J. Kockelkorn, *J. Less-Common Met.* **97** (1984) 205⊥ -214.
[7] H. Jacobs, J. Birkenbeul, D. Schmitz, *J. Less-Common Met.* **85** (1982) 79⊥ -86.

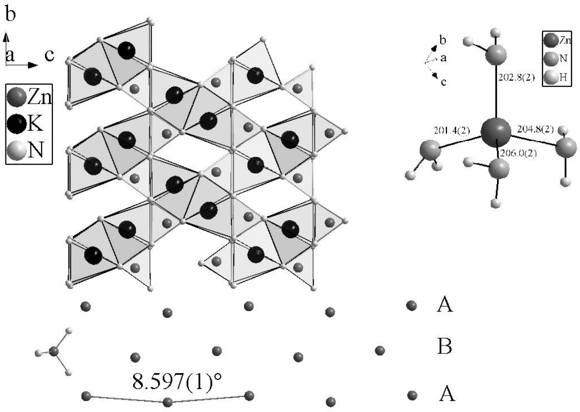

Figure 1: Structure of $K_2[Zn(NH_2)_4]$ without hydrogen atoms, $[Zn(NH_2)]_2$⊥ $^{4-}$ substructure and surrounding of Zn^{2+} ions by 4 amide ions.

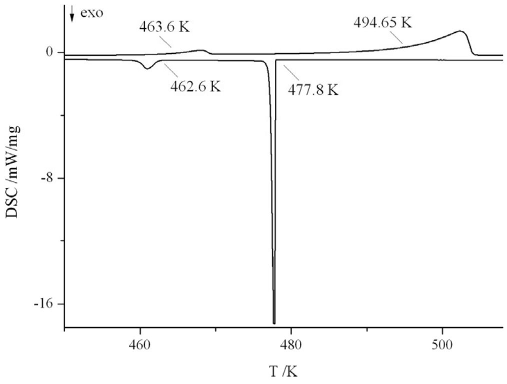

Figure 2: DSC measurement of the monoclinic $K_2[Zn(NH_2)_4]$ (297 - 523 K, heating and cooling rates 5 K/min).

PS05-P19

A Potential Redox-System Captured from Aqueous Solution: Synthesis and Crystal Structure of BaCl[MnO$_4$]

H. Henning[1], T. Schleid[1]
[1]*Universität Stuttgart, Institut für Anorganische Chemie, Stuttgart, Germany*

The established route for the synthesis of any salt-like permanganate, other than K[MnO$_4$], is to use aqueous solutions of Ba[MnO$_4$]$_2$, synthesized according to the *Muthmann* method [1], and a sulfate $M^{n+}([SO_4]^{2-})_{n/2}$ in order to isolate the desired permanganate $M^{n+}([MnO_4]^{-})_n$ after the precipitation of Ba[SO$_4$] by subsequent drying of the remaining brine. In some cases, more specifically with Sr^{2+} or Ca^{2+}, where the sulfate itself is poorly soluable as well, a detour via the unstable free acid H[MnO$_4$] has to be taken.

In an attempt to circumvent this step, a new pathway to prepare permanganates was tested, where a cation-exchange column loaded with a $BaCl_2$ solution should exchange the K^+ cations of K[MnO$_4$]. By an insufficient loading of the column, BaCl[MnO$_4$] was obtained as a by-product first, but could be reproduced later as pure phase through the mixing of equimolar amounts of $BaCl_2$ and

$Ba[MnO_4]_2$ in aqueous solution and subsequent removal of water with a rotary evaporator.

The crystal structure of $BaCl[MnO_4]$ shows a general structural motif that was also observed for $LaCl[MoO_4]$ (monoclinic, $P2_1/c$) [2] and $LaBr[MoO_4]$ (monoclinic, *Pc*) [3] before, but the title compound crystallizes in the orthorhombic space group *Pnma* with lattice parameters of a = 1923.18(9), b = 550.24(3), c = 472.31(2) pm and Z = 4 (CSD-424746). One crystallographically distinguishable Ba^{2+} and Cl^- ion as well as three different oxygen atoms, which form together with the unique Mn^{7+} cation the discrete permanganate anion $[MnO_4]^-$ (d(Mn−O) = 160 - 163 pm), occur in $BaCl[MnO_4]$. Ba^{2+} is coordinated by four Cl^- anions (d(Ba−Cl) = 315 - 317 pm) and five permanganate units (d(Ba−O) = 276 - 295 pm), two of them attached via edges. The Cl^- anions on the other hand are coordinated tetrahedrally by four Ba^{2+} cations to form two dimensional layers (Figure 1) by edge-fusion of $[ClBa_4]^{7+}$ tetrahedra (d(Cl−Ba) = 315 - 317 pm), in between which the $[MnO_4]^-$ anions arrange in zigzag-chains with the top of the tetrahedra pointing towards (00−1) or (001), respectively (Figure 2). At first glance, this structure looks like a fusion of the crystal structures of $BaCl_2$ and $Ba[MnO_4]_2$, although it shows many characteristics of the above mentioned series LnCl[MoO_4] with Ln = La, Ce, Pr [2] and LnBr[MoO_4] with Ln = La, Ce [3] and is also placeable within the *Bärnighausen* tree [4] at the same position as the isopuntal compound $LaCl[WO_4]$ [5] with similar lattice parameters to the expected values for an $AX[MO_4]$ compound crystallizing in space group *Pnma*.

[1] W. Muthmann, *Ber. Deut. Chem. Ges.* **1893**, *26*, 1016.

[2] I. Hartenbach, Th. Schleid, S. Strobel, P. K. Dorhout, *Z. Anorg. Allg. Chem.* **2010**, *636*, 1183.

[3] I. Hartenbach, H. Henning, Th. Schleid, T. Schustereit, S. Strobel, *Z. Anorg. Allg. Chem.* **2013**, *639*, in press.

[4] H. Bärnighausen, *MATCH − Comm. Math. Chem.* **1980**, *9*, 139.

[5] L. H. Brixner, H.-Y. Chen, C. M. Foris, *J. Solid State Chem.* **1982**, *45*, 80.

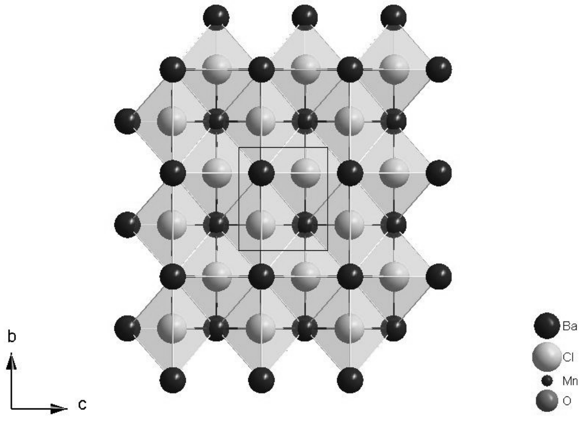

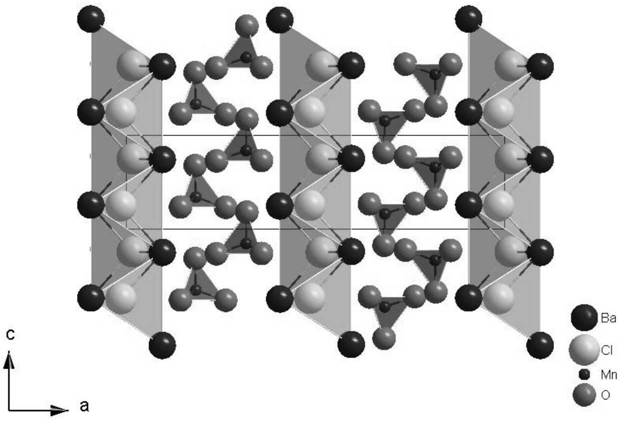

PS05-P20

Neue Rubidiumsulfidoferrate $Rb_8[Fe_4S_{10}]$, *m*-$Rb_6[Fe_2S_6]$, *o*-$Rb_6[Fe_2S_6]$

M. Schwarz[1], M. Haas[1], C. Röhr[1]
[1]*Universität Freiburg, Institut für Anorganische und Analytische Chemie, Freiburg, Germany*

In der Reihe der Rb-Sulfidoferrate Rb-Fe-S waren bislang vier Glieder bekannt. Allen ist ein Anionenbauverband aus FeS_4-Tetraedern gemeinsam, der je nach Verhältnis Fe:S unterschiedliche Kondensationsgrade aus kantenverknüpften Tetraedern enthält: $Rb_9Fe_2^{II/III}S_7$ [1] enthält neben isolierten $Fe^{III}S_4$-Tetraedern planare $Fe^{III}S_3$-Einheiten. Die Anionenbauverbände der Kettenferrate $RbFe^{III}S_2$ [2], welches antiferromagnetische Kopplung der Fe^{III}-Ionen entlang der Ketten aufweist [3], und $Rb_3Fe_2^{II/III}S_4$ [4] bestehen aus SiS_2-analogen $FeS_{4/2}$-Tetraedersträngen aus über Kanten verknüpften Tetraedern. Das synthetische Analogon des Minerals Rasvumit mit der Zusammensetzung $RbFe_2S_3$ [5] ist aus zu Ketten verknüpften gemischtvalenten $[Fe_2S_6]$-Doppeltetraedern aufgebaut. Mößbauerspektren der zu den letztgenannten gemischtvalenten Verbindungen isotypen Phasen $Na_3Fe_2S_4$ und KFe_2S_3 zeigen keine Ausordnung der $Fe^{II/III}$-Ionen [6,7].

Mittels Schmelzreaktionen bei 600/800°C aus Rb_2S, Fe und S ist uns die Synthese und strukturelle Aufklärung durch Einkristallstrukturanalyse dreier weiterer Rb-Sulfidoferrate(III) gelungen: $Rb_6[Fe_2S_6]$, welches $Fe_2S_6^{6-}$-Tetraederdoppel bestehend aus über zwei Kanten verknüpfte FeS_4-Tetraeder enthält und in zwei Modifikationen kristallisiert: *m*-$Rb_6[Fe_2S_6]$ ($P2_1/c$, a=796.06(5), b=1291.35(8), c=1032.40(6) pm, β=127.163(4)°) sowie *o*-$Rb_6[Fe_2S_6]$ (*Cmca*, a=1884.36(3), b=695.660(10), c=1296.09(2) pm). Die Abstände Fe-S und Fe-Fe innerhalb der Anionen sind in den beiden Modifiaktionen fast gleich, während sich die Koordinationszahlen und -abstände der Kationen deutlich unterscheiden. Damit reiht sich die Verbindung als struktureller Übergang vom monoklinen Strukturtyp der Sulfidoferrate $A_6[Fe_2S_6]$ mit A=Na,K [8,9] hin zum orthorhombischen Strukturtyp der Cs-Verbindung [10] ein. Desweiteren ist uns die Synthese eines Tetraferrates $Rb_8[Fe_4S_{10}]$ (*P*-1, a=744.65(3), b=851.21(3), c=1042.77(4) pm, α=77.990(2), β=85.244(2), γ=81.051(2)°) mit Kettenstücken aus je vier kantenverknüpften FeS_4-Tetraedern gelungen. Die Tetramere sind längs der Raumdiagonalen [-111], jeweils getrennt durch zwei Rb-Kationen, aufgereiht und senkrecht dazu in einer hexagonalen Stabpackung angeordnet (siehe Abb.). Die Phase bildet das Bindeglied zwischen den Tetraederdoppeln $Fe_2S_6^{6-}$ mit ausschließlich endständigen FeS_4-Tetraedern und den Kettenferraten, die ausschließlich verknüpfte $FeS_{4/2}$-Tetraeder enthalten, was sich in den Abständen Fe-S und Fe-Fe in den Anionen widerspiegelt, die denen der Di- und Kettenferrate sehr ähnlich sind.

[1] W. Bronger *et al.*, *J. Alloys. Compd.* **1993**, *197,* 83.
[2] W. Bronger, Z. Anorg. *Allg. Chem.* **1968**, *359,* 225.
[3] W. Bronger *et al.*, *J. Sol. St. Chem.* **1987**, *70,* 262.
[4] W. Bronger *et al.*, *J. Alloys. Com.* **1995**, *218,* 22.
[5] R. H. Mitchell *et al.*, *J. Sol. St. Chem.* **2004**, *177,* 1867.
[6] J. Ensling *et al.*, *Hyperfine Interact.* **1986**, *28,* 599.
[7] G. Amthauer *et al.*, *Naturwissenschaften* **1983**, *70,* 146.
[8] P. Müller *et al.*, *Z. Naturforsch.* **1979**, *34b,* 1264.
[9] M. Schwarz *et al.*, im Druck, DOI:10.1002/zaac.201200397
[10] W. Bronger *et al.*, *J. Alloys Compd.* **1992**, *187,* 95.

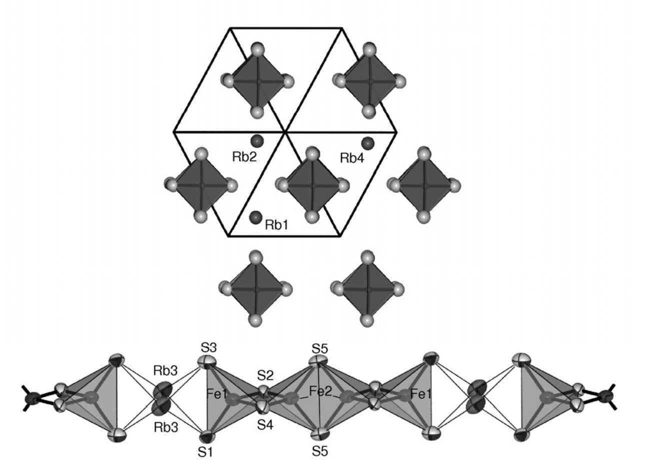

PS05-P21

$[N_2C_6H_{14}][CuX_3]$ - 1,4-Diazoniabicyclo[2.2.2]octane trihalocuprate(I), (*X* = Cl, Br, I): Synthesis, crystal structure and optical properties

S. Maderlehner, M. Leitl, H. Yersin, A. Pfitzner

S. Maderlehner[1], M. Leitl[2], H. Yersin[2], A. Pfitzner[1,2]
[1] *Universität Regensburg, Institut für Anorganische Chemie, Regensburg, Germany*
[2] *Universität Regensburg, Institut für Physikalische Chemie, Regensburg, Germany*

The compounds $[N_2C_6H_{14}][CuCl_3]$ (**1**), $[N_2C_6H_{14}][CuBr_3]$ (**2**) and $[N_2C_6H_{14}][CuI_3]$ (**3**) were synthesized in a hydrothermal reaction in organic solvents such as acetone or acetonitrile in silica ampoules at 130 °C. They were obtained as colourless plate like crystals. All three compounds are isotypic and crystallize orthorhombic, space group *Pnma*, $Z = 4$, with $a = 14.132(5)$ Å, $b = 7.831(3)$ Å, $c = 9.354(4)$ Å, $V = 1035(1)$ Å^3 (**1**), $a = 14.7119(8)$ Å, $b = 8.0193(5)$ Å, $c = 9.3718(4)$ Å, $V = 1105.7(1)$ Å^3 (**2**), and $a = 15.659(2)$ Å, $b = 8.315(1)$ Å, $c = 9.668(1)$ Å, $V = 1258.8(4)$ Å^3 (**3**). The refinements converged at $R_1 = 0.0472$ and $wR_2 = 0.0874$ (**1**), $R_1 = 0.0523$ and $wR_2 = 0.1115$ (**2**) and $R_1 = 0.0662$ and $wR_2 = 0.0867$ (**3**) (all data).

The complex anion is a trigonal monomer with all atoms located on the 4*c* Wyckoff position. Three different bond lengths between copper and halide are observed in all compounds which is in agreement with FIR-spectra. The cation is a twofold protonated 1,4-diazabicyclo[2.2.2]octane (dabco) which takes an eclipsed conformation. These cations form hydrogen bonds to two of the halide ligands of the complex anions, thus forming an infinite chain structure via hydrogen bonding, see Figure 1. The copper halide bond lengths correlate strongly with the $H\cdots X$ distances showing an inverse proportionality. The formation of chain structures via hydrogen bonding has been also observed in the hydrates of dabco dihydrohalides [1-3].

1, **2** and **3** show visible luminescence upon excitation with UV-light. **1** has a blue emission at room temperature with the emission maximum at 430 nm, while **2** and **3** have a violet emission with the emission maxima at 395 (**2**) or 405 nm (**3**), respectively. Upon cooling to liquid nitrogen temperature a narrowing of the emission band and a small blue-shift of 5 - 10 nm of the emission maximum can be observed for all compounds.

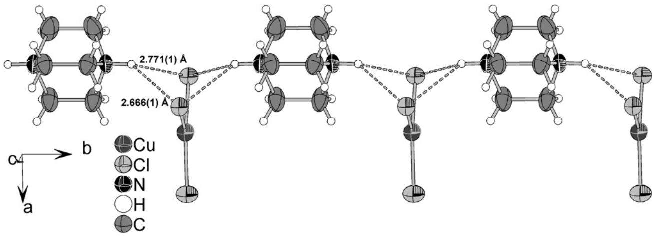

Figure 1. Section of the chain structure formed via hydrogen bonding in **1**

References

[1] T. C. Lewis, D. A. Tocher, *Acta Crystallogr., Sect. E: Struct. Rep. Online*, **2005**, *61*, o2202.

[2] M. Andrzejewski, A. Olejniczak, A. Katrusiak, *Cryst. Growth&Design* **2011**, *11*, 4892-4899.

[3] S. Maderlehner, A. Pfitzner, *Z. Kristallogr.* **2012**, *227*, 569-574.

PS05-P22

The Crystal Structure of $Ce_4Mo_7O_{27}$ and its Relationship to the Structures of $La_4Mo_7O_{27}$ and $Ln_4Mo_7O_{27}$ (*Ln* = Eu, Gd)

T. Schleid[1], C. Dobos-Wolfer[1], S. Strobel[1], I. Hartenbach[1]
[1] *University of Stuttgart, Institute for Inorganic Chemistry, Stuttgart, Germany*

In attempts to obtain the oxomolybdate(VI) $Ce[MoO_4]_2$ with tetravalent cerium, using CeO_2 and MoO_3 (molar ratio 1 : 1) in a classical solid-state synthesis approach, orange-coloured, coarse single crystals of $Ce_4Mo_7O_{27}$, containing trivalent cerium emerged.

The title compound crystallizes monoclinically in space group *C*2/*c* (*a* = 4612.17(6) pm, *b* = 748.02(1) pm, *c* = 1432.58(2) pm, *β* = 100.946(1)°, CSD-425495) with eight formula units per unit cell. In its crystal structure four crystallographically distinguishable Ce^{3+} cations occur, of which $(Ce1)^{3+}$ and $(Ce2)^{3+}$ are surrounded by irregular polyhedra with coordination numbers of nine, while $(Ce3)^{3+}$ and $(Ce4)^{3+}$ show eight-membered coordination spheres in the shape of distorted bicapped trigonal prisms, each. The latter two build up $[(Ce3)(Ce4)O_{13}]^{20-}$ dimers by sharing triangular faces, whereas those around the $(Ce1)^{3+}$ and $(Ce2)^{3+}$ cations arrange themselves in chains of the composition $[(Ce1)(Ce2)O_{13}]^{20-}$ along [010] by their fusion via common faces and edges. Furthermore, five crystallographically different *ortho*-oxomolybdate(VI) tetrahedra $[(Mo1\text{-}5)O_4]^{2-}$ and one oxodimolybdate(VI) unit $[(Mo6)(Mo7)O_7]^{2-}$ are found in the crystal structure of the title compound. While the entities around $(Mo1)^{6+}$, $(Mo2)^{6+}$, $(Mo4)^{6+}$, and $(Mo5)^{6+}$ can be considered as isolated, one of the oxide ligands within the $[(Mo3)O_4]^{2-}$ tetrahedra is found approximately 263 pm apart from $(Mo7)^{6+}$ and therefore the coordination number of the latter is enlarged to CN = 4+*1*. Thus, instead of completely isolated oxodimolybdate(VI) units, moieties of the composition $[Mo_3O_{11}]^{4-}$ can be identified in this structure. These units are arranged in a loosely packed layer perpendicular to [100] at $x/a \approx {}^1/_8$, ${}^3/_8$, ${}^5/_8$, and ${}^7/_8$. The $[(Mo1)O_4]^{2-}$ and $[(Mo2)O_4]^{2-}$ tetrahedra also assemble in sheets parallel to (100), but at $x/a \approx {}^1/_4$ and ${}^3/_4$ with the $(Ce1)^{3+}$ and $(Ce2)^{3+}$ cations separating them from the aforementioned layers built of the $[Mo_3O_{11}]^{4-}$ units. The same is true for the $[(Mo4)O_4]^{2-}$ and $[(Mo5)O_4]^{2-}$ tetrahedra at $x/a \approx 0$ and ${}^1/_2$ with $(Ce3)^{3+}$ and $(Ce4)^{3+}$ as cationic spacers (see Figure, Ce^{3+}: black spheres, $[MoO_4]^{2-}$ tetrahedra: dark grey polyhedra, $[Mo_3O_{11}]^{4-}$ units: light grey polyhedra).

Basically, all these building blocks are also found in the crystal structures of *non*-centrosymmetric $La_4Mo_7O_{27}$ (orthorhombic, *Pca*2_1 [1]) as well as in $Eu_4Mo_7O_{27}$ [2] and, $Gd_4Mo_7O_{27}$ [3] (monoclinic, *C*2/*c*). Slight, but critical differences do exist, however, which lead to structural arrangements that are similar to each other at first glance, but exhibit variations in detail.

[1] B. van der Wolf, P. Held, P. Becker, *Acta Crystallogr.* **2009**, *E 65*, i59.

[2] H. Naruke, T. Yamase, *J. Solid State Chem.* **2001**, *161*, 85.

[3] H. Naruke, T. Yamase, *Acta Crystallogr.* **2002**, *E 58*, i62.

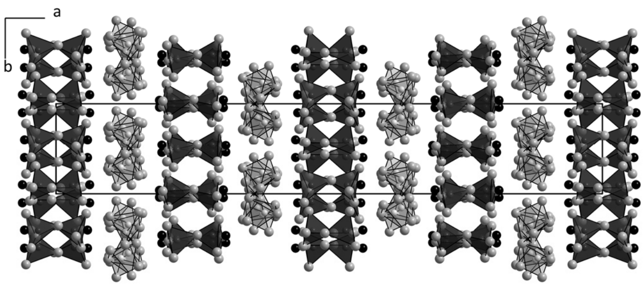

PS05-P23

Synthesis and Structural Characterization of the Terbium(III) Chloride Oxotungstate(VI) TbCl[WO4]

T. Schustereit[1], T. Schleid[1], I. Hartenbach[1]

[1]*University of Stuttgart, Institute for Inorganic Chemistry, Stuttgart, Germany*

More than 30 years ago, rare-earth metal chloride oxotungstates with the composition *RE*Cl[WO_4] (*RE* = Y, Eu - Tm) were synthesized by *Brixner et al.* [1]. The crystal structure of GdCl[WO_4] was determined only by X-ray powder diffraction and served as model for the whole *RE*Cl[WO_4] series (*RE* = Y, Eu - Tm). Colourless, transparent single crystals of TbCl[WO_4] could now be obtained by heating a mixture of Tb_4O_7, Tb, $TbCl_3$, and WO_3 (molar ratio: 3 : 2 : 35 : 21) in evacuated fused silica ampoules for seven days at 950 °C. $TbCl_3$, which was used with a fivefold excess as both educt and flux, was able to be removed from the crystals of the title compound by washing with water.

TbCl[WO_4] crystallizes monoclinically in space group *C*2/*m* (*a* = 1028.06(5), *b* = 728.58(3), *c* = 687.13(3) pm and β = 107.293(2)°, CSD-425496) with four formula units per unit cell. Thus, the title compound is not only isostructural with GdCl[WO_4], but also with most representatives of the analogous rare-earth metal(III) chloride oxomolybdates(VI) *RE*ClMoO$_4$ (*RE* = Y, Sm - Yb) [2, 3]. The structure contains crystallographically unique Tb^{3+} cations, which are surrounded by two Cl^- and six O^{2-} anions (*d* (Tb - Cl) = 272 - 276 pm), *d* (Tb - O) = 230 - 263 pm), forming a distorted trigonal dodecahedron (CN = 8). These polyhedra are fused together via three common edges, which consist of two oxide anions (twice) and two chloride anions (once), respectively, to form anionic $[TbClO_4]^{6-}$ layers parallel to the *ab* plane (see Figure 1). Finally, those layers become interconnected by W^{6+} cations along [001] to build up the complete structure by forming discrete $[WO_4]^{2-}$ tetrahedral (*d* (W - O) = 174 - 180 pm). Since the title compound emerged as pure phase, which was confirmed by X-ray powder diffractometry, vibrational and optical spectroscopy could also be performed. Furthermore, TbCl[WO_4] exhibits a Tb^{3+}-typical yellow-green bulk luminescence upon excitation with UV light (λ = 254 nm).

[1] L. H. Brixner, H.-Y. Chen, C. M. Foris, *Mater. Res. Bull.* **1982**, *17*, 1545.

[2] Th. Schleid, S. Strobel, P. K. Dorhout, P. Nockemann, K. Binnemans, I. Hartenbach, *Inorg. Chem.* **2008**, *47*, 3728.

[3] I. Hartenbach, S. Strobel, Th. Schleid, K. Krämer, P. K. Dorhout, *Z. Anorg. Allg. Chem.* **2009**, *635*, 966.

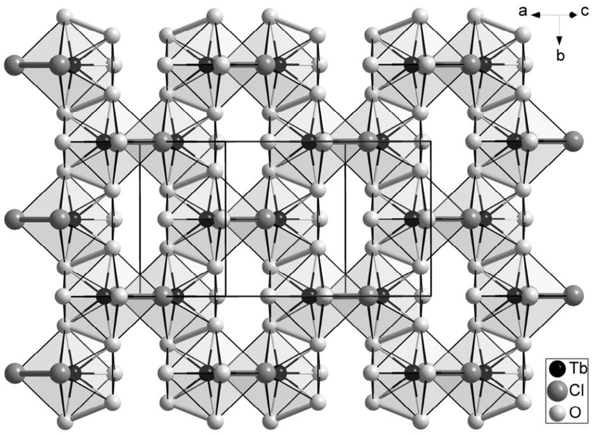

PS05-P24

Crystal Structure of a New Monoclinic Modification of Cu_2SnSe_3

J. Fan[1], W. Carrillo-Cabrera[1], Y. Grin[1]
[1]*Max Planck Institute for Chemical Physics of Solids, Dresden, Germany*

Recently, the ternary compound Cu_2SnSe_3 with diamond-like crystal structure has gained much attention as promising thermoelectric material. Nevertheless, a controversy still exists about its crystal structure. Besides the early reported cubic phase[1-3], recently two monoclinic modifications were reported[4,5]. During our studies, Cu_2SnSe_3 was found to crystallize with thin twin domains, being difficult to find individual single crystals suitable for X-ray single-crystal data acquisition. Therefore, we use Electron Diffraction Tomography (EDT[6]) on a tiny crystal fragment to evade the problem of twinning. In this study, the crystal structure of a new monoclinic modification of Cu_2SnSe_3 was determined from EDT and refined using the full-profile method on X-ray diffraction (XRD) powder data: modification II, space group *Cc*, a_2 = 6.9684(4) Å, b_2 = 12.078(1) Å, c_2 = 13.3942(9) Å, β_2 = 99.838(6)°.

Conventional TEM microscopy and manually controlled diffraction tomography were employed. The selected area electron diffraction (SAED) mode was used for data collection. ADT3D software package[6] was used for reconstruction of the diffraction volume and the space group *Cc* was chosen. Structure solution was confirmed by Rietveld refinement of the XRD powder data. $R_w(p) = 0.042$, $R(F^2) = 0.041$, $R(F) = 0.038$ were achieved with 696 reflections, 40 refined parameters.

The new monoclinic modification (II) along with the known monoclinic modifications I and III reported before are all ordered superstructures of the cubic Cu_2SnSe_3 pattern, which is a derivative of the sphalerite structure. Therefore each Se anion is coordinated by four cations and, similarly, Cu and Sn cations are coordinated by four Se anions. There is distinct ordering of Sn and Cu, forming different zig-zag chains of corner sharing $SnSe_4$ tetrahedra along the *c* axis (Fig. 1). So the three monoclinic modifications have different but related *c* axis lengths, while practically same *a* and *b* axes. The relationship is as follows: $c_1 = a_c{\cdot}6^{1/2}/2$, $c_2 = a_c{\cdot}6^{1/2}$, $c_3 = a_c{\cdot}2{\cdot}6^{1/2}$.

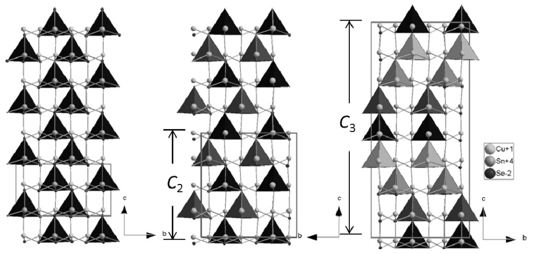

Fig. 1. The packing of the Sn-centered tetrahedra in modifications of Cu_2SnSe_3: I (left), II (middle) and III (right). Different colors of the tetrahedra indicate different crystallographic Sn positions.

References

1. Palatnik, L. S.; Koshkin, V. M.; Galchinetskii, L. P.; Kolesnikov, V. I.; Komnik, Y. F., *Soviet Physics-Solid State* **1962,** *4*, 1052-1053.
2. Rivet, J.; Laruelle, P.; Flahaut, J., *Comptes Rendus Hebdomadaires Des Seances De L Academie Des Sciences* **1963,** *257*, 161-&.
3. Sharma, B. B.; Ayyar, R.; Singh, H., *Physica Status Solidi a-Applied Research* **1977,** *40*, 691-696.
4. Delgado, G. E.; Mora, A. J.; Marcano, G.; Rincon, C., *Materials Research Bulletin* **2003,** *38*, 1949-1955.
5. Gulay, L. D.; Daszkiewicz, M.; Ostapyuk, T. A.; Klymovych, O. S.; Zmiy, O. F., *Acta Crystallographica Section C-Crystal Structure Communications* **2010,** *66*, I58-I60.
6. Kolb, U.; Mugnaioli, E.; Gorelik, T. E., *Crystal Research and Technology* **2011,** *46*, 542-554.

PS05-P25

Crystal Structures and Isometricity Comparison of Bisphenol F Derivatives

T. Gruber[1], R. Nestler[1], W. Seichter[1], P. Bombicz[2]
[1]*TU Bergakademie Freiberg, Institute of Organic Chemistry, Freiberg, Germany*
[2]*Hungarian Academy of Sciences, Department of Structural Chemistry, Budapest, Hungary*

The term ‘bisphenol’ is used for a class of chemical compounds bearing two hydroxyphenyl moieties connected via a carbon or sulfur bridge. For many decades, they are widely used in industry and manufacturing of polymers.[1] One member of this particular family is bisphenol F featuring a bridging methylene group between the two aromatic units. It is believed to interfere in environmental processes and human health, *e.g.* was found to establish estrogenic activity in *in-vitro* bioassays.[2] Humans can be exposed to bisphenol F and its derivatives as environment and food contaminants.[3] Their solubility and bioavailability is directly connected to the intermolecular interactions in the solid state and in solution. Here we discuss in detail the crystal structures and solid state behavior of three bisphenol F derivatives and one respective analogue (**1**-**4**), including their synthesis, conformational analyses and an extensive structural comparison.

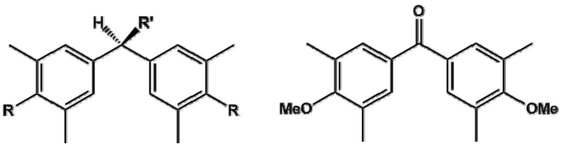

1: R = OH, R' = H
2: R = OMe, R' = H
3: R = H, R' = OH

4

Fig. 1 Compounds studied in this work.

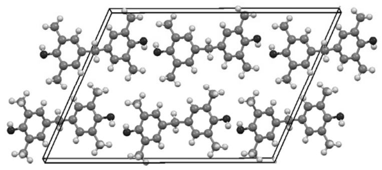

Fig. 2 Packing diagram of **1** in direction of the crystallographic *b* axis.

---

[1] H.-G. Franck, *Industrial Aromatic Chemistry: Raw Materials, Processes, Products*, Springer, Heidelberg, **1988**; H. Zhang, H. Wu, Q. Tang, *Reguxing Shuzhi* **1996**, 11, 43-45.

[2] Y. Hashimoto, M. Nakamura, *Dent. Mater. J.* **2000**, *19*, 245-262.

[3] N. Cabaton, C. Dumont, I. Severin, E. Perdu, D. Zalko, M. Cherkaoui-Malki, M. C. Chagnon, *Toxicology* **2009**, *255*, 15-24.

PS05-P26

Crystallography and crystal chemistry of alkaline earth monochloroacetate hydrates

R. Kaden[1], H. Pöllmann[1]
[1]*Martin Luther University Halle/Wittenberg, Mineralogy and Geochemistry, Halle (Saale), Germany*

Organic as well as inorganic additives are used to control the setting behaviour of calcium aluminate cements (CAC). While LiCl and Li_2CO_3 typically act as accelerators (Scrivener & Chapmas 1998, Stöber & Pöllmann 2003), organic acids like citric, formic, benzoic, oxalic or tartaric acid and their Ca-salts retard the hydration reaction (Scrivener & Chapmas 1998 and Pöllmann 1988, 1989, 1990). In a detailed report on the hydration behaviour of a CAC using Ca-salts of chlorinated acetic acids, Ca-monochloroacetate was pointed out as the strongest retarder (Schmidt & Pöllmann 2008). Thus, the present studies are focused on the influence of the cations of alkaline earth and alkaline chloroacetates and occurring derivatives. However, for the phase identification of such compounds by XRD, appropriate database entries are lacking. Crystal-structural data are only available for the monochloroacetates/-hydrates of NH_4^+ (Ichikawa 1972), Li^+ (Ehrenberger *et al.* 1999), Na^+ (Elizabé *et al.* 1997), Ca^{2+} (Karipides & Peiffer 1988), Ag^+ (Epple & Kirschnick 1997) and Ni^{2+} (Solans & Miravitlles 1981). Thus, the crystal structures, their thermal stabilities as well as their chemical behaviour and influence on a hydraulic binder system are objects of investigation, starting with the monochloroacetates. The compounds were synthesised by reaction of chloroacetic acid with the carbonates in aqueous solution and crystallised by slow evaporation of the solvent water.

Owing to their high alkalinity, for all the alkaline compounds stored in mother liquor, a hydrolysis of monochloroacetate into glycolic acid and chloride results, according to Drushel & Simpson (1917):

$$ClCH_2COO\mathit{A} + H_2O \leftrightarrow ClCH_2COOH + \mathit{A}^+ + OH^- \rightarrow HOCH_2COOH + \mathit{A}^+ + Cl^-$$

Only for *A* = Li this conversion reaction is not complete and an addition compound $Li(ClCH_2COO)(HOCH_2COOH)$ with a chain like crystal structure crystallised.

The alkaline earth monochloroacetates $Mg(ClCH_2COO)_2 \times 4H_2O$, $Ca(ClCH_2COO)_2 \times 1H_2O$, $Sr(ClCH_2COO)_2$, $Ba(ClCH_2COO)_2 \times 1H_2O$ were found to be stable in the mother liquor and to form layered structures. Each single layer consists of a chain like arrangement of the alkaline earth metals connected by 2 or 3 oxygen (2 for Ca, 3 for Sr and Ba) from the carboxylic groups and one water in $Ba(ClCH_2COO)_2 \times H_2O$ (Fig. 1). The linking of adjacent chains is realised by bridging carboxylic groups, differently for Ca, Sr and Ba. Characteristic for all of these compounds the chloromethyl groups are roughly directed in stacking direction on both outsides of the layers.

The setting of a typical CAC (Secar51, W/C = 0.5, T = 20°C) was retarded when a 0.025 molar solution of Ca-, Sr-, Ba-monochloroacetates was used (Ca > Sr > Ba). The Li-addition-compound strongly accelerates the setting.

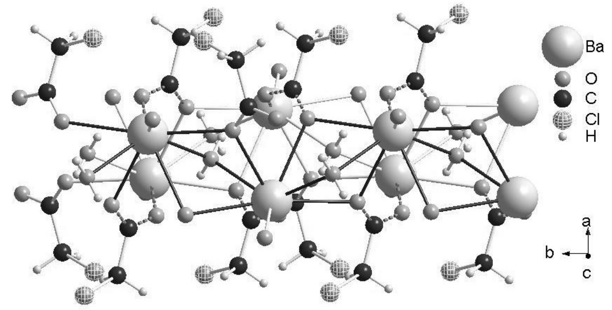

Fig. 1. Crystal structure of $Ba(ClCH_2COO)_2 \times H_2O$ ($1a_0 \times 1.75b_0 \times 1c_0$), intra chain connection of Ba-3O-Ba are drawn as black bonds, inter chain linking by carboxylic groups are drawn as doted bonds.

PS05-P27

Raman-spectroscopic and crystal structure investigation of solvo- and ionothermal prepared metal-aluminophosphate zeotypes

A. Bieniok[1], U. Brendel[2], P. Sereni[3], M. Musso[3]
[1]*Univerity of Salzburg, Geography & Geology, Salzburg, Austria*

[2]*University of Salzburg, Mol.Biology, Salzburg, Austria*
[3]*University of Salzburg, Mat. Research & Physics, Salzburg, Austria*

Aluminophosphate zeotypes are microporous solids with framework structures of strictly alternating phosphate and aluminate tetrahedra. We have prepared Fe- and Mn-bearing aluminophosphates zeotypes with the laumontite framework topology using two different synthesis procedures - solvothermal and ionothermal. Imidazole acts as structure directing agent (SDA) and as charge balancing cation. $(C_3N_2H_5)_{7.5}[Al_{16.5}Fe_{7.5}P_{24}O_{96}]$ was solvothermal synthesized with ethyleneglycol as solvent, for $(C_3N_2H_5)_{5.7}[Al_{18.3}Mn_{5.7}P_{24}O_{96}]$ an ionothermal synthesis procedure was performed with the ionic liquid 1-ethyl-3-methylimidazolium-tosylate, [emim][tos]. It comprises an imidazole-based cation similar to the SDA molecule. The ionothermal synthesis provided well-crystallized crystals with perfect {110} faces, 3 x larger than that of the solvothermal synthesis. Single-crystal diffraction measurements and structure analyses showed that both zeotypes crystallize in C2/c with the LAU framework structure. 31 % and 24 % of aluminium at the tetrahedral sites are replaced by iron and manganese, respectively. The imidazole-rings reside inside the narrowest part of the 1-D channels. Raman spectroscopy measurements of FeAPO- and MnAPO-LAU additionally confirm the presence of protonated imidazole inside the compounds. But the Raman spectra differ in 3 smaller bands at 2968, 1337 and 597 cm^{-1}, which are present in the Mn-bearing phase but are absent in the Fe-bearing zeotype. A comparison with the Raman spectrum of [emim] reveals that the 3 bands fit very well with the strongest bands of the ionic liquid. It appears that in the ionothermal synthesis of MnAPO-LAU not only protonated imidazole but also the charged cation of the solvent was incorporated into the pores of the laumontite framework structure. The amount seems to be very small and its distribution in the 1D-channel is totally disordered so that it is not possible to identify it in the crystal structure analysis. The different properties of both zeotype compounds show that the SDA and the choice of the solvent determine the rate of the transition metal substitution and the quality of the resulting crystals.

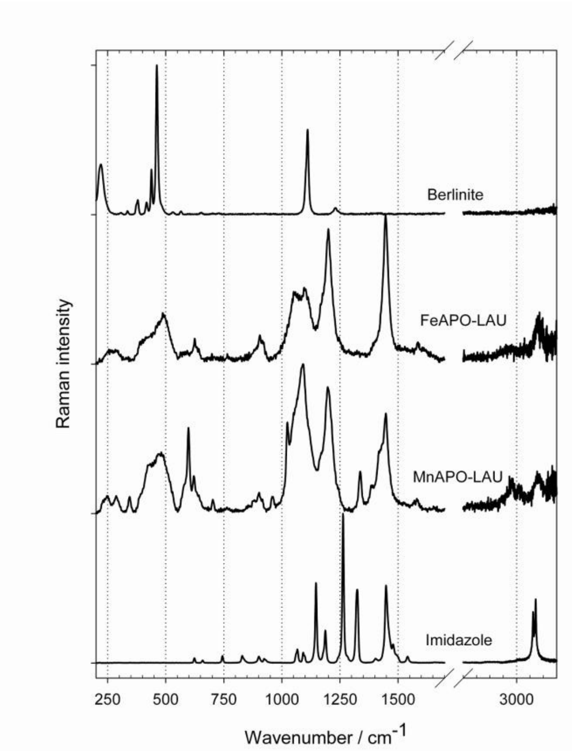

PS05-P28

$Na_2GeGa_2O_6$ - a new octahedra helix backbone structure

L. Robben[1], T. M. Gesing[1]
[1]*Uni Bremen, Chemische Kristallographie fester Stoffe, Bremen, Germany*

The novel gallogermanate $Na_2GeGa_2O_6$ was synthesized in a hydrothermal process at 363 K. 1 g $NaGaGeO_4$, 0.5 g $NaBH_4$ and 3 mL 2M NaOH solution were heated for 96 hours. After this period a mixture of berillionite-type $NaGaGeO_4$ [1] and $|Na_6(H_2O)_8|[GaGeO_4]_6$ sodalite [2] powder as well as single crystals with columnar habitus were found in the precipitate. The tetragonal crystals have differently shaped upper and lower crystal faces indicating a possible polar axis as realized in $I4_1/acd$. Energy dispersive X-ray spectra show an enrichment of Gallium with respect to the initial feed in the tetragonal crystals (Ga/Ge ratio ≈ 1.5 - 1.75). A crystal of 20 x 20 x 140 μm^3 was selected for X-ray data collection on a Stoe IPDS1 diffractometer using graphite monochromized $Mo_{K\alpha}$-radiation (λ=71.073 pm). $Na_2GeGa_2O_6$ crystallizes in space group $I4_1/acd$ with lattice parameters a = 1303.5(2) pm and c = 876.2(2) pm. Numerical absorption correction was applied (XShape, Stoe & Cie GmbH) for the 4249 collected reflections ($-15 < h < 15$; $-15 < k < 15$; $-10 < l < 10$). Structure solution and refinement were carried out with the SHELX-97 package [3]. After merging (R_{int} = 0.063) 360 unique reflections were available for the anisotropic refinement of all atoms using 22 variable parameters (R_1 = 0.031, wR_2 = 0.087).

The backbone of the crystal structure is formed of helix-like chains of edge-sharing NaO_6 octahedra (Na - O distances: 2x O1 240.7(3) pm, 2x O1 246.5(4) pm, 2x O2 254.7(4) pm). To these sodium-octahedra helixes four different one-dimensional chains are connected which consist of cation four ring units. Both gallium and germanium cations are coordinated by oxygen atoms building corner sharing tetrahedra. The alternating pairs of GeO_4 (Ge-O2 distance: 176.1(3) pm) and GaO_4 (Ga-O distances: 2x O1 184.7(3) pm, 2x O2 185.6(3)) tetrahedra are rotated by 90° to each other. First results of Raman spectroscopy are also presented.

[1] L. Robben, I. Poltz, J.-Ch. Buhl: Z. Kristallogr. NCS 255 (2010) 421. [2] T.M. Nenoff, W.T.A. Harrison e.a. Inorg. Chem. 33 (1994) 2472-2480 [3] G.M. Sheldrick: Acta Crystallogr. A64 (2008) 112.

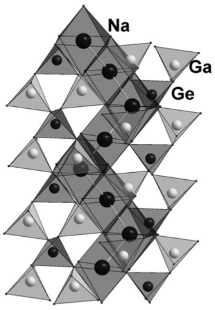

Figure 1: $Na_2GeGa_2O_6$ with helical chains of NaO_6 edge sharing octahedral (blue) which connect the chains of GaO_4 and GeO_4 four ring units.

PS05-P29

Synthesis and crystal structure of Ga-sillenite

M. Šehović[1], R. X. Fischer[1]
[1]*Universität Bremen, Fachbereich Geowissenschaften, Bremen, Germany*

Sillenite is the high-temperature modification of Bi_2O_3 usually designated as y-Bi_2O_3. The name is also used for the whole group of metal-doped phases ($Bi_{12}M_xO_{20}\pm\gamma$) being isostructural to y-Bi_2O_3. Due to the incorporation of cations (M^{n+}; II-VIII) the phase can be stabilized at ambient conditions. We synthesized sillenites with the initial molar composition of 92% Bi_2O_3 : 8% Ga_2O_3 by melting the educts in a platinum crucible at 900°C for 5 hours. Subsequently the melt was cooled down with 1°C/h from 835°C to 790°C to yield sillenite crystals large enough for single-crystal X-ray diffraction. The following cooling step was performed with 400°C/h down to 40°C to diminish the formation of a mullite-type phase.

In the literature two different structure models exist for Ga-sillenite, both derived in the same year. One is described in the cubic space group *I*23 with the chemical composition $Bi_{25}GaO_{39}$ (Radaev et al., 1989), whereas the other one was determined in the orthorhombic space group *I*222 with the chemical composition $Bi_{24}Ga_2O_{40}$ (Yudin et al., 1989). The main difference between these two models is the higher amount of Bi in the cubic compound where part of the Bi^{3+} with its lone electron pair statistically shares a position close to tetrahedrally coordinated gallium. The orthorhombic model can only be described properly in terms of charge balancing when the existence of two OH^- groups is considered.

Single-crystal X-ray diffraction data were collected on a Bruker diffractometer with an APEX II area detector and Mo-Kα radiation. Crystal-structure refinements were performed with the SHELXL-97 program (Sheldrick, 2008). It confirms the cubic space group *I*23 yielding residuals of R1=1.2% and wR2=2.9% with five Bi1-O distances between 2.068(5) Å and 2.628(6) Å, and Ga-O distances of 1.88(1) Å for the tetrahedrally coordinated gallium.

References

Radaev, S.F., Muradyan, L.A., Kargin, Yu.F., Sarin, V.A., Rider, E.E., Simonov, V.I. (1989): Atomic structure of bismuth gallium oxide ($Bi_{25}GaO_{39}$) and interpretation of the structure of sillenite-type crystals. Dokl. Akad. Nauk SSSR 306, 624-627.

Sheldrick, G.M. (2008): A short history of SHELX. Acta *Crystallogr.* A64, 112-122.

Yudin, A.N., Pobedimskaya, E.A., Terent'eva, I.E., Petrova, I.V., Kaplunnik, I.N., Malakhova, G.V. (1989): Crystal-chemical characteristics of gallium and vanadium sillenites. Izvestiya Akademii Nauk SSSR, Neoganicheskie Materialy 25, 1715-1718.

PS05-P30

The superstructure of $BaCaBO_3F$ grown by the Czochralski method

M. Teck[1], M. Burianek[2], M. Mühlberg[2], R. Fischer[1]
[1]*Universität Bremen, Fachbereich Geowissenschaften, Bremen, Germany*
[2]*Universität Köln, Institut für Kristallographie, Köln, Germany*

$BaCaBO_3F$ (BCBF) is a possible compound for nonlinear optical applications, such as converting infrared laser-light into the UV-Region (Xu et al., 2009). Especially Yb doped BCBF is known to have a high potential for self-frequency doubling (Schaffers et al., 1996). The crystal structure of BCBF was reported to crystallize in space group P-62m with Z=3 (Keszler et al., 1994) and recently determined and refined by Xu et al. (2009). A single crystal was grown by us by the Czochralski method. A small fraction of this crystal was cut off and used for the X-ray diffraction experiments. The analysis of this crystal by single-crystal X-Ray diffraction revealed weak superstructure reflections as shown in Fig. 1. Most of these reflections can be interpreted by a hexagonal superstructure in space group P-6m2 with a symmetry lowering of index 6. If all observed superstructure reflections are considered, the symmetry must be lowered from the original hexagonal space group to a monoclinic C-centered unit cell (most probably space group C2) with lattice parameters of *a*= 17.9024(8) Å, *b*= 9.0489(8) Å, *c*= 12.9771(4) Å, and γ= 118.89° also corresponding to a symmetry lowering of index 6. Here we are presenting the results of the crystal structure refinements comparing the average structure in P-62m with the possible superstructure models in space groups P-6m2 and C2.

Keszler, D.A., Akella, A., Schaffers, K.I., Alekel, T. (1994): New borate structures for NLO applications. Mat. Res. Soc. Symp. Proc. 329, 15-22.

Schaffers, K.I., DeLoach, L.D., Payne, S.A. (1996): Crystal growth, frequency doubling, and infrared laser performance of Yb^{3+} : $BaCaBO_3F$. IEEE J. Quantum Electronics 32, 741-748.

Xu, K., Loiseau, P., Aka, G.: BaCaBO$_3$F (2009): A nonlinear optical crystal investigated for UV light generation. J. Cryst. Growth 311, 2508-2512.

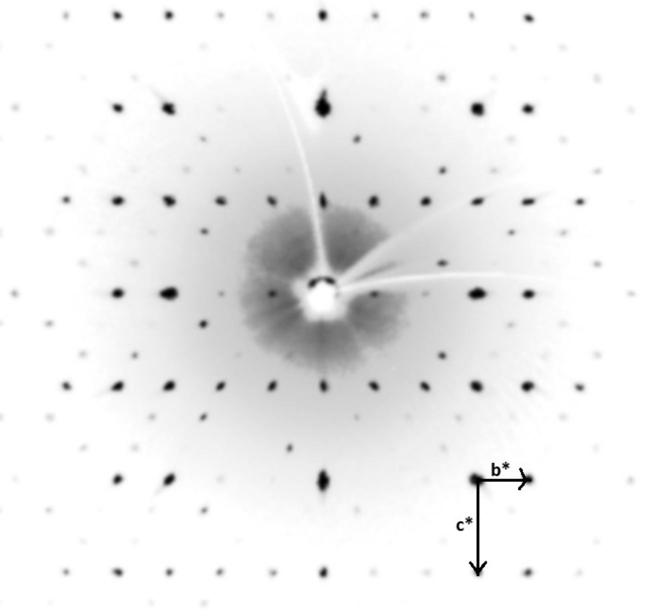

Fig. 1: BaCaBO$_3$F - 0kl-layer with b*and c* of the original hexagonal setting in P-62m with the superstructure reflections clearly indicating the symmetry lowering.

PS05-P31

New findings on *closo*-Hydroborates

K. Hofmann[1], E.- M. Felix[1], G. Bruhn[1], B. Albert[1]
[1]*Technische Universität Darmstadt, Eduard-Zintl-Institut für Anorganische und Physikalische Chemie, Darmstadt, Germany*

New methods to crystallize compounds with polyhedral hydroborate anions are highly desirable, due to the interesting structures and properties of these salts [1]. We synthesized different *closo*-hydoborates from liquid ammonia at low temperatures [2] and recently had success in growing single crystals in silica gels [3]. Earlier, we have shown for $[Li(NH_3)_4]_2B_6H_6 \cdot 2\ NH_3$ [4] and $N(C_4H_9)B_6H_7$ [5] that *closo*-hydroborates with the anion $B_nH_n^{2-}$ are very interesting for charge density analyses to gain more insight into the electronic situation of multi-center bonds as well as into the interaction between anions and cations and solvent molecules. Also, these investigations reveal weak attractive interactions like hydrogen and dihydrogen bonds. We now crystallized several new hydroborates like $[N(C_3H_7)_4]_2B_{10}H_{10} \cdot CH_3COOH$, $[PPh_4]_2B_{12}H_{12} \cdot C_3H_7OH$, or $[NH(C_3H_7)_3]_2B_{12}H_{12}$ and determined their structures. For $[NH(C_3H_7)_3]_2B_{12}H_{12}$ (Fig. 1), an experimental charge density analysis on basis of high-angle single crystal X-ray data was performed. It shows attractive (N)H$\cdots$B$_3$ interactions between the anion and the cation [6].

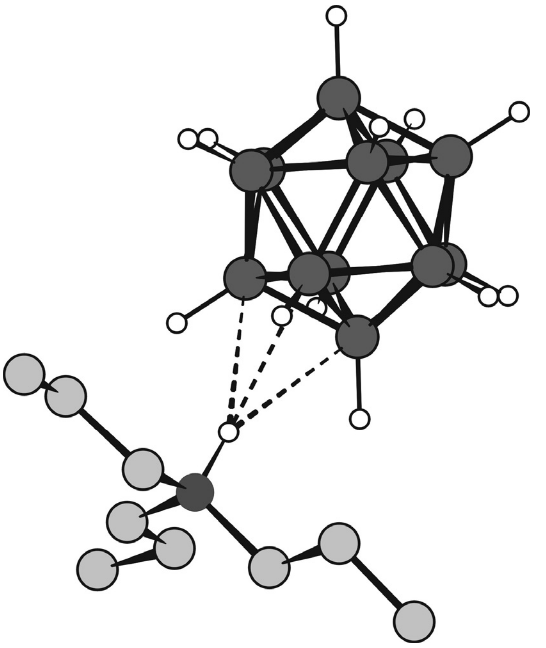

Fig. 1 $B_{12}H_{12}^{2-}$-anion and $NH(C_3H_7)_3^+$-cation in $[NH(C_3H_7)_3]_2B_{12}H_{12}$. The (C)H-atoms are omitted for clarity (blue: N, red: B, grey: C, white: H)

Our findings regarding our crystallization methods as well as the crystal structures and the bonding and electronic situation of different *closo*-hydroborates will be presented and discussed.

References
[1] K. Hofmann, B. Albert, *Z. Kristallogr.* 220 (2005) 142.
[2] F. Kraus, B. Albert, *Z. Anorg. Allg. Chem.*631 (2005) 152.
[3] E. Felix, M.Sc. Thesis, TU Darmstadt, 2012.
[4] M. Panda, K. Hofmann, M. H. Prosenc, B. Albert, *Dalton Trans*. (2008) 3956.
[5] K. Hofmann, M. H. Prosenc, B. Albert, *Chem. Commun*. (2007) 3097.
[6] G. Bruhn, B. Albert, unpublished results

PS05-P32

Crystal structure, polarised optical absorption spectra, and crystal field Superposition Model analysis of the new compound LiCo(SO$_4$)OH

M. Wildner[1], G. E. Büchel[2], L. Filak[2], C. Petautschnig[1], G. Giester[1]
[1]*Universität Wien, Institut für Mineralogie und Kristallographie, Wien, Austria*
[2]*Universität Wien, Institut für Anorganische Chemie, Wien, Austria*

Crystals of the new compound LiCo(SO$_4$)OH were synthesised at low-hydrothermal conditions, and the crystal structure was determined and refined from single crystal X-ray diffraction data. LiCo(SO$_4$)OH crystallises monoclinic, space group $P2_1/c$, $Z = 4$, $a = 9.586(2)$, $b = 5.425(1)$, $c = 7.317(1)$ Å, $\beta = 109.65(1)°$, $V = 358.3$ Å^3, wR2 = 0.0485 (2215 unique reflections, 78 variables). The only isotypic compound known so far is LiCd(MoO$_4$)OH (Kobtsev et al. 1968).

The crystal structure of LiCo(SO$_4$)OH is built from chains of edge-sharing, strongly distorted CoO$_3$(OH)$_3$ octahedra (<Co-O> = 2.126

Å), which are further linked by common corners and by properly shaped SO_4 tetrahedra (<S-O> = 1.476 Å) to sheets parallel (100). These sheets are finally connected to a three-dimensional structure by sharing corners with distorted LiO_4 polyhedra (<Li-O> = 1.956 Å). An oxygen atom which is only shared by one S and one Li atom acts as acceptor of the moderately strong hydrogen bond ($O\cdots O$ = 2.831 Å). The most remarkable feature of the structure is the strong bond length distortion of the CoO_6 polyhedron (point symmetry 1), with three short bonds to OH groups (Co-O = 2.045 - 2.097 Å) and three long bonds to oxygen atoms of SO_4 tetrahedra (Co-O = 2.166 - 2.216 Å). The two longest bonds are *trans*-located, thus forming a roughly pseudo-tetragonally elongated octahedron.

Polarised optical absorption spectra of $LiCo(SO_4)OH$ were measured on (100) plates parallel to the *b*- and *c*-directions (Fig. 1). According to the strong distortion of the CoO_6 polyhedron, the spin-allowed $^4T_1(P)$ band system of d^7-configurated Co^{2+} [cubic ground state $^4T_1(F)$] is strongly split up and covers a prominent part (~ 15500 - 24500 cm^{-1}) of the visible spectral range. In contrast, the weaker spin-allowed $^4T_2(F)$ band in the NIR region (centred around 7500 cm^{-1}) shows only weak splitting, and the spin-allowed but electronically forbidden $^4A_2(F)$ band (at ~14800 cm^{-1}) is non-degenerate and hence not split up. As a consequence of the strong splitting and broadening of the intense spin-allowed $^4T_1(P)$ state in $LiCo(SO_4)OH$, generally weak spin-forbidden levels are now located at the onset or within the $^4T_1(P)$ band system and can ‘steal’ significant intensity from the spin-allowed bands due to spin-orbit coupling [i.e. $^2T_{1,2}(G)$ at 16110 cm^{-1}, $^2T_1(P)$ at 19990 cm^{-1}, and $^2A_1(G)$ at 20540 cm^{-1}]. The detailed assignment of split levels and a numerical analysis of the crystal field effects in $LiCo(SO_4)OH$ in terms of semiempirical Superposition Model calculations are still in progress.

References: B.M. Kobtsev, Y.A. Kharitonov, E.A. Pobedimskaya, N.V. Belov (1968) Sov. Phys. Doklady, 13, 193-195.

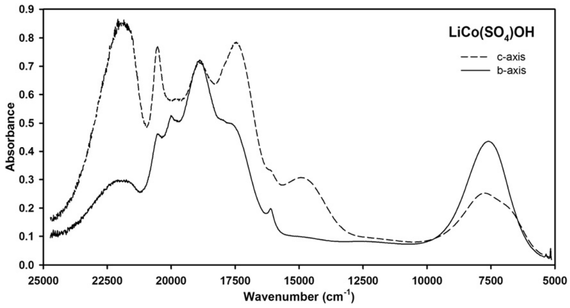

Fig. 1. Polarised optical absorption spectra of $LiCo(SO_4)OH$ measured on (100) plates.

PS05-P33

Formation and Characterisation of Lesukite

A. Neumann[1], H. Curtius[1], M. Klinkenberg[1], G. Kaiser[1], D. Bosbach[1]
[1]*Forschungszentrum Jülich GmbH, Institute of Energy and Climate Research, Jülich, Germany*

In corrosion experiments with non-irradiated fuel elements the formation of lesukite was observed. Fuel plates of UAlx-Al and U3Si2-Al were put into an autoclave which contains a standardized MgCl2 rich solution to account for conditions of a final repository in salt formations. The experiment was carried out under initial anoxic conditions and at a temperature of 90 °C. The corrosion process was monitored by the pressure which developed due to the formation of hydrogen. Within a time period of few months the reaction ceased and the secondary phases, which have been formed during the decomposition of the fuel plates, were obtained. Subsequently these solids were subjected to a grain size separation. We used therefore wet sieving and applied the Atterberg method to obtain the grain fraction of 63 µm, 2 - 63, < 2 µm. As major method to identify the corrosion products, i.e. the secondary phases we applied powder X-ray diffraction. The samples were prepared on a sample holder which was put into a climate chamber being mounted on the diffractometer. With this device the samples were investigated under non-ambient conditions because a constant flow of nitrogen was purged through the climate chamber. The qualitative analysis of the diffractograms showed that lesukite was mainly enriched in the fraction < 2 µm. This is valid for UAlx-Al and U3Si2-Al fuel samples. In the fractions > 2µm lesukite is also present yet the presence of other phases became also evident. We observed various layered double hydroxides like green rust, iron oxy hydroxides and chlorides, and even residues of non-corroded fuel compounds. For the quantification of the secondary phases we applied the Rietveld method. It was therefore necessary to derive a sound structural model for lesukite because the related structure is not known until present. By means of additional analysis, performed with HRTEM, EDX, and SEM, a model for the unit cell of lesukite was derived successfully. Considering the chemical composition, the lattice parameter, morphology, and the X-ray density the results we obtained were in very good agreement with the literature data [VER 97, WIT 97]: Lesukite is a cubic aluminium chloro hydrate which exhibits a specific weight of approx. 2 g/cm³ and a lattice parameter of approx. 19.8 Å.

References

[VER 97] L. P. Vergasova, E. L. Stepanova, E. K. Serafimova,S. K. Filatov (1997). Lesukite Al2(OH)5Cl•2H2O - a new mineral from volcanic exhalation. Zapiski Vserossiyskogo Mineralogicheskogo Obshchestva Proceedings of the Russian Mineralogical Society 126: 104-110.

[WIT 97] T. Witzke (1997). A new aluminium chloride mineral from Oelsnitz near Zwickau, Saxony, Germany. Neues Jahrbuch für Mineralogie - Monatshefte (7): 301-308.

PS05-P34

Tetrapropylammonium Tetrathiorhenate(VII) $(C_3H_7)_4N[ReS_4]$: A New *n*-Alkylammonium Thioperrhenate with an Ordered Crystal Structure

K. K. Wolff[1], I. Grau[1], T. Schleid[1]
[1]*University of Stuttgart, Institute for Inorganic Chemistry, Stuttgart, Germany*

The first attempts for the synthesis of tetrathioperrhenates from $[ReO_4]^-$ anions with hydrogen sulfide in aqueous solutions were undertaken by *Feit* [1]. By introduction of hydrogen sulfide in a very dilute solution of Re_2O_7 in aqueous ammonia *Müller et al.* [2, 3] was able to prove the existence of the intense violet $[ReS_4]^-$ tetrahedron. This anion could be isolated in salts with tetraphenylarsonium, tetraphenylphosphonium and tetramethylammonium as counter-cations [3]. The only two tetrathioperrhenates, which are so far characterized by single-crystal studies in some detail are the tetraethylammonium ($(C_2H_5)_4N[ReS_4]$ [4] with a lot of disorder) and the tetrabutylammonium salts ($(C_4H_9)_4N[ReS_4]$ [5], perfectly ordered).

Phase-pure, polycrystalline, deep purple tetrapropylammonium tetrathiorhenate(VII) was obtained by launching of a strong hydrogen sulfide stream in a hot solution of potassium perrhenate ($K[ReO_4]$) in aqueous ammonia. The mixture turned slowly from yellow via orange and red to violet with a simultaneous deposition of a black precipitate. After boiling for 10 min and adding potassium hydroxide (KOH) the new precipitation was filtered off and a solution of tetrapropylammonium bromide was added dropwise under argon. Recrystallization from ethanol yielded deeply violet crystals, which were suitable for single crystal X-ray measurement. The product is covering itself with a brown lining after several weeks in consequence of decomposition.

Tetrapropylammonium tetrathioperrhenate ($(C_3H_7)_4N[ReS_4]$) crystallizes in the monoclinic space group $P2_1/c$ with eight formula units per unit cell and the lattice constants a = 1306.74(9) pm, b = 1788.91(12) pm, c = 1622.68(11) pm and β = 91.449(3)° at 100 K. There are two crystallographically different nitrogen as well as rhenium atoms, each, which are tetrahedrally surrounded either by C_3H_7 chain fragments or S^{2-} anions, respectively (Figure 1). The Re-S distances range from 212 to 214 pm, while the N-C bond lengths cover the interval from 149 to 154 pm. The $[ReS_4]^-$ tetrahedra are arranged as zigzag chains along the a axis (Figure 2), without being linked to each other and the crystallographically identical tetrahedra align almost linearly along [100]. The $[ReS_4]^-$ anions exhibit just a slightly distorted tetrahedral geometry with angles in a range from 108.6 to 110.3°. Through solid-state Raman spectroscopy the existence of isolated $[ReS_4]^-$ tetrahedra could be clearly proven for this compound additionally.

[1] W. Feit, *Z. Anorg. Allg. Chem*. **1931**, *199*, 262; *Z. Angew. Chem.* **1931**, *44*, 65.
[2] A. Müller, B. Krebs, E. Diemann, *Z. Anorg. Allg. Chem*. **1967**, *353*, 259.
[3] A. Müller, E. Diemann, V. V. Krishna Rao, *Chem. Ber.* **1970**, *103*, 2961.
[4] A. Müller, E. Krickemeyer, H. Bögge, *Z. Anorg. Allg. Chem.* **1987**, *554*, 61.
[5] Y. Do, E. D. Simhon, R. H. Holm, *Inorg. Chem.* **1985**, *24*, 4635.

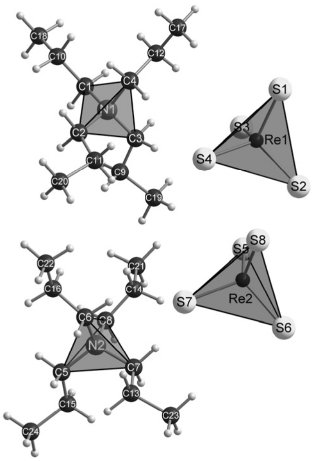

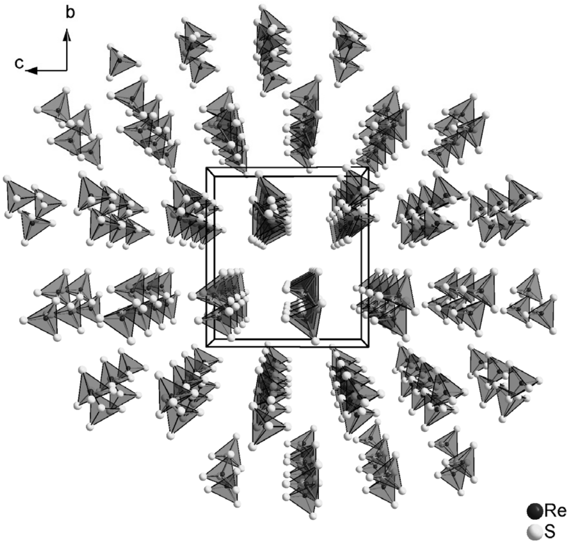

PS05-P35
The $[Pt(S_2O_7)_3]^{2-}$-anion

J. Bruns[1], H. Bülter[1], M. Wickleder[1]
[1]C.v.Ossietzky University, IRAC, Oldenburg, Germany

Recently we presented several examples of new, partly unprecedented polysulfates. e.g. the *bis*-(disulfato)-aurate $[Au(S_2O_7)_2]^{2-}$, the *tris*- and *tetrakis*-(disulfato)-silicates $[Si(S_2O_7)_3]^{2-}$ and $[Si(S_2O_7)_4]^{4-}$ bearing octahedral silicon coordination[1,2]. Furthermore we presented the unique disulfate $Pd(S_2O_7)$ with octahedral Pd^{2+} coordination and ferromagnetic ordering below 11.7 K.[3] Our attempts to prepare also polysulfates of the heavier palladium congener platinum have now afforded the ternary platinum disulfates $A_2[Pt(S_2O_7)_3]$ (A = K, NH_4, NO) via the reaction of the respective alkaline or ammonium tetrachloroplatinates or, for the NO compound, of the Pt(III) complex $(NO)_4[Pt_2(SO_4)_5]$ (P-1, Z=4, a = 978.2(2) pm, b = 1319.0(3) pm, c = 1511.1(3) pm, α = 105.14(3)°, β = 95.10(3)°, γ = 102.27(3)°), with SO_3 at higher temperature in torch sealed glass ampoules. In the isotypic triclinic compounds (e.g. $K_2[Pt(S_2O_7)_3]$: P-1, Z=2, a = 900.72(4) pm, b = 1076.74(4) pm, c = 1093.23(4) pm, α = 62.721(3)°, β = 69.721(3)°, γ = 69.054(6)°) the central Pt atoms are coordinated by three crystallographically independent disulfate anions. Each anion coordinates in a bidentate chelating mode via terminal oxygen atoms. The charge compensation is achieved by two potassium, ammonium or nitrosylium cations. Switching to oleum (65% SO_3) and using the large bivalent counter cation Ba^{2+}, we were able to isolate a slight amount of yellow block-shaped single crystals of $Ba[Pt(S_2O_7)_3]\cdot(H_2SO_4)(H_2S_2O_7)$. As well as found for the potassium and ammonium species, in the barium compound the central Pt(IV) is coordinated octahedrally by six oxygen atoms belonging to three crystallographically independent bidentate chelating disulfate anions. Furthermore, in the triclinic compound (P-1, Z=2, a = 992.05(2) pm, b = 1069.07(3) pm, c = 1114.22(3) pm, α = 69.497(1)°, β = 72.962(1)°, γ = 72.930(1)°) the barium cations are interconnected by molecules of H_2SO_4 and $H_2S_2O_7$.

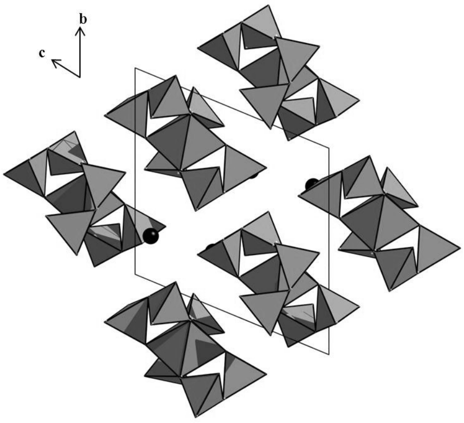

Figure 1. Structure of $K_2[Pt(S_2O_7)_3]$ along [100].

[1] C. Logemann, M. S. Wickleder, *Inorg. Chem.* **2011**, 50, 11111-11116.
[2] C. Logemann, K. Rieß, M. S. Wickleder, *Chem. Asian J.* **2012**, DOI: 10.1002/asia.201200661.
[3] J. Bruns, M. Eul, R. Pöttgen, M. S. Wickleder, *Angew. Chem.* **2012**, *124,* 2247-2250; *Angew. Chem. Int. Ed.*, **2012**, *51,* 2204-2207.

PS05-P37

Monoclinic CuLa₃OS₄: An Ordered Variation of this Copper(I) Lanthanum(III) Oxide Sulfide

M. Eberle[1], T. Schleid[1]
[1]*University of Stuttgart, Institute for Inorganic Chemistry, Stuttgart, Germany*

$CuLa_3OS_4$ was first presented in the orthorhombic space group $Pnma$ (a = 1187.76(9), b = 408.61(3), c = 4684.6(3) pm, Z = 12) crystallizing as dark grey needles [1]. The crystal structure consists of O^{2-} anions centering tetrahedra formed by La^{3+} cations with bond lengths of 233 - 280 pm. These highly distorted $[OLa_4]^{10+}$ units are first connected via common vertices, forming straight chains $[OLa_3]^{7+}$ along the b axis. Three of those chains become further fused again via common vertices, resulting in a band of the composition $[O_3La_7]^{15+}$. All Cu^+ cations are also fourfold coordinated in the shape of tetrahedra, now erected by S^{2-} anions (d = 228 - 251 pm). Again, these tetrahedra are connected by shared corners to form strings along [010]. Additionally to single chains, strands of tetrahedra fused by common vertices and faces occur as well. Considering the face-connected tetrahedra, only half of them can be occupied with Cu^+ cations in a disordered way.

During attempts to synthesize $TlCuLa_2S_4$ by mixing the elements (Tl, Cu, La, and S) along with NaCl as fluxing agent, single crystals of the known compound $CuLa_3OS_4$ emerged again, but now with different colour (dark red) and structure. The reaction took place in evacuated silica ampoules, which were heated up to 850 °C for eight days. It turned out, that the lanthanum metal was partly oxidized on its surface, which provided enough oxygen to yield this oxide sulfide, crystallizing in the monoclinic space group $C2/m$ with the lattice constants a = 3034.26(22), b = 403.98(3), c = 1231.29(9) pm and Z = 8. Here, the O^{2-} anions again reside in the centers of tetrahedra formed by La^{3+} cations (d = 235 - 264 pm). Yet, these units are connected to each other by sharing only two common vertices, building straight single chains along [010] (Figure 1). The surrounding of the Cu^+ cations is similar as well. While $[(Cu1)S_4]^{7-}$ units share corners and so build single chains along the b axis (Figure 2, *bottom*), chains consisting of $[(Cu2)S_4]^{7-}$ tetrahedra are further vertex-connected to form double strands (Figure 2, *top*) along the same direction. The bond lengths within $[(Cu1)S_4]^{7-}$ tetrahedra are longer than in $[(Cu2)S_4]^{7-}$ units, which share an additional common vertex (d = 235 - 237 pm versus d = 230 - 233 pm).

[1] P. Lauxmann, Th. Schleid, *Z. Kristallogr.* **2001**, *Suppl. 18*, 113.

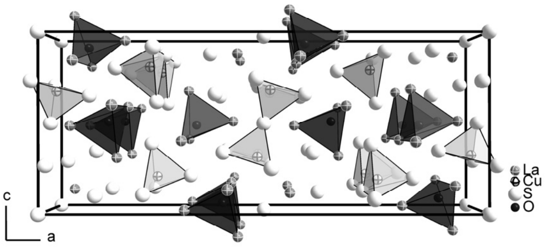

Figure 1: Unit cell of monoclinic $CuLa_3OS_4$ with vertex-shared $[OLa_4]^{10+}$ and $[CuS_4]^{7-}$tetrahedra.

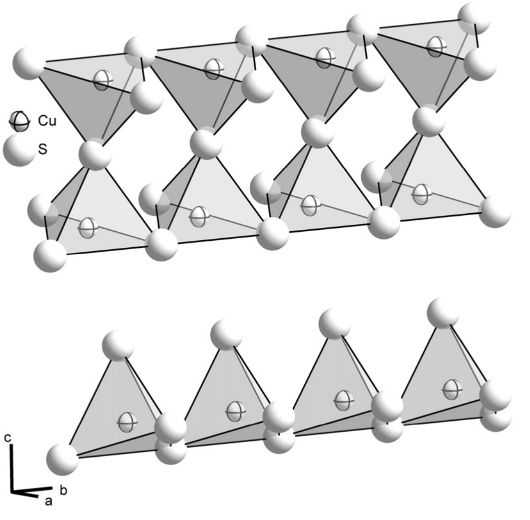

Figure 2: Interconnection of $[(Cu2)S_4]^{7-}$ tetrahedra via vertices in the crystal structure of monoclinic $CuLa_3OS_4$.

PS05-P39

$NaLa_6O_3F_9S_2$: A Chemical Extension of the Formula Type M_3OF_5S (M = Nd, Sm, Gd - Ho)

D. D. Zimmermann[1], T. Schleid[1]
[1]*University of Stuttgart, Institute for Inorganic Chemistry, Stuttgart, Germany*

Syntheses with sulfur, the lanthanoid metals, their sesquioxides and trifluorides of the light representatives usually result in the formation of compounds with the formula type $M_6O_2F_8S_3$ (M = La - Nd, Sm and Gd) [1]. Recently it was possible to synthesize crystals of the putative compound "La_3OF_5S", but so far the series of lanthanoid(III) oxide fluoride sulfide with the composition M_3OF_5S started normally with the element neodymium [2]. Treated isotypically at first glance it crystallizes hexagonally with the space group $P6_3/m$ (no. 176) and the lattice parameters a = 986.25(9) pm, c = 393.16(3) pm (c/a = 0.3986) with Z = 2 as rod-shaped specimens (Figure 1). The La^{3+} position is coordinated as tricapped trigonal prism with nine anions. The basis and the top are each formed by one F1, F2/O and S atoms, the threefold capping motif is built up by one F1 and two F2/O atoms. The light-anion positions are coordinated as triangular non-planar $(F1)^-$ and as tetrahedral arrangement of La^{3+} cations $(F2/O)^{n-}$, the allocation of oxygen only to the F2/O (ratio F:O = 2:1) position is already approved by the calculation of the Madelung Part of the Lattice Energy based on the prototypic compound Dy_3OF_5S [3]. The tetrahedra $[(F2/O)La_4]^{m+}$ are creating one-dimensional chains by *cis*-edge sharing along the c axis. Sulfur is coordinated by six La^{3+} cations as trigonal prism $[SLa_6]^{16+}$ and those get associated by *trans*-faces showing chains along the c axis as well. Remarkable for this lanthanum compound is the unusual size of the lattice parameters, however by extrapolating a linear trend of the lattice constants for the other members of the M_3OF_5S series, La_3OF_5S should have only about 975 pm for the a axis and 387 pm for the c axis. This expansion of the lattice parameters indicates the presence of a light cation in the channel sub-structure formed by the $(F1)^-$ anions. Using NaCl as flux material it is supported and highly probable that sodium takes room in the structure and gets coordinated octahedrally by six $(F1)^-$ anions about 243 pm apart. First electron-beam microprobe measurements are supporting the presence of sodium in this lanthanum compound, which thus should be re-addressed as $NaLa_6O_3F_9S_2$ with Z = 1 and a F2:O-ratio of 1:1. Furthermore with the existence of the lanthanum compound it should be possible to synthesize the analogous compounds with cerium and praseodymium.

[1] H. Grossholz, *Dissertation,* Universität Stuttgart **2003**.

[2] H. Grossholz, O. Janka, Th. Schleid, *Z. Naturforsch.* **2011**, *66 b*, 213.

[3] H. Grossholz, Th. Schleid, *Z. Anorg. Allg. Chem.* **2002**, *628,* 1012.

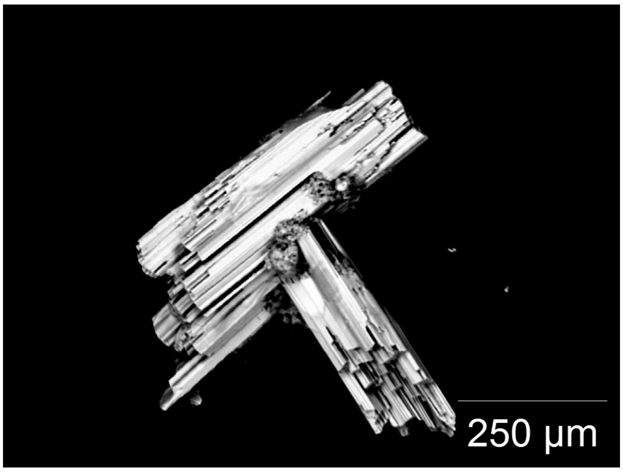

PS05-P40

Synthesis and characterization of mullite-type $(Al_{1-x}Ga_x)_4B_2O_9$.

K. Hoffmann[1,2], M. M. Murshed[2], R. X. Fischer[1], H. Schneider[3], T. M. Gesing [2]
[1]*Universität Bremen, Fachbereich Geowissenschaften, Bremen, Germany*
[2]*Universität Bremen, Chemische Kristallographie fester Stoffe, Institut für anorganische Chemie, Bremen, Germany*
[3]*Universität Köln, Institut für Kristallographie, Köln, Germany*

Aluminum borates represent an important class of materials. Their chemical properties are of considerable research interest because of a high tensile strength, relatively high elastic moduli and a low thermal expansion [1, and references therein]. Aluminum borate $Al_4B_2O_9$ (A_2B) and gallium borate $Ga_4B_2O_9$ (G_2B) belong to the family of mullite-type materials. We found A_2B well crystallized as the monoclinic $C2/m$ polymorph [2]. The corresponding gallium containing mullite-type compound G_2B is described in the monoclinic symmetry $C2/m$ as well [3], but its structure differs significantly from that of A_2B. G_2B was transformed here into space group $I112/m$ and A_2B was transformed into space group $B112/m$ to conform to the mullite-type setting. The Ga-doped A_2B structures were synthesized following the glycerine method [4], showing an incorporation limit of $x \approx 0.7$, using a final heating temperature of 1223K. With synthesis modified in temperature and time, slightly higher x-values could be reached. The synthesis of the Al-doped G_2B structures was performed according to Cong et. al. [3]. The incorporation limit of aluminum at 923K is again approximately $x \approx 0.7$. The crystalline powder samples were studied by means of X-ray diffraction data refinements using the Rietveld method. For the Ga-doped A_2B structures, the boron positions were determined by DLS calculations, the most probably coordination of the metal atoms was calculated with respect to their bond valence sum (BVS). With an increase of the initial amount of gallium, the metal-oxygen distances in the A_2B structures show a tendency towards longer distances as expected for an incorporation of the bigger gallium atoms. For the Al-doped G_2B structures, a poor crystallinity aggravates a successful structure refinement.

Successfully synthesized $(Al_{1-x}Ga_x)_4B_2O_9$ samples were characterized between 298 K and 1423 K by means of temperature-dependent X-ray powder diffraction Rietveld refinements as well. Pure A_2B decomposes to $Al_{18}B_4O_{33}$ (A_9B_2) + B_2O_3 above 1323 K, while Ga-doping in the A_2B structure leads to decreasing decomposition temperatures. Pure G_2B is reported to be stable up to 923 K [3] before decomposing to the binary oxides. Opposite to the findings in Ga-doped A_2B, Al-doping of the G_2B structures leads to an increase of the decomposition temperature.

[1] Zhang, J., Lin, J., Song, H.S., Elssfah, E.M., Liu, S.J., Luo, J.J., Ding, X.X., Tang, C., Qi, S.R. (2006): *Mater. Lett.*, **60**, 3292-3295. [2] Fischer, R. X., Kahlenberg, V., Voll, D., MacKenzie, K. J. D., Smith, M. E., Schnetger, B., Brumsack, H. J., Schneider, H. (2008): Am. Mineral. 93, 118. [3] R. Cong, T. Yang, K. Li, H. Li, L. You, F. Liao, Y. Wang, J. Lin (2010): Acta Crystallogr., B66, 141-150. [4] Th. M. Gesing, R. X. Fischer, M. Burianek, M. Mühlberg, T. Debnath, C. H. Rüscher, J. Ottinger, J.-Ch. Buhl, H. Schneider J. Eur. Ceram. Soc. 31 (2011) 3055-3062.

PS05-P41

Synthesis and crystal structure of body-centered gallogermanate chloride/hydrate sodalite

I. Poltz[1,2], L. Robben[2], J.- C. Buhl[1], T. M. Gesing[2]
[1]*Leibniz Universität Hannover, Institut für Mineralogie, Hannover, Germany*
[2]*Universität Bremen, Chemische Kristallographie fester Stoffe, Institut für Anorganische Chemie, Bremen, Germany*

Reports on body-centered sodium containing sodalites with two types of framework forming cations are rare [1]. The sodium chloride and water enclathrated gallogermanate sodalite described here was synthesized under mild hydrothermal conditions in Teflon coated steel autoclaves in two steps. First, 1.39 g $NaGaO_2$, 1.85 g Na_2GeO_3 and 15 g NaCl were mixed. After the addition of 5 mL deionized H_2O, the resulting gel was heated at 453 K for 48 h. The solid precipitate was washed, dried and again mixed with 6 g NaCl and 2 mL H_2O for further heating at 453 K for 48 h. The final product was washed with deionized water and dried at 353 K. While investigating the sample in a scanning electron microscope cubo-octahedral shaped single crystals with a size between 10 and 50 µm were observed. From X-ray powder data analysis more than one sodalite phase could be deduced. A big crystal was selected for a single-crystal structure analysis finally showing the body-centered symmetry. X-ray data were collected on a Stoe IPDS1 diffractometer using MoK_α radiation. 5038 reflections in the range up to 51.75° 2 Theta (-11 < h < 11, -11 < k < 11, -11 < l < 11) were integrated resulting in 164 unique reflections after merging (R_{int} = 0.062). The crystal structure was solved and refined in the space group I-43m (a= 914.00(11) pm) using SHELX-97 [2]. Beside the positional parameters, anisotropic displacement ellipsoids were refined for all atoms, except the water molecule oxygen, resulting in residuals of R_1 = 0.028 and wR_2 = 0.077. Usually, the T-atom ratio in sodalites containing two different framework cations is equal to 1, leading to an alternating occupancy of the T-atom sites and primitive space group symmetry. Here, a body centered symmetry was found as a result of the Ga : Ge ratio > 1, due to the Ga enrichment relative to Ge during the two step synthesis. Therefore, Ga and Ge share the I-43m 12d position. The final Ga : Ge ratio was calculated from the average T-O distance observed during the structure refinement with respect to Ga-O and Ge-O distances known from gallogermanate hydro sodalites [3]. The higher Ga amount leads to a more negative framework charge (-6.32 v.u.), which is compensated by 6.32 Na^+. With a maximum of eight sodium cations per unit cell, the remaining one cannot serve for the charge compensation of sodalite cages fully occupied with chloride anions. The anion free cages are then occupied by four water molecules, which are provided by the hydrothermal solution during the synthesis, resulting in a composition of $|Na_{7.98(7)}Cl_{1.66(7)}(H_2O)_{1.3(3)}|[Ga_{6.32(5)}Ge_{5.68(5)}O_{24}]$. The water content was confirmed by the presence of H_2O bending modes observed in Raman spectra measured on the same crystal as the X-ray data collection was carried out.

[1] Th. M. Gesing, Z. Kristallogr. 215 (2000) 510-517. [2] G.M. Sheldrick: Acta Crystallogr. A64 (2008) 112. [3] T.M. Nenoff, W.T.A. Harrison, T.E. Gier, N.L. Keder, C.M. Zaremba, V. I. Srdanov, J.M. Nicol, G.D. Stucky, Inorg. Chem. 33 (1994) 2472-2480.

PS05-P42

New coordination polymers with aniline-2,5-disulfonic acid and 2,3,5,6-tetrachloro-1,4-benzenedisulfonic acid

M. Gudenschwager[1], M. S. Wickleder[1], J. Christoffers[1], T. W. T. Muesmann[1]
[1]*University of Oldenburg, Institute of pure and applied chemistry, Oldenburg, Germany*

Since a couple of years our group is studying the syntheses of metal-organic frameworks (MOFs) and coordination polymers based on new polysulfonate linkers. These are intended to replace the well-known carboxylate linkers in order to increase the thermal stability of the compounds.[1,2] Some results using aniline-2,5-disulfonic acid (H_2BDSNH_2) and 2,3,5,6-tetrachloro-1,4-benzenedisulfonic acid (p-H_2BDSCl_4), will be shown here. The solvothermal reaction of $Ni(OH)_2$, with H_2BDSCl_4 or *p*-H_2BDSNH_2 and DMA yielded single crystals of $Ni(BDSCl_4)(DMA)$ (triclinic, P-1, Z = 1, a = 918.74(6), b = 974.53(6), c = 990.79(6) pm, α = 88.637(3)°, β = 85,842(3)°, γ = 86,295(2)°, V = 796,33(9)$Å^3$) and $Ni(BDSNH_2)(DMA)_2(H_2O)\cdot 2DMA$ (triclinic, P-1, Z = 4, a = 932.04(6), b = 978.29(7), c = 1763.5(1) pm, α = 88.069(4)°, β = 75.146(4)°, γ = 80.419(4)°, V = 1532.4(2)$Å^3$). Single crystals of $Cu(BDSNH_2)(NMP)_2(H_2O)$ are obtained via the reaction of $CuCO_3$, H_2BDSNH_2, and NMP (triclinic, P-1, Z = 2, a = 1032.08(2), b = 1039.95(2), c = 1160.37(2) pm, α = 63.755(1)°, β = 73,537(1)°, γ = 85,468(1)°, V = 1069,70(3)$Å^3$). Its structure is similar to the one of $Ni(BDSNH_2)(DMA)_2(H_2O)\cdot 2DMA$. All of the three compounds exhibit chains in which the Ni^{2+} and Cu^{2+} ions are linked by the respective disulfonate anions. In $Cu(BDSNH_2)(NMP)_2(H_2O)$ the central atoms are connected by one sulfonate ligand. Then non-coordinating $[SO_3]$ moiety forms hydrogen bonds to the solvent molecules of the adjacent chain, which contributes to the stabilization of the structure. Hydrogen bonds between the individual chains play also a crucial role in the structures of $Ni(BDSNH_2)(DMA)_2(H_2O)\cdot 2DMA$ and $Ni(BDSCl_4)(DMA)_4$. The compounds were further characterized by DSC/TG measurements and X-ray powder diffraction.

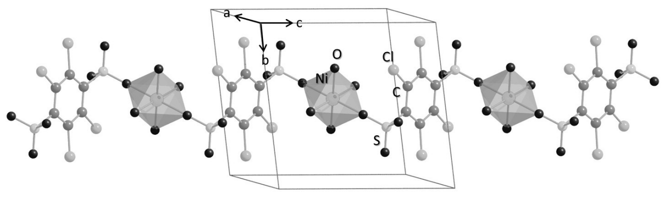

Figure 1: 1D-structure of Ni(BDSCl$_4$)(DMA)$_4$ (DMA molecules omitted for clarity)

References:

[1] A. Mietrach, T. W.T. Muesmann, J. Christoffers, M. S. Wickleder, *Eur. J. Inorg. Chem.,***2009**, *35*, 5328.

[2] T.W.T. Muesmann, C. Zitzer, A. Mietrach, T. Klüner, J. Christoffers, M. S. Wickleder, *Dalton Trans.,* **2011**, *40*, 3128.

PS05-P43

Applying a Novel Ligand Class: Synthesis and Structures of Metal Complexes with 'Normal' 1,2,3-Triazolylidene Ligands

A. Pöthig[1], L.- A. Schaper[1], X. Wei[1], F. E. Kühn[1], W. A. Herrmann[1]
[1]*TU München, Catalysis Research Center, Garching b. München, Germany*

A new NHC ligand and its complexes are presented, representing the first example of a 1,2,3-triazolylidene with a 1,2,4-substitution pattern, thus opening a new subclass of sterically and electronically tunable N-heterocyclic carbenes to serve as ligands in the growing new class of homogenous catalysts.

PS05-P44

U_2PTe_2O - Ein neues Pniktidchalkogenid des Urans mit P_2^{4-}-Einheiten

K. Stolze[1], U. Schwarz[2], T. Doert[1]
[1]*TU Dresden, Chemistry and Food Chemistry, Dresden, Germany*
[2]*Max Planck Institute for Chemical Physiscs of Solids, Dresden, Germany*

Die Kristallstruktur von U_2PTe_2O wurde durch Röntgenbeugung am Einkristall aufgeklärt. U_2PTe_2O kristallisiert tetragonal in der Raumgruppe *I*4/*mmm* (Nr. 139) mit Gitterparametern von a = 4.037(1) Å und c = 32.069(3) Å. Die Struktur von U_2PTe_2O besteht aus einer Stapelfolge von [U_2P_2]-, [U_2O_2]- und [Te_2]-Schichtpaketen (s. Abbildung) und kann als eine partiell oxidierte Stapelvariante des Uranphosphidtellurids UPTe beschrieben werden, bei der die Strukturmotive des UPTe mit PbO-analogen Motiven aus Uran- und Sauerstoffatomen abwechseln. Die Uranatome sind dabei entweder von jeweils vier P- und Te-Atomen oder von jeweils vier O- und Te-Atomen in Form eines verzerrten quadratischen Antiprismas umgeben, wobei die Te-Grundfläche jeweils von einem weiteren Te-Atom überkappt wird.

Das Phosphoratom befindet sich auf 0.079, ½, 0 (Wyckoff-Lage 8*j*, Lagesymmetrie *m*2*m*) und ist damit etwa 0.35 Å vom Inversionszentrum in 0, ½, 0 (Lage 4*c*) entfernt. Der geringe Abstand zwischen den Phosphor-Positionen *x*, ½ , 0 und -*x*, ½ 0 sowie die gefundene Elektronendichtemaxima sind lediglich mit einer Halbbesetzung verträglich. Die kürzesten P-P-Abstände von 2.40 Å sind vergleichbar mit denen der Diphosphideinheiten in $BaPd_2P_2$ (2.40 Å, [1]) und weisen auf (fehlgeordnete) P_4^{2-}-Anionen hin.

Nach kürzlich durchgeführten Untersuchungen zeigt U_2PTe_2O somit die gleiche Phosphor-Lagefehlordnung wie das ternäre UPTe; hier konnte die Existenz der fehlgeordneten P_4^{2-}-Anionen bereits durch ihr charakteristisches Raman-Signal bei etwa 450 cm^{-1} nachgewiesen werden [2].

Der kristallchemische Befund steht im Einklang mit dem Valenzzustand U(IV) für das Actinoidmetall, welcher am ehesten kompatibel mit den magnetischen Daten der Pniktid-Chalkogenide U*XY* ist [3]. U_2PTe_2O kann daher als normale Valenzverbindung gemäß *Zintl-Klemm*-Konzept formuliert werden: $(U^{4+})_4(P_2^{4-})(Te^{2-})_4(O^{2-})_2$.

[1] A. Mewis, Z. Naturforsch. b **1984**, 39, 713-720.
[2] K. Stolze, U. Schwarz, Th. Doert, unveröffentlichte Ergebnisse.
[3] A. Zygmunt, A. Czopnik, Phys. Status Solidi A **1973**, 18, 731-734.

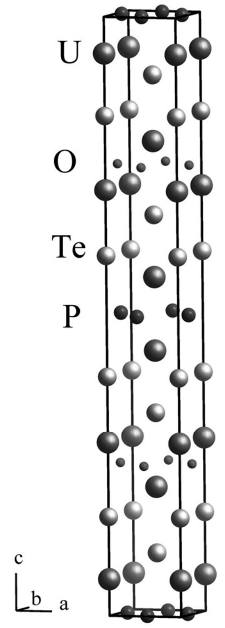

PS05-P45

Anisotropy study of the magnetoelectric properties of $LiFeSi_2O_6$

M. Ackermann[1], T. Lorenz[2], P. Becker[1], L. Bohatý[1]
[1]*Institut für Kristallographie, Köln, Germany*
[2]*II. Physikalisches Institut, Köln, Germany*

$LiFeSi_2O_6$ belongs to the class of pyroxenes with the general composition AMT_2O_6 (A = mono- or divalent metal, M = di- or trivalent metal, T = Si, Ge). The crystal structure of pyroxenes with either orthorhombic or monoclinic symmetry consists of zig-zag chains of edge-sharing [MO_6] octahedra running along the crystallographic *c*-axis. Within the planes (110) and the octahedra chains are connected by chains of [TO_4] tetrahedra. In case of an occupation of the *M*-sites by ions with magnetic moment the mutual arrangement of the octahedra chains can result in frustration of magnetic interactions that can lead to unusual spin arrangements. In the case of the pyroxene compounds $NaFeSi_2O_6$ and $NaFeGe_2O_6$ this is the source of multiferroicity [1, 2]. The title crystal $LiFeSi_2O_6$ shows the linear magnetoelectric effect a_{ij} (with $P_i = a_{ij} H_j$; P_i = electric polarization, H_j = applied magnetic field). At room temperature $LiFeSi_2O_6$ possesses space group symmetry $C2/c$, it undergoes a structural phase transition at 230 K with a symmetry change to $P2_1/c$ [3, 4]. Below the magnetic ordering temperature T_N » 18 K the magnetic structure of $LiFeSi_2O_6$ can be described by the Shubnikov group $P2_1/c'$, this symmetry allows the components of the magnetoelectric tensor a_{11}, a_{22}, a_{33}, a_{13} and a_{31}. In this contribution we present a detailed investigation of the linear magnetoelectric properties of $LiFeSi_2O_6$ and their anisotropy.

This work was supported by the DFG though SFB 608.

[1] S. Jodlauk, P. Becker, J. A. Mydosh, D. I. Khomskii, T. Lorenz, S. V. Streltsov, D. C. Hezel, L. Bohatý, *J. Phys.: Condens. Matter* **19** (2007) 432201.

[2] I. Kim, B.-G. Jeon, D. Patil, S. Patil, G. Nénert, K.H. Kim, *J. Phys.: Condens. Matter* **24** (2012) 306001.

[3] M. Behruzi, Th. Hahn, C.T. Prewitt, K. Baldwin, *Acta Cryst. A* **40** (1984) Suppl. C-247.

[4] G.J. Redhammer, G. Roth, W. Treutmann, M. Hoelzel, W. Paulus, G. André, C. Pietzonka, G. Amthauer, *J. Solid State Chem.* **182** (2009) 2374-2384.

PS05-P46

Temperaturabhängige Kristallstrukturuntersuchung an $TlFe_{2-x}Se_2$ ($x \approx 0{,}4$)

E. Ahrens[1], T. Doert[1], M. Ruck[1]
[1]*TU Dresden, Chemistry and Food Chemistry, Dresden, Germany*

Bei den derzeit stark untersuchten eisenhaltigen Supraleitern wird u. a. eine Reihe von Verbindungen $A_{1-x}Fe_{2-y}Se_2$ (A = K, Rb, Cs; $x \leq 0.2$; $y \leq 0.4$) mit $ThCr_2Si_2$-Typ Strukturen bearbeitet. Die Sprungtemperaturen entsprechender Proben hängen stark von der chemischen Zusammensetzung, der Kristallstruktur und der Herstellung ab. Wir haben in diesem Zusammenhang die Kristallstruktur der isostrukturellen Verbindung $TlFe_{2-x}Se_2$ bei verschiedenen Temperaturen und Probenvorbehandlungen untersucht.

Die Grundstruktur von $TlFe_2Se_2$ wurde von *Klepp* und *Boller* in der Raumgruppe $I4/mmm$ mit Zellparametern von a = 3.9(1) Å und c = 14.0(1) Å beschrieben [1]. Wie nachfolgende Untersuchungen ergaben, fällt das Thalliumeisenselenid jedoch stets eisendefizitär an [2, 3]. Neben einer statistischen Verteilung von Leerstellen und Eisen-Atomen, die ebenfalls in der Subzelle in $I4/mmm$ beschrieben werden kann, wurde für eine leerstellengeordnete Variante der Zusammensetzung $TlFe_{1.6}Se_2$ eine $\sqrt{5}\times\sqrt{5}$-Überstruktur in $I4/m$ mit a = 8.7(1) Å, c = 14.0(1) Å vorgeschlagen [3]. Unsere Arbeiten zeigen, dass beide Strukturmotive bei einem gegebenen Eisendefizit in einer Probe gefunden und ineinander überführt werden können. Neben den starken Reflexen der hochsymmetrischen Substruktur finden wir im Beugungsbild bei Raumtemperatur auch sehr viel schwächere Überstrukturreflexe. Diese können mit der genannten $\sqrt{5}\times\sqrt{5}$-Überstrukturzelle unter Berücksichtigung partiell meroedrischer Zwillinge erklärt werden. Die Strukturverfeinerung dieser Daten ergibt allerdings lediglich eine teilweise geordnete Leerstellenverteilung. Erhitzt man den Kristall auf 200°C verschwinden die Überstrukturreflexe und man erhält das Beugungsbild der (gemittelten) Substruktur mit statistischer Leerstellenverteilung. Der Übergang ist reversibel, nach Abkühlung wird wieder die verzwillingte $\sqrt{5}\times\sqrt{5}$-Überstruktur gefunden, es bilden sich jedoch kleinere Zwillingsdomänen aus (s. Abbildung).

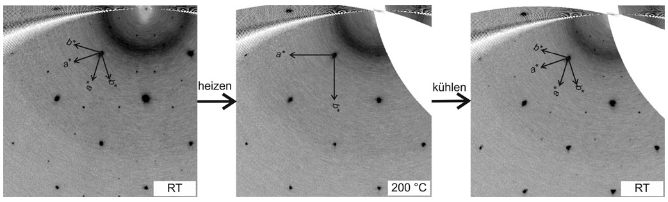

Abbildung: Reziproke *hk*0-Schichten eines verzwillingten $TlFe_{2-x}Se_2$ Kristalls bei unterschiedlichen Temperaturen.

[1] K. Klepp et al, *Monatsh. Chem.* **1978**, *109* (*5*), *1049-1057.*
[2] B. C. Sales et al., *Phys. Rev. Lett.* **2012**, *109*, *077003.*
[3] L. Häggström et al., *J. Solid State Chem.* **1986**, *63*, *401-408.*

PS05-P47

Towards anhydrous rare earth triflates

Syntheses, crystal structures and characterization of $RE(CF_3SO_3)_3(H_2O)_3$ (RE=Eu-Lu,Y) and $(NO)[Sm_2(CF_3SO_3)_7(H_2O)_3]$

J. Bruns[1], A. Weiz[1], M. Wickleder[1]
[1]*C.v.Ossietzky University, IRAC, Oldenburg, Germany*

Our knowledge on the structures of rare earth triflates is extraordinary limited with respect to their importance, especially in homogenous catalysis. The nona-hydrates $RE(CF_3SO_3)_3(H_2O)_9$ are the only class of compounds for which structures have been sufficiently elucidated [1]. They show the RE^{3+} ions in exclusive coordination of water molecules. Our efforts to shed some light on the structures of lower triflate hydrates or even the anhydrous species have now led to the trihydrates $RE(CF_3SO_3)_3(H_2O)_3$ (RE = Eu-Lu, Y) (**I**), The compounds are formed in reactions of the oxides RE_2O_3 with triflic acid in fuming HNO_3 at 150 °C. In the isotypic triclinic structures (e.g. RE = Eu: P-1, Z=2, a = 7.9542(4), b = 10.9660(7), c = 11.2817(7) Å, α = 98.567(3)°, β = 108.990(3)°, γ = 101.326(3)°) all triflate anions are coordinating ligands, and the coordination sphere around RE^{3+} is filled by three molecules of water (Fig. 1) [2]. For the large rare earth elements RE = La-Sm the monoclinic complex triflates $(NO)[RE_2(CF_3SO_3)_7(H_2O)_3]$ (**II**) are formed (e.g. RE = Sm: $P2_1/c$, Z = 4, a = 11.5436(3) Å, b = 20.7287(6) Å, c = 16.6324(4) Å, β = 102.446(1)°). It is worthwhile to mention that for RE = Eu and Gd both types of compounds exist. The thermal decompositions of the compounds **I** and **II** lead essentially to the oxide-fluorides REOF as revealed by DSC/TG/EGA measurements and XRD analysis.

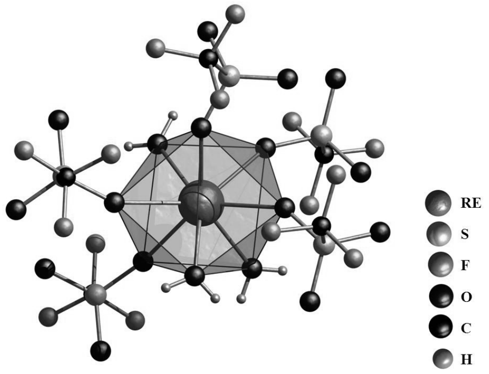

Figure 1. Slightly distorted square-antiprismatic oxygen coordination of the RE^{3+} ions in the structures of RE$(CF_3SO_3)_3(H_2O)_3$ (RE = Eu - Lu, Y). The coordination sphere is built up by five triflate anions and three H_2O molecules.

[1] A. Abbasi, P. Lindqvist-Reis, L. Eriksson, D. Sandström, S. Lidin, I. Persson, M. Sandström, *Chem. Eur. J.* **2005**, *11*, 4065, and references therein.

[2] J. Bruns, A.Weiz, M. S. Wickleder, *Z. Anorg. Allg. Chem.* **2012**, 1635.

PS05-P48

Fe^{2+}-linking by novel polysulfonate anions

C. Zitzer[1], M. Wickleder[1], J. Christoffers[1], T. Muesmann[1]
[1]*C.v.Ossietzky University, IRAC, Oldenburg, Germany*

The anion of terephthalic acid (1,4-benzenedicarboxylate, BDC^{2-}), is one of the most frequently used linkers in the synthesis of coordination polymers and metal-organic Frameworks (MOFs), e.g. in the famous MOF-5.[1] As sulfo analogue to terephthalic acid we recently presented the synthesis of 1,4-benzene-disulfonic acid(H_2BDS).[2] Using this new sulfonate linker we have already prepared salts of Cu(II) and Zn(II).[2,3] Here we present the first Fe^{2+} compounds, namely Fe(BDS)$(NMP)_3$(**1**)(NMP-*N*-methylpyrrolidone) and Fe(BDS)$(NMP)_2(H_2O)_3$(**2**). For the respective carboxylates Fe(BDC)(DMF) is a well decscribed three-dimensional example.[4] Compound **1** has been synthesized by solvothermal reaction. It crystallizes in the space group *P*-1 with the following parametrs: a = 911.98(5), b = 960.75(5), c = 1432.41(8) pm, α = 94.951(2), β = 98.050(3), γ = 92.029(2)°. The Fe^{2+} ion is octahedrally coordinated by two sulfonate anions and three solvent molecules. In the asymmetric unit, there are two crystallographically distinguishable benzenedisulfonates. One of these acts as bidentate bridging ligand, the second one is even a tetradentate bridging ligand (Fig. 1) The linking leads to chains in the [100] direction which are further connected in [001] direction yielding two-dimensional layers. Compound **1** is highly hygroscopic and the hydratisation leads to single crystals of compound **2**. The monoclinic compound has a monomeric structure with the following lattice parameters: *Pc*, a =1468.49(5), b = 778.56(2), c = 2011.74(7) pm, β = 98.020(2)°.

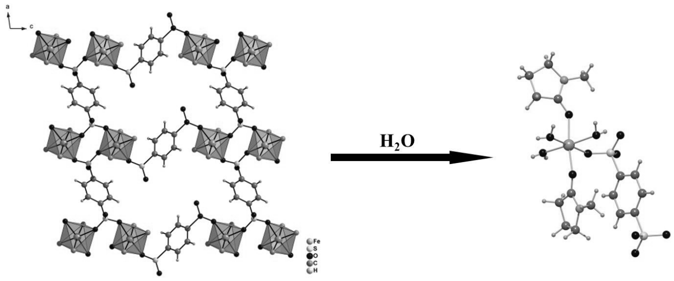

Figure 1. Left: Projection of the structure of Fe(BDS)$(NMP)_3$ onto the (010) plane. The oxygen atoms are shown as blue (sulfonate oxygen) and light blue spheres (oxygen of NMP). For clarity the NMP-molecules are not shown. Right: Monomer of Fe(BDS)$(NMP)_2(H_2O)_3$.

[1] H. Li, M. Eddaoudi, M. O'Keeffe, O. M. Yaghi, *Nature* **1999**, *402*, 276-279.[2]A. Mietrach, T. W. T. Muesmann, J. Christoffers, M. S. Wickleder, *Eur. J. Iorg. Chem.* **2009**, 5328-5334.[3]T. Muesmann, C. Zitzer, A. Mietrach, T. Klüner, J. Christoffers, M. S. Wickleder,*Dalton Trans.***2011**, *40*,3128-3141.[4] T. R. Whitfield, X. Wang, L. Liu, A. J. Jacobson, *Solid State Sciences* **2005**,*7*,1096-1103.

PS05-P49

Kokristallisation und Kristallmorphologie der Zeolithe LTA und X (FAU) bei der Hydrothermalsynthese silikatreicher Gele

V. Petrov[1], T. Koglin[1], J.- C. Buhl[1]
[1]*Mineralogie, Kristallographie, Hannover, Germany*

Zusammenfassung: Die vorliegende Arbeit befasst sich mit der Gelsynthese der technisch wichtigen Zeolithe A (Strukturtyp Linde Typ A) und X (Strukturtyp Faujasit, FAU). In insgesamt acht Syntheseansätzen unter Variation des Si:Al-Verhältnisses konnte gezeigt werden, dass der Strukturübergang LTA↔FAU ohne Gelalterung problemlos möglich ist. Änderungen der Kristallitgröße und Morphologie werden beschrieben.

1. Einleitung

Der Syntheseübergang von LTA zu FAU wurde durch Erhöhung der eingesetzten Natriumsilikatmenge experimentell geprüft [1, 2] um ein einfaches Reaktionssystem für eine Übertragung der Kristallisationsbedingungen auf industrielle Reststoffe zu entwickeln. Weiterhin interessierte auch, ob ein Einfluss der Gelzusammensetzung auf die Kristallitgröße und Kristallmorphologie zu beobachten ist. Zur Analyse der Produkte diente die Röntgen-Pulverdiffraktometie (BRUKER Endeavor D4) sowie Rasterelektronenmikroskopie mit EDX-Analyse (JEOL JSM6390A mit BRUKER Quantax 2000 EDX-System).

2. Experimentelles

Die Herstellung des Gels erfolgte in herkömmlicher Weise aus 10 ml Natriumaluminat-Lösung und 10 ml Natriumsilikat-Lösung unter Verwendung von Natriumaluminat $NaAlO_2$, Riedel-deHaen, Nr. 13404 und Natriummetasilikat Na_2SiO_3, Aldrich, Nr. 30.781-5. Für die Syntheseansätze wurde entsprechend Tabelle 1 lediglich der Anteil an Natriummetasilikat variiert und die $NaAlO_2$-Menge mit 0,9g konstant eingewogen. Das nach Zugabe der Silikat- zur Aluminat-Lösung entstandene Gel wurde anschließend in 50 ml Stahl-Autoklaven mit Teflon-Einsatz überführt und kristallisierte jeweils bei 363 K für 16 Stunden aus. Auf eine übliche Gelalterung der Si-reichen Ansätze wurde bei den hier beschriebenen Experimenten verzichtet, um für spätere Übertragungen der Synthese auf industrielle Reststoffe kürzere Synthesezeiten zu erreichen.

3. Ergebnisse

In insgesamt acht Syntheseansätzen unter Variation des Si:Al-Verhältnisses konnte gezeigt werden, dass der Strukturübergang LTA↔FAU ohne Gelalterung problemlos möglich ist (Abbildung 1). Für Gele mit Gewichtsverhältnissen von Na_2SiO_3:$NaAlO_2$ von 1,4 kristallisiert noch LTA, für 1,67 erfolgt eine Kokristallisation von LTA und FAU und für 1,94 lag dann phasenreiner Zeolith X (FAU) vor. Für sehr Si-reiche Gele (Na_2SiO_3:$NaAlO_2$ von 2,8 und 3,5) konnte gezeigt werden, dass die Kristallitgröße statt rund 2 µm hier nur noch 1µm beträgt und gleichzeitig eine Änderung der Morphologie eintritt. Anstelle oktaederförmiger Faujasite liegt eine Verwachsung kleiner Kristallite mit plättchenförmigen Habitus vor.

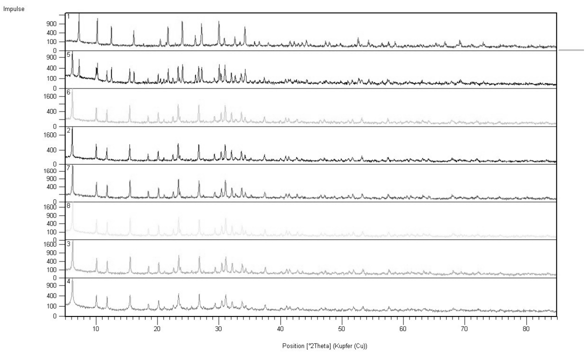

Abb. 1: Röntgen-Pulverdiffraktogramme der Produkte (S. Tab. 1.)

Litheratur: [1] Breck, D. W.: Zeolite Molecular Sieves. Wiley & Sons, New York, London, Sydney, Toronto, 1974.

[2] Жданов, С. П., Хвощев, С. С., Самулевич Н. Н., Синтетические цеолиты, Москва «Химия», 1981.

Tabelle 1: Einwaage der Edukten

Proben Nr.	$NaAlO_2$ (g)	Na_2SiO_3 (g)	Produkt
1	0,9	1,25	LTA
2	0,9	1,88	FAU
3	0,9	2,50	FAU
4	0,9	3,13	FAU
5	0,9	1,50	FAU+LTA
6	0,9	1,75	FAU
7	0,9	2,00	FAU
8	0,9	2,25	FAU

PS05-P50

Pyroelectric properties of the monoclinic rare earth nitrates $A_2Ln(NO_3)_5 \cdot 4H_2O$

M. Ackermann[1], L. Andersen[1], P. Becker[1], L. Bohaty[1]
[1]*University of Cologne, Institut of Crystallography, Köln, Germany*

Crystals of the isomorphic series of rare earth nitrates of type $A_2Ln(NO_3)_5 \cdot 4H_2O$ (A = Rb, NH_4; Ln = La, Ce, Pr, Nd) crystallize in the non-centrosymmetric space group *Cc* [1-4]. Single crystals of the compounds with La and Ce can easily be grown from aqueous solutions containing a surplus of HNO_3, using our standard evaporation method at 38°C [3, 4]. During a growth period of 12-15 weeks large single crystals (up to 50 g) of optical quality can be obtained. The point group *m* of the title crystals allows a rotational degree of freedom of the pyroelectric vector $\boldsymbol{p}$ within the mirror plane, with $\boldsymbol{p} = p_1\boldsymbol{e}_1 + p_3\boldsymbol{e}_3$ (the reference Cartesian system $\{\boldsymbol{e}_i\}$ being defined as $\boldsymbol{e}_2 \| b$, $\boldsymbol{e}_3 \| c$, $\boldsymbol{e}_1 = \boldsymbol{e}_2 \times \boldsymbol{e}_3$). For the determination of the pyroelectric components p_1 and p_3 and their temperature dependence three differently oriented plate-shaped samples from the zone [010] were used for each compound under investigation. The components p_1 and p_3 were derived from the measurement of the pyroelectric current that arises as a consequence of an applied heating/cooling rate dT/dt [5, 6]. An improved experimental setup for these measurements is presented. At room temperature the relative large pyroelectric coefficients of the title compounds show values of up to 10 times p_3 of tourmaline. Most strikingly the orientation of the pyroelectric vector is very sensitive to temperature changes and shows a remarkable orientational variation, e.g., in the case of $(NH_4)_2La(NO_3)_5 \cdot 4\,H_2O$ a rotation of ~140° occurs in the temperature range between 100 K and 300 K.

[1] A. G. Vigdorchik, Y. A. Malinovskii, A. G. Dryuchko, V. B. Kalinin, I. A. Verin, S. Y. Stefanovich, *Sov. Phys. Crystallogr.* **37** (1992) 783-791.
[2] N. Audebrand, J. P. Auffrédic, M. Louër, N. Guillou, D. Louër, *Solid State Ionics* **84** (1996) 323-333.
[3] L. Bohatý, P. Held, P. Becker, *Z. Anorg. Allg. Chem.* **635** (2009) 2236-2241.
[4] L. Bohatý, R. Fröhlich, P. Held, P. Becker, *Eur. J. Inorg. Chem.* **2010** 2642-2648.

[5] S.B. Lang, F. Steckel, *Rev. Sci. Inst.* **36** (1965) 929-932.
[6] R.L. Byer, C.B. Roundy, *Ferroelectrics* **3** (1972) 333-338.

PS05-P51

On the dehydration mechanism of NaB(OH)$_4$-sodalites investigated by micro-Raman spectroscopy

A. Schulz[1], C. H. Rüscher[1], J.- C. Buhl[1]
[1]*Mineralogie, Kristallografie, Hannover, Germany*

NaB(OH)$_4$-sodalite can be seen as the end-member of the hydrogen release reaction of NaBH$_4$-sodalite under wet conditions at temperatures between 150 and 450°C:

$$Na_8(Al_6Si_6O_{24})(BH_4)_2 + 8\ H_2O \rightarrow Na_8(Al_6Si_6O_{24})(B(OH)_4)_2 + 8\ H_2$$

Under dry (say open atmospheric conditions) and in a partly reacted NaBH$_4$-sodalite details of the de- and rehydration reaction of NaB(OH)$_4$ sodalite become important, too. For this the main question is how water becomes released in the two well known steps [1-4]

$$Na_8(Al_6Si_6O_{24})(B(OH)_4)_2 \rightarrow Na_8(Al_6Si_6O_{24})(BO(OH)_2)_2 + H_2O \rightarrow Na_8(Al_6Si_6O_{24})(BO_2)_2 + 2\ H_2O,$$

i.e., if and how water could be transported for a further hydrogen release reaction, beside the most fundamental question concerning the hydrogen release itself.

In this circumstance it is interesting to note that the dehydration steps of NaB(OH)$_4$-sodalite single crystals to NaBO(OH)$_2$- and NaBO$_2$- species were observed by micro Raman spectroscopy [5]. It could be shown that single crystals could be grown which are large enough for obtaining depth profiles by micro Raman spectroscopy. Preliminary estimations using the solution of Fick's first law reveal a diffusion coefficient according to $D = z^2/t$, z = characteristic dehydrated zone depth, in the range of 10^{-10} cm²/s for dehydration experiments at 400°C. This method could be consequently improved and now systematically used for carrying out detailed depth profile analysis with Fick's 2nd law according to:$[n(x)=(n0-ns)\mathrm{erf}(X/2\sqrt{Dt})+ ns]$

The results are shown in Fig. 1. It is observed that dehydration occurs in a diffusion controlled process which could be described by $D = D_0\exp(-E_a/kT)$ with $E_a = 1.3$ eV, $D_0 = 0.3$, as deduced for experiments at temperatures between 300 and 400°C.

The dehydration effect could be determined by the change in intensity of the B-(OH) vibration and could also be seen by small and systematic shift in the "hard mode" Si-O lattice vibration according to the change in cage filling. Further experiments are required in order to distinct between the possibility of a separated transport mechanism as OH$^-$ and H$^+$ or as a H$_2$O molecules. For this exchange experiments using D$_2$O were carried out in order to determine H$^+$/D$^+$ Tracer diffusion coefficients. Some preliminary experiments could be carried out with single crystals put into Teflon cups together with water of concentration 50%D$_2$O/50%H$_2$O. The samples were heated at 50, 100 and 150 °C for times between 1 h and 48 h. Depth profiles by micro Raman analysis could be carried out using relative intensities of OH- and OD-vibrations. First results show a very high mobility of protons through the sodalite framework already at 50°C, 100°C and 150°C (Fig.1). So the dehydration of NaB(OH)$_4$-sodalite can be described via a rather fast diffusion of protons and a slower diffusion of OH-groups during dehydration. It could be shown that the micro-Raman spectrometer technique (Bruker Senterra) reveal a rather high precession of better than 2 µm in local resolution and better than 0.5 µm in relative spectral resolution of the main lattice vibration.

[1] H.-H. E. Pietsch, M. Fechtelkord, J.-Chr. Buhl, J. Alloys Comp. 257 (1997) 168-174.
[2] A. Schulz, C. H. Rüscher, J.-C. Buhl, Z. Krist. Suppl. 31 (2011) 93.
[3] C. H. Rüscher, J.-Chr. Buhl, Z. Krist. Suppl. 15 (1998) 113.
[4] C. H. Rüscher, Microp. Mesop. Mat. 86 (2005) 58-68.
[5] A. Schulz, C. H. Rüscher, J.-Chr. Buhl: Z. Krist. Supplement Issue 32 (2012) 81-82.

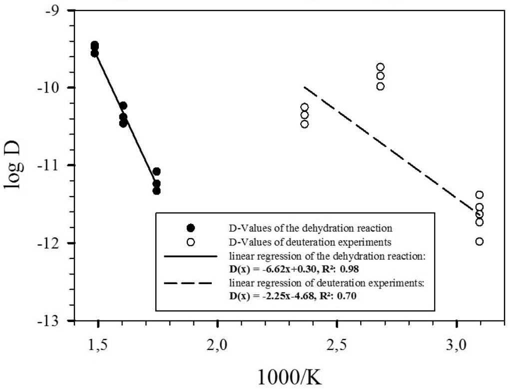

Fig. 1: Arrhenius-Plot of the determined diffusion coefficients of the dehydration reaction of NaB(OH)$_4$-sodalite at 300°C, 350°C and 400°C (closed circle). First estimated diffusion coefficients of deuteration experiments at 50°C, 100°C and 150°C (open circle).

PS05-P52

$\chi^{(3)}$-nonlinear optical effects in topaz, $Al_2(F_{1-x}(OH)_x)_2SiO_4$

A. A. Kaminskii[1], O. Lux[2], H. Rhee[2], H.- J. Eichler[2], L. Bohatý[3], P. Becker[3]
[1]*Russian Academy of Sciences, Institute of Crystallography, Moscow, Russian Federation*
[2]*Technical University Berlin, Institute of Optics and Atomic Physics, Berlin, Germany*
[3]*University of Cologne, Institute of Crystallography, Köln, Germany*

The $\chi^{(3)}$-nonlinear optical inelastic process of stimulated Raman scattering (SRS) in SRS-active crystals can be successfully used for various treatment of laser light, for example, applications such as effective laser frequency conversion (Raman laser wavelength shifter) or improvement of the quality of laser light (Raman laser beam cleaner) (see, e.g., [1, 2]). Consequently, there is an ongoing demand for new suitable nonlinear optical, SRS-active crystals that fit the requirements of miscellaneous applications. In contrast to $\chi^{(2)}$-nonlinear optical processes such as second harmonic generation (SHG), SRS is possible in media of any symmetry. In the present contribution a study of SRS and Raman induced four wave mixing (RFWM) in crystals of centrosymmetric topaz, $Al_2(F_{1-x}(OH)_x)_2SiO_4$, with space group *Pbnm* (e.g. [3, 4]) is presented. The (OH) content of our used natural crystals of high optical quality was determined by the established method of precise measurement of main refractive indices and precise measurement of the Bragg reflection 120 with internal standard NaCl [5], and was found to be $x \approx 0.04$. Topaz turned out to be an efficient SRS and RFWM medium: By single-wavelength excitation with $\lambda_{f1} = 1.06415$ µm and with $\lambda_{f2} = 0.53207$ µm the generation of octave-spanning Stokes and anti-Stokes lasing combs was observed. In addition, by dual-wavelength excitation using λ_{f1} and λ_{f2} simultaneously, cascaded $\chi^{(3)} \leftrightarrow \chi^{(3)}$ nonlinear photon-phonon interactions were found. Topaz crystals show two SRS-promoting vibration modes with $\omega_{SRS1} \approx 265$ cm^{-1} and $\omega_{SRS2} \approx 238$ cm^{-1}, which are also manifest in the spectrum of spontaneous Raman scattering, and additionally two combined modes with $\omega_{SRS3} \approx 503$ cm^{-1} and $\omega_{SRS4} \approx 27$ cm^{-1}.

[1] A.A. Kaminskii, *Laser Photon. Rev.* **1** (2007) 93-177.

[2] J.T. Murray, W.L. Austin, R.C. Powell, *Opt. Mater.* **11** (1999) 353-371.

[3] J. Leonhardt, Z. Kristallogr. **59** (1924) 216-229.

[4] Y.V. Ivanov, E.L. Belokoneva, J. Protas, N.K. Hansen, V.G. Tsirelson, *Acta Cryst. B* **54** (1998) 774-781.

[5] P.H. Ribbe, P.E. Rosenberg, *Am. Mineral.* **56** (1971) 1812-1821.

PS05-P53

Kokristallisation und Kristallmorphologie von Zeolith (LTA) und Sodalith (SOD) bei der Hydrothermalsynthese aluminiumreicher Gele und Einfluss der Alkalinität auf den Kristallisationsablauf.

V. Petrov[1], P. Törber[1], J.- C. Buhl[1]
[1]*Mineralogie, Kristallographie, Hannover, Germany*

1. Einleitung

Die Ableitung des Kristallisationsverhaltens von Zeolith LTA bei maximaler Alkalinität ist für eine Übertragung der Bedingungen auf industrielle Reststoffe von Bedeutung. Diese werden oftmals in hochalkalischen Prozessen aufbereitet. Kokristallisation- oder Kristallisation von SOD allein soll dabei unterdrückt bleiben. Daher wird der Syntheseübergang von LTA zu SOD durch Erhöhung der eingesetzten Natronlauge experimentell geprüft. Darüber hinaus war der Zusammenhang von Gelzusammensetzung auf die Kristallitgröße und Kristallmorphologie von Interesse.

2. Experimentelles

Die Herstellung des Gels erfolgte mit Natriumaluminat ($NaAlO_2$, Riedel-deHaen, Nr. 13404) und Natriummetasilikat (Na_2SiO_3, Fluka, Nr. 2299129). Vor der Gelfällung wurde die Alkalinität durch Zugabe von NaOH-Granulat (Merck, 1.06467) zur Aluminat- und zur Natriumsilikat-Lösung entsprechend der Einwaagen in Tab. 1 eingestellt. Erst dann wurden die Lösungen (je 10 ml) zusammen geführt. Das entstandene Gel wurde anschließend in Stahlautoklaven mit 50 ml Teflon-Einsatz überführt und kristallisierte jeweils bei 353 K für 16 Stunden aus.

3. Ergebnisse

Es wurden insgesamt 12 Syntheseansätze durchgeführt, wobei die erste Probenreihe (Versuche: 1 bis 6) zur Untersuchung von Kristallitgröße- und Kristallmorphologie bei niedriger Alkalinität diente. Die zweite Probenreihe (Versuche: 7 bis 12) erfolgte bei höher Alkalinität, um die Umwandlung von LTA zu SOD zu erreichen und den Einfluss auf die Kristallmorphologie und Kristallitgröße zu untersuchen. Aus Gelen mit einem Molverhältniss (Si/Al) von 1,0 kristallisierten noch ideal kubische LTA-Kristallite. Bei aluminiumreichen Gelen (Si/Al: 0,7 und 0,5) entstanden abgerundete Kristalle bei einer gleichzeitigen Verringerung der Kristallitgröße (1. Probenreihe, Versuche 1-3, Tab. 1). Der Zusatz von 1 M NaOH ergab keinen Einfluss auf das Kristallwachstum (1. Probenreihe, Versuche 4-6). In Serie 7-12 wurden dann Gele mit einem Molverhältnissen Si/Al von 1,0 mit unterschiedlichen Laugenkonzentrationen behandelt. Während Zusätze von 1,5M und 2,0M NaOH noch zu LTA führten (Versuch 7 und 8), ergab 2,5M NaOH-Lsg eine Kokristallisation von SOD und LTA (Versuch 9). Der Anteil von SOD nahm weiter mit ansteigender Laugenkonzentration zu bis schließlich phasenreiner SOD vorlag (Versuch 12). Außerdem konnte gezeigt werden, dass die Kristallitgröße von etwa 2µm unter 1µm fiel bei einer gleichzeitigen Änderung der Kristallit-Morphologie. Anstelle würfelförmiger Kristallite (LTA) zeigte sich mit zunehmender Alkalinität die Tendenz über abgerundete LTA-Kristalle hin zu Verwachsungen linsen- bis plättchenförmiger SOD-Kristallite.

Litheratur: [1] Breck, D. W.: Zeolite Molecular Sieves. Wiley & Sons, New York, London, Sydney, Toronto, 1974.

[2] Жданов, С. П., Хвощев, С. С., Самулевич Н. Н., Синтетические цеолиты, Москва «Химия», 1981

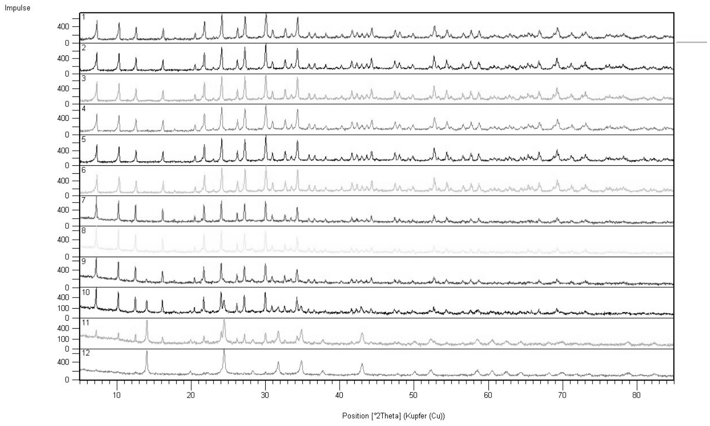

Abb. 1: Röntgen-Pulverdiffraktogramme der Produkte (S. Tab. 1.)

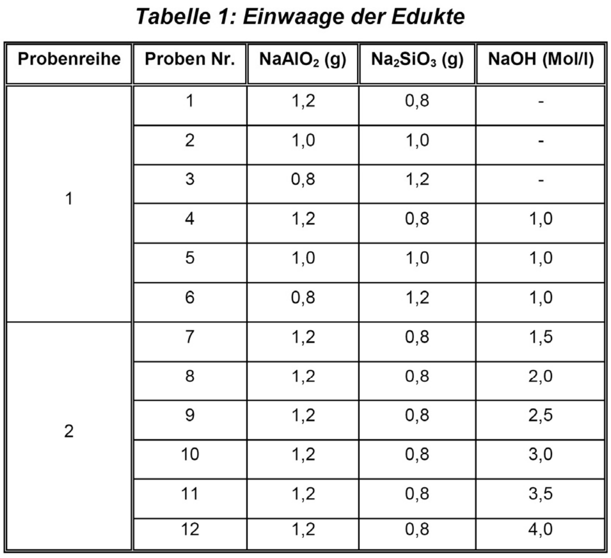

Tabelle 1: Einwaage der Edukte

Probenreihe	Proben Nr.	$NaAlO_2$ (g)	Na_2SiO_3 (g)	NaOH (Mol/l)
1	1	1,2	0,8	-
	2	1,0	1,0	-
	3	0,8	1,2	-
	4	1,2	0,8	1,0
	5	1,0	1,0	1,0
	6	0,8	1,2	1,0
2	7	1,2	0,8	1,5
	8	1,2	0,8	2,0
	9	1,2	0,8	2,5
	10	1,2	0,8	3,0
	11	1,2	0,8	3,5
	12	1,2	0,8	4,0

Tabelle 1: Einwaage der Edukte

PS05-P54

Metastability of metamict titanite and thermal behaviour of its elastic properties

U. Bismayer[1], C. Paulmann[1], T. Beirau[1], B. Mihailova[1], T. Malcherek[1], P. Guglielmi[2], G. Schneider[2], L. Groat[3], E. K. H. Salje[4]
[1]*Mineralogie, Uni Hamburg, Geowissenschaften, Hamburg, Germany*
[2]*Technical University Hamburg-Harburg, Institute of Advanced Ceramics, Hamburg-Harburg, Germany*
[3]*University of British Columbia , Department of Earth and Ocean Sciences, Vancouver, Canada*
[4]*University of Cambridge, Department of Earth Sciences, Cambridge, United Kingdom*

Metamict minerals incorporate various impurities like the radiogenic elements U and Th which lead to emission of alpha-particles. The related recoil processes change the originally periodical structure into a state with quasi-amorphous disordered areas adjacent to long-range ordered crystalline clusters. Crystalline and quasi-amorphous areas are separated by interfaces. The interfaces are relatively broad rims and represent regions which are transition areas between the amorphous and crystalline material (1). On thermal treatment the metamict material recrystallises and its macroscopic physical properties change drastically with increasing structural order. One of the properties concerned is the materials hardness which is expected to increases as a result of increasing order in the system. The elastic properties of metamict titanite were studied using by nanoindentation to investigate in detail the behaviour of the elastic modulus (E) and the hardness (H). The observed average hardness decreases on annealing at temperatures below 950K and only increases at higher temperatures while the elastic modulus increases with rising annealing temperature over the whole annealing range (2). Raman and X-ray diffraction are used to better understand the phenomena.

(1) Salje E.K.H., D.J. Safarik, J.C. Lashley, L.A. Groat, U. Bismayer
American Mineralogist 96, 1254-1261, 2011

(2) Beirau T., P. Guglielmi, C. Paulmann, G.A. Schneider, L.A. Groat, T. Malcherek, E.K.H. Salje, U. Bismayer
Phase Transitions iFirst, 1-10, 2012

PS05-P55

Kristallisationsprozesse in stark alkalischen Aufschlusslösungen von Aschen aus der Verbrennung von Schlämmen der Altpapieraufbereitung

A. Hartmann[1], V. Petrov[1], J.- C. Buhl[1], K. Rübner[2]
[1]*Leibniz Universität Hannover, Institut für Mineralogie, Hannover, Germany*
[2]*Bundesanstalt für Materialforschung und -prüfung (BAM), Fachgruppe VII.1 Baustoffe, Berlin, Germany*

Bei Aschen, die bei der Verbrennung von Schlämmen der Altpapieraufbereitung anfallen, handelt es sich um industrielle Reststoffe. Sie enthalten hohe Anteile an Calcium- und Silikatverbindungen, die bei geeigneten Kristallisationsbedingungen in Wertstoffe überführt werden können. Am Beispiel einer calcit- und gehlenitreichen Asche (PA-D) sowie einer calcitreichen Asche (PA-NL) werden hier Möglichkeiten für geeignete Kristallisationsprozesse bei niedriger Temperatur von nur 60°C sowie kurzer Reaktionszeit (4h) untersucht und hochalkalische Bedingungen mit 8 M-, 12 M- und 16 M NaOH eingesetzt. Ziel der Arbeiten ist die Entwicklung neuartiger Herstellungsmöglichkeiten technisch nutzbarer Recyclingmaterialien.

Da für Synthesechemikalien (Gele aus Natriumsilikat- und Natriumaluminat-Lösungen) unter hochalkalischen Niedertemperaturbedingungen eine Zeolithkristallisation möglich ist [1-2], erfolgten hier Experimente mit dem Additiv $NaAlO_2$ als Al-Quelle zur Kristallisation von Na-Ca-Alumosilikaten. Zur Prozesscharakterisierung dienten chemische, röntgenographische und elektronenmikroskopische Analysen.

Für PA-D konnte gezeigt werden, dass Calcium in Abhängigkeit von der Alkalinität nach 4h Laugung in Portlandit überführt wird, der Calcitanteil geht völlig zurück und der Gehlenitanteil bleibt erhalten (Abb. 1). Zusatz von $NaAlO_2$ führt bei 8 M NaOH zur Bildung von Katoit (Hydrogranat) neben Portlandit, wobei das eingesetzte Aluminat nicht in Zeolith sondern in Katoit eingebunden wird. Eine höhere Alkalinität drängt die Katoitbildung zu Gunsten der neuen Phase „Calcium-Aluminiumoxid-Carbonat-Hydrat“ [3] zurück. Der Gehlenitanteil der PA geht bei Reaktion unter Zusatz von $NaAlO_2$ in 12 M NaOH merklich sowie in 16 M NaOH stark zurück (Abb. 1). Die alkalische Reaktion führte nicht zur Zeolithbildung.

Die mit PA-NL, ebenfalls bei einer Reaktionszeit von 4h durchgeführte Versuchsserie zeigte, dass bereits nach Reaktion in 8 M NaOH Portlandit und Katoit vorhanden sind. Die Aufschlussreaktion in 12 M und 16 M NaOH führt zu hohen Anteilen an Portlandit im Feststoff, während der gesamte Silikatanteil in die alkalische Aufschlusslösung überführt wird. Der Zusatz von $NaAlO_2$ ergibt bei der Laugung in 8 M NaOH Katoit und Portlandit, der Calcitanteil geht merklich zurück. Höhere Alkalinität führt zu „Calcium-Aluminiumoxid-Carbonat-Hydrat“ neben hohen Portlanditanteilen, anstelle der Katoitkristallisation.

Sehr geringe Calcitanteile bleiben erhalten. Dieses Ergebnis findet sich sowohl für die 12 M Serie als auch für 16 M NaOH (Abb. 1).

Die Arbeiten besitzen Modellcharakter für neue Ansätze des Reststoff-Recycling durch alkalischen Hydrothermalaufschluss unter Optimierung des Energiebedarfs (60°C) und der Reaktionszeit (4h) sowie einer Weiterverwendung der Aufschlusslaugen im Kristallisationsprozess.

[1] Hadan, M., Fischer, F.: Cryst. Res. Technol. 27 (1992) 343 - 350.

[2] Fischer, F., Hadan, M., Horn, A.: Chem. Tech. 43 (1991) 191 - 195.

[3] International Centre for Diffraction Data, 12 Campus Boulevard, Newton Square, Pennsylvania 190073-3272, U.S.A.

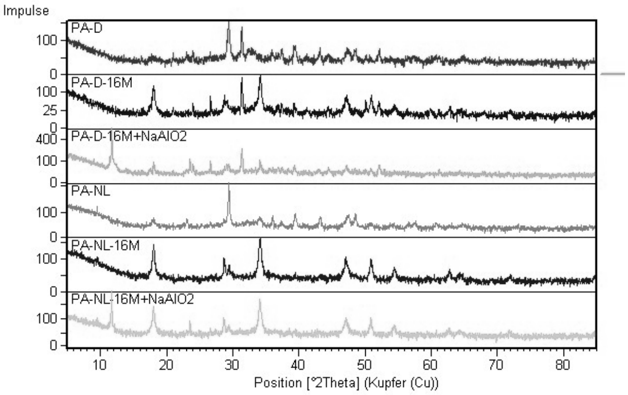

PS05-P56

Kristallographische Untersuchungen zu Zinn(II)-Thiocyanat und seinen Komplexen

H. Reuter[1], F. Ye[1], P. Harpel[1]
[1]*Institut für Chemie neuer Materialien, Osnabrück, Germany*

Unter den Pseudohalogeniden des zweiwertigen Zinns nimmt die Verbindung Zinn(II)-Thiocyanat, $Sn(NCS)_2$, eine Sonderstellung ein, da sie präparativ relativ einfach in großen Menge herzustellen ist [1]. Diese Verbindung stellt, wie die Zinn(II)-Halogenide, eine starke Lewis-Säure dar und sollte daher mit vielen Lewis-Basen Komplexe bilden, was in der Vergangenheit intensiv untersucht und für zahlreiche Komplexliganden IR-spektroskopisch dokumentiert wurde [2].

Da bisher jedoch außer zum reinen Zinn(II)-Thiocyanat [1] keine kristallographischen Untersuchungen zu solchen Komplexen vorlagen, schließen wir diese Lücke im vorliegenden Fall mit den Verbindungen $Sn(NCS)_2 \cdot 2dmpu$ (**1**), $Sn(NCS)_2 \cdot 2dmso$ (**2**), $Sn(NCS)_2 \cdot phen$ (**3**) und $Sn(NCS)_2 \cdot dmso \cdot phen$ (**4**) für die ein- und zweizähnigen O- und N-Komplexliganden dmpu = 1,3-Dimethyl-3,4,5,6-tetrahydro-2(1H)-pyrimidinon, bipy = 2,2'-Bipyridin, phen = 1,10-Phenanthrolin und dmso = Dimethylsulfoxid. In allen Fällen handelt es sich in erster Linie um Molekülstrukturen (Abb. 1), in denen das zweiwertige Zinnatom ψ-trigonal-bipyramidal (**1**, **2**, **3**) bzw. ψ-oktaedrisch (**4**) koordiniert ist. Darüber hinaus sind die Thiocyanat-Ionen, wie in der Ausgangsverbindung, jeweils über die Stickstoffatome an die Zinnatome gebunden, wobei die Zinn-Stickstoff-Abstände mit der axialen bzw. äquatorialen Stellung des Thiocyanat-Ions innerhalb der trigonalen Bipyramide variieren.

[1] Chamberlain, B.R.; Moser, W.: Tin(II) Thiocyanate and Complex Thiocyanates. J. Chem. Soc. A, **1969**, 354-358.

[2] Absi, T.B.; Makhija, R.C.; Onyszchuk, M.: Synthesis and vibrational spectra of tin(II) isothiocyanates adducts with some O- and N-donor ligands. Can. J. Chem. **56** (1978) 2039-2041.

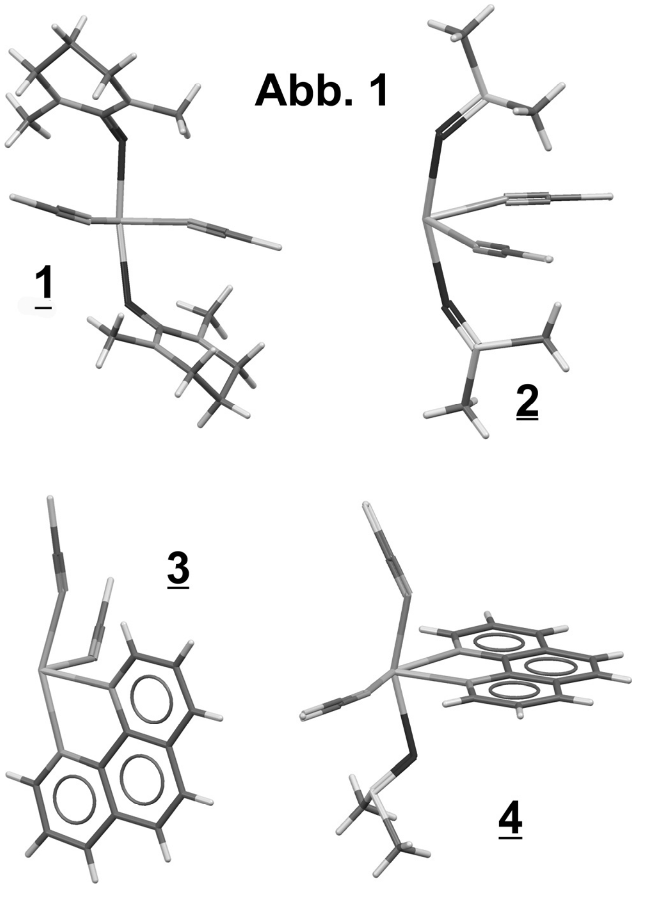

PS05-P57

2,2'-Bipyridin Komplexe von Diethylzinn(IV)-Verbindungen

H. Reuter[1], I. Mastall[1]
[1]*Institut für Chemie neuer Materialien, Osnabrück, Germany*

2,2'-Bipyridin (bipy) Komplexe von Diorganozinn(IV)-Verbindungen sind in der Vergangenheit vielfach hergestellt und kristallographisch untersucht worden, wobei der Schwerpunkt der Untersuchungen auf den Komplexen der Diorganozinndichloride, R_2SnCl_2, lag, [[1], R = Methyl, Isopropyl, n-Butyl, Benzyl], während die entsprechenden Komplexe der analogen *Dibromide*, R_2SnBr_2, und *Diiodide*, R_2SnI_2, bisher vollständig unbeachtet blieben. Dementsprechend liegen bis heute keine Daten zum Einfluss der Größe und Elektronegativität des Halogens auf die Strukturparameter (Bindungslängen, Bindungswinkel, Torsionswinkel) innerhalb der oktaedrischen Komplexe solcher Verbindungen vor.

Um diese Lücke zu schließen, haben wir daher im Falle der Diorganozinndihalogenide mit R = Et = Ethyl neben der bereits seit längerem bekannten Chlorverbindung, $Et_2SnCl_2 \cdot$ bipy (**1**) [2], erstmals auch die entsprechende Brom-, $Et_2SnBr_2 \cdot$ bipy (**2**), und Iodverbindung, $Et_2SnI_2 \cdot$ bipy (**3**), hergestellt und kristallographisch untersucht (Abb. 1), wobei wir im Falle der Iodverbindung nicht weniger als drei polymorphe Modifikationen (**3**α, **3**β, **3**γ) isolieren konnten. In allen Fällen liegt im Hinblick auf die beiden Ethylgruppen und die beiden Halogenatome eine *trans*,*cis*,*cis*-Konfiguration der oktaedrisch aufgebauten Komplexe vor. Demgegenüber macht sich der Einfluss des Halogenatoms auf die Strukturparameter der Komplexe unter anderem in einer Änderung der Stellung der Ethylreste relativ zu den Halogenatomen und in einer starken Verdrillung des Komplexliganden bemerkbar, während sich die Bindungsabstände und -winkel nur in Bezug auf die Halogenatome deutlich unterscheiden.

[1] Tiekink, E.R.T.; Hall, V.J.; Buntine, M.A.; Hook, J.: Examination of the effect of crystal packing forces on geometric parameters: a combined crystallographic and theoretical study of 2,2'-bipyridyl adducts of R_2SnCl_2. Z. Kristallogr. **215** (2000) 23-33.

[2] Chadha, S.L.; Harrision, P.G.; Molloy, K.C.: Structural studies in main group chemistry XXVI. The reaction between di-μ_3-oxobis[μ-chlorodiethyltin(IV)]-bis[*o*-chlorodiethyltin(IV)] and 2,2'-bipyridyl. J. Organomet. Chem. **202** (1980) 247-256.

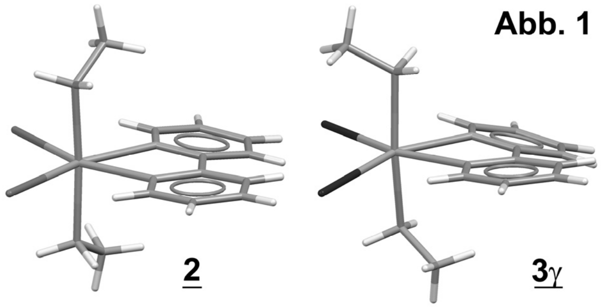

PS05-P58
Neue ternäre Barium-Triel-Mercuride

C. Röhr[1], M. Wendorff[1]
[1]*Institut für Anorganische und Analytische Chemie, Freiburg, Germany*

Für die lange bekannte ($BaHg_{11}$ [1]) bzw. die kürzlich neu synthetisierten und strukturell charakterisierten ($BaHg_6$ [2] und $Ba_{20}Hg_{103}$ [3]) Quecksilberreichen Barium-Mercuride wurden Untersuchungen zur 'Kolorierung' des Mercurid-Anions mit Metallen erhöhter Valenzelektronenzahl vorgenommen. Dazu wurden mit Gallium bzw. Indium jeweils ein etwas kleineres bzw. größeres Element mit geringerer Elektronegativität ausgewählt. Die Phasenbreite des $BaHg_{11}$-Typs [1] reicht bis $BaIn_{2.7}Hg_{8.3}$ (kubisch, Raumgruppe *Pm*3*m*, *a* = 961.81(1) pm, *R*1 = 0.0245), wobei Indium alle Positionen ausser der Hg-Lage, die ausschliesslich von Hg-Atomen umgeben ist, statistisch besetzt. Mit der neuen 1:7-Verbindung $BaIn_{2.6}Hg_{4.4}$ (orthorhombisch, *Cmmm*, *a* = 509.2(5), *b* = 1233.8(14), *c* = 668.8(9) pm, *R*1=0.0617) konnte ein weiterer neuer Strukturtyp erhalten werden, der Ähnlichkeiten mit der 1:8-Phase $SrHg_8$ [4] und $BaHg_6$ [2], aber auch mit $BaHg_{11}$ [1] aufweist: Ebene Netze aus Vier-, Sechs- und Achtringen, ähnlich denen in $SrHg_8$ und $BaHg_6$, sind so gegeneinander verschoben angeordnet, dass benachbarte Vierringe Hg_8-Würfel wie in $BaHg_{11}$ bilden (s. Abb.). Die Ba-Kationen sind in den Achtringen positioniert, ihre Koordinationszahl beträgt 20. Diese $BaHg_{20}$-Polyeder und die Würfel parkettieren den Raum vollständig. Als weiteres Strukturelement sind Zick-Zack-Leitern wie in der Zintl-Phase $BaIn_2$ und dem isotypen Mercurid $BaHg_2$ (KHg_2-Typ) vorhanden (Abb.: gestrichelte Markierung). Für diese Phasenbreite $BaIn_xHg_{2-x}$ sowie für $Ba(In/Ga)_xHg_{4-x}$ ($BaAl_4$-Strukturtyp) wurden kristallographische (neue Überstrukturvarianten) und bindungstheorische Untersuchungen durchgeführt. Die neuen 3:11-Phasen Ba_3MHg_{10}, die nur durch Ga/In als Minoritätskomponente *M* stabilisiert werden und keine bzw. nur minimale Phasenbreiten aufweisen, kristallisieren abhängig von der Größe von *M* isotyp zu Ba_3ZnHg_{10} [5] in einem eigenen Strukturtyp (Ba_3GaHg_{10}) bzw. im La_3Al_{11}-Typ (Ba_3InHg_{10} und Ba_3CdHg_{10}).

[1] E. Biehl, H. J. Deiseroth, *Z. Anorg. Allg. Chem.*, **625**, 1073-1080 (1999).
[2] M. Wendorff, C. Röhr, *J. Alloys Compd.* **546**, 320-328, (2013).
[3] M. Wendorff, C. Röhr, *Z. Naturforsch.* **67b**, 893-906 (2012).
[4] A. V. Tkachuk, A. Mar, *Dalton Trans.*, **39**, 7132-7135 (2010).
[5] M. Schwarz, M. Wendorff, C. Röhr, *J. Solid State Chem.* (im Druck).

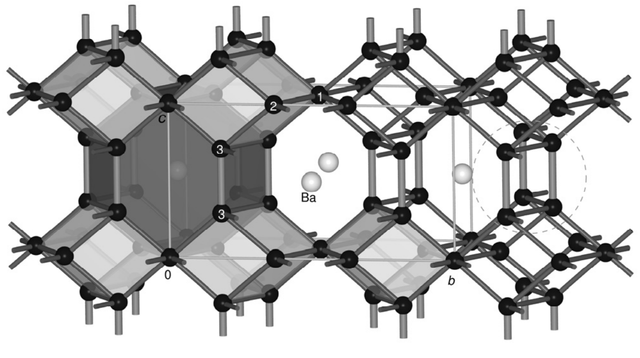

PS05-P59
1,4-Dithian-1,4-dioxid als potentiell zweizähniger Komplexligand gegenüber anorganischen und organischen Zinnverbindungen

H. Reuter[1], S. Budau[1]
[1]*Institut für Chemie neuer Materialien, Osnabrück, Germany*

Ähnlich wie Dimethylsulfoxid, DMSO, stellt 1,4-Dithian-1,4-dioxid, dithiox, das durch Oxidation von 1,4-Dithian mittels Wasserstoffperoxid einfach herzustellen ist, eine Lewis-Base dar, die über ihre Sulfoxid-Funktion an geeignete Lewis-Säure-Zentren koordinieren sollte. Im Gegensatz zum einzähnigen Dimethylsulfoxid, von dem einige Komplexe mit rein anorganischen Zinn(II)- und Zinn(IV)-Verbindungen aber auch Organozinnverbindungen bekannt sind, liegen vom 1,4-Dithian-1,4-dioxid jedoch bisher keine Untersuchungen an Zinnverbindungen vor, obwohl es als potentiell zweizähniger Komplexligand in der Lage sein sollte sich an zwei Zinnatome zu koordinieren, wodurch interessante Molekül- und Kettenstrukturen resultieren sollten. Allerdings dadurch erschwert, das die Verbindung bei der Synthese in zwei nur schwer voneinander trennbaren Konstitutionsisomeren entsteht, die als α- (beide S=O-Gruppen axial) [1] oder β- (eine S=O Gruppe axial die andere äquatorial) [2] 1,4-Dithian-1,2-dioxid bezeichnet werden (Abb. 1).

Bei ersten Voruntersuchungen mit solchen Produktgemischen konnten wir folgende Verbindungen herstellen und deren Kristallstrukturen (Abb. 2) aufklären: $SnCl_2 \cdot$ α-dithiox (**1**), $Me_3SnCl(H_2O) \cdot$ α-dithiox (**2**), $Et_2SnCl_2 \cdot$ α-dithiox (**3**) und $2iPrSnCl_3 \cdot$ β-dithiox (**4**). Mit Ausnahme von **2**, wo das Dithiandioxid-Molekül über Wasserstoffbrücken im Kristall fixiert ist, agiert es gegenüber den Zinnatomen in den anderen Verbindungen immer als zweizähnige Lewis-Base. Dabei resultiert in **1** eine Kettenstruktur, in der die zweiwertigen Zinnatome ψ-trigonal-bipyramidal koordiniert sind. Kettenstrukturen finden sich auch in **2**, hier sind die Zinnatome trigonal-bipyramidal von den drei Methylgruppen und je einem Chloratom und Wassermolekül umgeben, als auch in **3**, wo die Zinnatome oktaedrisch koordiniert sind. Demgegenüber handelt es sich bei **4** um eine Molekülstruktur, in der ein b-Dithiandioxid-Molekül beidseitig zwei trigonal-bipyramidal koordinierte Zinnatome verbrückt. Letztere Verbindung ist bisher die Einzige von uns gefundene, in der das β- und nicht das α-Isomer eingebaut ist.

[1] Shearer, H.M.M.: The Structure of the α-Modification of 1 : 4-Dithian 1:4-Dioxide. J. Chem. Soc. (1959) 1394-1397.

[2] Montgomery, H.: The Crystal Structure of Beta Dithiane Disulphoxide. Acta Crystallogr. **13** (1960) 381-384.

Abb. 1

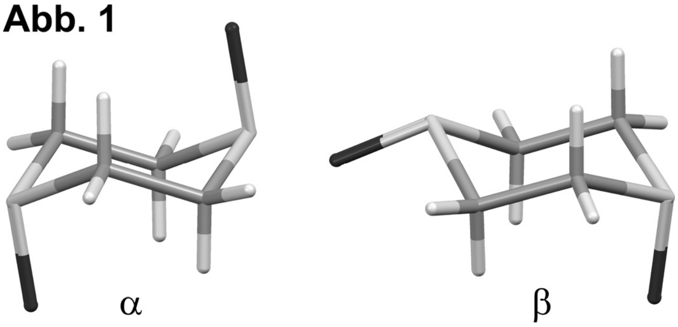

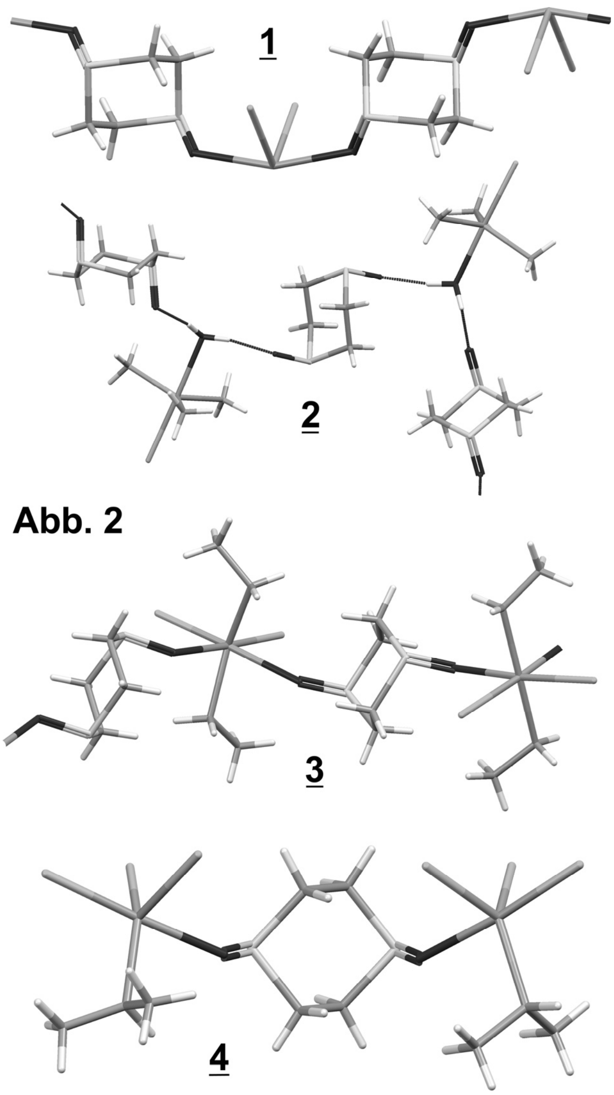

Abb. 2

PS05-P60

Synthesis and crystal structure of $Ba_3B_6Si_2O_{16}$

M. Krzhizhanovskaya[1], L. Gorelova[1,2], R. Bubnova[1,2], S. Filatov[1]
[1]*Saint Petersburg State University, St. Petersburg, Russian Federation*
[2]*Institute of Silicate Chemistry RAS, St. Petersburg, Russian Federation*

Single crystals of $Ba_3B_6Si_2O_{16}$ silicoborate were obtained by slow cooling a melt of stoichiometric composition. Crystal structure was determined by direct methods from X-ray single crystal diffractometry data (Bruker KAPPA APEX DUO, MoKa, CCD detector) using a small colorless plate. It is triclinic, P-1, a = 5.038(1), b = 7.657(1), c = 8.526(1) Å, α = 77.68(1)°, β = 77.88(1)°, γ = 86.32(1)°, R1 = 0.07 (2940 Refl.), 0.09 (Total 3922 Refl.). The structure consists of layered silicoborate anion formed by four crystallographically independent polyhedra: one BO_3 triangle, two BO_4 tetrahedra and one SiO_4 tetrahedron. Ba atoms occupy two different positions in the structure: one of them is inside the layer and another one between the layers. Silicoborate layers are located parallel to (010) plane.

According to triangulation reported in (Levin, Ugrinic, 1953) $Ba_3B_6Si_2O_{16}$ is only one stable compound in the $BaO-B_2O_3-SiO_2$ ternary system. In a wide field of compositions near 3BaO x $3B_2O_3$

x $2SiO_2$ we obtained $Ba_3B_6Si_2O_{16}$ by solid state reaction at 800, 900 and 950 °C mixed with barium borates and/or silicates depending on the composition of initial mixture. Powder XRD data obtained by us for the pure $Ba_3B_6Si_2O_{16}$ synthesized by cooling a melt are in well agreement with the reported before in PDF database and with structural data presented here.

The studied have been supported by Russian Foundation for Basic research (grant for young scientists 12-03-31829). The XRD measurements are performed in the XRD Research Center of Saint Petersburg State University.

PS05-P61
β-$LiSbS_2$ is $Li_{1.250}Sb_{0.917}S_2$: Synthesis, crystal structure and impedance spectroscopy

S. Huber[1], C. De Giorgi[1], A. Pfitzner[1]
[1]*Universität Regensburg, Institut für Anorganische Chemie, Regensburg, Germany*

The crystal structure of the title compound was determined from dark red rectangular single crystals. It becomes obvious that it is closely related to the formerly reported β-$LiSbS_2$.[1, 2] A reinvestigation of "β-$LiSbS_2$" shows that the correct composition is $Li_{1.250}Sb_{0.917}S_2$. The compound crystallizes in the space group R-3 (No. 148) with $Z = 18$, $a = 13.972$ Å, and $c = 9.241$ Å. The refinement converged at $R_1 = 0.0234$ and $wR_2 = 0.0529$ for all data. The purity of the sample was confirmed by powder X-ray diffraction. $Li_{1.250}Sb_{0.917}S_2$ crystallizes in an ordered NaCl superstructure. Antimony is 3+2 coordinated by sulfur. Six of these SbS_5-units arrange around a vacancy in the anion lattice, with the lone pairs of the antimony atoms pointing to the center of the vacancy, see Figure 1. Impedance spectroscopic measurements of the title compound show an ionic conductivity of $\sigma = 3.2 \times 10^{-9}\ \Omega^{-1}\ \mathrm{cm}^{-1}$ at 332 K and of $\sigma = 1.7 \times 10^{-5}\ \Omega^{-1}\ \mathrm{cm}^{-1}$ at 569 K. The activation energy is $E_A = 0.60$ eV.

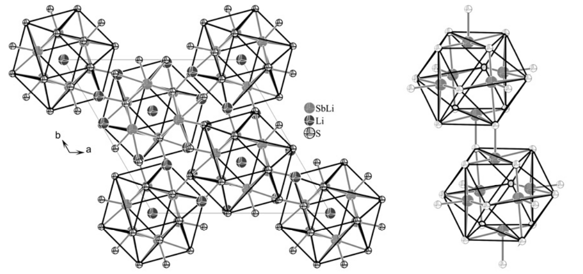

Figure 1 Unit cell projection (left) and cuboctahedral enviroment of six SbS_5-units arranged around vacancies in the anion lattice (right).

[1] J. Olivier-Fourcade, L. Izghouti, M. Maurin, E. Philippot, *Rev. Chim. Miner.* **1983**, *20*, 186.

[2] J. Olivier-Fourcade, M. Maurin, E. Philippot, *Rev. Chim. Miner.* **1983**, *20*, 196.

PS05-P62
New Sodium Ion conducting Chalcogenides - Structure analyses and Impedance Measurements of Na_3SbQ_3 - (Q = S, Se)

C. Pompe[1], A. Pfitzner[1]
[1]*Universität Regensburg, Regensburg, Germany*

The compounds Na_3SbQ_3 (Q = S, Se) were prepared by solid state reactions of stoichiometric amounts of the anhydrous sodium chalcogenides Na_2Q (Q = S, Se), antimony and the chalcogens (Q = S, Se) at 870 K.[1, 2] Crystals were obtained after annealing the samples at 720 K. The structures were determined by single-crystal X-Ray diffraction at 123 K. They crystallize in the cubic space group $P2_13$ (No.198) and are isotypic with Na_3AsS_3. For Na_3SbS_3 the cell parameters were refined to $a = 8.4620(1)$ Å, $V = 645.42(1)$ Å^3, and $Z = 4$. The structure refinement converged to $R = 0.0099$ and $wR = 0.0181$. The lattice constant and cell volume of Na_3SbSe_3 are significantly higher than in the case of the sulfide compound, *i.e.*, $a = 9.0227(2)$ Å, $V = 734.53(3)$ Å^3, and $Z = 4$ ($R = 0.0243$, $wR = 0.0475$). Three different sodium sites are coordinated by a distorted octahedral arrangement of chalcogenide atoms. These NaQ_6 polyhedra form an interpenetrating network, with SbQ_3 units acting as mono-, bi-, and three-dentate ligand, see Fig.1. Impedance measurements reveal temperature dependent sodium conductivity up to $2 \cdot 10^{-6}\ \Omega^{-1}\mathrm{cm}^{-1}$ for Na_3SbS_3 and $3 \cdot 10^{-6}\ \Omega^{-1}\mathrm{cm}^{-1}$ for Na_3SbSe_3 at 570 K.

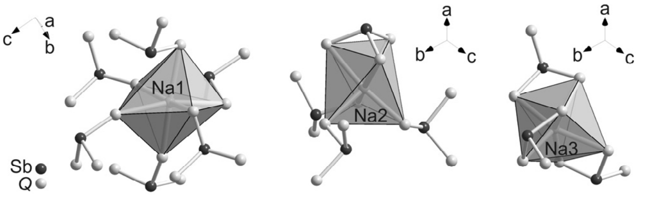

Fig1: Coordination modes for the SbQ_3-units in Na_3SbQ_3 around Na1, Na2, and Na3.

[1] H. Sommer, R. Hoppe, *Z. anorg. allg. Chem.,* **1977**, *430*, 199.

[2] C. Pompe, A. Pfitzner, *Z. anorg. allg. Chem.,* **2012**, *638*, 2158.

PS05-P63
Investigation of microscopic origin of piezoelectric effect in $Bi_{12}SiO_{20}$ single crystals

S. Gorfman[1], M. Zhao[1], A. Huesecken[1], M. Burianek[2], M. Mühlberg[2], U. Pietsch[2]
[1]*University of Siegen, Department of Physics, Siegen, Germany*
[2]*University of Cologne, Department of Physics, Cologne, Germany*

Piezoelectric effect is the generation of a dielectric polarization in response to applied mechanical stress, or, conversely, mechanical strain in response to an external electric field. The piezoelectric materials (e.g. a-SiO_2, a-$GaPO_4$ or $PbZr_{1-x}Ti_xO_3$, $Na_{0.5}Bi_{0.5}TiO_3$) are used in the number of devices such as pressure sensors, actuators, frequency controllers, etc. In spite of the great importance the number of well-studied and widely implemented piezoelectric materials is very limited. The reason for that is a little understanding of the microscopic origin of piezoelectric effect, which is mandatory for designing new materials with optimized properties.

The aim of this work is to investigate the microscopic origin of piezoelectric effect in $Bi_{12}SiO_{20}$ (BSO) single crystals. BSO belongs to one of a very few non-polar materials with high piezoelectric response (by the factor of 20 higher than that of the a-quartz). The cubic point symmetry group (*23*) of the BSO excludes the possibility of ferroelectric (ferroelastic) domains, i.e. piezoelectric effect must be purely intrinsic (lattice related). The high intrinsic piezoresponse in bismuth based materials is particularly interesting as the piezoelectric effect of the same magnitude was recently found in another (BiB_3O_6) Bi-based material. It is the second aim of this work to analyze if the property of Bi atom - the existence of a lone electron pair - is responsible for the high piezoelectric effect.

We approach the problem by investigating small electric field induced displacements of atoms and focusing on the displacements of Bi sub-lattice. We used a special X-ray diffraction based stroboscopic technique (see [1,3] for more details) to probe the tiny structural changes induced in a single crystal by electric field (the example output of the data collection is shown on Figure 1). We collected the rocking curves of a series of Bragg reflections and analyzed both macroscopic strain (by monitoring the shift of an angular position of a rocking curve) and atomic displacements (by measuring small changes in integrated intensities and structure factor analysis). The results will be discussed in the presentation.

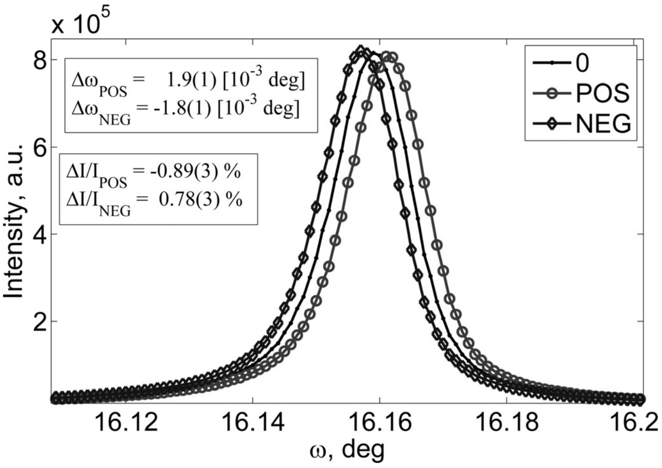

Figure 1. A typical modification of a Bragg rocking curve under applied external electric field. The right and left curves correspond to the positive and negative polarities of applied voltage, while the middle curve corresponds to the average between two zero states of the electric field. Shifts of the angular positions and relative change of intensity are extracted from the curves and analysed independently from each other.

[1] Schmidt, O., Gorfman, S., Bohaty, L., Neumann, E., Engelen, B., Pietsch, U. *Acta Cryst* **A**65, 267-275, (2009)

[2] Haussuhl, S., Bohaty, L., Becker, P. *Appl. Phys.* A 82, 495 (2006).

[3] Schmidt O., Gorfman, S., Pietsch U. *Cryst Res Technol.* 43(11), 1126 -1132

PS05-P64

Detailed studies on silicates using neutron diffraction

M. Meven[1], G. D. Gatta[2]
[1]*RWTH Aachen, Institut für Kristallographie, Aachen, Germany*
[2]*Universita` degli Studi di Milano, Dipartimento di Scienze Della Terra, Milan, Italy*

Minerals of the silicate family are is up to the present day an interesting topic of research. Various members from the epidote, lithium tourmaline and beryl group with very different crystallographic space groups were studied on the single crystal diffractometer HEIDI at the hot source of the Maier-Leibnitz Zentrum in Garching (FRM II) in the recent past. The combination of neutron and X-ray diffraction in combination with other methods revealed for each of the studied minerals - zoisite, elbaite and pezzottaite - valuable information about their structural details like its thermal evolutions, mixed occupancies or details of hydrogen bonds.

[1] F. Cámara, G.D. Gatta, M. Meven und D. Pasqual; Thermal expansion and high temperature structure evolution of zoisite by single-crystal X-ray and neutron diffraction; Physics and Chemistry of Minerals, 39(1):27-45 (2011).

[2] G. Diego Gatta, Rosa M. Danisi, Ilaria Adamo, Martin Meven und Valeria Diella; A single-crystal neutron and X-ray diffraction study of elbaite; Physics and Chemistry of Minerals, 39(7):577-588 (2012).

[3] G. Diego Gatta, Ilaria Adamo, Martin Meven und Erica Lambruschi, A single-crystal neutron and X-ray diffraction study of pezzottaite, Cs(Be2Li)Al2Si6O18, Physics and Chemistry of Minerals, (39):829-840 (2012).

PS05-P65

MTEX for Texture, Fabric, and Anisotropic Properties

H. Schaeben[1], F. Bachmann[1], R. Hielscher[2], D. Mainprice[3]
[1]*TU Bergakademie Freiberg, Institut für Geophysik und Geoinformatiki, Freiberg, Germany*
[2]*TU Chemnitz, Angewandte Funktionalanalysis, Chemnitz, Germany*
[3]*Université Montpellier 2, Geosciences Montpellier, Montpellier, France*

MTEX is a free and open-source MATLAB toolbox for texture and fabric analysis and calculations of tensor properties of 2nd, 3rd, and 4th rank. MTEX features: - all kind of symmetries, different Euler angle conventions, import from crystallographic information files (CIF); - pole figure data analysis; inversion of pole figures to an ODF for any experimental design; - EBSD data analysis; ODF estimation from EBSD data with optimized kernel width; - ODF analysis including modal orientations, volume portions, entropy, texture index, Fourier coefficients; - ODF modeling in terms of uniform, unimodal, fibre and Bingham ODFs, simulation of pole figure and individual orientation data; - grain detection, fabric analysis, misorientation analysis; - material property tensors, average tensors from EBSD data and ODFs, elastic stiffness tensor, elastic compliance tensor, Young's modulus, shear modulus, Poisson's ratio, linear compressibility, compressional and shear elastic wave velocities, wavefront velocities. Emphasis is put on the explicit statement of modeling assumptions and the unified mathematical approach applying radial basis functions and fast Fourier methods.

PS05-P66

Determination of Niobium precipitations in micro alloyed steels

I. Janßen[1], H. Klein[1], C. Klinkenberg[2]
[1]*Universität Göttingen, GZG, Kristallographie, Göttingen, Germany*
[2]*SMS Siemag AG, Düsseldorf, Germany*

Niobium micro-alloyed high strength low alloy (HSLA) steels are widely used in civil construction, automobile and line pipe applications. These steels rely on thermo-mechanical rolling, a technique that simultaneously provides high strength and toughness by grain refinement. Since these steels typically contain low carbon contents, they also have excellent welding and cold forming properties.

The most important role of niobium as a micro-alloying element in thermo-mechanically rolled steel is the retardation of austenite recrystallization, which provides more nuclei for the γ/α-Fe transformation and thus a finer grain size. Besides niobium's role in solid solution by delaying all diffusion controlled processes, its tendency to form carbides provides the dominant effect [1,2].

Depending on the hot rolling parameters, such as the deformation amount and rate, temperature and interpass time, niobium carbide precipitation is generally incomplete with regard to the thermodynamic equilibrium state. As a result, a part of the niobium stays in solid solution in the austenite phase after rolling and is effective in retarding the transformation or allowing a strong increase by precipitation hardening in the ferrite phase [3].

It is very time consuming to locate and determine the crystallographic structure of Niobium carbide precipitations using electron microscopy, because of its low Nb content (~0.05 wt. %). Hard X-ray investigations can solve this problem because of the high penetration depth and so allowing a large diffracting volume [4]. First experiments were carried out at the beam line BW5 (l=0.12 Å, ~100keV) at HASYLAB, later at the beam line P02.1 (l=0.26 Å, ~60keV) at PETRA III. In a first step commercial HSLA-steels were measured. Because of the content of other alloy elements (Ti, Mn, Si, …) it was very difficult to separate and locate the diffraction lines of the Nb-Precipitations. This was the reason to use a model-alloy consisting of iron, carbon (~0.1 wt. %) and Niobium (~0.05 wt. %). From sets of 2-dimensional area detector images - because of the preferred orientation - 1-dimensional diffraction diagrams were constructed. From these diagrams - beside the strong diffraction lines of a-Fe - peaks of Fe$_3$C and of Niobium carbides were found. Some diffraction lines of the phases overlap. For this reason a Rietveld algorithm is used to separate the lines and determine the volume fraction.

In order to follow the dissolving and forming processes of the Niobium precipitates in-situ annealing experiments were carried out in a next step.

References

[1] C. Klinkenberg, K. Hulka, W. Bleck (2004). Niobium carbide precipitation in micro-alloyed steel. Steel Research int. **75**, 1-11.

[2] M. Beres, T. E. Weirich, K. Hulka and J. Mayer (2004). TEM Investigations of fine niobium precipitates in HSLA steel. Steel Research int. **75**, 10-15.

[3] Christian Klinkenberg et al. (2010), 20 years of experience in thin slab casting and rolling state of the art and future developments . Mat. Science Forum **638-642**, 3610-3615.

[4] H. Klein (2009). Principles of highly resolved determination of texture and microstructure using high-energy synchrotron radiation. Adv. Eng. Mat. **11**, 6, 452-458

PS05-P67

Structural characterization of Cu$_2$ZnSn(S, Se)$_4$ thin films

S. Schorr[1], G. Gurieva[1], L. I. Bruc[2], D. A. Sherban[2], T. Unold[3]
[1]*Helmholtz-Zentrum Berlin für Materialien und Energie, Kristallographie, Berlin, Germany*
[2]*Institute of Applied Physics, Chisinau, Moldova, Republic of*
[3]*Helmholtz-Zentrum Berlin für Materialien und Energie, Institut für Technologie, Berlin, Germany*

The compound semiconductor Cu$_2$ZnSn(S,Se)$_4$ (CZTSSe) are promising candidates for an absorber material in 2nd generation solar cells due to their direct band gap in the range 1- 1.5 eV and high absorption coefficient (> 10^4cm^{-1}) for solar radiation in the corresponding spectral range [1,2]. All constituents of these thin films are abundant, low cost and non-toxic. The highest conversion efficiency of CZTSSe based thin film solar cells is till now 11% [3]

We will present structural investigations of CZTS polycrystalline thin films grown by different processes: physical vapour deposition (PVD-coevaporation) and spray pyrolysis. Moreover we studied CZTSe thin films, obtained by a selenization process of PVD co-evaporated CZTS thin films.

For the structural characterization we used grazing incidence X-ray diffraction (GIXRD), obtained on a PANalytical X'pert Pro MPD diffractometer eqipped with CuKα-radiation. The incident angle was chosen varied in between 0.5° and 10^{o} in order to probe different depth of the polycrystalliine thin films. The Rietveld analysis of the diffraction data was performed using the FullProf software [5]. The kesterite type structure (space group) was used as starting model for the refinement procedure.

The obtained lattice parameters and microstructural features of the thin films will be discussed with regard to the different deposition processes and probed film depth.

Financial supports from BMBF-MDA 11/002 and from FP7-PEOPLE-2010-IRSES (PVICOKEST) projects are acknowledged.

[1] J.M. Raulot, C. Domain, J.F. Guillemoles*, J. Phys. Chem. Solids* **66** (2005) 2019.

[2] P.A. Fernandes, P.M.P. Salomé, A.F. da Cunha, *Phys. Status Solidi C 7* (2010) 901.

[3] D. Aaron R. Barkhouse, Oki Gunawan, Tayfun Gokmen,Teodor K. Todorov, David B. Mitzi, *Progress in Photovoltaics: Research and Applications* **20** (2012) 6-11.

[4] A. V. Simashkevich, D. A. Sherban, L. I. Bruk, A. Coval, V. Fedorov, E. Bobeico, Yu. Usatyi, Proc. of the 20th European Solar Energy Conf. 2005, Barcelona, pp. 980-982.

[5] Juan Rodriguez-Carvajal and Thierry Roisnel,www.ill.eu/sites/fullprof/

PS05-P68

Structural Investigations of the MgO-$MgCl_2$-H_2O-CO_2 system: the Sorel Cement Phases

R. Dinnebier[1], T. Runcevski[1]
[1]*Max-Planck-Institute for Solid State Research, Suttgart, Germany*

One and half century ago it was found that high quality cement can be formed by mixing magnesium oxide with an aqueous solution of magnesium chloride.[1] This so called Sorel cement has a remarkable capacity to bond with and contain other organic and inorganic materials. In some cases, this cement has superior properties to those of Portland, namely the high fire resistance, low thermal conductivity, high resistance to abrasion etc. The main applications are ranging from grindstones, tiles, artificial stone (cast stone), cast floors, to artificial ivory (e.g. for billiard-balls).

During the binding process, ternary magnesium oxychloride phases are formed, which are of key importance for the physical properties. A detailed knowledge of the ternary phase diagram MgO-$MgCl_2$-H_2O is necessary to understand the properties and to perform any type of qualitative or quantitative phase analysis. A series of magnesium oxychloride phases have been studied by means of X-ray powder diffraction and their structures have been solved and refined. Herein we present a short overview of crystal structures present in the MgO-$MgCl_2$-H_2O-CO_2 system (Figure).[2-4]

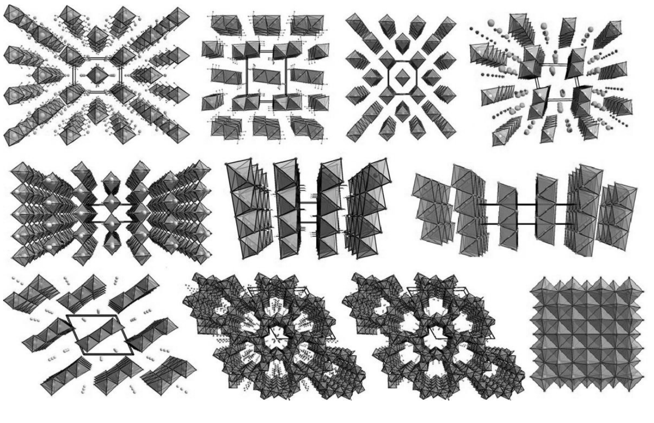

Figure: Packing diagrams of selected crystal phases in the MgO-$MgCl_2$-H_2O-CO_2 system.

References:

[1] Sorel S. *Cement. Compt Rend*, **1867**, *65*, 102.
[2] Dinnebier et al., *J. Appl. Crystallogr.* **2006**, *39*, 739.
[3] Dinnebier et al., *Acta Crystallogr.* **2006**, *63B*, 805.
[4] Dinnebier et al., *Inorg. Chem*, **2010**, *49*, 9770.

PS05-P69

Oxygen Content in $SrFeO_3$ obtained from Neutron and X-ray Powder Diffraction modeled by Distribution Functions

M. Etter[1], A. Wedig[1], D. Samuelis[1], R. Merkle[1], A. Senyshyn[2], J. Maier[1], R. E. Dinnebier[1]
[1]*Max-Planck-Institut für Festkörperforschung, Stuttgart, Germany*
[2]*Research Neutron Reactor ZWE FRM II, TU Munich, München, Germany*

Strontium ferrite ($SrFeO_{3-\delta}$) is a cubic perovskite with unordered oxygen vacancies, consisting of up to 4 different phases up to a temperature of around 300°C which can be distinguished in the way how the oxygen vacancies are ordered. These phases are $Sr_2Fe_2O_5$, $Sr_4Fe_4O_{11}$, $Sr_8Fe_8O_{23}$ and $SrFeO_{3-\delta}$[1]. Above 300°C only the cubic $SrFeO_{3-\delta}$ phase is observed in powder diffraction experiments. In our X-ray and Neutron powder diffraction experiments we controlled not only the temperature during the measurements but also the environmental pressure. In doing so we observed that the annealing time at 300°C is a crucial parameter. For a certain annealing time peak splitting for every peak (sample S1 in Fig. 1) was observed in one measurement, while for another measurement with the same annealing time a significantly peak broadening (sample S2 in Fig. 1) occurred. Both can be an indicator for a second phase or at least additional phases with different lattice parameters. The same effect also appeared in neutron measurements as can be seen in Fig. 2 with the small additional peaks.

Under the precondition that we have different phases in dependence on the oxygen content, we use successfully several numbers of Rietveld phases which are bonded together by distribution functions to model a feasible peak shape. This bonding and the use of the distribution functions was achieved by using the TOPAS macro language. As a result quantitative phase analysis can then give a weighted oxygen content.

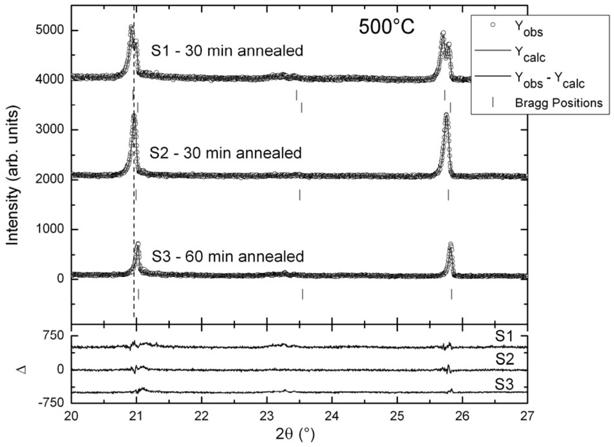

Fig 1: Laboratory X-ray powder diffraction measurements of $SrFeO_{3-\delta}$ with different annealing times and corresponding Rietveld refinements.

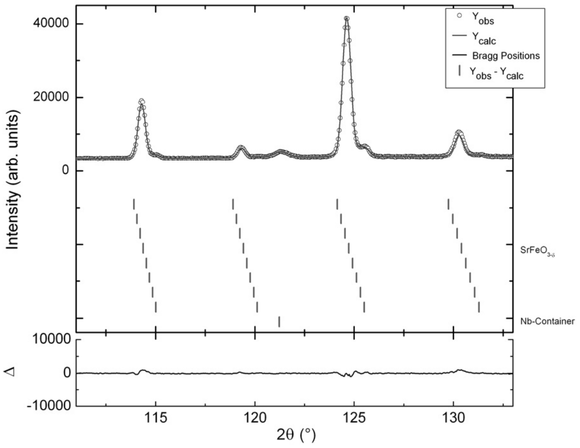

Fig 2: Neutron powder diffraction measurement of $SrFeO_{3-\delta}$ and corresponding Rietveld refinements with 8 different phases bonded together with the assumption of a Gaussian distribution.

References:

[1] **Hodges, J.P., Short, S. & Jorgensen, J.D.:**

Evolution of Oxygen-Vacancy Ordered Crystal Structures in the Perovskite Series $Sr_nFe_nO3_{n-1}$ (n=2, 4, 8, and 8), and the Relationship to Electronic and Magnetic Properties.

Journal of Solid State Chemistry, **151**, 190-209, (2000)

PS05-P70

Double-crystal-diffraction measurements of oxygen clusters in single-crystalline silicon

C. Bergmann[1], J. Will[1], A. Gröschel[1], M. Weisser[1], A. Magerl[1]
[1]Lehrstuhl für Kristallographie und Strukturphysik, Universität Erlangen-Nürnberg, Germany, Erlangen, Germany

Semiconductor-grade silicon being close to structural perfection is the basic material for nowadays integrated circuits with structural dimensions reaching the nano-regime. In Czochralski-grown single crystals, oxygen is incorporated due to the growth process which upon thermal treatment forms clusters in size range of nanometers. The investigation of such kind of defects has been carried out with various methods in the past.

Recently, new approaches to the treatment of diffraction data of lattice distortions as arising from clusters were proposed by Molodkin et al. [1]. With this approach it is possible to describe both the coherent Bragg scattering and the defect-induced diffuse scattering within a dynamical formalism. This enables one to simulate the effect of lattice distortions of various sizes on the profiles of Bragg reflections.

We present X-ray diffraction data obtained with synchrotron and laboratory sources of CZ-Si being distorted by small and medium size clusters (4nm - 25nm, compare Fig.1: line profiles of (400)-Bragg reflections of different samples). By recording the Bragg peaks with a double crystal setup, it is possible to derive information about the oxygen clusters' size, density and morphology. The data is compared with TEM measurements.

[1] V. B. Molodkin et al., Phys. Rev. B 78, 224109 (2008)

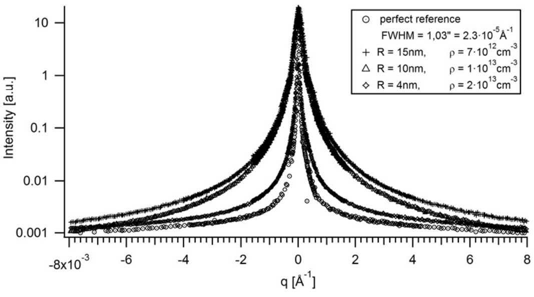

PS05-P71

Investigation of Grain Boundaries in Multi-crystalline Silicon

E.- R. Carl[1], A. N. Danilewsky[1], T. Geiger[2], E. Meißner[2]
[1]Kristallographie, Institut für Geowissenschaften, Freiburg, Germany
[2]Fraunhofer-Institut für Integrierte Systeme und Bauelementetechnologie IISB, Erlangen, Germany

Multi-crystalline silicon is one of the most important photovoltaic materials. However, its microstructure lowers the efficiency of the cells with grain boundaries and highly dislocated areas acting as effective recombination centers. This is why the main challenge is to optimize the structural properties. For this, detailed knowledge about the formation of the microstructure is needed.

Grain boundaries in multi-crystalline silicon grown by directional solidification were analyzed by means of Electron Backscatter Diffraction (EBSD) and Synchrotron X-Ray Topography (SXRT). Two nearest neighbor samples of one column were analyzed in order to get information about the development of grain boundaries during crystal growth. Thereby, the emphasis was placed on the evolution of one selected and its neighboring grains.

From the analysis of the EBSD data for the large angle grain boundaries and twins, it was found that the common interface of adjacent grains that forms the grain boundary is not correlated to the rotation axis that defines the type of boundary. The results show that the interfaces formed by lower symmetry operations are responsible for the trace of the grain boundary.

In the samples, significant changes with respect to non-"straight line" twin boundaries were found during the growth process. Grain boundaries of this type were formed or eliminated very quickly, while other types of grain boundaries experienced only small changes.

By means of SXRT, the microstructure of the analyzed grain shows numerous small-angle grain boundaries with angles in the range between 0.05 and 0.15 degrees, which is well below the EBSD angular resolution of about ± 0.5°. The experiments give evidence that the small-angle grain boundaries with larger angles extend, while the smaller ones vanished. This enlargement from 0.1° to 30° finally results in the formation of a twin boundary.

Furthermore it will be shown, that the "dislocation clusters" proposed from etch pit patterns are small angle grain boundaries with angles of 0.01 - 0.18 degrees, corresponding to a minimum theoretical dislocation density of about 10^8 cm^{-2} responsible for such a tilt value.

PS05-P72

Effect of domains on a multiferroic mineral, huebnerte (MnWO4)

S. PARK[1], D. Behal[2], U. Gattermann[1], B. Pedersen[2], C. Paulmann[3]
[1]*LMU, Geo- and Environmental Sciences, Kristallographie, Munch, Germany*
[2]*TUM, FRM II, Garching, Germany*
[3]*Univ. Hamburg, Mineralogisch-Petrographisches Institut, Hamburg, Germany*

The naturally occurring multiferroic compound huebnerite ($MnWO_4$) has three antiferromagnetic phases below 13 K [1-7]. We have intended to resolve the degree of lattice misfits at observed domain boundaries in the paramagnetic state of hübnerite at 300 K in order to check a loss of symmetry. This could be impact the appearance of antiferromagnetic transition at higher temperatures. X-ray single crystal diffraction at the beamline F1, HASYLAB equipped with a long-distance focus polarisation microscope was performed with a hübnerite thin slice cut parallel (001) to characterize the local domain boundary structure. Its three magnetic superstructures have been re-investigated with neutron single crystal diffraction data subsequently collected at RESI at FRM II. F1 data from the domain boundaries (**Figure**) showed a misorientation angle of 7°. The understanding of the presence of domains in paramagnetic state will be discussed based on results from both diffraction studies.

1. D. Khomskii (2009), Physics 2, 20
2. S.-W. Cheong & M. Mostovoy (2007), Nature materials, V6, 13-20; literatures therein
3. H. Dachs (1969), Solid St. Comm. V7, 1015-1017
4. B. Kundys et al. (2008), Phys. Rev. B77, 172402
5. G. Lautenschläger et al. (1998) Phys. Rev. B, V48, No. 9, 6089
6. Ehrenberg et al. (1997), J. Phys.: Condens. Matter 9, 3189
7. H.O. Heyer et al. (2006), J. Phys.: Condens. Matter 18, L471

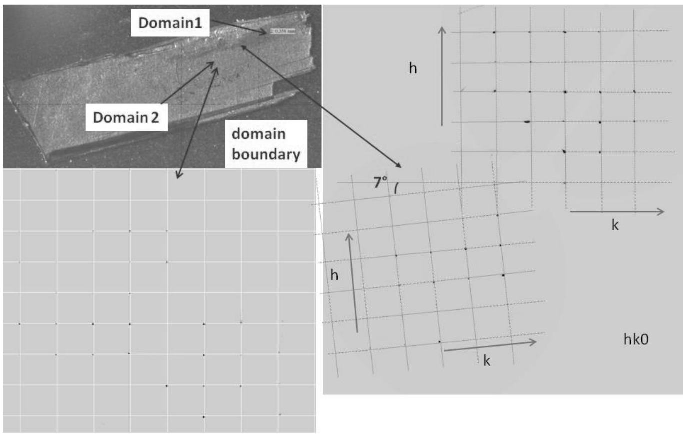

Figure Birefringence contrast between micro twins is viable within a single huebnerite ($MnWO_4$) crystal under polarisation microscope (left, top). Reconstructed reciprocal hk0 plane obtained diffraction from a single domain region (left, bottom) and from the domain boundary (right) show typical single crystal pattern and superimposed two reciprocal lattices with a misfit of 7°, respectively.

PS05-P73

Crystal Structure of $5Mg(OH)_2$-$MgSO_4$-$7H_2O$: a new Magnesium Oxysulfate Cement Phase

T. Runcevski[1], W. Chengyou[2], Y. Hongfa[2], Y. Bo[2], R. Dinnebier[1]
[1]*Max-Planck-Institute for Solid State Research, Suttgart, Germany*
[2]*Qinghai Institute of SaltLake, ChineseAcademy of Sciences, Xining, China*

Magnesium oxysulfate (MOS) cement poses light density, high resistance to fire and water, low corrosion to steal and low thermal conductivity. Accordingly, this cementitious material is widely used in the production of insulation boards and fire resistive materials. The low mechanical strength and high production cost, however, are major drawbacks in its large scale applications. Taken that the compressive strength highly depends on which MOS phases are present in the system, a systematic study of its phase diagram is needed.

Four ternary (MgO-$MgSO_4$-H_2O) phases are known to be formed in the MOS system, with chemical formulae: $5Mg(OH)_2{\cdot}MgSO_4{\cdot}3H_2O$ (5-1-3), $3Mg(OH)_2{\cdot}MgSO_4{\cdot}8H_2O$ (3-1-8), $Mg(OH)_2{\cdot}2MgSO_4{\cdot}3H_2O$ (1-2-3) and $Mg(OH)_2{\cdot}MgSO_4{\cdot}5H_2O$ (1-1-5). In addition, we report the synthesis and crystal structure of a new MOS phase, $5Mg(OH)_2{\cdot}MgSO_4{\cdot}7H_2O$ (5-1-7) which has significant influence on the mechanical properties of the MOS cement. This phase crystallizes as micro-meter sized needles (Figure 1a), its crystal structure was solved *ab initio* from X-ray powder diffraction data, using charge flipping, and refined by the Rietveld method (Figure 1b). It is characterized by one dimensional infinite chains built by three neighbouring MgO_6 octahedra and statistically distributed SO_4 tetrahedra and H_2O molecules in the interstitial space (Figure 1c).

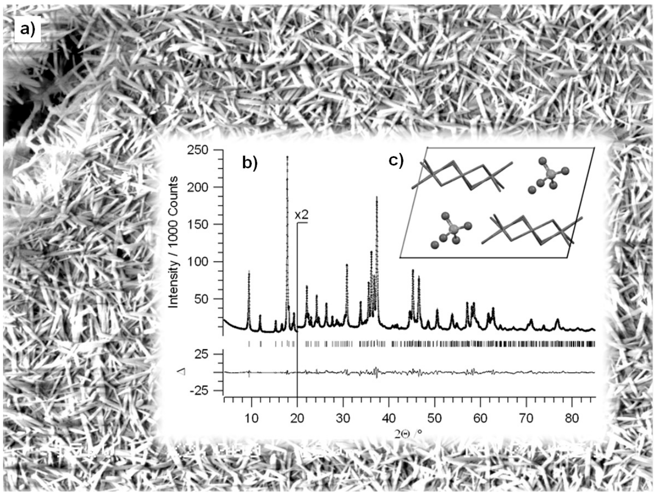

Figure1: a) SEM image, b) Rietveld plot and c) *Packing diagram of 5-1-7.*

PS05-P74
Optical characterization of the protonation and deprotonation of pyroelectric single crystals

T. Köhler[1], E. Mehner[1], J. Hanzig[1], H. Stöcker[1], D. C. Meyer[1]
[1]TU Bergakademie Freiberg, Institut für Experimentelle Physik, Freiberg, Germany

Pyroelectric crystals are used in many optical devices, therefore, understanding of structural defects is essential. It is easy to incorporate hydrogen in air-grown $LiNbO_3$ and $LiTaO_3$, however, the exact processes are only partially understood. Hence, the incorporation of hydrogen in both materials was investigated via FT-IR and UV/VIS absorption spectroscopy. Specifically the hydrogen in the congruent crystals leads to OH absorption bands with two components at 3468 cm^{-1}, 3485 cm^{-1} in $LiNbO_3$ and at 3463 cm^{-1}, 3481 cm^{-1} in $LiTaO_3$, respectively.

It is observed that the OH bands decrease in reduced and increase in protonated and reprotonated crystals. A third component at about 3500 cm^{-1} is discernible in the protonated $LiNbO_3$. Reduced crystals show no reprotonation - only in $LiNbO_3$ crystals deprotonated above 900 °C the return of the OH band was observed. Furthermore, the varying degree of reduction of the samples has influence on the absorption in the visible range. A broad band is observed in heavily reduced crystals, which is assigned to the formation of polarons [1]. The formation of polarons is different in the two material systems and shows influence on their optical behavior and their defect structure.

[1] A. Dhar, A. Mansingh. J. Appl. Phys. 1990, 68 (11), 5804-5809.

PS05-P75
Lattice controlled corrosion marks in pyrite single crystals of weathered ore veins of the polymetallic sulfide deposit of Freiberg

F. Haubrich[1], A. Kluge[2]
[1]TU Bergakademie Freiberg, Institute of Mineralogy, Freiberg, Germany
[2]TU Bergakademie Freiberg, Universitaetsrechenzentrum, Freiberg, Germany

Pyrite crystals from the weathering zone of the polymetallic sulfide deposit of Freiberg show microscopic rhombic and hexagonal corrosions marks mirroring [100] and [111] crystal faces. The corroded crystals were in contact with acid mine drainage (AMD) of pH values between 0.7 to 2.4, and $E_H > 750mV$. Experiments on corrosion of fresh pyrite crystals by AMD yielded equal corrosion marks after 3 months of exposure. It remains unclear whether the corrosion marks are developed by sterile attack of Fe^{3+} ions and/or microbial mediated processes.

PS05-P76
Structure and thermal behaviour of a new Zn^{II} squarate complex, $[Zn(HC_4O_4)_2(OH_2)_4]$

F. Dumitru[1], M.- D. Şerb[1], B. Braun[2]
[1]Politehnica University of Bucharest, Bucharest, Romania
[2]Humboldt-Universität zu Berlin, Institut für Chemie, Berlin, Germany

Metal carboxylates represents a class of compounds extensively studied both with regard to fundamental scientific aspects and to application-oriented problems. Among metal carboxylates, the simplest metal formates, acetates and oxalates have been more intensely investigated but other unsaturated and aromatic carboxylates such as squarate have gained increased importance in the last decades. Squaric acid, with versatile modes of coordination, is a suitable ligand for the design and construction of metal-organic coordination polymers, which exhibit structures of various topologies.

As part of a project focused on coordination polymers, a new Zn^{II}-squarato complex: $[Zn(HC_4O_4)_2(OH_2)_4]$, has been synthesized and its thermal behavior is reported here.

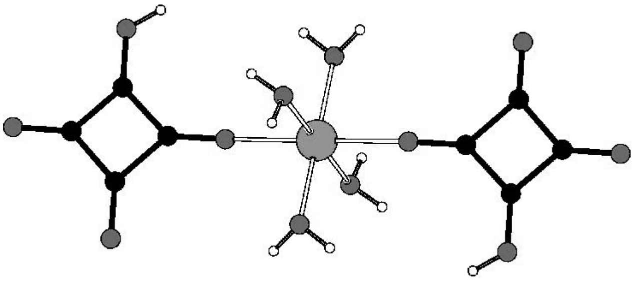

The complex $[Zn(HC_4O_4)_2(OH_2)_4]$ crystallizes in the space group *P-1*. In the crystal structure of the complex, the Zn^{II} ion is in a distorted octahedral coordination geometry composed of six O atoms, two from the monodentate squarato group and four from water molecules.

TG/DSC measurements were performed in the air atmosphere under dynamic conditions. Their results indicate dehydration in a first step (99-121ºC) and decomposition in two subsequent steps (178-214ºC; 390ºC); the total weight loss of 78.1% corresponds to the formation of ZnO.

The authors acknowledge financial support from the European Social Fund through POSDRU/89/1.5/S/54785 project: ‘Postdoctoral Program for Advanced Research in the field of nanomaterials’.

X. Solans, M. Aguilo, A. Gleizes, J. Faus, M. Julve, M. Verdaguer, Inorg. Chem. 1990, 29, 775.

M.-D. Şerb, M. Speldrich, H. Lueken, U. Englert, Z. Anorg. Allg. Chem., 2011, 637, 536.

Y. Wang, M. Şerb, U. Englert, Struct. Chem., 2010, 21, 203.

PS05-P77

Very short intermolecular hydrogen bonds in a tren:hydrogen succinate salt

M.- D. Şerb[1], F. Dumitru[1]
[1]*Politehnica University of Bucharest, Bucharest, Romania*

Hydrogen bonds represent probably the most widely used interactions in crystal engineering and are intensively exploited to generate supramolecular systems by design.

We are interested in supramolecularly hydrogen-bonded systems formed by organic amines and dicarboxylic acids. Succinic acid can act both as a donor as well as an acceptor for hydrogen bonding. Bases such as *tren* = tris(2-aminoethyl)amine represent interesting partners for dicarboxylic acids: They incorporate multiple sites that can donate or accept hydrogen bonds, thereby directing molecular recognition and association.

In the solid state, the title compound consists of one cation and three monanions as shown in the scheme below.

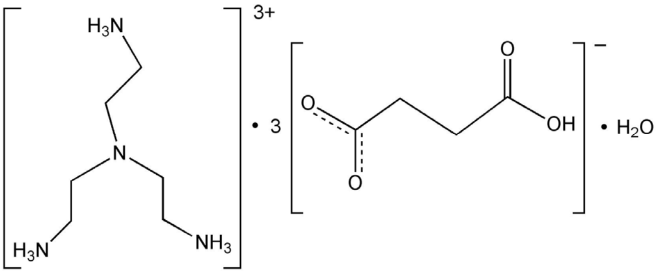

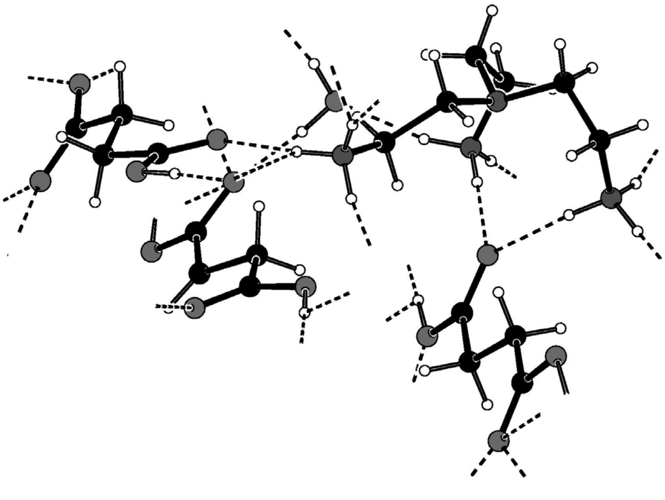

The above mentioned system with very short O-H---O bonds (D---A< 2.5 Å: d_1(O···O) = 2.4408(18) Å; d_2(O···O) = 2.4688(17) Å; d_3(O···O) = 2.4848(17) Å) represents an ideal candidate for neutron diffraction and high resolution X-ray diffraction.

The authors acknowledge financial support from the European Social Fund through POSDRU/89/1.5/S/54785 project: 'Postdoctoral Program for Advanced Research in the field of nanomaterials'.

Braga, D., Maini, L., Polito, M., Tagliavini, E. & Grepioni, F. (2003). Coord. Chem. Rev. 246, 53-71.

Prins, L. J., Reinhoudt, D. N. & Timmerman, P. (2001). Angew. Chem.Int. Ed. 40, 2382-2426.

Roesky, H. W. & Andruh, M. (2003). Coord. Chem. Rev. 236, 91-119.

Şerb, M.-D., Wang, R., Meven, M., Englert, U. (2011), Acta Cryst., B67, 552-559.

PS06 - Cutting edge Techniques in Analysis and Preparation

PS06-P01

X-ray powder diffraction analysis of disordered dioctahedral Si-Al layer silicates by the Rietveld method and a recursive method for modeling stacking faults

K. Ufer[1], R. Kleeberg[2]
[1]*BGR/LBEG, Hannover, Germany*
[2]*TU Bergakademie, Mineralogy, Freiberg, Germany*

Minerals like the 1:1 layer silicate kaolinite, $Al_4Si_4O_{10}(OH)_8$ or the 2:1 layer silicate pyrophyllite, $Al_2Si_4O_{10}(OH)_2$ occur in natural environment commonly in a wide variability of disorder, mainly caused by faults in layer stacking. The types of disorder in natural kaolinites have been well investigated by modeling of the diffraction patterns using the explicit calculation method (Drits & Tchoubar, 1990, and citations herein). The models commonly used consist in different stacking of layers having vacant B or C octahedral sites (kaolinite) or different translation directions of identically oriented layers (pyrophyllite, Kogure et al., 2006). Such stacking models have been adapted for the use in a recursive calculation (Treacy et al., 1991) within the structure description language of the Rietveld program BGMN (Bergmann et al., 1998). This approach has been found to be suitable for the successful fitting of diffraction patterns of several natural minerals. The X-ray powder diffraction patterns of disordered kaolinites may be modeled by a statistical stacking of B and C layers. In agreement with Drits & Tchoubar (1990), the "better ordered" varieties of natural kaolinites could not described by a single model. A combination of a defective B-layer stacking and a nearly ideally stacked structure modes has been found to be able to fit a number of kaolinitic materials. This two-phase approach was successfully tested for the quantification of kaolinite in several mineral mixtures.

Bergmann, J., Friedel, P., and Kleeberg, R. (1998) BGMN, a new fundamental parameter based Rietveld program for laboratory X-ray sources, its use in quantitative analysis and structure investigations. CPD Newsletter, Commission of Powder Diffraction, International Union of Crystallography, 20, 5-8.

Drits, V.A. and Tchoubar, C. (1990) X-ray Diffraction by Disordered Lamellar Structures. Springer-Verlag, Berlin,Heidelberg.

Kogure, T., Jige, M., Kameda, J., Yamagishi, A., Miyawaki, R., and Kitagawa, R. (2006) Stacking structures in pyrophyllite revealed by high-resolution transmission electron microscopy (HRTEM). American Mineralogist, 91, 1293-1299.

Treacy, M.M., Newsam, J.M., and Deem, M.W. (1991) A General Recursion Method for Calculating Diffracted Intensities From Crystals Containing Planar Faults. Proceedings of the Royal Society of London, A433, 499-520.

PS06-P02
New abilities and performance of neutron powder diffraction at E9

A. Franz[1], D. M. Többens[1], M. Tovar[2]
[1]*Helmholtz-Zentrum Berlin für Materialien und Energie, Department Crystallography, Berlin, Germany*
[2]*Helmholtz-Zentrum Berlin für Materialien und Energie, Institute for Complex Magnetic Materials, Berlin, Germany*

The fine-resolution neutron powder diffractometer E9 [1] at the BER II reactor at the Helmholtz-Zentrum Berlin für Materialien und Energie [2] has undergone major alterations, which improved both the performance and the flexibility of the instrument. The new detector bank consists of eight individual 2D detectors, arranged at an optimized, non-constant distance from the sample, and a radial collimator to reduce background noise. Position-sensitive data integration results in a strongly reduced asymmetry of the peaks. The foremost result of the upgrade is an intensity increase by factor 5. Through the choice of sample diameter, axial focus length, and primary collimation a wide range of combinations of intensities, resolution curves, and sample volume can be obtained.

In its default mode, the instrument is dedicated to collect diffractograms suited for crystal structure determinations and Rietveld refinements. In example, hydrogen positions in zeolites or metal-organic framework structures can be determined from fast measurements. This is especially interesting when combined with the new option to equip more than 10 different gas-adsorption modules, covering a wide pressure and temperature range from 4 K to 1500 K and up to 10000 bar. Possible load gasses include nitrogen, hydrogen, heavy hydrogen, argon, helium, vapour and chemisorption.

Additionally, four of the individual detectors can be placed closer to the sample, for higher intensity and coverage of large angular ranges. This is useful for data collection with fixed detector position, allowing for rapid parameterized scans, e.g. the temperature dependency of cavity fillings or phase transitions. In example, structural, magnetic and magnetostrictive phase transitions could be analysed using data collection times of only 10 minutes per temperature step, measuring low angle magnetic peaks with high intensity, while simultaneously measuring peak shifts from magnetostriction with high resolution at high diffraction angles.

Of course, the upgraded instrument still allows the use of the usual suit of sample environments, covering a wide range of low and high temperatures (1.5 - 2000 K), pressure (up to 2.5 kbar), variable magnetic fields (up to 5 T). With BER II back in operation, E9 is now once again open to applications [2] from external users.

[1] D. M. Többens et al., Mat. Sci. Forum. 378-381, 288 (2001)

[2] Helmholtz-Zentrum Berlin für Materialien und Energie, http://www.helmholtz-berlin.de

PS06-P03
DIFFaX-Analyses of faulted phases like $Ni(OH)_2$ with a MATLAB^{TM}-based software tool

B. Priehs[1], J. Birkenstock[1]
[1]*Universität Bremen, Bremen, Germany*

XPRD data of nickel hydroxide samples have been collected with a Bruker D8 Advance diffractometer. The nickel hydroxide samples, kindly provided by P. Vishnu Kamath, were synthesized by Ramesh et al, 2006 to generate samples with different amounts of stacking faults. The attempt of reproducing the results has been made in order to gain knowledge of the nature and simulation of XRPD patterns faulted crystals.

The DIFFaX computer program (Treacy et al, 1991) constitutes an excellent tool for simulating XRPD patterns of layered materials with planar faults. DIFFaX lacks a profile-refinement environment and thus only enables a qualitative comparison between observed and calculated patterns. A software tool, using MATLAB^{TM}, was programmed that allows for fitting of the scaling factor as well as for the correction of background and zero point offset (ZPO). In the $Ni(OH)_2$ analyses, the scaling factor was fitted by using the integrated intensity of the (001) reflection. The background was corrected using the spline interpolation function implemented in MATLAB^{TM}. The ZPO was corrected by shifting the simulated pattern incrementally along 2θ and calculating the R_{wp} between observed and calculated pattern.

Additionally, the program generates complete series of structure files with incrementally changing fault probabilities. The results of the simulation series can be compared with the observed patterns and be evaluated using R_{wp} values as well as graphical inspection.

The application of the software to extensively faulted clay minerals such as kaolinite, montmorillonite or nontronite is in progress. It is also intended to implement a least-squares algorithm to further accelerate the analyses and extend its applicability, with a similar approach as used in the program DIFFaX+ written by Leoni et al., 2004.

Ramesh, T. N., Vishnu Kamath, P., Shivakumara, C. (2006). *Classification of stacking faults and their stepwise elimination* *during the disorder à order transformation of nickel hydroxide.* Acta Cryst. B62, 530-536.

Treacy, M. M. J., Newsam, J. M., Deem, M. W. (1991). *A general recursion method for calculating diffraction intensities from crystals containing planar faults.* Proc. R. Soc. London Ser. A, 433, 499-520.

Leoni, M., Gualtieri, A.F., and Roveri, N. (2004). *Simultaneous refinement of structure and microstructure of layered materials.* Journal of Applied Crystallography, 37, 166-173.

PS06-P04
Analysis of 2D diffraction data for the fast determination of crystallite size distributions

S. Neher[1], M. Chaouachi[1], H. Klein[1], W. F. Kuhs[1]
[1]Universität Göttingen, GZG Abt. Kristallographie, Göttingen, Germany

While diffraction data from 2D detectors are routinely used nowadays for both standard single crystal and powder structural analysis there is some considerable potential also for the analysis of polycrystalline materials. Here we describe our novel approach to extract crystallite size distributions (CSDs) of powders and polycrystalline materials, which we like to call *fast diffraction CSD analysis*. In an accompanying paper (1) we show the importance of CSD for material science, in particular for samples where the widespread (electron-) optical methods are not suitable or for *in-situ* investigations of changing CSDs and give examples of the application of this method. Here we concentrate on the description of the method of intensity extraction from 2D detector data from both, laboratory and synchrotron sources. At the basis of our approach are 2D diffraction data from powders or polycrystalline aggregates with separated Bragg diffraction spots on the Debye-Scherrer rings. Two extraction methods are described: (1) 2D-analysis of one frame obtained by an omega-rotation of a few degrees, (2) 3D-analysis of a stack of 2D frames obtained by stepping in omega. The intensity extraction is handled by the interpreter programming language Python (2) using an integrated development environment in the following steps: (i) selection of the Debye-Scherrer ring of interest, (ii) thresholding (with respect to background), (iii) peak detection in the pre-selected Debye-Scherrer ring, (iv) if necessary peak separation for partly overlapping peaks by a watersheding algorithm and (v) assignment of Bragg spot objects and (vi) Bragg intensity extraction. Given that a representative number of crystallites has been measured via their Bragg diffraction spots, the unknown CSD of the material under investigation can be established *via* a calibration using a material with known CSD, measured under identical conditions. Examples for the intensity extraction procedures will be given for diffraction data from a Bruker APEX II CCD-detector on a laboratory X-ray source as well as from a PerkinElmer XRD 1622 detector installed at PETRA/ DESY/ Hamburg. The advantages of the more involved 3D-analysis will be demonstrated.

1. M Chaouachi, S Neher, S Stracke, A Falenty, H Klein, and WF Kuhs (this conference)

2. available athttp://www.python.org

PS06-P05
Neutron radiography: a quantitative tool to study dehydration of bentonite bonded molding sand

G. Jordan[1], C. Eulenkamp[1], E. Calzada[2], B. Schillinger[2], M. Hoelzel[2], W. W. Schmahl[1]
[1]LMU, Dept. Geo Umwelt, München, Germany
[2]TUM, FRM II, Garching, Germany

Bentonite bonded quartz sand is one of the most common mold materials used by the casting industry. In comparison to other mold materials, bentonite bonded molding sands are excellent regarding sustainability and reusability. However, the reusability of bentonite bonded mold material is still limited. A continuous reuse of the material leads to a noticeable decrease in its bonding quality. In order to investigate the causes of the decrease of bonding quality, the dehydration behavior of molding sands induced by thermal impacts has been studied with neutron radiography. Neutron radiography records the attenuation of a neutron beam radiating through a material with a CCD sensor. Because water has a high neutron attenuation coefficient, a change in the local water concentration within the radiographed material results in a change of the image grayscales obtained by the CCD sensor.

The image greyscales of radiographed molding sand can be converted into absolute water concentrations. The conversion requires a normalization of the greyscales with respect to the maximum beam intensity, the background intensity, and the temporal intensity variations. Relating these normalized values to fully dehydrated molding sand as a reference yields the absolute water concentration within the radiographed mold material.

Data of local water concentrations were obtained in-situ during dehydration of pure mixtures of quartz, bentonite, and water. These data were compared to the data of identical mixtures which previously were subject to four dehydration-rehydration cycles. The data indicate that dehydration kinetics is dominated by material compaction and that a potential decrease in bonding quality may likely be a consequence of industrial conditions rather than intrinsic properties of the pure bentonite.

PS06-P06
Complete characterization MOFs using CCD and CMOS detector based SC-XRD systems

A. Gerisch[1], M. Adam[1], I. Eryazici[2], O. K. Farha[2], E. Hovestreydt[1], H. Ott[1], M. Ruf[1], A. A. Sarjeant[2], K. Yoza[1]
[1]Bruker AXS, Karlsruhe, Japan
[2]Northwest University, Department of ChemistryChemistry, Evanston, United States

Metal Organic Framework (MOF) structures are well known for their many interesting applications, such as gas storage and separation, chemical sensing, and catalysis [[i]]. The same structural features that allow for such excellent chemical properties [[ii]] cause difficulty in characterization by crystallographic methods. Owing to the highly porous nature of MOFs, crystalline samples tend to lose solvent rapidly, degrading the quality of diffraction. Additionally, a high degree of disorder over long ranges frustrates single crystal structure determination efforts.

In assessing the suitability of a certain MOF system for various applications, it is necessary not only to elucidate the structural features via single-crystal diffraction, but also to confirm the purity of the bulk sample by comparative PXRD techniques. In order to completely characterize difficult MOF samples, we have investigated the complementary techniques of single crystal and powder diffraction utilizing single crystal diffractometers equipped with APEX II CCD detectors.

Very recently, the D8 CRYSTALLOGRAPHY SOLUTIONS family became available addressing the MOF specific demands for high-end in-house instrumentation even more efficiently. These systems feature the latest generation of microfocus X-ray sources, X-ray optics and dedicated software. However, the most significant contribution to the improved data quality, typically resulting in lower R-values, often observed within a shorter exposure time, can be assigned to the CMOS-based PHOTON 100 detector.

A number of successful investigations, including two highly porous MOF-structures based on the hexacarboxylic acid ligand LH_6 will be presented [[iii]]. Details on the structure solution and the comparison of SC-XRD and XRD data will be discussed.

[[i]] (a)Murray, L. J.; Dinca, M.; Long, J. R. *Chem. Soc. Rev.* **2009**, *38*, 1294-1314. (b) Li, J.-R.; Kuppler, R. J.; Zhou, H.-C. *Chem. Soc. Rev.* **2009**, *38*, 1477-1504. (c) Allendorf, M. D.; Bauer, C. A.; Bhakta, R. K.; Houk, R. J. T. *Chem. Soc. Rev.* **2009**, *38*, 1330-1352; (d) Kreno, L. E.; Hupp, J. T.; Van Duyne, R. P. *Anal. Chem.* **2010**, *82*, 8042-8046. (e) Lee, J.-Y.; Farha, O. K.; Roberts, J.; Scheidt, K. A.; Nguyen, S. T.; Hupp, J. T. *Chem. Soc. Rev.* **2009**, *38*, 1450-1459; (f) Ma, L.; Abney, C.; Lin, W. *Chem. Soc. Rev.* **2009**, *38*, 1248-1256.

[[ii]] (a) Ferey, G. *Chem. Soc. Rev.* **2008**, *37*, 191-214; (b) Tranchemontagne, D. J.; Mendoz-Cortes, J. L.; O'Keeffe, M.; Yaghi, O. M. *Chem. Soc. Rev.* **2009**, *38*, 1257-1283.

[[iii]] Eryazici, I.; Farha, O.K.; Hauser, B.G.; Yazaydın, A.Ö.; Sarjeant, A.A.; Nguyen, S.T.; and Hupp, J.T. *Cryst. Growth Des.* **2012**, *12*, 1075-1080.

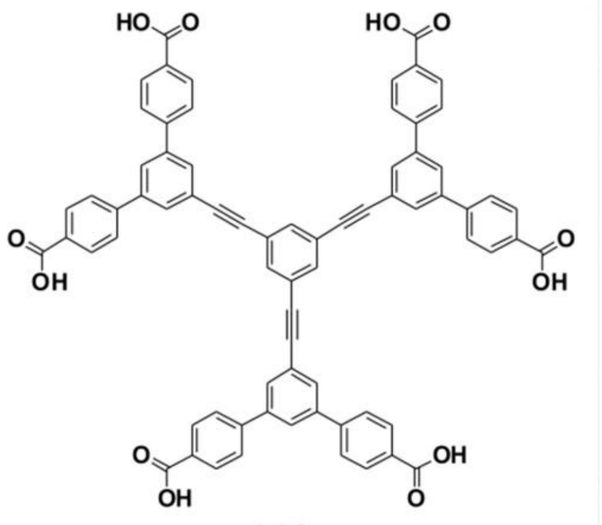

LH_6

PS06-P08

Serial femtosecond X-ray crystallography of *in vivo* crystallized proteins opens new routes in structural biology

L. Redecke[1,2], K. Nass[3,4], D. P. DePonte[3], D. Rehders[1,2], T. A. White[3], A. Barty[3], F. Stellato[3], M. Duszenko[3], H. N. Chapman[3,4], C. Betzel[5]
[1] *Universities Hamburg and Lübeck c/o DESY, Joint Laboratory for Structural Biology of Infection and Inflammation, Hamburg, Germany*
[2] *University of Lübeck, German Centre for Infection Research, Lübeck, Germany*
[3] *Centre of Free-Electron Laser Sciences (CFEL) , Hamburg, Germany*
[4] *University of Hamburg, Department of Physics, Hamburg, Germany*
[5] *University of Hamburg, c/o DESY, Institute of Biochemistry and Molecular Biology, Hamburg, Germany*

Protein crystallization within living cells has been observed several times in nature, e.g. for storage proteins in seeds. *In vivo* crystal growth can also occur spontaneously during over-expression of proteins, as reported for the baculovirus/Sf9 insect cell system. However, *in vivo* grown crystals were not considered for structural biology so far, largely attributed to the small crystal size.

We observed spontaneous crystallization of cathepsin B from *Trypanosoma brucei* (TbCatB) within insect cells (1). Since this cysteine protease is involved in host protein degradation by the parasite, it is a promising target to develop new treatments against sleeping sickness. The emerging technique of free-electron laser (FEL)-based serial femtosecond crystallography (SFX) (2) was applied on isolated TbCatB *in vivo* crystals injected across the pulsed laser beam. The collected and combined single-pulse diffraction pattern allowed the elucidation of the room-temperature 2.1 Å resolution structure of the fully glycosylated precursor complex (3), revealing the mechanism of native TbCatB inhibition that may aid the design of specific inhibitors.

Our study demonstrates for the first time that new high-resolution biomolecular information can be obtained by the “diffraction-before-destruction” approach of x-ray FELs from hundreds of thousands of individual crystals. Moreover, we show that *in vivo* grown crystals are suitable targets for structural biology applying

SFX, which offers exciting new possibilities for proteins that do not form crystals suitable for conventional X-ray diffraction *in vitro*.

(1) R. Koopmann*, K. Kupelli*, L. Redecke* *et al*. *Nat. Methods* **9**, 259-262 (2012).
(2) H.N. Chapman *et al*. *Nature* **470**, 73-77 (2011).
(3) L. Redecke*, K. Nass* *et al*. *Science* **339**, 227-231 (2013).

PS06-P09

High-Efficiency Laboratory GISAXS Instrument and its Applications

Paul Pennartz, Lixin Fan, Mike Degen, Nick Grupido
Rigaku Innovative Technologies Inc., Auburn Hills, MI 48326, USA

P. U. Pennartz[1]
[1] *Rigaku, Eschweiler, Germany*

GISAXS experiments have commonly been implemented on SAXS cameras with a sample stage that allows reflection mode. The Rigaku SAXS instrument S-MAX-3000 with a dedicated GISAXS sample stage provides excellent GISAXS capabilities. This instrument is designed for working with various types of X-ray sources including rotating anode and microfocusing sealed tube source for your own choice. The source, coupled with a confocal multilayer focusing optic, yields a high intensity X-ray beam spot. Combining this intense beam with three-pinhole collimation, a fully evacuated beam path and a photon-counting MWPC detector, this instrument is capable of making highly sensitive GISAXS measurements from both isotropic and anisotropic materials without needing desmearing corrections. Recently, additional capability is added by replacing the MWPC with a comparably sized pixelated detector, such as the Pilatus 300K or scanning a smaller pixelated detector, such as the Pilatus 100K. Three types of GISAXS stages are available. A high weight capacity stage provides better than 5 arc second angular precision and motion ranges of ±8^o in plane, ±10^o out of plane and ±12.5mm vertical. The high weight capacity can be utilized to support in-situ vessels or samples of all types. A high precision stage is available with sub-arc second motion but lower weight capacity. The GI-V stage has the capabilities of the high weight capacity stage and except that the out-of-plan stage is replaced with sample rotation. All stages are fully automated. The zero incident angles can be precisely and automatically determined using software. New beamstop setup allows minimum beam alignment and simple and fast exchange between SAXS and GISAXS measurements. High throughput GISAXS data can be collected automatically using software. A second optional sample chamber allows access to a middle Q range without moving the detector or realigning the beam. The Rigaku S-Max3000 is capable of characterizing a large variety of materials, ranging from colloids of all types, cements, nanoparticles, oils, polymers, plastics, proteins, surfactants, foods and pharmaceuticals. In this presentation, we demonstrate its GISAXS capabilities in studying various materials. The structural morphology from weak scattering polymer thin films can be determined using this laboratory setup.

PS06-P10

The new Kappa-diffractometer at beamline P24 (ChemCryst, PetraIII.14, Hasylab/Desy)

C. Paulmann[1], A. Berghäuser[1], D. Ropers[1], U. Bismayer[1]
[1] *Mineralogisch-Petrographisches Institut, Universität Hamburg, Hamburg, Germany*

The shutdown of DORIS III discontinues some successful beamlines (eg. F1, D3, BW1) which served as main stations for a wide field of crystallographic applications ranging from diffuse scattering studies, charge density analysis, phase transitions, disordered and modulated structures all at ambient and non-ambient conditions. As result of a joint research BMBF project (coordination: University Hamburg) to build up a new beamline at PetraIII.14 dedicated to all fields of crystallographic research, layout and specifications for a new diffractometer were defined and a european call for tenders was placed in spring 2012. The diffractometer (Fig. 1) is in production process and delivery to Desy is expected in summer 2013.

The four-circle diffractometer (ca. 3.5 tons), designed in Kappa-geometry, offers two independent detector circles able to take loads of 30 kg each equipped with motorized counter-weights to balance a detector travel of 500 mm. The sphere of confusion (SOC) of the main circles (incl. Omega) for multi axis movements is below 10 µm and repeatability below 2x10^{-4} degrees. The inner circles (Kappa, Phi) provide a SOC below 25 µm for loads up to 5 kg with a maximum load of 10 kg. The Phi circle includes a motorized xyz-stage offering an accuracy in the micrometer range. The available space for sample environments is 190 mm, extendable to 250 mm by removing the stage. In combination with a modular mounting system, an easy exchange of different detectors, sample environments or microscopes is possible. A high-precision secondary optics system (slits, collimator) including a millisecond shutter system is under development.

The diffractometer will be installed with a short undulator (N < 20) as source, optimized for energies in the range of 17 to 40 keV using a CEMO-type water-cooled DCM (Si111/Si311). Options are designated to upgrade to a standard PetraIII-type undulator in combination with a cryo-cooled monochromator. The preliminary optics layout will consist of the following parts (downstream): 1. Horizonally focusing CRLs (>25 keV), 2. CEMO-type DCM, 3. Horizontally focusing mirror (< 25 keV), 4. Bendable plane mirror (vertical focusing), 5. (Rotatable) CRLs for final focusing. The optic specifications will be laid out to give a (collimated) homogenous beam of 0.3 mm².

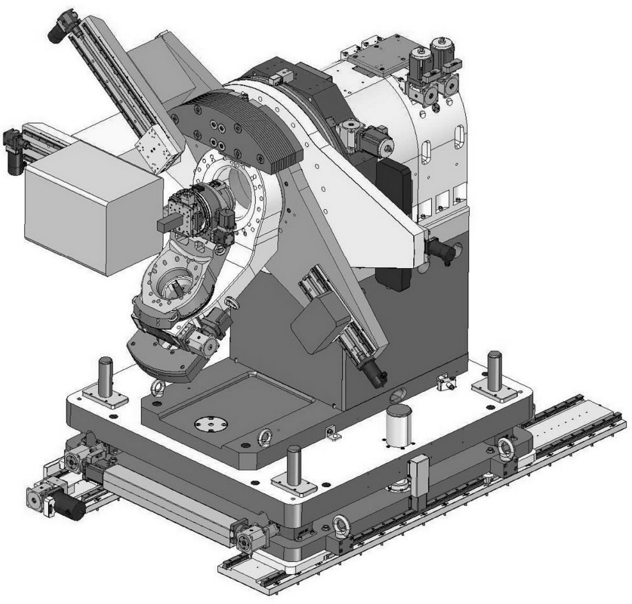

PS06-P11

Multi-purpose X-ray diffractometer platform with versatile SAXS / WAXS options

J. Bolze[1], V. Kogan[2], D. Beckers[1], P. Munk[1], M. Fransen[1]
[1]*PANalytical B.V., Almelo, Netherlands*
[2]*DANNALAB B.V., Enschede, Netherlands*

A multi-purpose laboratory X-ray diffractometer is used as a platform for SAXS and WAXS measurements. The modular concept of the instrument uses pre-aligned optical components and sample stages and thus allows for a quick and easy reconfiguration for a wide variety of applications. Besides SAXS/WAXS options, these include powder X-ray diffraction, pair distribution function (PDF) analysis, stress and texture measurements, X-ray reflectivity, grazing incidence diffraction as well as computed tomography (CT).

For the SAXS/WAXS setups one can choose among various incident beam optics (focusing and parallel beam mirrors or slit collimation system), sample stages and detectors. The highest performance can be achieved with a solid state pixel detector (PIXcel^{3D}) that excels by a high linearity and dynamic range, and by a very small point spread function of only 55 µm. The latter, when combined with a focusing X-ray mirror, allows for a rather compact SAXS setup. WAXS data can be collected within a very wide angular range by making use of the 2Theta arm of the goniometer. For data reduction and analysis comprehensive SAXS software (EasySAXS®) has been developed. Its graphical user interface facilitates easy and efficient operations.

In this contribution we will give an overview and comparison of the various experimental setups and show typical SAXS / WAXS measurement data and analysis results obtained from different nanostructured materials. An overview about the functionalities of the SAXS data analysis software will also be given.

PS07 - General Crystallography: Modelling and Analysis Bridging the Scales

PS07-P01

INVESTIGATION OF THE STRUCTURE OF NANOSIZED Na_nCl_n (n = 4, 8, 12, 16) CLUSTERS USING GLOBAL OPTIMIZATION

J. Zagorac[1,2], C. J. Schoen[1], M. Jansen[1]
[1]*Max Planck Institute, Solid State Research, Stuttgart, Germany*
[2]*Institute of Nuclear Sciences Vinca, Materials Science Laboratory, Belgrade, Germany*

The structure and stability of alkali halide clusters has long been a focus of research in an effort to understand crystal growth. In our study, several global optimization methods have been applied to determine both the global and metastable minima of Na_nCl_n (n = 4, 8, 12, 16) clusters. Global search for local minima was performed using stochastic (Monte Carlo) moves simulated annealing (SA) and multiquench (MQ) where both single and multi-atom moves were used to generate new atom configurations. As energy function, empirical potentials (Lennard-Jones + Coulomb terms) were employed. For SA, the temperature schedule was defined as: T_n = (decrease) × T_{n-1}; nTmax = number of temperature adjustements; stepsmax = number of Monte Carlo moves at each temperature. For MQ, one alternates short random walks at $T = \infty$ and quenches ($T = 0$). The schedule is defined by the parameters: tnum = number of steps for each random walk; mqnum = number of quenches and mqloop = number of blocks. Each block consists of mqnum quenches and (mqnum - 1) heating phases. Following moves were applied: displacement of individual atoms (move 1); exchange of atoms (move 2); shift of cell vector with adjustement of atom positions (move 3) and shift of cell vector without adjustement of atom positions (move 4). Both the moveclass (i. e. the percentage of the moves) and the temperature (control parameter) schedule of the optimization algorithm were systematically varied. For the larger clusters (n = 12, 16), the multiquench method found on average lower energy minima than simulated annealing (Fig. 1). For SA, decrease = 0.99; Tinit = T_0 = 0.1; nTmax = 1000; stepsmax = 1000; moveclass: 90 % move 1 + 5 % move 3 and 5 % move 4 parameters gave the best energies for all cluster sizes. For MQ, tnum = 1000; mqnum = 20; mqloop = 40; and 100 % move 1 gave the best energies for clusters with 8 and 16 atoms. tnum = 10; mqnum = 40; mqloop = 20; moveclass: 90 % move 1 + 5 % move 3 and 5 % move 4 gave the best energies for clusters with 24 and 32 atoms. The most relevant lowest-energy structures for the Na_nCl_n clusters are visualized (Fig. 2) and analysed with the structure drawing and analysis program KPLOT where we analyze the degree to which the clusters found resemble cut-outs of bulk NaCl using the CCL (compare cluster) algorithm [1].

[1] R. Hundt, J. C. Schön, S. Neelamraju, J. Zagorac and M. Jansen, J. Appl. Cryst., submitted.

Cluster size	8	16	24	32
SA	-2.435249	-2.670798	-2.726342	-2.785314
MQ	-2.435249	-2.670798	-2.728406	-2.809213

Fig 1. Comparison of the best energies (eV per atom) obtained via SA and MQ methods.

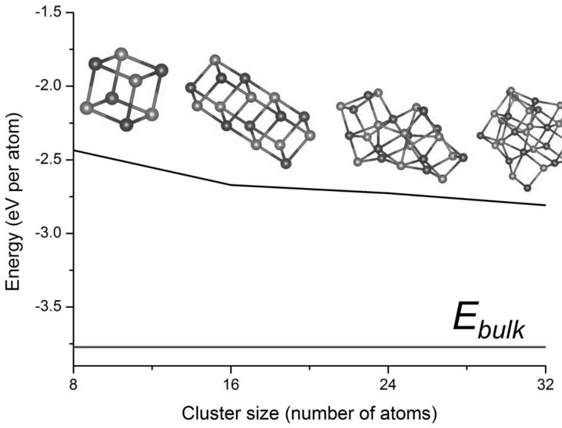

Fig. 2. Lowest energy vs. cluster size.

PS07-P02

Mosaic Structure of Single Crystals: Investigation of Mosaicity and Anisotropy of Pyrite.

A. K. Hüsecken[1], S. Gorfman[2], U. Pietsch[2]
[1]*Universität Siegen / DELTA, Physik, Dortmund, Germany*
[2]*Universität Siegen, Physik, Siegen, Germany*

Extinction is long-standing problem in X-ray crystal structure analysis, occurring due to multiple scattering in crystals. Over the years several extinction correction theorems have been formulated, but the used parameters have never been proved to be valid for a certain crystal under investigation. The measured intensities of real crystals do not fulfil the kinematical ($I \sim |F|^2$) nor the dynamical theory ($I \sim |F|$). They are in between both cases and an extinction correction, y ($I = y|F|^2$) is needed to fulfil the kinematic approach.

Present theories of extinction in single crystals are based on the model of a mosaic crystal with different shapes and dimensions of mosaic blocks. They describe intensities of X-ray diffraction in terms of the kinematical approach and using certain "correction terms" to implement the mosaic structure of a real crystal **[1, 2, 3]**. At the moment crystallographers use the extinction correction as a black box. They don't prove whether the extinction model used is valid or invalid because the parameters are typically not verified by the experiment.

The mosaic blocks within a real crystal are disorientated relative to each other and are also affected by lattice strain. In addition both 3D shape and size of the blocs are not known. All these parameters can be determined by high-resolution X-ray diffraction techniques performing ω- and ω-2θ-scans through certain reciprocal lattice nods. The measured widths of these scans can be used as fixed model parameters in different kinds of extinction correction.

The aim of this work is to test this approach for the case of a pyrite crystal, which is the material that shows significant effect of extinction (up to 50%, **[4]).** It is therefore a perfect model system for our studies. In addition pyrite is expected to have anisotropic mosaic block sizes, so the approach can be tested for the case of anisotropic extinction correction. The final goal of our studies is to verify if the new approach to extinction problem can improve the quality of X-ray electron density studies.

[1] Becker, P. J. & Coppens, P. (1974). *Acta Cryst.* A**30**, 129. [2] Suortti, P. (1982). *Acta Cryst.* A**38**, 642. [3] Zachariasen, W. H. (1967). *Acta Cryst.* **23**, 558. [4] Templeton, D. H. & Templeton, L. K. (1992). *Acta Cryst.* A**53**, 6227.

PS07-P03

Charge density study in three isomorphous salts containing different "tetrahalide" groups

F. Pan[1], U. Englert[1]
[1]*RWTH Aachen University, Department of Inorganic Chemistry, Aachen, Germany*

Halogen bonding interactions, with the nature of electron density "belt" in the equatorial region of the covalently-bound halogen atom (halogen bond acceptor) pointing towards the σ-hole in the polar region of the halogen bond donor[1], have received considerable attention in the past decades[2]. Recently, an unexpected mechanism was presented by Lyssenko and coworkers in their tetraiodide-group-containing structure[3]. They considered the different type of the halogen bond coming as the result of crystal field and the nature of the donor species. To further investigate this point, we exploit three isomorphous compounds with different "tetrahalide" ions ($[Cl...I\text{-}I...Cl]^{2-}$, $[Br...I\text{-}I...Br]^{2-}$, and $[I...I\text{-}I...I]^{2-}$). As shown in Fig. 1, when X1 changing from Cl^- via Br^- to I^-, I-I bond lengths increase and the distances between X1 and I1 decrease. Though the variations are moderate, they might cause the nature of the halogen bonds to differ. Detailed analyses of the experimental electron density distribution based on Bader's "Atoms in Molecules" (AIM) theory[4] will be discussed in this contribution.

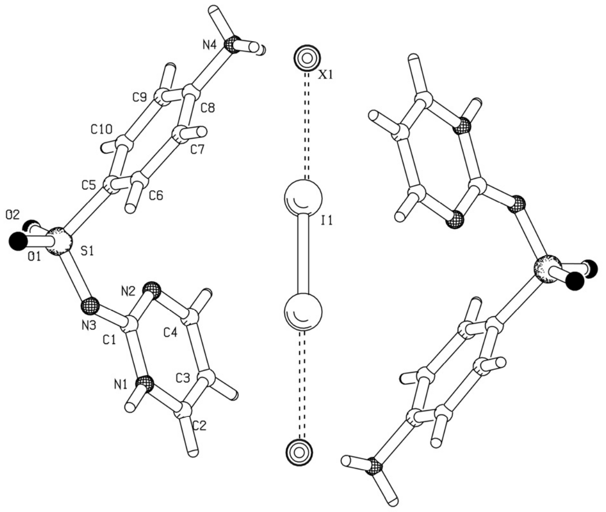

Figure 1. The structure of isomorphous salts containing "tetrahalide" groups

1. T. T. T. Bui, S. Dahaoui, C. Lecomte, G. R. Desiraju and E. Espinosa, *Angew. Chem., Int. Ed.,* 2009, **48**, 3838.
2. a) G. Cavallo, P. Metrangolo, T. Pilati, G. Resnati, M. Sansotera and G. Terraneo, Chem. Soc. Rev., 2010, **39**, 3772;
b) P. Metrangolo, H. Neukirch, T. Pilati and G. Resnati, *Acc. Chem. Res.*, 2005, **38**, 386;
c) S. K. Ritter, *Chem. Eng. News*, 2009, **87**, 39.
3. Y. V. Nelyubina, M. Y. Antipin, D. S. Dunin, V. Y. Kotov and K. A. Lyssenko, *Chem. Commun.*, 2010, **46**, 5325.
4. R. F. W. Bader, *Atoms In Molecules. A Quantum Theory*, Clarendon Press, Oxford, 1990.

PS07-P04

Computational adsorption experiments by comparison: Molecular dynamic simulations for the (100)-FeS_2-H_2O interface with Materials Studio 5.0

S. Meis[1], U. Magdans[2], H. Gies[1]
[1]*Ruhr-Universität Bochum, Institute for Geology, Mineralogy and Geophysics, Bochum, Germany*
[2]*RWTH Aachen University, Physics, Aachen, Germany*

It is of great importance to study mineral-adsorbate interfaces, because mineral surfaces are able to function as templates for organic molecules and water. The periodically ordered surface atoms induce an ordering of adsorbates, so that specific chemical reactions can take place near surfaces. The (100)-pyrite (FeS_2) surface plays an important role in many environmental, biological and natural processes, e.g. in the Iron-Sulphur world scenario, that describes one possibility for the origin of life[1].

The structures of the dry (100)-pyrite surface and the interface of the (100)-pyrite surface with water were determined with grazing incidence X-ray diffraction experiments previously[2]. An adsorption model for water on the pyrite surface was determined including three adsorption layers, a transitional zone of partial ordered water molecules and water molecules that occupy vacancies of the topmost FeS_2-layer.

In this study we present two different computational experiments, especially molecular dynamic simulations using the forcefield COMPASS27, for the adsorption of water at the (100)-pyrite surface. Simulations were carried out with the program package Materials Studio 5.0, particularly the program "Adsorption Locator", from Accelrys Inc. The start models consist of a 4x4 (100)-pyrite surface, where the four topmost substrate layers were marked as target layers and their occupation factors were assigned using the experimental values. A maximal adsorption distance of 15Å was assigned for the H_2O-molecules. Whereas in the first experiment the surface is loaded with a certain amount of water that is introduced statistical to the simulation space in one step, within the second experiment the water molecules are added in several steps to the simulation space executing a simulation after each loading step. Simulated annealing was carried out for both experiments with a total of 30 cycles consisting of 250000 steps and a time step of 1fs, a geometry optimization including the smart method, the Ewald-summation method for electrostatic and the atom based calculation method for van-der Waals interactions.

Both experiments yielded results that are in good agreement with the previously determined experimental model and with molecular dynamic simulations after Philpott et. al.[3] and ab-initio simulations [4]. Additional it was possible to determine the orientation of the H_2O-molecules within the adsorption layer, to determine the exact positioning of the H-atoms and to supply information about the influence of the H_2O-density to the amount of defects within the adsorption layers. The comparison of both experiments is well suited to get information about the difference of interface systems under perfect adsorption conditions and interface systems exposed to higher entropy.

References:

[1] G. Wächtershäuser; C. Huber, *Science* **281** (1998) 670-672
[2] Meis, S.; Magdans, U.; Torrelles, X.; *Acta Cryst.* **A67** (2011) , C338-C339
[3] M.R. Philpott, I.Y. Goliney, T.T. Lin, *J. Chem. Phys.* **120(4)** (2004), 1943-1950
[4] A. Stirling, M. Bernasconi, M. Parrinello, *J. Chem. Phys.* **118(19)** (2003), 8917-8926

PS07-P05

The symmetry and electronic structure of a new, predicted carbon phase

T. Weißbach[1], S. Bahmann[1], J. Kortus[1]
[1]*TU Bergakademie Freiberg, Institute of Theoretical Physics, Freiberg, Germany*

A new metastable structure of carbon was predicted using a a genetic search algorithm. The crystal structure contains building blocks of diamond and graphite and exhibits tubular pores, similar to the carbon foam structures. This contribution concentrates on the symmetry and its reflection in the calculated electronic and phonon band structures. We find a band crossing at the Fermi level and zero band gap as in graphite. The mechanical stability is enhanced by the links between the graphene sheets.

PS07-P06

Extent and relevance of stacking disorder in "cubic ice"

W. F. Kuhs[1], C. Sippel[1], T. Hansen[1], A. Falenty[1]
[1]*Universität Göttingen, GZG Abt. Kristallographie, Göttingen, Germany*

A solid water phase commonly known as ”cubic ice”, or ”ice I_c”, is frequently encountered in various transitions between the solid, liquid and gaseous phases of the water substance. There was multiple, compelling evidence that this phase is not truly cubic but composed of disordered cubic and hexagonal stacking sequences. The complexity of the stacking disorder, however, appears to have been largely overlooked in most of the literature.

We review the various approaches to the description of stacking-disorder that have been suggested in the past and show their interrelation. The concept of a *reichweite* (1) allows the investigation of possible correlations within a stack of layers. The recursive model proposed by Treacy et al. (2), cast into the modelling program DIFFaX, includes first-order memory effects and is the basis of the work by Malkin et al. (3). Second-order memory effects are included in a more general model proposed by Hansen et al. (4). Our analysis of neutron diffraction data show that such correlations between next-nearest layers are clearly developed, leading to marked deviations from a simple random stacking in almost all investigated cases (5). The stacking disorder is so extensive that the name “cubic ice” is no longer justified and we propose to name this phase of macroscopic trigonal symmetry ice I_{ch} (where the indices indicate that the stacking is between cubic (c) and hexagonal (h)).

We follow the evolution of the stacking disorder in ice I_{ch} as a function of time and temperature at conditions relevant to atmospheric processes; a continuous transformation towards normal hexagonal ice, ice I_h, is observed. Fresh samples of vapour-deposited ice were found to consist of spherulitic agglomerates of µm-sized units, which in turn are composed of aggregated nanoparticles; their size ranges from ~ 50 to 200 nm. We establish a quantitative link between the crystallite size established by diffraction and electron microscopic images; the crystallite size evolves from several nm into the µm-range with progressing annealing. The crystallites are isometric with markedly rough surfaces parallel to the stacking direction. We show that stacking disorder persists up to 240K, thus ice I_{ch} must be a frequent encounter in cirrus and noctilucent clouds as well as in planetary environments; the surface defect sites related to the stacking disorder may well promote chemical reactivity and affect the resulting physical properties (like vapour pressure) of atmospheric ice; this is highly relevant in the context of efforts of climate modelling and understanding climate change.

1. Jagodzinski H (1949) *Acta Cryst* 2:201-207; 2:208-214; 2:298-304.
2. Treacy MMJ, Newsam JM, Deem MW (1991) *Proc Royal Soc London A* 433:499-520.
3. Malkin TL, Murray BJ, Brukhno AV, Anwar J, Salzmann CG (2012) *PNAS* 109:1041-1045.
4. Hansen T, Koza MM, Kuhs WF (2008) *J Phys-Condens Mat* 20:285104.
5. Kuhs WF, Sippel C, Falenty A, Hansen TC *PNAS* accepted

PS07-P07

Structure determination from X-RAY powder diffraction data: A systematic survey of a new global optimization algorithm.

G. Roth[1], J. M. Simons[1]
[1]*RWTH Aachen University, Institut für Kristallographie, Aachen, Germany*

Structure determination from resolution limited XRD data is still a challenging field in inorganic structures due to the high dimensionality of the problem. Using a real space modelling approach with n scatterers in the asymmetric unit one has to find the global optimum in a 3n-dimensional solution space. For medium sized structures this poses a major problem as the size of this solution space simply gets too large to find the global optimum in reasonable time. A possible solution to this could be the optimal configuration search (ocs) algorithm: The ocs algorithm first discretises the solution space with a specially built grid transforming the continuous problem into a combinatoric problem. Further abstractions and approximations of the scatterers then simplify the problem even more. Now this derived problem can be evaluated for all possible combinations in acceptable time. Doing this one is guaranteed to actually find the global optimum (= best fitting structural model) of the derived problem against the observed XRD intensities. This solution can then be used as a starting model for structure refinement in the continuous problem.

We present the results of our systematic survey of the limitations and features of this ocs algorithm. To obtain these results we used this approach: First we took a set of a few hundred model structures of different complexities. We then calculated simulated XRD patterns and integral intensities for each model structure using FullProf[1]. Using the integral intensities we then tried to find fitting trial structures using our own programme (PowPySol) with the ocs algorithm. Those trial structures were then fed into FullProf for a final Rietveld analysis/refinement and to judge if the trial structure could be used to find the original model structure.

[1] by J. Rodriguez-Carvajal - http://www.ill.eu/sites/fullprof/

PS07-P08

Structural analysis of Yersinia enterocolitica pyruvate kinase PykF

W. Li[1], J. Hofmann[2], C. Marschall[2], G. Wilharm[2], D. Heinz[1], J. Krause[1]
[1]*Helmholtz center for infection research, Molecular structure biology, Braunschweig, Germany*
[2]*Robert Koch Institute, Wernigeroder, Germany*

The glycolytic enzyme pyruvate kinase (PK) converts phosphoenolpyruvate into pyruvate and thereby generates ATP via substrate-level phosphorylation [1,2]. In contrast to most bacteria, Enterobacteriaceae, such as Yersinia enterocolitica, harbor two pyruvate kinases encoded by the genes pykA and pykF, but the particular role of these isoenzymes is poorly understood. Y. enterocolitica PykF and PykA are phylogenetically distant and share only 39% amino acid sequence identity. PykF can be activated by fructose 1,6-bisphosphate (FBP) whereas PykA is not affected by the presence of FBP [3]. In order to elucidate the correlation between the structure and the function, recombinant PykF was produced in E. coli and purified to homogeneity through a combination of ion exchange and size exclusion chromatography. The complex of PykF and FBP could be crystallized but PykF alone could not, a fact that indicates that FBP binding causes a substantial comformational change in PykF. The crystal structure of PykF with FBP was determined to 1.85 ? resolution in space group is C2. The asymmetric unit contains two monomers with the physiological tetramer being formed through the twofold crystallographic symmetry. The FBP binding sites are located on the surface of the tetramer and are different from the ones of Saccharomyces cerevisiae pyruvate kinase, as were revealed by a superposition of both structures [4]. Currently, co-crystallization experiments with FBP, oxalate and ATP/ADP are carried out in order to explore the catalytic site of PykF. Initial crystals have been obtained, and optimization of crystallization condition is ongoing.

References

1. E. Ponce, N. Flores, A. Martinez, F. Valle, F. Bolívar, J. Bacteriol. 177 (1995) 5719-5722.

2. K.A. Siddiquee, M.J. Arauzo-Bravo, K. Shimizu, FEMS Microbiol. Lett. 235 (2004) 25-33.

3. E.B. Waygood, B.D. Sanwal, J. Biol. Chem. 249 (1974) 265-274.

4. M.S. Jurica , A. Mesecar , P.J. Heath, W. Shi, T. Nowak, B.L. Stoddard, Structure. 1998 6(2): 195-210.

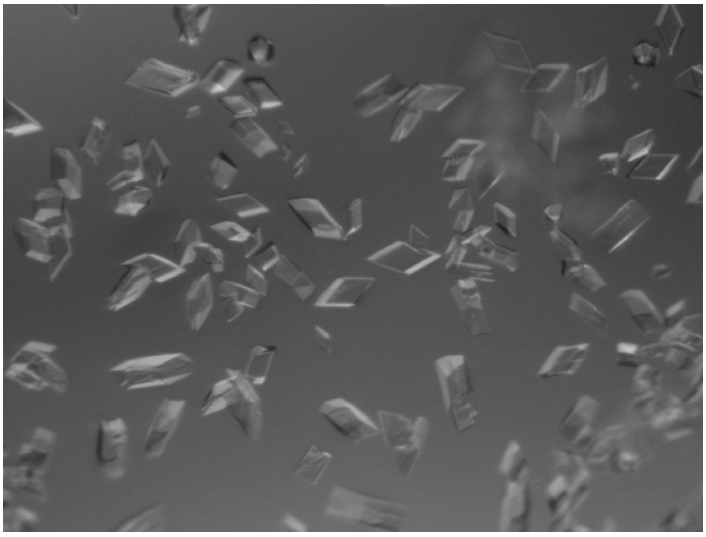

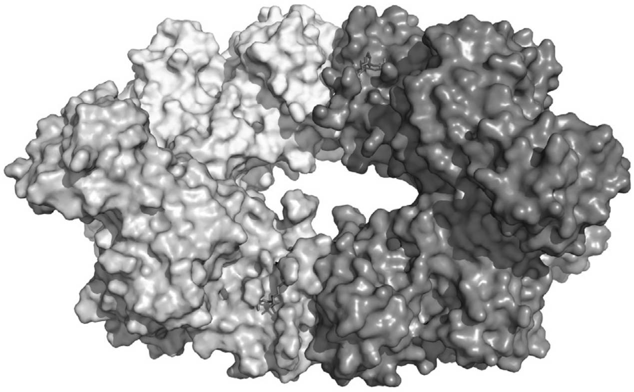

PS07-P09

Sequential proton ordering as a mechanism for the low-temperature phase transitions in $(NH_4)_3H(SO_4)_2$: single-crystal neutron diffraction studies

Y. J. Sohn[1], K. Sparta[1], M. Meven[1,2], G. Roth[1], G. Heger[1]
[1]Insitut für Kristallographie, RWTH Aachen University, Aachen, Germany
[2]JCNS Outstation@FRM II, FZ Jülich, Garching, Germany

$(NH_4)_3H(SO_4)_2$ (TAHS) has been investigated so far with regard to its rich polymorphism and superprotonic conductivity [1-4]. Using single-crystal X-ray diffraction, extensive crystal structure studies have been done in a wide temperature range of 120 - 420 K [5, 6]. However, little has been known up to now about the H-disorder of TAHS with decreasing temperature, which plays a key role in the low-temperature phase transitions. Owing to the strength of neutron diffraction, localizing proton precisely and describing its thermal behaviour better, more detailed crystal structure analyses have been carried out in the present work, focusing on the proton ordering of TAHS as a function of temperature. Large TAHS single crystals of optical quality were grown from aqueous solution by the cooling method. A complete data set of Bragg reflection intensities was collected at various temperatures up to $(\sin\theta/\lambda)_{max} = 0.7$ Å^{-1} on the four-circle diffractometer HEiDi at the FRM II in Garching.

As a result, sequential proton ordering in a complex system of hydrogen bonds was identified as the driving force for the successive structural phase transitions in TAHS. The rotational disorder of the ammonium groups at room temperature occurs based on the competing $N\text{-}H\cdots O$ hydrogen bonds. These approximately equidistant hydrogen bonds dissociate into stronger and weaker ones with decreasing temperature. Hence, different ammonium groups start freezing one after the other at different phase transitions. A group-subgroup relationship between space group symmetries of the different phases of TAHS is also presented.

[1] K. Gesi (1976) *Phys. Status Solidi* **33**, 479-482.
[2] K. Gesi (1980) *Jap. J. Appl. Phys.* **19**, 1051-1053.
[3] L. Schwalowsky, V. Vinnichenko, A. Baranov, U. Bismayer, B. Merinov & G. Eckold (1998) *J. Phys. Condens. Matter* **10**, 3019-3027.
[4] R. H. Chen, T. M. Chen & C.S. Shern (2000) *J. Phys. Chem. Solids* **61**, 1399-1406.
[5] P.M. Dominiak, J. Herold, W. Kolodziejski & K. Wozniak (2003) *Inorg. Chem.* **42**, 1590-1598.
[6] K. Friese, M. I. Aroyo, L. Schwalowsky, G. Adiwidjyjy & U. Bismayer (2002) *J. Solid State Chem.* **165**, 136-147.

PS07-P10

Inhibition of magnesite growth kinetics by acute kink-blocking

U.- N. Berninger[1], Q. Gautier[1], G. Jordan[2], J. Schott[1]
[1]UPS-CNRS-IRD, Géosciences Environnement Toulouse, Toulouse, France
[2]LMU, Dept. f. Geo- und Umweltwissenschaften, München, Germany

The high stability of magnesite in natural environments makes this mineral a promising candidate for long-term CO_2 sequestration. However, the causes for the reluctance of magnesite to form under earth surface conditions are still poorly understood. To better decipher the mechanisms controlling magnesite growth, experiments need to be performed at high temperature ($T \geq 100$) to be compatible with the laboratory time scale.

Recently the effects of various carboxylic ligands on magnesite growth were investigated and citrate was found to cause the highest degree of inhibition [1]. Surface active ligands that efficiently inhibit growth kinetics necessarily interfere with the growth controlling mechanisms. Therefore, applying in-situ high-resolution and time-resolved surface techniques to such a system holds the promise to identify the active growth sites by gaining insights in the competing inhibition-growth processes.

In this study we applied hydrothermal atomic force microscopy (HAFM) to investigate magnesite growth on the (104) surface as a function of saturation state and citrate concentrations up 10 mM. Experiments were conducted at 100 °C, pH 8 and pressures to 4 bars.

HAFM observations showed that spiral growth is the rate controlling mechanism over a wide range of saturation states in both ligand-free and citrate-containing solutions. However, citrate was found to exert a significant effect on the morphology of growth hillocks. Since no reduction of obtuse step velocity was observed, these results are interpreted as resulting from the preferential adsorption of citrate to acute kink-sites. The rotation frequence of spirals and thus the growth rate are controlled by the slowest process. Efficiently slowing acute step propagation, the presence of 1 mM citrate reduced magnesite growth rates by a factor of more than 3.

In summary, this study demonstrates the control exerted by acute steps on magnesite spiral growth kinetics. Such a control indicates that impurities adsorbing preferentially on magnesite acute steps may have a stronger inhibiting influence on magnesite growth than ligands which are less specific to step orientations.

[1] Gautier *et al*. (2013) in prep.

PS07-P11
ShelXle - A graphical user interface for SHELXL

C. Hübschle[1], B. Dittrich[1,2], G. Sheldrick[1]
[1]*Georg-August-University, Intstitute of Inorganic Chemistry, Göttingen, Germany*
[2]*Universität Hamburg, Institut für Anorganische und Angewandte Chemie, Hamburg, Germany*

ShelXle is a graphical user interface for *SHELXL*, currently the most widely used program for small-molecule structure refinement. It combines an editor with syntax highlighting for the *SHELXL*-associated .ins (input) and .res (output) files with an interactive graphical display for visualization of a three-dimensional structure including the electron density (F_o) and difference density (F_o-F_c) maps. Special features of *ShelXle* include intuitive atom (re-)naming, a strongly coupled editor, structure visualization in various mono and stereo modes, and a novel way of displaying disorder extending over special positions.

ShelXle is completely compatible with all features of *SHELXL*, including the latest version (shelxl2012) version and is written entirely in C++ using the Qt4 library. It is available at no cost for Windows, Linux and Mac-OS X and as source code. The latest versions of Debian and Ubuntu include ShelXle directly from the package manager.

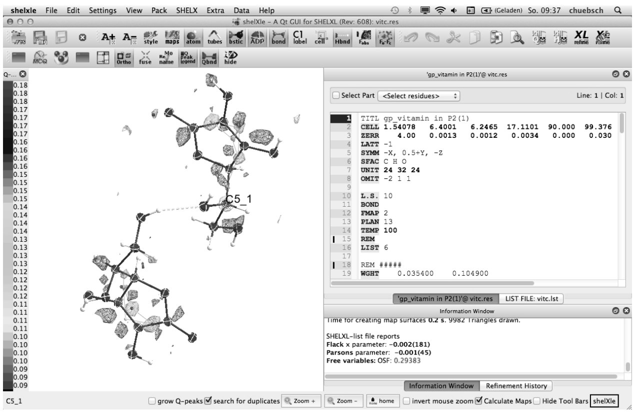

```
TITL gp_vitamin in P2(1)
CELL 1.54078   6.4001   6.2465  17.1101  90.000  99.376
ZERR    4.00   0.0013   0.0012   0.0034   0.000   0.030
LATT -1
SYMM -X, 0.5+Y, -Z
SFAC C H O
UNIT 24 32 24
OMIT -2 1 1

L.S. 10
BOND
FMAP 2
PLAN 13
TEMP 100
REM
LIST 6

REM #####
WGHT    0.035400    0.104900
```

```
Time for creating map surfaces 0.2 s. 9982 Triangles drawn.

SHELXL-list file reports
Flack x parameter: -0.002(181)
Parsons parameter:  -0.001(45)
Free variables: OSF: 0.29383
```

Figure 1: Screenshot of ShelXle on MacOS showing a Vitamin C structure.

PS07-P12
DRAWxtl 5.6

M. Kroeker[1], B. Toby[2], L. Finger[3]
[1]*Universität Freiburg, Institut für Anorganische und Analytische Chemie, Freiburg, Germany*
[2]*ANL, X-Ray Science Division, Argonne,IL, United States*
[3]*Carnegie Institution (retired), Geophysical Laboratory, Washington, D.C., United States*

DRAWxtl is a free and open-source drawing program that supports all the conventional elements of crystal structure drawings such as atomic spheres, thermal ellipsoids and polyhedra of arbitrary complexity. Although it is mainly designed for the rendering of inorganic crystal structures, with import filters for CIF, CSD, Fullprof, GSAS, JANA and Shelx format, it is equally well suited for displaying the results of DFT calculations done with the popular VASP, WIEN2k and ELK codes.

The upcoming version 5.6 contains many improvements across the board, from support for new modulation functions introduced in recent updates to JANA2006, to significant speedup in reading of electron density map files, improvements in drawing Bader surfaces and numerous enhancements in object rendering styles.

Special attention has been put on the novel possibilities provided by the recent advances towards affordable, high-quality printing of accurate 3D structural models. To this end, the long since available VRML output has been improved and a new output format has been added to address printing service providers that do not yet handle VRML sufficiently well.

As always, the program is freely available under the GPL license from http://www.lwfinger.net/drawxtl/ in the form of ready-to-run binaries for Linux, OS X and Microsoft Windows, as well as C++ source code for building on other platforms.

Finger L.W., Toby B.H. Kroeker, M., *J.Appl.Cryst.*, 2007, 40, 188.

PS07-P13
Role of XRD/XRF Reference Materials and Values Benchmarks on macro and micro scales.

G. Berti[1], F. de Marco[2], M. E. Del Seppia[2]
[1]*University of Pisa, Lab. R&D on X-ray Diffraction , Pisa, Italy*
[2]*XRD-Tools s.r.l., Pisa, Italy*

The material rheology to external solicitations is in general determined according to macroscopic parameters. The classic theory of elasticity assumes continuity and isotropy as two basic properties of the space around the investigated point from where the deformation vector is observed. This deformation is the macroscopic result of a microscopic arrangement of atoms and molecules; this arrangement is discontinuous and anisotropic in nature. As a consequence, said external solicitations result in effects that are on average isotropic and continuous in appearance. The description of the creep propagation mechanism from its nucleation to fracture is an excellent example. By starting from the concept of the real Mean Equivalent Lattice, which considers the short and long range vibrations, induced by internal elastic wavelengths, the modeling of the progressive lattice deformation unifies several distinct creep mechanisms. Creep is in fact capable to disaggregate and rearrange systems composed by several distinct elementary units. These rearrangements result in either cure or reparation (restoration) and either in pathologies or damages of biomolecule or atomic systems respectively. Theories and modeling methods shall be accompanied by appropriate technologies for inspections on site and appropriate benchmarks values of the most relevant properties of the material under investigation. The effective qualification of the material (or its re-qualification) for its intended uses is obtained from comparing the values of the same property from Reference Materials (RM). This RM is not a generic one but exactly the most appropriate one for that specific value: the Reference Value Material (RVM). RVM supplies the benchmark value for the measurement ranking scale. The role of said RVM is quite different from the specimens used to verify either the instrument alignment or the instrument calibration [1], [2]. The x-ray diffraction patterns obtained from RVM indicate the minimum perceivable effect on the pattern from those particular properties. The orthogonal relation between uncertainty and accuracy of the results descends from the completeness of the adopted model where the instrument contribution and the RVM are considered as well.

[1] EN13925-2 CEN© 2003

[2] EN13925-3 CEN© 2005

PS07-P14
Crystallography of bis(nitrilotriacetato)zirconates with divalent cations.

P. Held[1], M. Fridrichová[2], L. Bohatý[1]
[1]*University of Cologne, Institute for Crystallography, Cologne, Germany*
[2]*Charles univerity, Department of Inorganic Chemistry, Prague, Czech Republic*

Zirconium(IV) forms, together with the quadridentate ligand nitrilotriacetic acid, $N(CH_2COOH)_3$, the anionic complex $[Zr(NTA)_2]^{2-}$ (NTA = $[N(CH_2COO)_3]^{3-}$), which is stable in aqueous solutions throughout a wide pH range [1]. Therefore, salts of this anionic complex can be synthesized and crystallized easily in aquatic systems, as was first shown by [2] and later e.g. by [3-6].

A statistical analysis of space group symmetry of crystals containing $[Zr(NTA)_2]^{2-}$ as a structural unit shows, that there is a strong preference for bis(nitrilotriacetato)zirconates to crystallize non-centrosymmetrically. The bulky (non-chiral) complex group $[Zr(NTA)_2]^{2-}$ possesses a marked polar symmetry, which seems to "enforce" the non-centrosymmetry of a crystal structure. While the crystal structures and physical properties of bis(nitrilotriacetato)zirconates of monovalent cations have been studied intensively (see, as a selection, e.g. [2-6]), our knowledge about structural and physical properties of bis(nitrilotriacetato)zirconates of divalent cations is limited, with lattice constants and symmetry of the Sr, Ba and Pb compounds [7] and a more detailed study of possibly ferroelectric $Ni[Zr(NTA)_2]\cdot 8.5H_2O$ [8].

The contribution presents synthesis and crystal structures of the non-centrosymmetric isomorphic compounds $M^{II}[Zr(NTA)_2]\cdot 6H_2O$ (M = Ca, Mn, Fe, Co, Zn;), and reports on our attempts to crystallize bis(nitrilotriacetato)zirconates of various further divalent cations.

[1] B. I. Intorre, A. E. Martell, *J. Amer. Chem. Soc.* **82** (1960) 358-364.
[2] J. L. Hoard, E. W. Silverton, J. V. Silverton, *J. Amer. Chem. Soc.* **90** (1968) 2300-2308.
[3] U. Richter, S. Haussühl, *Cryst. Res. Technol.* **22** (1987) 539-545.
[4] S. Haussühl, U. Richter, *Z. Kristallogr.* **211** (1996) 101-105.
[5] P. Held, B. Listl, E. Tillmanns, S. Ahrweiler, H. Hellwig, L. Bohatý, *Z. Kristallogr.* **215** (2000) 65-71.
[6] A. S. Antsyshkina, G. G. Sadikov, V. S. Sergienko, R. L. Davidovich, L. M. Shkol´nikova, *Russ. J. Inorg. Chem.* **41** (1996) 1914-1923.
[7] C. Hoffmann, E. Tillmanns, E. Utz, L. Bohatý, *Z. Kristallogr. Suppl.* **8** (1994) 269.
[8] E. Haussühl, S. Haussühl, E. Tillmanns, *Z. Kristallogr.* **213** (1998) 559-562.

PS07-P15
The Collection of Crystal Models of Abraham Gottlob Werner

B. Heide[1], A. Massanek[1], G. Heide[1]
[1]*TU Bergakademie Freiberg, Geoscientific Collections , Freiberg, Germany*

A. G. Werner has developed his teaching method „Von den äußerlichen Kennzeichen der Foßilien“ (Leipzig 1774) to identify minerals. In connection with this matter he has dealt with crystal shapes and made models of lead himself. 48 of these models are still in the Geoscientific Collections of the TU Bergakademie Freiberg. They belong to the collection of crystal models of A. G. Werner together with more than 400 models made of wood from Freiberg, twin models of brass and models made of wood and porcelain in R. J. Hauy's workshop in Paris.

This collection will be tapped in the project „Aufbau eines webbasierten Systems zur Erschließung, Digitalisierung und Visualisierung des Bestandes der historischen mineralogischen Kennzeichen-Sammlung von Abraham Gottlob Werner an der TU Bergakademie Freiberg“ in the DFG announcement „Erschließung und Digitalisierung von objektbezogenen wissenschaftlichen Sammlungen“. The exhibition „Mineralogische Sammlung Deutschland“ in the Krüger-Haus in Freiberg shows some of the models.

Fig.: Photo of Werner's lead models

PS08 - Materials for Electronics: Energy and Data Storage through the Eyes of Crystallographers

PS08-P01
Benzylidene-Oxazolones: Photoreactivity in the Crystal State

T. Runcevski[1], M. Cejuela[2], M. Blanco-Lomas[2], D. Sampedro[2], R. Dinnebier[1]
[1]Max-Planck-Institute for Solid State Research, Suttgart, Germany
[2]Universidad de La Rioja, La Rioja, Spain

The potential applicability of organic solids as controllable molecular media in the photon-based molecular devices, that is, memories and switches, has turned such materials into an expanding research field.[1] In the search for new systems, inspiration from nature can provide useful insights. One example of biomolecules that undergo photoinduced *Z*/*E* isomerization and/or [2+2] dimerization is the chromophore of the green fluorescent protein.[2] Although the photoreactivity of this system is well-studied, little is known about the oxazolone analogues. Herein, we report the photoswitching ability of benzylidene-oxazolones (**B-O**) in the solid state, as a biomimetic system with promising applications in crystal engineering.

The synthesis and photochemistry in solution of **B-O** was recently reported; upon irradiation with UV-light, these molecules underwent *Z*/*E* isomerization in solution.[3] In the solid state, however, irradiation of some **B-O** leads to [2+2] dimerization. Other members of the family showed no photoinduced changes, even after prolonged exposition to UV light. Accordingly, it can be assumed that the molecular conformation, together with the crystal packing play significant role in the photoreactivity.

X-ray crystallography was used to solve the crystal structures and to draw structure-photoreactivity relationships. Obtaining single crystals of **B-O** turned-out to be a challenging task, thus powder diffraction was used as the method of choice. The crystal structure analysis gave insights into the topochemical control of the photoreactivity and the mechanisms of molecular motions (hula twist vs. one-bond flip).

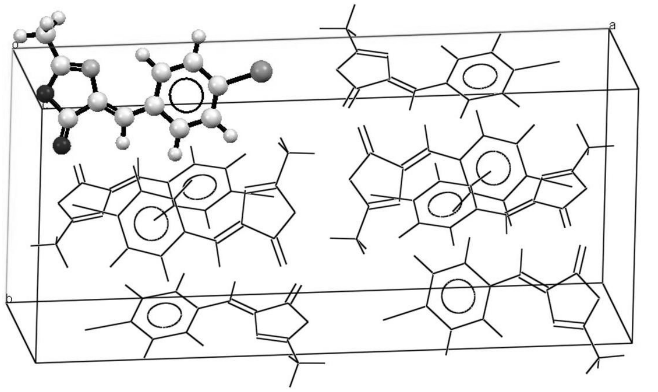

Figure: Molecular structure and packing diagram of

*(Z)-4-(4-bromobenzylidene)-2-methyloxazol-5(4H)-one, a member of the **B-O** family.*

References:

[1] Naumov et al., *J. Am. Chem. Soc.*, **2002**, *124* (29), 8540.

[2] Moerner et al., *Nature*, **1997**, *388* (6640), 355.

[3] Sampedro et al., *Org. Lett.*, **2012**, *14* (17), 4334.

PS08-P02
Production and characterization of LLTO thin films

J. Derr[1,2], J. Birkenstock[2], F. Andre[1]
[1]Fraunhofer IFAM Bremen, Elektrische Energiespeicher, Bremen, Germany
[2]Universität Bremen, Fachbereich Geowissenschaften/ Kristallographie, Bremen, Germany

Lithium lanthanum titanate (LLTO) is a promising material for applications as solid state electrolyte in lithium ion secondary batteries. With an ideal chemical composition of $Li_{0.31(1)}La_{0.56(1)}TiO_{2.94(2)}$ it exhibits a perovskite structure (of general composition ABO_3) and, an excellent bulk ionic conductivity at room temperature of more than 10^{-3} S/cm, as first reported by Inaguma et al. (1993).

LLTO thin films were deposited on sapphire (Al_2O_3) substrates by RF magnetron sputtering and analyzed with grazing incidence X-ray diffraction (GIXRD). GIXRD measurements at various temperatures were carried out on Philips X'Pert Pro MPD equipped with a hybrid monochromator providing a parallel beam of pure Cu-Kα_1 radiation. Initially the deposited thin films were amorphous and crystallized between 640 and 650°C. However, the observed reflections didn't match any of the expected phases in this system.

To verify if the phase identification might have been hindered by strong texture effects, which could easily occur in thin films by directional growth, some of the deposited amorphous sample was separated from the substrate, filled into a capillary and investigated with X-ray diffraction. Indeed, the received powder pattern is more detailed than that of the thin film, but again none of the expected phases could be matched with the observed pattern. Investigations are currently underway to determine whether it is new and phase pure, to allow for more detailed phase analyses. Furthermore ionic conductivities of the various samples shall be determined by electrochemical impedance spectroscopy (EIS).

Y. Inaguma, C. Liquan, M. Itoh, T. Nakamura, T. Uchida, H. Ikuta, M. Wakihara, Solid State Commun. 1993, 86, 689-693.

PS08-P03

Photo chromatic sensors of multinary mixed valence inorganic micro needles

K. Xhaxhiu[1], C. Kvarnström[2], P. Damlin[2], R. Schmidt-Grund[3], K. Bente[4]
[1]*University of Tirana, Faculty of Natural Sciences, Chemistry, Tirana, Albania*
[2]*University of Turku, Faculty of Mathematics and Natural Sciences, Department of Chemistry, Turku, Finland*
[3]*University of Leipzig, Institute for Experimental Physics II, Leipzig, Germany*
[4]*University of Leipzig, Institute of Mineralogy, Crystallography and Material Science , Leipzig, Germany*

The recent *I-U* measurements on the individual micro needle-shaped crystals, of the ternary mixed valence compound In_5Se_5Cl, crystallizing in the monoclinic crystal system ($P2_1/m$) [1], showed significant light sensitivities. Micro needles of In_5Se_5Cl “glued” on Si- and Cu- substrates (Fig. 1a) were measured under seven different wavelengths with various irradiation intensities to investigate their photo chromatic sensing behavior along with the substrate’s influence. In the measuring voltage range 0 - 3 V and maximal LED illumination intensity, current jumps above two orders of magnitude were observed for white light (4100 K; 200 lm), followed by the blue light (460 nm; 976 mW). The amber light (590 nm; 203 mW) exhibited the lowest response. Green- and blue light were selected to determine the substrate’s effect. The micro-needles chips prepared with Si-substrates displayed higher currents for the same voltages in comparison to those prepared with Cu-substrates. These differences decreased with the voltage increase (Fig. 1b) for both employed wavelengths.

The mutual structural substitution of a selenium with sulfur, led to the compound In_5SSe_4Cl [2]. The later crystallizes similarly to In_5Se_5Cl. Its *I-U* measurements recorded with green and blue light, on Cu-substrate chips within the voltage range 0 -3 V, revealed more pronounced photo chromatic sensorial for both wavelengths used. These differences increased with the voltage increase for both employed wavelengths (Fig. 1c). At 3 V, current increases up to 2.2 times and 2.4 times were observed for the green light and blue light respectively. Typically high and better distinguishable sensorial activity was observed for all the employed wavelengths using chips with In_5SSe_4Cl crystals on Cu-substrate, even at minimal irradiation LED power (0.25 %) Fig. 1d. The micro-reflection measurements of both needle-shaped crystals displayed a substitution dependent band-gap. For In_5Se_5Cl the band gap was estimated at 580 nm. Thickness interference oscillations strongly damped due to structural inhomogeneity or defect-related absorption suggest two possible band gaps for In_5SSe_4Cl; at 540 nm or at 620 nm.

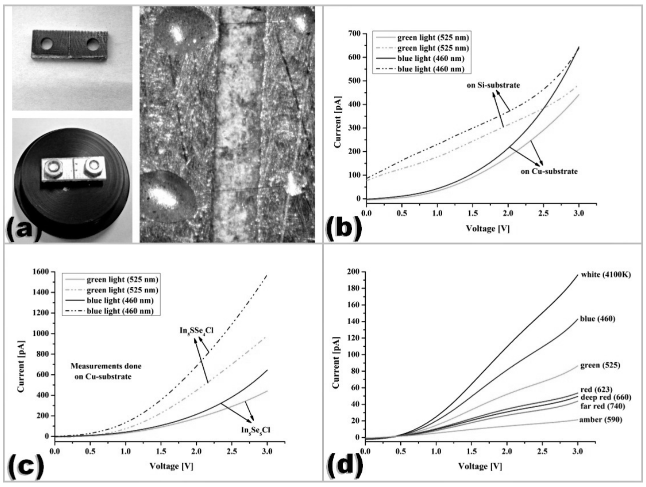

Fig. 1. (a) Cu-substrate (left-up), measuring cell (left-down), chip with two crystals "glued" on a Cu-substrate (right); (b) effect of substrate for two wavelenghs (green, blue) in case of In_5Se_5Cl; (c) effect of mutual substitution of Se with S using two wavelengths (green, blue); (d) the chip (In_5SSe_4Cl crystals on Cu-substrate) response toward minimal LED illumination power for seven different wavelengths

[1]] H.-J. Deiseroth, C. Reiner, K. Xhaxhiu, M. Schlosser, L. Kienle, (**2004**) “X-Ray and Transmission Electron Microscopy Investigations of the New Solids In_5S_5Cl, In_5Se_5Cl, In_5S_5Br and In_5Se_5Br” *Zeitschrift für Anorganische und Allgemeine Chemie*, ***630*, 2319-2328.**

[2] Xhaxhiu, K., (**2005**). The use of supercritical carbon dioxide in Solid State Chemistry and basic structural investigations with chalcogenide halides of the third main group. PhD thesis, University of Siegen (Germany).

PS09 - Non-ambient Conditions: Pressure, Temperature and Fields at Work

PS09-P01

Unexpected Low Temperature Behaviour of Piroxicam Monohydrate

K. Fucke[1], A. J. Edwards[2], M. R. Probert[3], S. E. Tallentire[3], J. A. K. Howard[3], J. W. Steed[3]
[1]*Julius-Maximilians-Universitaet Wuerzburg, Anorganische Chemie, Wuerzburg, Germany*
[2]*Australian Nuclear Science and Technology Organisation, The Bragg Institute, Lucas Heights, Australia*
[3]*University of Durham, Department of Chemistry, Durham, United Kingdom*

Pharmaceutical compounds can crystallise in different polymorphic forms with the same chemical composition, which remains a major issue in the pharmaceutical industry. Additional problems arise from solvated crystal forms, which incorporate one or more types of solvent from the crystallisation medium into the crystal. As part of our study of pharmaceutical hydrates, we investigated piroxicam (PIR), a non-steroidal anti-inflammatory drug (NSAID) used in the treatment of chronic pain in rheumatoid arthritis and osteoarthritis. PIR is listed in the European[1] and the US Pharmacopoeias,[2] and is reported to exist in three different unsolvated crystal forms,[3] a monohydrate,[4] and several multi-component crystals and salt forms.[5] After cooling a large single crystal (ca. 0.5 mm^3) of PIR monohydrate from 120 K to 22 K at 180 K h^{-1} for thermal neutron Laue diffraction, we observed an undesirable and marked splitting in the diffraction peaks, which normally would have resulted in the abortion of the experiment assuming degradation of the crystal. Nonetheless, data collection was commenced and remarkably the peaks coalesced within 11 hours to give a diffraction pattern consistent with an essentially single crystalline sample. A phase transition of the crystal form could be ruled out by X-ray diffraction single crystal diffraction experiments. During these, we observed unusual thermal behaviour of the monohydrate. For a continuously cooled sample the unit cell volume decreases in a smooth fashion to about 50 K, below which the contraction of the cell volume levels off and stays approximately constant below 35 K. A sample quenched to 120 K, however, reveals an initially larger cell volume than that found for the continuously cooled sample. During the subsequent cooling, the unit cell volume contracts more quickly, but levels off at about 70 K. Between 70 K and 50 K the cell volume stays nominally unchanged, but continues to decrease below 50 K and levels off again below 25 K. Surprisingly, the final cell volume of the initially quenched sample lies below that of the continuously cooled one. This behaviour can be explained by the strongly hydrogen bonded, isolated chains present in the crystal structure, which can contract separately from each other. It can be expected that a crystal structure stabilised by comparably strong hydrogen bonds, as for example observed in very stable hydrates, may be prone to this type of thermal behaviour.

References

[1] *Pharmacopoeia Europaea 6.8*, Deutscher Apotheker Verlag, Stuttgart & Govi-Verlag GmbH, Eschborn, **2007**.

[2] *United States Pharmacopoeia Vol 32*, The Stationary Office, Norwich, England, **2008**.

[3] F. Vrecer, M. Vrbinc, A. Meden, *Int. J. Pharm.* **2003**, *256*, 3-15.

[4] J. Bordner, J. A. Richards, P. Weeks, E. B. Whipple, *Acta Crystallogr., Sect. C: Cryst. Struct. Commun.* **1984**, *C40*, 989-990.

[5] S. L. Childs, K. I. Hardcastle, *Cryst. Growth Des.* **2007**, *7*, 1291-1304.

PS09-P02

Polarized Raman spectroscopy on multiferroic $MnWO_4$ under an applied electric field

M. Adrian[1], H. Gibhardt[1], J. Leist[1], L. Bohatý[2], P. Becker[2], G. Eckold[1]
[1]*Georg-August Universität Göttingen, Institut für Physikalische Chemie, Göttingen, Germany*
[2]*Universität zu Köln, Institut für Kristallographie, Köln, Germany*

Multiferroic materials, such as $MnWO_4$, received increasing interest in recent years due to their distinctive properties. They exhibit simultaneously two or more ferroic properties and the corresponding order parameters (electric, magnetic, elastic) are strongly coupled. Due to the coupling of ordering of charge and spin degrees of freedom, the electric polarization of magneto electric multiferroic materials could be controlled by an external magnetic field and vice versa. It is assumed, that the formation of a macroscopic spontaneous polarization within a cycloidal spin structure originates in the inverse of the Dzyaloshinskii-Moriya effect [1].

In the group of magneto electric multiferroic materials, mangane tungstate is a likely chosen example to study the coupling mechanism of electric and magnetic properties, because it contains only one kind of ion exhibiting a magnetic moment (Mn^{2+}). Mangane tungstate undergoes three antiferromagnetic phase transitions at low temperatures (at 13.5 K, 12.5 K and 7 K). In the range of 7 K to 12.5 K a spontaneous polarization is formed and mangane tungstate becomes multiferroic. The magnetic behavior was found to be influenceable by the application of an external electric field [2,3].

Mangane tungstate was studied by polarized Raman scattering by L. Dura et al. [4], extending the work of Iliev et al. [5] and Hoang et al. [6]. In the work of L. Dura et al. some anomalies in the linewidth of certain Raman vibration modes could be related to the multiferroic phase and high order magnon scattering was proven in all three antiferromagnetic phases. In this work, the influence of an applied external electric field on the magnetic excitations was studied. The behavior of the low frequency excitations, which were found by L. Dura et al., were related to the strength of the applied electric field.

[1] M. Mostovoy, *Phys. Rev. Let.* **2006**, *96*, 067601.
[2] F. Finger, D. Senff, K. Schmalzl, W. Schmidt, L. P. Regnault, P. Becker, L. Bohatý, M. Braden, *Phys. Rev. B* **2010**, 81, 054430.
[3] D. Meier, N. Leo, M. Maringer, Th. Lottermoser, M. Fiebig, P. Becker, L. Bohatý, *Phys. Rev. B* **2009**, *80*, 224420.
[4] L. Dura, H. Gibhardt, J. Leist, P. Becker, L. Bohatý, G. Eckold, *J. Phys.: Condens. Matter* **2012**, *24*, 335901.
[5] M. N. Iliev, M. M. Gospodinov, A. P. Litvinchuk, *Phys. Rev. B* **2009**, *80*, 212302.
[6] L. H. Hoang, N. T. M. Hien, W. S. Choi, Y. S. Lee, K. Taniguchi, T. Arima, S. Yoon, X. B. Chen, I.-S. Yang, *J. Raman Spectrosc.* **2010**, *41*, 1005-1010.

PS09-P03

Intermediates during Ammono-basic Crystal Growth of GaN

S. Zhang[1], R. Niewa[1]
[1]*Institut für Anorganische Chemie, Universität Stuttgart, Stuttgart, Germany*

The ammonothermal process employs basic mineralizers (alkali metals or their amides) in supercritical ammonia and was proven to be capable of growing free standing GaN wafer up to 2 inch [1]. However, the growth mechanism with respect to intermediate species involved was rarely discussed.

We obtained $Li[Ga(NH_2)_4]$ under ammonothermal conditions (400 ^oC, 2.5 kbar, 72 h) from Ga and $LiNH_2$. In the crystal structure ($P2_1/n$, a = 5.817(1) Å, b = 12.442(3) Å, c = 6.829(1) Å, β =

92.99(3)º) both Li and Ga are tetrahedrally coordinated by NH_2^- ions, connected via vertex-sharing along [100] (**Fig. 1**). N atoms are arranged in the motif of a hexagonal closed packing. The isotypic compound $Na[Ga(NH_2)_4]$ was earlier synthesized in liquid ammonia [2]. Under ammonothermal conditions, however, the new amidogallate amide $Na_2[Ga(NH_2)_4]NH_2$ was obtained after heating Ga and $NaNH_2$ at 580 °C and 1.3 kbar for 48 hours. In the crystal structure (*Pnma*, a = 11.748(2) Å, b = 6.681(1) Å, c = 9.665(2) Å) each Ga atom is situated in tetrahedral coordination by NH_2^- ions. Due to site disorder of Na atoms, two sites are half occupied by sodium ions. Twin sets of edge-sharing chains of tetrahedrally coordinated Na form columns running along [010] (**Fig. 2**). The bond lengths d(Ga-N) in the $[Ga(NH_2)_4]^-$ tetrahedra are close to those found in $Na[Ga(NH_2)_4]$.

The existence of negatively charged complex ion $[Ga(NH_2)_4]^-$ in supercritical ammonia will influence the growth kinetics of GaN on different faces and could provide explanation to the discovery of polarity dependence of GaN seed crystal growth nature under ammono-basic conditions [3, 4].

References:

[1] Dwilinski, R.; Doradzinski, R.; Garczynski, J.; Sierzputowski, L.; Kucharski, R.; Zajac, M.; Rudzinski, M.; Kudrawiec, R.; Serafinczuk, J.; Strupinski, W. *J. Cryst. Growth* **2010**, *312*, 2499.

[2] Jacobs, H.; Nöcker, B. *Z. Anorg. Allg. Chem.* **1993**, *619*, 381.

[3] Saito, M.; Kamber, D. S.; Baker, T. J.; Fujito, K.; DenBaars, S. P.; Speck, J. S.; Nakamura, S. *Appl. Phys. Express* **2008**, *1*, 121103.

[4] Hashimoto, T.; Wu, F.; Saito, M.; Fujito, K.; Speck, J. S.; Nakamura, S. *J. Cryst. Growth* **2008**, *310*, 876.

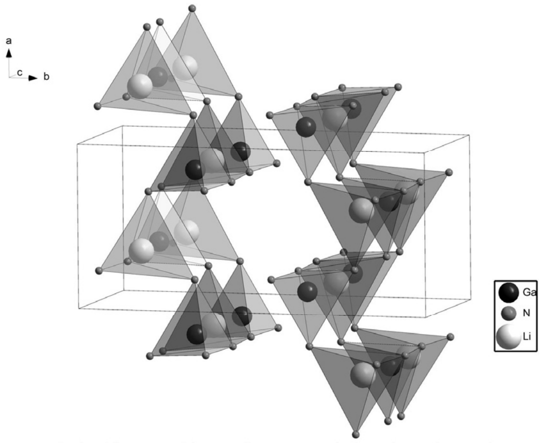

Fig. 1 $Li[Ga(NH_2)_4]$: section of the crystal structure emphasizing chains of vertex-sharing tetrahedra $[Ga(NH_2)_4]$ and $[Li(NH_2)_4]$.

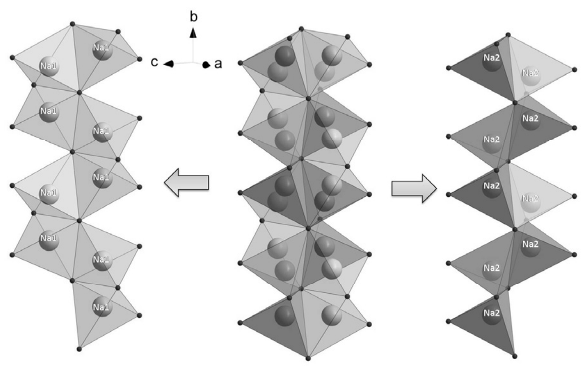

Fig. 2 $Na_2[Ga(NH_2)_4]NH_2$: chains of tetrahedra surrounding of sodium; middle: with sodium positions occupied to 50%; left and right: microscopic picture with fully occupied sites.

PS09-P04
High-pressure high-temperature phase diagram of TaN

A. Friedrich[1], W. Morgenroth[1], L. Bayarjargal[1], N. Rademacher[1], F. Schröder[1], E. A. Juarez-Arellano[2], J. Biehler[1], J. D. Bauer[1], B. Winkler[1]
[1]Goethe-University Frankfurt am Main, Insitut für Geowissenschaften, Kristallographie, Frankfurt am Main, Germany
[2]Universidad del Papaloapan, Instituto de Química Aplicada, Tuxtepec, Mexico

The tantalum nitrides are a complex system of phases with a variety of stoichiometries [1]. They have been extensively explored at high temperatures in the last decades, while fewer studies on the phase stabilities at high pressures and temperatures have been reported in the recent years. The ground state structure of tantalum mononitride, ε-TaN, is of the hexagonal CoSn-structure type. From the analysis of quenched samples it was reported that hexagonal θ-TaN in the WC-structure type is the stable phase at 2-10 GPa and 673-2073 K, while cubic δ-TaN (NaCl-type structure) is stable in this pressure range at a higher temperature of 2073 K [2,3]. Recently, a new phase, Ta_3N_5-II, was predicted to be formed from ε-TaN at 17-25 GPa and 2800 K [4]. Our aim was the in situ investigation of the ε-TaN phase stability at 6-20 GPa and 1400-3100 K and the determination of the compressibilities of the high-(p,T) mononitrides.

Commercially available ε-TaN was pressurized in the diamond anvil cell and laser heated at different pressures between 6-20 GPa at 1400-3100 K. Experiments were conducted with and without excess nitrogen using nitrogen or salt as pressure-transmitting medium, respectively. Powder synchrotron X-ray diffraction was performed in situ at high pressure and temperature at both the ALS (Berkeley, beamline 12.2.2) and PETRA III (Hamburg, beamline P02.2).

At different starting pressures we observed on temperature increase the transformation from ε-TaN to θ-TaN, which is the main stable tantalum nitride phase at 6-20 GPa and 1700-3000 K. Further heating of θ-TaN to >3000 K at 20 GPa led to the appearance of new diffraction lines indicating the formation of a novel tantalum nitride phase, which also remained stable after pressure and temperature release. This observation supports the prediction of another stable phase in this (p,T)-range [4], and further studies are currently in progress. Under nitrogen excess ε-TaN reacted with nitrogen to the high-(p,T) phase η-Ta_2N_3 [1] as the main stable phase at 8-13 GPa and about 2000 K. This behaviour is similar to the reaction of pure Ta with nitrogen at high-(*p*,*T*) conditions [1]. In addition, we have determined the bulk modulus of θ-TaN, which is less compressible than ε-TaN.

Financial support from the DFG within SPP1236 (Wi1232, Fr2491/2-1) and the BMBF (project 05K10RFA) is gratefully acknowledged. We thank ALS, HASYLAB, COMPRES and the VFF of the Goethe University for beamtime and financial support, and the ALS beamline scientists for their help.

[1] A. Friedrich, B. Winkler, L. Bayarjargal, E.A. Juarez-Arellano, W. Morgenroth, J. Biehler, F. Schröder, J. Yan, S.M. Clark, *J. Alloys Compd.*, 502, 5, 2010.
[2] L.G. Boiko, S.V. Popova, *JETP Letters USSR*, 12, 70, 1970.
[3] G. Brauer, E. Mohr, A. Neuhaus, A. Skokan, *Monatsh. Chem.*, 103, 794, 1972.
[4] P. Kroll, T. Schröter, M. Peters, *Angew. Chem.-Int. Ed.*, 44, 4249, 2005.

PS09-P05

High-pressure polymorphs of spinel-type $LiMn_2O_4$ as cathode materials for lithium-ion batteries

C. Braun[1,2], N. Kiziltas Yavuz[2], K. Nikolowski[3], J. Gallardo-Amores[4], M. E. Arroyo-de Dompablo[4], H. Ehrenberg[3,2], C. Braun[1,2], N. Kiziltas Yavuz[2], K. Nikolowski[3], J. Gallardo-Amores[4], M. E. Arroyo-de Dompablo[4], H. Ehrenberg[3,2]
[1]*Technische Universität Dresden, Institut für Werkstoffwissenschaft (IfWW), Dresden, Germany*
[2]*Karlsruher Institut für Technologie (KIT), Anorganische Chemie, Karlsruhe, Germany*
[3]*Karlsruher Institut für Technologie (KIT), Institute für Angewandte Materielien (IAM), Leopoldshafen, Germany*
[4]*Universidad Complutense de Madrid, Facultad de Ciencias Químicas, Madrid, Spain*

In order to enhance the electrochemical properties of cathode materials for lithium-ion batteries, new synthesis strategies have to be developed and investigated. Usual strategies as doping and/or coating of materials tend to only slightly increase parameters like capacity or energy density. To significantly increase these parameters, phases which are only accessible by applying extreme conditions are possible candidates. High pressure driven transformations of several electrode materials have so far been studied and reported, for example Li_xFePO_4,[1,2] V_2O_5,[3] Li_2MSiO_4 (*M* = Mn, Co),[4] $LiMO_2$ (*M* = Ni, Mn).[5] It is proven that after exposure to high pressure/high temperature conditions, the electrochemical properties varied compared to the ambient pressure materials.

The spinel type $LiMn_2O_4$ is well known as cathode material for lithium-ion batteries. Furthermore, various studies report structural examinations at high pressure of these spinel phases [6,7]. Nevertheless, only little is known about the electrochemical behaviour of these phases, when they are used as intercalation compound for an electrode in a lithium ion battery.[5,8] In this communication we present the structural transformation, measured by X-ray diffraction, the spinel type $LiMn_2O_4$ undergoes when high pressures are applied. Finally the electrochemical behaviour is analysed and discussed.

References:

[1] M. E. Arroyo de Dompablo, N. Biskup, J.M. Gallardo-Amores, E. Morán, H. Ehrenberg, U. Amador, *Chem. Mater.* **2010**, *22*, 994.
[2] M. E. Arroyo-de Dompablo, J.M. Gallardo-Amores, U. Amador, *Electrochem. Solid St.* **2005**, *8*, A564-A569.
[3] M. E. Arroyo de Dompablo, J. M. Gallardo-Amores, U. Amador, E. Morán, *Electrochem. Commun.* **2007, *9***, 1305-1310.
[4] D. Santamaría-Pérez, U. Amador, J. Tortajada, R. Dominko, M. E. Arroyo-de Dompablo, *Inorganic chemistry* **2012**, *51*, 5779-86.
[5] C. R. Fell, D. H. Lee, Y. S. Meng, J. M. Gallardo-Amores, E. Morán, M. E. Arroyo-de Dompablo, *Energy & Environmental Science* **2012**, *5*, 6214.
[6] P. Piszora, W. Nowicki, J. Darul, B. Bojanowski, S. Carlson, Y. Cerenius, *Radiat. Phys. Chem.* **2009**, *78*, S89-S92.
[7] J. Darul, W. Nowicki, C. Lathe, P. Piszora, *Radiat. Phys. Chem.* **2011**, *80*, 1014-1018.
[8] K. Yamaura, Q. Huang, L. Zhang, K. Takada, Y. Baba, T. Nagai, Y. Matsui, K. Kosuda, E. Takayama-Muromachi, *J. Am. Chem. Soc.* **2006**, *128*, 9448-9456.

PS09-P06

The nanoscale structure of Pb-based relaxor ferroelectrics as revealed by in situ temperature-dependent Raman spectroscopy under an external electric field.

T. Steilmann[1], B. Maier[2], M. Gospodinov[3], U. Bismayer[1], B. Mihailova[1]
[1]*Universität Hamburg, Fachbereich Geowissenschaften, Hamburg, Germany*
[2]*Ludwig-Maximilians Universität, Department für Geo- und Umweltwissenschaften, München, Germany*
[3]*Institute of Solid State Physics, Sofia, Bulgaria*

Relaxor ferroelectrics are advanced functional materials with strong structural and chemical heterogeneities on the mesoscopic scale. Their structure is comprised of polar nanoregions (PNRs) dispersed into a paraelectric matrix. Dynamic PNRs that flip between different orientation states nucleate at the so-called Burns temperature TB, which is several hundreds Kelvins above the temperature of the dielectric-permittivity maximum Tm. At an intermediate temperature T* which is between Tm and TB the preexisting PNRs merge into larger PNRs of slower flipping dynamics. At temperatures slightly below Tm the PNRs freeze or evolve into long-range ordered ferroelectric domains, although a part of the material can still be in a paraelectric state. In situ temperature-dependent Raman-spectroscopy under different electric fields has been applied to perovskite-type (ABO3) Pb(Sc1/2Nb1/2)O3 relaxor ferroelectric to better understand the nanoscale process of polar coupling near the intermediate characteristic temperature T*. The polarized Raman spectra were collected at different temperatures and under an electric field applied along the cubic crystallographic directions [100], [110] and [111], respectively. The temperature evolution of the Raman peak positions and widths in zero and non-zero field measured for Pb(Sc1/2Nb1/2)O3 will be discussed in detail and compared with the results obtained for Pb(Sc1/2Ta1/2)O3 and (Pb0.78Ba0.22)(Sc1/2Ta1/2)O3 [1], which showed that the Pb2+ cations experience antiferroelectric coupling in the vicinity of T*, while the B-site cations couple ferroelectrically.

[1] B.J. Maier, T. Steilmann, M. Gospodinov, U. Bismayer, B. Mihailova, Influence of electric field on local phase transformations in relaxor ferroelectrics PST and PBST. accepted by J. Appl. Phys.

PS09-P07

Time-resolved X-ray diffraction study of elastic vibrations in piezoelectric crystals generated by alternating electric field

M. Al Taani[1], S. Gorfman[1], M. Ziolkowski[1], S. Heidbrink[1], U. Pietsch[1]
[1]*University of siegen , physics, siegen, Germany*

Piezoelectricity is the physical phenomenon describing mechanical deformation of a crystal under external electric field. It has a lot of technical application and still an interesting subject for fundamental crystallography: atomistic origin of piezoelectricity has recently been a focus of numerous researches works [1,2]. The aim of this work is to apply X-ray diffraction to investigate the piezoelectric deformation, produced by the alternating external electric field of a frequency close to that of an eigen-vibration mode, i.e. at the resonance. The magnitude of macroscopic deformation at resonance is significantly enhanced. In addition, different resonance frequencies correspond to mechanically different vibrations modes - either predominantly deformation (longitudinal, sheared) or bending ones.

We used a specially developed X-ray diffraction based experimental technique to follow the time dependence of a selected Bragg peak under electric field, periodically applied to a crystal. We implemented the stroboscopic approach, i.e. synchronization of electric field application with the diffraction intensity collection. The signals coming from an X-ray counter were redistributed between large numbers of time channels; the first channel was triggered to the beginning of the period, the time-duration of the channel was fixed (100 ns) and the total number of channels covered the whole period of applied electric field. The technique was realized using the programming of the FPGA (Field-Programmable Gate Array) board and described in more details in [3].

We investigated eigen vibration of a-quartz single crystal plate. The rocking curves of selected Bragg peaks were collected using the novel experimental approach at the frequency (~8.405 kHz) corresponding to the specific bending vibration mode. The shift of the position, integrated intensity and width of the Bragg peak were extracted from the rocking curve and plotted as a function of time or applied electric field (Figure 1). This way the dynamics of lattice constants, domain misorientation and atomic positions can be investigated simultaneously and compared with each other. We found, however, that the change of the integrated intensity under the resonance conditions cannot be described by the kinematical X-ray diffraction theory. This further result will be discussed in the presentation.

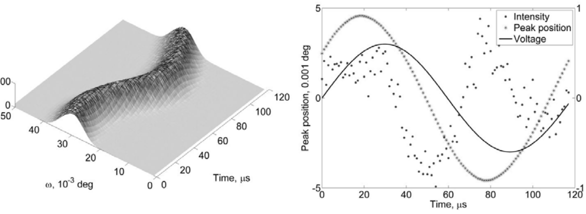

FIG.1. (left) Time-resolved behaviour of the rocking curve of the (-3, 2, 0) refection. (Right) The shift in peak position (black stars) and the relative change in the intensity (Gray dots) of (-3, 2, 0) reflection. The black line is the applied electric field as sine function with amplitude (3kV) at frequency (8.405 kHz).

[1] R. Guillot, P.Fertey, N.K.Hansen, P. Alle, E.Elkaım, C. Lecomte. Eur. Phys. J. B42, 373-380, (2004)

[2] O. Schmidt, S. Gorfman, L. Bohaty, E. Neumann, B. Engelen, U. Pietsch. Acta Cryst. A65, 267-275, (2009)

[3] S. Gorfman, O. Schmidt, M. Ziolkowski, M. von Kozierowski, U. Pietsch, J.Appl. Phys., 108, (2011)

PS09-P08

Lattice thermal expansion modeling of mullite-type $PbFeBO_4$

T. M. Gesing[1], D. Hansmann[2], G. Nénert[3], M. M. Murshed[1]
[1]*Chemische Kristallographie fester Stoffe, Institut für Anorganische Chemie, Universität Bremen, Bremen, Germany*
[2]*Universidad Nacional de Mar del Plata, Instituto de Física, FCEyN, Mar del Plata, Argentina, Argentina*
[3]*Institut Laue Langevin, Grenoble, France, France*

The lattice thermal expansion behavior of $PbFeBO_4$ has been investigated between 2 K and 1000 K using low-temperature neutron and high temperature X-ray diffraction data. The ^{11}B enriched powder sample was synthesized using the glycerin method [1]. The orthorhombic lattice parameters (*a* = *697.90(1) pm*, *b =835.20(1) pm*, *c* = *597.59(1) pm* and *V* = *348.32(3)* 10^{-6} pm^3 *at room-temperature*) were determined from the respective powder data Rietveld refinements in the non-standard space group *Pnam* that fits to mullite-type settings [2]. Number of observed anomalies considerably limits the quantitative treatment of the thermal expansion of the material, in particular of the negative thermal expansion of *a* cell parameter for the entire temperature range. Einstein model using a single harmonic oscillator with fixed frequency cannot satisfactorily fit the volume expansion, nor can the Debye model with characteristic temperature. The thermal expansion coefficients (TEC) $\alpha(a)$, $\alpha(b)$ $\alpha(c)$ of $PbFeBO_4$ do not saturate at high temperatures. As a consequence the temperature dependent $\alpha(V)$ showed a sigmoid behavior. Moreover, the second derivative of the anisotropy factor (with respect to temperature) is still non-linear. All these three factors require intrinsic anharmonicity terms to better fit the observed non-linearity of the expansion behavior. For the simulation of the thermal expansion of the unit cell volume with meaningful physical parameters we use the first-order Grüneisen approximation. Four independent characteristic temperatures were obtained for the Einstein and Debye approximations by least squared parameterization. We propose a weighted average for the calculation of the anharmonic contribution to the internal energy from two different Debye temperatures and the associated fitting constants using Oganov and Dorogokupets [3] approach. The Debye function values were calculated by numerical method. Although the applied model (DDEEA = double Debye double Einstein Anharmonic) fits well to our observed cell volume data set, still the significance of using four independent characteristic temperatures is an open question. Since the *a* cell parameter of $PbFeBO_4$ shows negative thermal expansion even at the high temperature paramagnetic region, the low temperature antiferromagnetism [4] is assumed not to significantly contribute as magnetostriction, nor does to anharmonicity of the phonon density of states.

[1] Th. M. Gesing, R. X. Fischer, M. Burianek, M. Mühlberg, T. Debnath, C. H. Rüscher, J. Ottinger, J.-Ch. Buhl, H. Schneider, J. Eur.Ceram. Soc. 31 (2011) 3055.
[2] R.X. Fischer, H. Schneider, Eur. J. Mineral. 20 (2008) 917.
[3] A.R. Oganov, P.I. Dorogokupets P I, J. Phys: Condens. Matter 16 (2004) 1351.
[4] H. Park, R. Lam, J. E. Greedan, J. Barbier, Chem. Mater. 15 (2003) 1703.

PS09-P09

Thermal excitation of superionic Li-mobility: Interatomic potentials from (an)-harmonic temperature factors of Li_2Te

J. Schneider[1], T. Schröder[2], M. Hölzel[3], O. Oeckler[4], W. Schmahl[1]
[1]*Ludwig-Maximilians-Universität München, Geo- und Umweltforschung, München, Germany*
[2]*Ludwig-Maximilians-Universität München, Chemie, München, Germany*
[3]*Technische Universität München, FRM II, München, Germany*
[4]*Universität Leipzig, Chemie, Leipzig, Germany*

Li ion conductors are highly important for the production of Li-ion batteries. Especially substances exhibiting a transition to a "superionic" phase at temperatures Tc are expected to be of technological relevance. From the isostructural series Li_2M (antifluorite structure type) with M=(O, S, Se, Te) only Li_2O [1] and Li_2S [2] have been investigated by neutron diffraction. A diffuse transition to a "Li-superionic" phase was found at Tc~1000K and Tc~900K, respectively. Details of Li-O and Li-S batteries have been reviewed very recently [3]. For technological reasons a lowering of Tc is highly desireable. As Tc scales with the melting temperature and inversely with the cell dimensions, we investigated the series end member Li_2Te by temperature dependent neutron powder diffraction.

The microcrystalline sample was synthesized from the elements in liquid ammonia and dried using the Schlenk technique. It was sealed into thin walled Nb-tubes in an Ar dry box. Neutron powder diffraction was performed with a standard furnace at the diffractometer SPODI at FRMII in Munich. Data were taken from ambient temperature up to 1073K in steps of 100K .

Rietveld analysis of the simple antifluorite structure model assuming harmonic temperature factors yielded strikingly nonlinear temperature dependence of Li atom displacement parameters (adp's). Therefore, anharmonic temperature factors up to 4th order for Li were refined [5]. A nonlinear temperature dependence of 3rd order adp's and an abrupt increase of 4th order adp's above 800K indicate a transition to "superionic" Li mobility. Joint probability density function (jpdf) maps show a tetrahedral arrangement of lobes for Li pointing towards the empty central octahedron and thus indicate possible Li diffusion pathways.

A similar delocalization pattern for Li is obtained by a split atom model setting Li on 32f sites (xxx). Analogous results had been found for the isostructural compound Ag_2Te [4]. A linear increase of (xxx) with temperature above 500K is accompanied by a change of slope of harmonic, anisotropic adp's above 800K. Interatomic potentials along [111] obtained from corresponding jpdf's show strong deviation from simple square form for Li above 800K, suggesting again the onset of "superionic" mobility (hopping) of Li via the empty 4b site at (½ ½ ½).

Keywords: fast ion conductor, neutron powder diffraction, atom displacement factors

[1] Farley T.W.D. et al. J. Phys.: Condens. Matter **3** (1991) 4761
[2] Buehrer W. et al. J. Phys.:Condens. Matter **3** (1991) 1055
[3] Bruce P.G. et al. Nature Materials **11** (2012) 19
[4] Schneider J. et al. Z. Kristallogr. **203** (1993) 1
[5] Petricek V. et al. Jana2006. The crystallographic computing system.
Institute of Physics, Praha, Czech Republic

PS09-P10

Measurement of pyroelectric properties and ferroelectric to paraelectric phase transition

S. Jachalke[1], E. Mehner[1], H. Stöcker[1], D. C. Meyer[1]
[1]*TU Bergakademie Freiberg, Institut für Experimentelle Physik, Freiberg, Germany*

The Olsen-Cycle can be utilized to build a pyroelectric energy converter by cycling temperature and electrical field. Beside several pyroelectric, non-centrosymmetric materials like lead zirconate stannate titanate (PZST) the perovskite-related $LiTaO_3$- and $LiNbO_3$-single-crystals or the co-polymer poly(vinylidene fluoride-trifluoroethylene) [P(VDF-TrFE)] offer a great potential for harvesting wasted heat and transform it into usefull electric energy. Pyroelectric materials are known for their ability to change their polarization while they are heated or cooled. This accumulates charges on their surface, which can flow trough an external circuit. This work focusses on a setup for the characterization of pyroelectric materials with the help of a computer controlled thermal stimulation and simultaneous recording of the arising pyroelectric current, including the ferro- to paraelectric phase transitions. Data analysis with the Lang-Steckel- and Shap-Garn-method [1] yields temperature depended pyroelectric coefficients and polarization, by separating the pyroelectric from the non-pyroelectric signal. Furthermore we are able to determine the Curie-temperature. First measurements where performed at $LiTaO_3/LiNbO_3$ single crystals and 50µm 70/30 %mol P(VDF-TrFE).

[1] I. Lubomirsky and O. Stafsudd, "Invited Review Article: Practical guide for pyroelectric measurements.," *Rev Sci Instrum*, vol. 83, no. 5, p. 051101, May 2012.

PS09-P11

Low Temperature Structural Phase Transitions of $Fe_{1+y}Te$

C. Koz[1], S. Roessler[1], A. A. Tsirlin[1,2], S. Wirth[1], U. Schwarz[1]
[1]*Max Planck Institute for Chemical Physics of Solids, Dresden, Germany*
[2]*National Institute of Chemical Physics and Biophysics, Tallinn, Germany*

Antiferromagnetic $Fe_{1+y}Te$ with a simple PbO-type crystal structure displays a complex phase diagram with several structural and magnetic phase transitions within the homogeneity range $0.06 \leq y \leq 0.15$. The magnetic and structural phase transitions are extremely sensitive to the tuning parameters such as Fe composition and application of external pressure, and both parameters influence the phase transition with regards to critical temperature and symmetry of the resulting polymorph [1-3]. The temperature of first-order magnetic and structural transitions to the monoclinic phase systematically decreases from 70 K to 57 K with an increase in y from 0.06 to 0.11. For $y = 0.12$, two distinct transitions occur: a λ-like shape continuous transition is followed by a first-order one. Further, for $y \geq 0.13$, the low-temperature structure adopts orthorhombic symmetry by undergoing a continuous phase transition. Here, we focus on the detailed analysis of the powder diffraction patterns and the temperature dependence of the peak-width in $Fe_{1+y}Te$ within the range $0.11 \geq y \geq 0.15$. We present a revised temperature-composition phase diagram for $Fe_{1+y}Te$ based on the temperature dependence of the crystal structure, specific heat, and magnetization measurements.

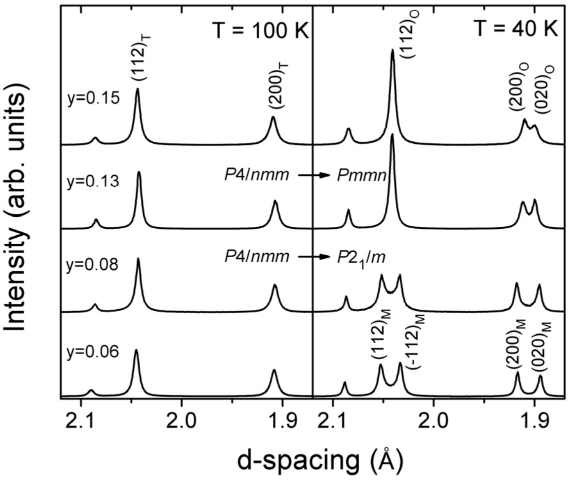

Figure 1: Representative powder XRD patterns of $Fe_{1+y}Te$ in the high- (left) and low-temperature form (right).

[1] W. Bao *et al., Phys. Rev. Lett.,* **2009**, *102*, 247001
[2] S. Rössler *et al., Phys. Rev. B.,* **2011**, *84*, 174506
[3] C. Koz *et al., Phys. Rev. B.,* **2012**, 86, 094505

PS09-P12

A polymorphic transition induced by hydrostatic compression of the a-polymorph of chlorpropamide in saturated ethanol solution, accompanied by twinning

E. Boldyreva[1,2], T. N. Drebushchak[1,3], Y. V. Seryotkin[1,2]
[1]*Novosibirsk State University, REC-008, Novosibirsk, Russian Federation*
[2]*Institute of Geology and Mineralogy, Novosibirsk, Russian Federation*
[3]*Institute of Solid State Chemistry and Mechanochemistry, Novosibirsk, Russian Federation*

The studies of the thermodynamic and kinetic control of polymorphism are of primary importance for understanding the factors determining crystal structures and structural transformations. Chlorpropamide, 4-chloro-N-(propylaminocarbonyl)benzenesulfonamide, is an antidiabetic drug, which is widely used as a model system for studying the polymorphism of molecular crystals. The aim of the present work was to follow the effect of hydrostatic compression of the a-polymorph of chlorpropamide in the saturated ethanol solution as pressure-transmitting liquid. The crystal structure of the high-pressure monoclinic polymorph of chlorpropamide has been determined. It is formed at ~ 2.8 GPa on hydrostatic compression of the orthorhombic stable a-polymorph. The phase transformation is reversible, and the original a-polymorph is restored on decompression. The structure of the high-pressure polymorph is related to that of the a-form, although it is of a lower symmetry, and differs from the latter in molecular conformation and the number of molecules in the asymmetric unit. Interestingly enough, structural compression is accompanied by a slight expansion of hydrogen bonds, which enables a denser packing of the molecules.

The phase transition is accompained by twinning. The twinning of a-chlorpropamide on hydrostatic compression differs from that observed in another polymorph, β-chlorpropamide, on cooling. In a-chlorpropamide, the twinning plane is normal to the hydrogen bonded z-type molecular bands. In β-chlorpropamide the twinning plane is parallel to the p-type molecular bands. This difference is likely to be related to the different response of the z- and p-type molecular bands to structural compression. A similarity in twinning in the two cases is that the twin components form layers. Besides, in both cases twinning disappears as the reverse transformations take place.

Seryotkin Yu.V., Drebushchak T.N., Boldyreva E.V. Effect of hydrostatic pressure on a-polymorph of chlorpropamide in saturated ethanol solution // Acta Cryst. B, 2013, B69, 77-85.

PS09-P13

Crystal and Magnetic Structures of Multiferroic $Ba_2CoGe_2O_7$

A. Sazonov[1,2], V. Hutanu[1,2], M. Meven[1,2], G. Roth[1], H. Murakawa[3], Y. Tokura[3], I. Kézsmárki[4], . Náfrádi[5], A. Gukasov[6], D. Chernyshov[7]
[1]*RWTH Aachen University, Institute of Crystallography, Aachen, Germany*
[2]*JCNS Outstation at FRM II, Garching, Germany*
[3]*University of Tokyo, Tokyo, Japan*
[4]*BME, Department of Physics, Budapest, Hungary*
[5]*Max-Planck-Institut für Festkörperforschung, Stuttgart, Germany*
[6]*Laboratoire Léon Brillouin, CEA-Saclay, Gif-sur-Yvette, France*
[7]*Swiss-Norwegian Beam Lines at ESRF, Grenoble, France*

Multiferroic materials in which more than one order parameter simultaneously appearing in a single phase have attracted extensive theoretical and experimental efforts. If an electric field controls the magnetism via magnetoelectric coupling, such process is much less dissipative in energy than the current control of magnetism in itinerant ferromagnets; thus multiferroics are interesting for potential use in spintronics and data storage.

Coupled electric and magnetic orderings were recently found in $Ba_2CoGe_2O_7$. To unravel the complex physics underlying magnetoelectric behavior of the title compound the symmetry information is essential. However, a close inspection of the available information about the $Ba_2CoGe_2O_7$ compound reveals that no detailed structural study of $Ba_2CoGe_2O_7$ has been performed up to now.

In order to fill the gap of structural information on $Ba_2CoGe_2O_7$ and to fully characterize its magnetic order in the multiferroic state, we have performed both x-ray synchrotron and neutron single-crystal diffraction experiments on $Ba_2CoGe_2O_7$ in the range between 2.2 K and room temperature.

We have found that the melilite tetragonal crystal structure (space group $P\text{-}42_1m$), widely accepted for the title compound, is indeed a rather good approximation. However, the real structure of $Ba_2CoGe_2O_7$ is more distorted and has a lower symmetry. Orthorhombic space group *Cmm*2 is proposed as a true crystal structure and the magnetic structure is described in the magnetic space group *Cm'm*2'.

PS10 - Spectroscopy and other Tools for Analysis

PS10-P01

A simple innovative method for X-ray absorption reduction in high temperature powder X-ray diffractometry

K. Xhaxhiu[1], M. Schlosser[2], H.- J. Deiseroth[3], K. Bente[4]
[1]*University of Tirana, Faculty of Natural Sciences, Chemistry, Tirana, Albania*
[2]*Institute of Inorganic Chemistry, University of Regensburg, Regensburg, Germany*
[3]*Institute of Inorganic Chemistry, University of Siegen, Siegen, Germany*
[4]*Institute of Mineralogy, Crystallography and Material Science, University of Leipzig, Leipzig, Germany*

For X-ray powder diffraction measurements, crystalline samples with particle sizes ranging from (5-50) µm are transferred into quartz capillaries. The choice of capillary diameter depends on the absorption coefficient of the material. For high absorbing materials, capillaries of 0.1 - 0.2 mm outer diameter are usually used. For medium and low absorbing materials, diameters between 0.5 and 1.0 mm are suitable. High absorbing samples are diluted with suitable low absorbing materials i.e. SiO_2, BN.

As a case study we considered the compound $K_2In_{12}Se_{12}Te_7$, crystallizing in the hexagonal system in the space group R3 with the lattice constants a = 14.175 (3) Å, c = 35.838 (9) Å and exhibiting superstructure reflections within 34 - 34.5° in 2θ scale [1]. Its preliminary measurements recorded with a step width 0.1° and time/step 60 sec, using a filled quartz capillary tube of 0.1 mm outer diameter and 0.01 mm wall thickness, exhibited a low signal/background noise ratio making the reflection indexing quite difficult.

The measurements using a quartz capillary with 0.1 mm outer diameter and 0.01 mm wall thickness covered from the outer surface with a thin film of silicon grease and rotated carefully over the spread powdered sample ($K_2In_{12}Se_{12}Te_7$) forming a cylindrical thin film of crystallites around it, revealed a much higher signal/background noise ratio. This method reduced the X-ray absorption and was limited to measurements at room temperature and to compounds which are inert in contact with grease.

The decrease of the sample's volume up to 1/3 of that contained in 0.1 mm capillary, through sample insertion between a system of two capillaries 0.1 and 0.2 mm (Fig. 1), led to a significant improvement of the diffraction patterns. The later were better reproducible and were comparable to those measured using silicon grease film around 0.1 mm capillary. With this method we could follow the thermal behavior of the superstructure reflections up to 550 K and were able to index the obtained patterns up to 733 K.

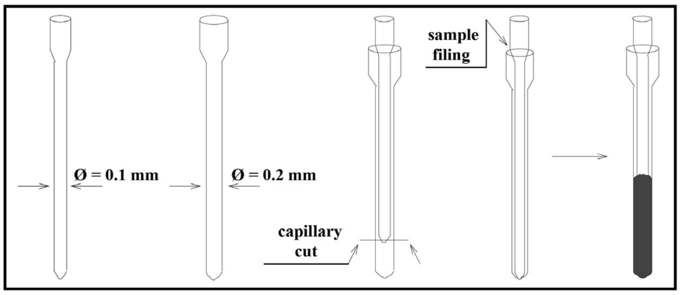

Fig. 1: Preparation of a double capillary using a combination of 0.1mm Ø and 0.2 mm Ø capillaries.

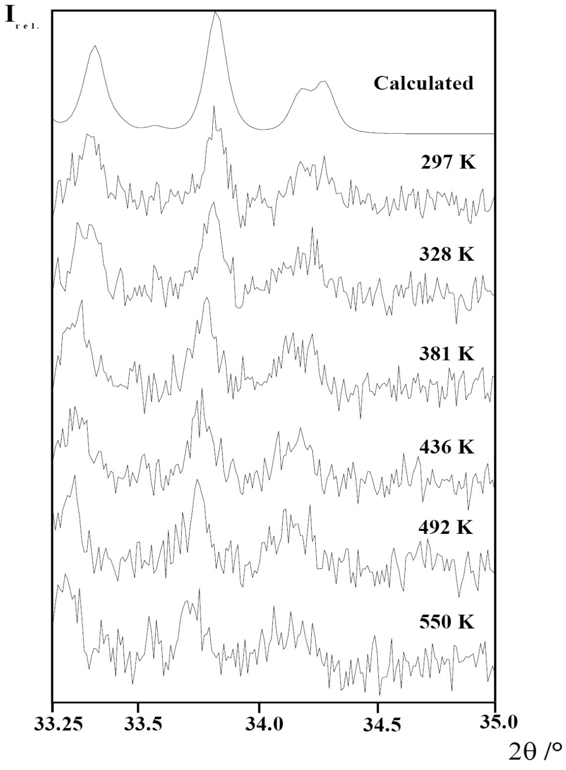

Fig. 2: Patterns of the measured superstructure reflections of $K_2In_{12}Se_{12}Te_7$ at different temperatures and compared with the calculated one.

[1] M. Schlosser, PhD thesis: Zur Micro- und Nanostruktur der neuen ternären Chalkogenide RbIn3S5, und K2In12Se19. University of Siegen **2005**.

PS10-P02

High-Resolution Imaging with Chemical Contrast by Using Hard X-Ray Ptychography

J. Reinhardt[1]
[1]*Institut für Strukturphysik, Dresden, Germany*

Monitoring the chemical state of catalysts on a large range of length scales is crucial to understand the function of the catalyst under realistic working conditions. Therefore high-resolution x-ray imaging is well suited due to the high-penetration depth and the consequently straightforward sample preparation and environment. Ptychography, a type of high-resolution coherent X-ray diffraction imaging, is combined with spectroscopy. Ptychography is a scanning coherent imaging technique. The sample is scanned through a coherent nanofocused beam (≈ 100 nm FWHM), recording a far-field diffraction pattern at each position of the scan. Appropriate overlap between the illumination at adjacent scan points allows for the unambiguous reconstruction of the complex transmission function of the object by numerical phase retrieval algorithms [1,2,3]. The transmission function gives access to both absorption and refraction inside the object. For strongly-scattering objects we have reached resolutions down to 9 nm [4].

For the spectroscopic part ptychographic datasets of the sample are recorded for a series of energies around an absorption edge. From these data, chemical information in the form of both an absorption and a resonant scattering spectrum is reconstructed at each location in the sample. Analysis of the resonant scattering spectrum show a significant decrease in negative phase shift along the absorption edge of the respective element. In this way we distinguished between two elements -platinum and gold- of a model sample [5].

This microscopy approach opens the way to in-operando studies of heterogeneous catalysts on the nanometer scale.

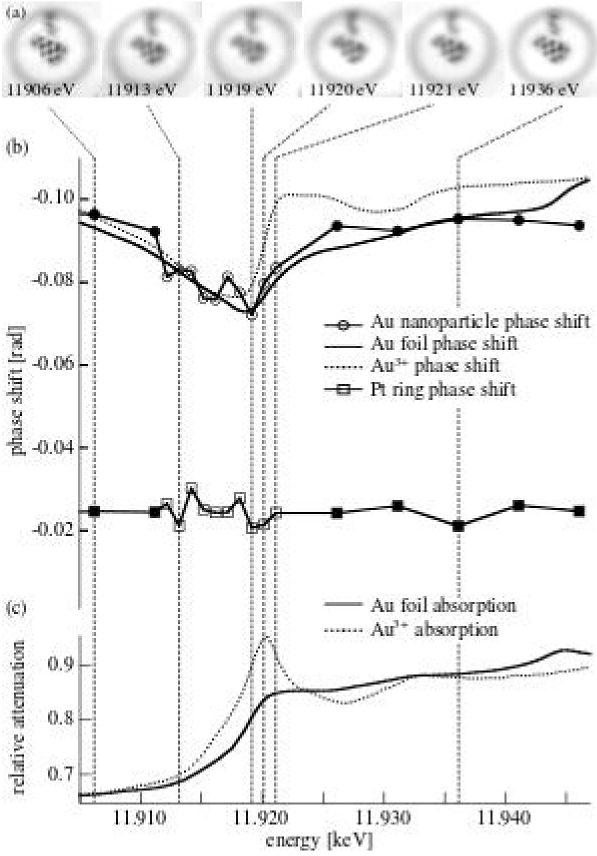

(a) Ptychographic reconstruction of the phase shift of the object at selected energies. (b) Phase shift of the gold nano particle as function of x-ray energy (circles), showing a reduced refraction at the gold L3 edge. The phase shift of the platinum ring shows no significant energy dependence. (c) As reference, the absorption of a metallic gold foil (solid curve) and of trivalent gold (dashed curve) are shown.

References:
1 A. M. Maiden and J. M. Rodenburg, Ultramicroscopy 109, 1256 (2009)
2 J. M. Rodenburg and H. M. L. Faulkner, Appl. Phys. Lett. 85, 4795 (2004)
3 P. Thibault et al., Science 321, 379 (2008)
4 A. Schropp et al., Appl. Phys. Lett. 100, 253112 (2012)
5 R. Hoppe et. Al, Appl. Phys. Lett. (2012, submitted)

PS10-P03

Pressure-induced structural changes in metamict zircon

F. A. Pina Binvignat[1], N. Waeselmann [1], T. Malcherek[1], C. Paulmann[1], J. Schlüter[1], B. Mihailova[1], R. J. Angel[2]
[1]*Universität Hamburg, Geowissenschaften, Hamburg, Germany*
[2]*Universita degli studi di Padova, Geoscienze, Padova, Italy*

The quest for encapsulation and permanent disposal of the increasing amount of nuclear waste in crystalline or glassy materials requires detailed studies of the structural stability and elastic response of the host matrix over a very long-term period. Metamict minerals possess structurally incorporated U and Th impurities and are characterized by a high degree of structural disorder consisting of coexistence of defect-rich crystalline and amorphous nanoregions, caused by the radioactive α-decay of the embedded actinides. In this regard, metamict minerals are ideal model systems for studying the behaviour of actinide-waste-form phases in specific geochemical environments over a geological time-scale period. Thus the analysis of the structural response to pressure of metamict minerals is vital for the better understanding of the long-term elastic stability of the matrix in which actinide-bearing radioactive waste is captured. Metamict zircon has been extensively studied by various methods because it is one the oldest minerals found in the Earth crust. Still high-pressure structural studies of metamict zircon are scarce. We have applied complementary polarized Raman spectroscopy and synchrotron single-crystal X-ray diffraction (XRD) to three representative zircon samples in order to analyze the pressure-induced structural alteration of both amorphous and crystalline regions up to 10 GPa. We have selected zircon samples free of chemical and structural zonation, as revealed by backscattering electron images and ambient-pressure Raman spectroscopy, which exhibit a low, moderate, and high degree of metamictization. The XRD data indicate a slightly larger volume compressibility for heavily metamict zircon as compared to the other two samples within the entire pressure range as well as a reduced mosaic spread of the crystallites above 6 GPa. The pressure evolution of the preexisting boson peak related to radiation-induced amorphous regions as well as the appearance of a new pressure-induced boson peak reveals a structural amorphous-to-amorphous transformation near 4 GPa. The widths of some Raman peaks generated by the crystalline regions indicate structural changes in the crystallites that accompany the pressure-induced alteration of the amorphous matter.

PS10-P04

The effect of chemical variations on the nanoscale structure of relaxor ferroelectrics studied by resonance Raman spectroscopy

A. Rohrbeck[1], G. de la Flor [2], M. Wehber[1], M. I. Aroyo[2], M. M. Gospodinov[3], U. Bismayer[1], B. Mihailova[1]
[1]*Universität Hamburg, Mineralogisch-Petrographisches Institut, Hamburg, Germany*
[2]*Universidad del Pais Vasco, Fisica de la Materia Condensada, Bilbao, Spain*
[3]*Bulgarian Academy of Sciences, Institute of Solid State Physics, Sofia, Bulgaria*

Relaxor ferroelectrics possess outstanding properties such as high dielectric permittivity and high electrooptic and electroelastic coefficients which result from their heterogeneous complex structure with cubic matrix and embedded polar nanoregions (PNR). Although the extensive application of a multitude of methods to analyze the structure of PNRs, the relationship between the local structural deviations and macroscopic properties of relaxor ferroelectrics is still not clarified, which requires the use of further advanced methods. The objective of this study is on one hand to explore the potential of resonance Raman scattering to selectively study phonon modes of PNR and on the other hand to compare the resonance Raman scattering of different doped materials in order to figure out how chemical variations influence the intrinsic electron-phonon coupling. Polarized resonance Raman spectroscopy has been performed on heavily doped ABO_3 perovskite-type relaxor ferroelectric model compounds $PbSc_{0.5}Ta_{0.5}O_3$ (PST) and $PbSc_{0.5}Nb_{0.5}O_3$ (PSN) with $\lambda = 325$ nm (~ 3.81 eV), which corresponds to the electron energy gap formed by the B-cation d level and oxygen p level. In situ measurements were conducted on cooling in the temperature range 800-100 K. Under resonance conditions first and second order Raman scattering of longitudinal optical phonon modes related to the antisymmetric intrinsic BO_6 vibrations was observed for all relaxors studied. Group theory analysis revealed that such a simultaneous enhancement is allowed only in non-centrosymmetrical structures and therefore resonance Raman spectra are dominated by the atomic dynamics of PNRs, which considerably facilitates the comparison of polar nanoregions in various relaxors. Doping of the perovskite A site with iso- and aliovalent cations (Ba^{2+}, Bi^{3+}, La^{3+} and Sr^{2+}) has been used in order to analyze the influence of local electric and elastic fields due to charge imbalance and varying ionic radii on the strength of electron-phonon coupling in related materials. It is shown that A-site substitution by cations which, in contrast to Pb^{2+}, have no lone-pair electrons (LPE) reduces the electron-phonon coupling. The chemically-induced BO_6 tilt order occurring due to the smaller ionic radius of the substituting element has significantly stronger impact on the average polarization of PNRs than the local charge imbalance. However, A-site doping with aliovalent cations having the same outermost electron shell and ionic radius as the host A-cations amplifies the resonance behavior, indicating stronger electron-phonon coupling due to enhanced random local electric field.

PS10-P05

Composition profiles across the metal-Nb_2O_5-metal stacks for resistive switching as studied by EDX and EELS

F. Hanzig[1], J. Veselý[1], M. Motylenko[1], A. Leuteritz[1], H. Mähne[2], T. Mikolajick[2], D. Rafaja[1]
[1]*TU Bergakademie Freiberg, Institute of Materials Science, Freiberg, Germany*
[2]*NaMLab gGmbH, Dresden, Germany*

Resistive switching in MIM (metal-insulator-metal) stacks is an effect that allows a promising technology which is able to overcome the size limitations of conventional non-volatile memories [1]. The resistive switching effect was already demonstrated for several transition metal oxides (TiO_2, NiO, HfO_2) [2]. The models of the switching mechanisms [3] suggest the important role of oxygen vacancies [4]. In this work Nb_2O_5 was used as switching insulator. An amorphous Nb_2O_5 layer was deposited on Pt bottom electrode by reactive dc magnetron sputtering from a metallic niobium target in an argon-oxygen atmosphere at room temperature [5]. In order to describe the effect of the oxygen vacancies on the switching, materials with different affinity to oxygen like Pt, Al and Ti were used for the top electrode. The composition variation at the $Nb_2O_5|Ti$ and $Nb_2O_5|Al$ interfaces due to the oxidation of the electrodes (Ti, Al) were studied both by energy dispersive X-ray spectroscopy (EDS) and by electron energy loss spectroscopy (EELS) in the scanning transmission electron microscope (STEM). While the quantification of oxygen by EDS proved difficult, the complementary EELS solved this problem and enabled us to distinguish different oxides based on their electron energy loss near edge structure (ELNES).

[1] T. Mikolajick, M. Salinga, M. Kund, T. Kever, Advanced Engineering Materials 11 (2009) 235.

[2] A. Sawa, Materials Today 11 (2008) 28.

[3] L. Chen, Q.-Q. Sun, J.-J. Gu, Y. Xu, S.-J. Ding, D.W. Zhang, Current Applied Physics 11 (2011) 849.

[4] B. Magyari-Köpe, S.G. Park, H.-D. Lee, Y. Nishi, J Mater Sci 47 (2012) 7498.

[5] H. Mähne, L. Berger, D. Martin, V. Klemm, S. Slesazeck, S. Jakschik, D. Rafaja, T. Mikolajick, Solid-State Electronics 72 (2012) 73.

PS10-P06

On site x-ray diffraction: a new approach for not destructive testing methods

G. Berti[1,2], F. de Marco[2], S. Aldrighetti[2]
[1]*University of Pisa, Lab. R&D on X-ray Diffraction , Pisa, Italy*
[2]*XRD-Tools s.r.l., Pisa, Italy*

New concepts are required when the applications of x-ray diffraction are used for investigation of critical points of industrial production. These concepts apply also to monitor the conservation of natural rocks, stones and other materials which are relevant for the maintenance or restoration of cultural heritage or simple for the current civil living and safety. There are circumstances, materials and structures, where the diagnosis shall be conducted on the same site where the manufacture is located for service. The “on site x-ray diffraction” extends the applicability of x-ray diffraction to all the manufactures, or natural rocks independently of their dimension, size, weight, shape and location [1], [2]. As an example, the understanding of the mineralogical composition of rocks gives relevant information for their uses and usability. Unfortunately, the observation of their characteristics through using x-ray diffraction requires specimen manipulation and preparation which could affect the original state of the of the sample. Fact is that the intentionally induced manipulation of specimens was intended to enhance the quality of the diffraction method (e.g. to magnify the reliability of the intensity distribution, the peak shaped as the diffraction line positioning). In facts this induced manipulation cancels the original finger print of the material and its properties in loco. The objective of the work is to investigate how to combine the traditional laboratory X-Ray diffraction measurements with results obtained from diffractometers which are adaptable to different environment and manufactures.

Among the most relevant features such a new technology is presented along with comparison of performances against the traditional x-ray diffractometers, thus evocating the great potentiality of the method. From the terminology point of view, we would avoid the use of “in situ” because it tends to be confused with experiments and measurements of x-ray diffraction carried on in laboratory and out of ambient conditions.

[1] G. Berti patents n. IT0001338588
[2] G. Berti patents n. IT 0001362652.

Authors and Presenters

Supplement Issue No. 33
Zeitschrift für Kristallographie